Biomarker proxies as quantitative indicators of climate variability in the Montcortés lake

MIN CAO

Biomarker proxies as quantitative indicators of climate variability in the Montcortés lake

PhD Thesis 2016

MIN CAO

Supervisor: Dr. **Antoni Rosell Melé**

ICTA - Institut de Ciència i Tecnologia Ambientals

Universitat Autònoma de Barcelona

icta

UAB Universitat Autònoma de Barcelona

Tesi doctoral

Institut de Ciència i Tecnologia Ambientals
Universitat Autònoma de Barcelona

Biomarker proxies as quantitative indicators of climate variability in the Montcortés lake

Memòria presentada per Min Cao per optar al títol de Doctor per la Universitat Autònoma de Barcelona, sota la direcció del doctor Antoni Rosell Melé.

Barcelona, July 2016

La Doctoranda
Min Cao

El Director de la Tesi
Antoni Rosell Melé

Cover photograph: Montcortés lake (Project: Tetraclim and Mont 500)

Aknowledgements

I am grateful to all the persons that contributed to the accomplishment of my PhD thesis:

First and foremost, I would like to express my deepest appreciation to my supervisor, Prof. Antoni Rosell Melé, who is definitely one of the most important persons to guide not only my PhD work, but also my career life in future. He introduced me to explore in organic geochemistry and encouraged me in scientific research all the time. This thesis would not have been written up without his patience, innovative thinking and valuable suggestions. Thanks for all his effort and help. I will never forget our experience of working in the field campaign, trying out lab experiments, solving problems that drive me to go further in my research career. It's my honor to be his PhD student.

I would give appreciation to Dr. Juan Pablo Corella, who provided the age-calibrated sediment core samples and basic climatic information as well as his previous work in Lake Montcortés which are very important to this thesis. Thanks to collaborators Dr. Teresa Vegal, who developed the idea of water column monitoring and Mª Carmen Trapote, Dr. Núria Cañellas-Boltà, Dr. Elisabet Safont who helped retrieve the sediment trap and provided their CTD data. Thanks to Santiago Giralt, Valentí Rull and Teresa Buchaca for collaborating in the field work. I felt very lucky to work with you in Montcortés. In addition, thanks to Francisco Sigró and Núria Perez for providing instrumental meteorological data (2013-2015) in La Pobla de Segur.

Thanks to the members in our group: Núria, who helped me a lot in analytical processes and all the equipment operation in the lab; Pau, who helped with performing isotopic analysis; Ferran for helping with my sampling and Carme Huguet, for leading me to do GDGT analysis and master the HPLC. Thanks to Pedro, as another PhD student, who companied with most of my work time, gave useful suggestions in developing methods, collecting samples and integrating data. Thanks to others: Maria, Mar, Elena, Raguel, Nadia, Gemma, Susanne, Raúl, Magdalena and Miryam. There are good memories with you all.

Thanks to other members in ICTA: Montserrat, Rafael, Marta, Sara and Cristina for their administrative help and thanks to Alba, Monserrat, Josep for providing technical help in GDGT analysis and Dr. Xavier Domene for soil pH measurement.

Thanks to Tish and Joanna for English improvement.

Thanks to my friends: Ana, Bea, Sara, Zhen Zhan, Liang Li, Qinyi Tan, Qiuyue Zhong, Qinglong Shao, Meng chen, Liu He,Tong Liu, Haijie Liu, Qin Liu, Ping sun, Shuangshang Qi, Dianfei Yuan, Yuan zhong, Wusheng Guo, Shujing Ding, Yangchun xin, Liying Wang, Yanan Zhu, Jin Huang. I am so graceful to share the life with you in Barcelona and I enjoyed our leisure time.

Thanks for the grant from the China Scholarship Council (CSC), who provided the opportunity for me to pursue the PhD degree and experience a wonderful life in Barcelona; for the financial contract from Antoni Rosell Melé. Thanks to Dr. Yongjun Jiang and Prof. Daoxian Yuan who supervised by master work for encouraging me to study abroad and thanks to Dr. Yuanzhu Zhang and Dr. Yunchuan Sun in Southwest University, China for their financial guarantee.

At last, I would like to thank my family: my lovely parents, grandparents and my little brother and sister for their understanding and support in my life.

Abstract

The main objective of this dissertation was to validate and undertake the application of biomarker climatic proxies in the context of a Mediterranean lake basin. To this end, the work consisted in the detailed observation of modern biomarker production, transport, deposition processes and compare them with instrumental records on a seasonal and interannual basins, to establish how the spatial and temporal patterns of variability of the biomarker signals integrated palaeonvironmental signals in the sedimentary record. The proxies studied are derived from *n*-alkyl and GDGT lipids. The site selected, Lake Montcortés in the Catalan Pre-Pyrenees, has been proven to be in previous studies a site sensitive to climate changes driven by Atlantic and Mediterranean influences and its sediments contain unique high resolution sequences deposited in the XX^{th} century. In order to identify the likely sources of terrigenous biomarkers in lake Montcortés sediments, and to study their spatial and temporal (monthly/seasonal) variability, we collected a number of plant specimens and soil samples across the catchment for over a year. Our results suggest that inputs of alkyl lipids differ among particular plant groups (woody plants, grasses, emergent and submerged macrophytes), and can be distinguished from their distributions and various indices. Our study does not provide evidence for seasonal effects on the abundance and proxies of *n*-alkanes and GDGTs in soils. While in the suspended and settling particulate matter in the water column, significant seasonal signals were observed from the concentration and flux of lipid biomarkers due to its production, transport as well as lake circulation in different seasons, e.g. C_{29} *n*-alkane abundance in the sediment trap was correlated to precipitation/soil runoff (especially the storm) or wind. The compound specific $\delta^{13}C$ values of long chain *n*-alkanes remained constant throughout the year in soils and sediments to faithfully preserve the initial $\delta^{13}C$ signals of dominant C3 higher plants. The variability of GDGT-derived TEX_{86}, temperature estimates were generally small on a short-time scale (monthly or seasonally) within the same soil type, but there was significant heterogeneity among soils in the abundance and distribution of GDGTs, which might be attributed to differences in pH and soil humidity. TEX_{86} values from the water column and sediment trap showed significant seasonal changes which were similar to the temperatures in the upper water column of Lake Montcortés. However, in the sediment core, TEX_{86}-estimated temperatures were potentially biased towards cooler temperatures due to contributions from methanogenic Archaea, or towards warmer signals due to allochthonous inputs from catchment soils. GDGT-MBT/CBT estimated temperatures showed a large heterogeneity in the different catchment soils, and together with other evidence leads us to conclude that MBT/CBT as a temperature proxy is not applicable in the lake on decadal time scales. Based on instrumental records and fractional abundance of some GDGTs, a new index was used to estimate the mean annual temperatures, which significantly recorded the onset of the Little Ice Age since the end of 15^{th} century in the study area. The results of this thesis in lake Montcortés can probably be extrapolated to similar lacustrine settings with caution. Thus, this thesis is also an example of the need to appraise at a catchment level the fidelity of biomarker proxies to reconstruct climate quantitatively in lacustrine sediments.

Resum

L'objectiu general d'aquest treball va ser validar i dur a terme l'aplicació de proxies climàtiques de biomarcadors en el context d'una conca mediterrània lacustre. Amb aquesta finalitat, el treball va consistir en l'observació detallada de la producció de biomarcadors, transport i processos de deposició i comparar-ho amb registres instrumentals estacionals i interanuals, per establir com els patrons espacials i temporals de la variabilitat dels senyals de biomarcadors integren senyals palaeoambientals en el registre sedimentari. Els proxies estudiats es deriven de n-alquil lípids i els GDGTs. El lloc seleccionat, l'estany de Montcortés al pre-Pirineu català, ha demostrat ser en estudis previs un lloc sensible als canvis climàtics impulsats per influències atlàntiques i mediterrànies, i els seus sediments contenen seqüències úniques d'alta resolució dipositats al segle XX. Per tal d'identificar les possibles fonts de biomarcadors terrígens en els sediments de Montcortés, i estudiar la seva variabilitat espacial i tempora, hem recopilat espècimens de plantes i mostres de sòl durant més d'un any. Els nostres resultats suggereixen que els aports lacustres de lípids contenen diferents contribucions de plantes (plantes llenyoses, herbes, i aquàtiques), i que poden distingir-se per les seves distribucions i diversos índexs. El nostre estudi no proporciona evidència d'efectes estacionals en l'abundància i les proxies de *n*-alcans i GDGTs en els sòls. Mentre que en el material particulat a la columna d'aigua, es van observar senyals estacionals significatives de la concentració i fluxos de biomarcadors a causa de la seva producció i transport, així com la circulació del llac en diferents estacions de l'any. Per exemple, l'abundància del n-alcà C_{29}en el sediments es va correlacionar amb la precipitació (especialment tempestes) o el vent. Els valors $\delta^{13}C$ de n-alcans específics es van mantenir constants durant tot l'any en els sòls i sediments, i conserven fidelment els senyals inicials de $\delta^{13}C$ de les plantes C3 d'on provenen. La variabilitat de TEX_{86} derivat dels GDGTs, i les estimacions de temperatura eren generalment petites en escalas mensuals i estacionals, dins el mateix tipus de sòl, però hi har una heterogeneïtat significativa entre els sòls en quant a l'abundància i distribució de GDGTs, que es podria atribuir a diferències en el pH i la humitat del sòl. Els valors de TEX_{86} de la columna d'aigua i sediments van mostrar canvis estacionals significatius que eren similars a les temperatures a la part superior de la columna d'aigua de l'estany. No obstant, en el testimoni de sediment, les temperatures estimades deTEX_{86} estaven esbiaixades cap a valors fred a causa de les contribucions d'arqueus metanogènics, o cap a senyals més càlides a causa dels aports de sòls. Les temperatures estimades de GDGT-MBT/CBT van mostrar una gran heterogeneïtat en els diferents sòls, i junta amb altres evidències ens porten a la conclusió que aquesta proxy de temperatura no és aplicable al llac en escales de temps de dècades. S'ha assajat un nou índex de GDGTs per estimar les temperatures mitjanes anuals, que registra significativament l'aparició de la petita edat de gel des de finals del segle XV en l'àrea d'estudi. Els resultats d'aquesta tesi probablement es poden extrapolar a d'altres conques lacustres similars amb precaució. No obstant, aquest estudi és també un exemple de la necessitat d'avaluar, per cada conca, la fidelitat dels proxies de biomarcadors per reconstruir el clima quantitativament mitjançant els seus sediments lacustres.

Index

Aknowledgements i
Abstract iii
Resum iv
Index v

Chapter 1

Introduction 1

1.1. Holocene climate drivers in the Western Mediterranean 3
1.2. Biomarkers 8
1.2.1. Introduction to biomarkers 8
1.2.2. *n*-Alkyl lipids 8
1.2.3. Glycerol dialkyl glycerol tetraethers (GDGTs) 10
1.2.4. Structures and sources of isoGDGTs 12
1.2.4.1 Structures and sources of brGDGTs 14
1.2.4.2 Proxy development and calibration 14
1.3. Thesis objectives and outline 17
1.4. References 18

Chapter 2

The study site and methods 25

2.1. Study site 27
2.2. Fieldwork sampling 30
2.2.1. Plant leaves 30
2.2.2. Soils 31
2.2.3. Suspended particulate matter (SPM) 32
2.2.4. Sediment trap 33
2.2.5. Sediment cores and surface sediments 34
2.3. Analytical procedures 35
2.3.1. Preparation of glassware 35
2.3.2. Freeze drying and sieving 36
2.3.3. Lipid extraction 36
2.3.4. Column chromatography 37
2.3.5. Sulphur removal 39
2.3.6. Instrumental analysis 39

2.3.6.1. Gas Chromatography Flame Ionization Detector (GC-FID)..... 39
2.3.6.2. Gas chromatography combustion isotope ratio mass spectrometry (GC-IRMS) ……..40
2.3.6.3. High Performance Liquid Chromatography Atmospheric Pressure Chemical Ionization Mass Spectrometry (HPLC-APCI-MS)..... 41
2.3.6.4. Analytical reproducibility and blank controls..... 43
2.3.7. Ancillary measurements..... 43
2.3.7.1. Loss on ignition of soils..... 43
2.3.7.2. pH analysis..... 44
2.4. Instrumental data support 44
2.5. Reference..... 46

Chapter 3

Heterogeneity and seasonality of biomarkers in the plant-soil system of Lake Montcortés catchment..... 49

3.1. Introduction..... 51
3.2. Material and Methods 53
3.2.1. The study area and sample collection..... 53
3.2.2. Sample preparation 54
3.2.3. *n*-Alkane and GDGT analyses 54
3.2.4. Biomarker ratios 55
3.3. Results and discussion 56
3.3.1. Environmental parameters in soils..... 56
3.3.2. *n*-alkanes..... 57
3.3.2.1. Spatial heterogeneity of *n*-alkane signatures in soils..... 57
3.3.2.2. Seasonality of *n*-alkane signatures in soils 58
3.3.2.3. Heterogeneity of *n*-alkane signatures in plants 60
3.3.2.4. Comparison of sediments signatures with those from soils and plants..... 62
3.3.2.5. Implications of *n*-alkane chain length ratios for paleoecology..... 64
3.3.2.6. Compound specific $\delta^{13}C$ of *n*-alkanes in plants and soils..... 65
3.3.3. GDGTs 67
3.3.3.1. Spatial heterogeneity of GDGTs in catchment soils 67
3.3.3.2. Seasonality of GDGT concentrations and indices 70
3.3.3.3. Comparison of GDGT signatures in surface sediments and soils..... 72
3.3.3.4. Implication of brGDGT-derived index..... 73
3.4. Conclusions..... 75
3.5. Reference..... 76

Chapter 4

Seasonality of alkyl lipid signatures in the water column of Lake Montcortés 81

4.1. Introduction 83

4.2. Methods and Materials 85

4.2.1. Study area 85

4.2.2. Sample collection 86

4.2.3. Analytical processes 87

4.2.4. *n*-alkyl lipid analysis in GC-FID 87

4.3. Results and discussion 88

4.3.1. Seasonal and vertical variability in the concentrations of SPM *n*-alkyl lipids in the water column 88

4.3.2. Seasonal and vertical variability in the ratios of *n*-alkyl lipids in SPM 94

4.3.3. Seasonality in the fluxes and ratios of *n*-alkyl lipids of in the sediment trap 96

4.3.4. Compound-specific $\delta^{13}C$ values of *n*-alkanes 99

4.3.5. Transport mechanism of alkyl lipids from higher plants 100

4.4. Conclusion 103

4.5. References 103

Chapter 5

Seasonal variations of glycerol dialkyl glycerol tetraether lipids (GDGTs) contents in the water column of a southern European lake 107

5.1. Introduction 109

5.2. Methods and Material 111

5.2.1. Study area 111

5.2.2. Sampling 112

5.2.3. Extract clean up 112

5.2.4. Instrumental analysis 113

5.3. Results and discussion 114

5.3.1. Environmental conditions 114

5.3.2. Seasonal variability in the concentrations and fluxes of GDGT classes in the water column and the sediment trap 115

5.3.3. Seasonal variability in GDGT distributions in the water column and sediment trap 119

5.3.4. TEX_{86} values and estimated temperatures in the water column and sediment trap 121

5.3.5. MBT/CBT index as temperature proxy in the water column and sediment trap 126

5.4. Conclusions 128

5.5. Reference 129

Chapter 6

Biomarker proxies in two high-resolution records in a Pyrenean lake spanning the last 110 years and the Spörer Minimum 135

6.1. Introduction 137

6.2. Materials and methods 139

6.2.1. Study area 139

6.2.2. Sediment coring and slicing 140

6.2.3. Sample analysis 140

6.3. Results and discussion 141

6.3.1. Climate records from previous study in Montcortes or nearby lakes during XX century and XV-XVII century 141

6.3.2. GDGTs 142

6.3.2.1. GDGT abundance and indices changed in the sediment core (the XX century and the XV-XVII century) 142

6.3.2.2. Validation of isoGDGT proxy with instrumental air temperature record 144

6.3.2.3. Validation of brGDGT estimates based on instrumental temperatures 146

6.3.2.4. Application of validated proxies in Montcortés core during XV-XVII century (covering the Spörer Minimum) 148

6.3.3. *n*-alkanes 149

6.3.3.1. *n*-alkane abundance and indices changed in the sediment core (the XX century and the XV-XVII century) 149

6.3.3.2. Compound specific $\delta^{13}C$ values changed in the sediment core (the XX century and the XV-XVII century) 151

6.3.3.3. Climatic implication of *n*-alkanes in the sediment core 151

6.3.3.4. Other implication of *n*-alkane proxy in the sediment core 152

6.4. Conclusion 154

6.5. References 154

Chapter 7

Conclusions and future work 159

List of Figures and Tables 163

Abbreviations 167

Appendix 168

Chapter 1
Introduction

1.1. Holocene climate drivers in the Western Mediterranean

Climate and weather are an important part of the daily experience of human beings and is essential for their health, food production and well-being (IPCC, Working Group I: Assessment Report, 2001). Precipitation and temperature are essential variables of climate change, which are also major drivers of terrestrial ecosystem processes (Gleixner & Mügler, 2007). According to the Intergovernmental Panel on Climate Change (IPCC), the globally averaged surface temperature exhibits substantial decadal and interannual variability. However, it is likely that more than half of the observed increase in global average surface temperature from 1951 to 2010 was caused by the anthropogenic increase in greenhouse gas concentrations. However, in this period of time, climate changes are induced both by the internal variability within the climate system and external factors that are either natural or anthropogenic (IPCC, 2014). To understand climatic drivers and eventually predict the human influence on climate in the future, we need to understand the climatic system at present and in the past, and which are the key processes that drive climate changes on Earth at different time-scales. However, deciphering the various drivers of climate is a major challenge. According to Ruddiman (1994), three fundamental kinds of natural climate forcing and anthropogenic forcing exist in our world: tectonic processes which operate very slowly over millions of years, Earth-orbital changes which take place over tens to hundreds of thousands of years and changes in the strength of the Sun that occurs over periods of decades to billions of years. These and arguably other processes are the driving forces that shape Earth's climate variability through different timescales, from the interannual to geological, and have given rise to the current climate on Earth.

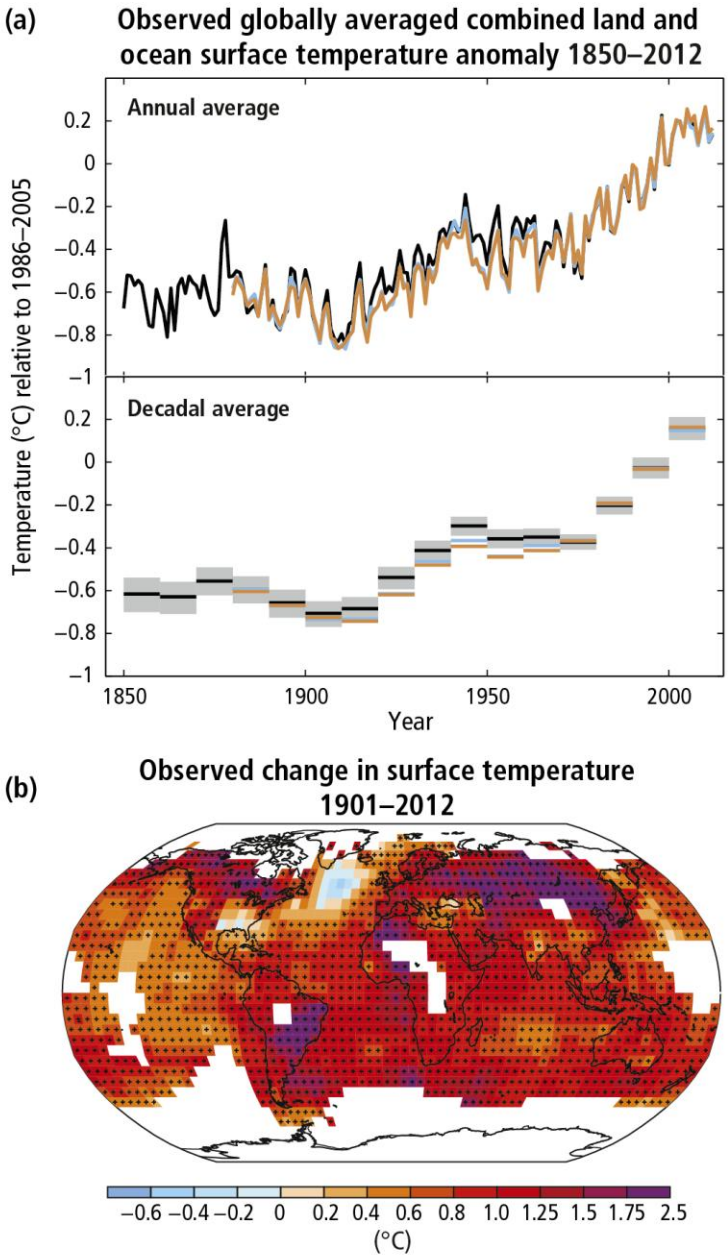

Figure 1-1 (a) Observed changes in global average surface temperature. The three surface temperature datasets are originated from Hadley Centre/Climate Research Unit of the University of East Anglia, UK (black line), US National Oceanic and Atmospheric Administration (orange line) and Goddard Institute for Space studies, NASA (blue line). Top panel: annual mean values, bottom panel: decadal mean values including the estimate of uncertainty for HadCRUT4. (b) Changes in annual surface temperatures between 1901 and 2012 derived from data maintained by US National Oceanic and Atmospheric Administration. (Source: IPCC AR5, 2014)

To understand the climate system requires the compilation of time series of data that span all the relevant time scales. This thesis is concerned with the study of the last few centuries (i.e. the late Holocene), and in this sense, the generation of reliable time series

of instrumental records of climate parameters on a global scale began in 1850 (Brohan et al., 2006). This is not much earlier that the onset of the current global warming trend ca. 1880 (Fig. 1-1). Beyond this time period, to evaluate climate changes , one must resort to the use of environmental proxy variables, which in the parlance of paleoenvironmental reconstruction field, are measurable descriptors, standing in for desired but unobservable variables (target parameters). A wide range of proxies can be measured to derive time series records in ice cores, tree rings, or sediments among many other natural climate archives. Proxies frequently rely on the measurement of some type of fossil remain (e.g. pollen or foraminifera) or chemical measurement such as the analysis of stable isotopes of inorganic compounds or molecular organic geochemical proxies. The latter are the focus of this thesis, and are based on the application of organic molecular geochemistry techniques to characterize and quantify the molecular components of organic matter (Philip A Meyers & Lallier-vergès, 1999). All proxies have in common, however, the utilization of a transforming algorithm to extract from the measurement information on a climatic relevant parameter, which is commonly referred to as the calibration of the proxy (Wefer et al., 1999).

Even though the Holocene climate (11,500 cal yr B. P. to the present) has a very close relationship with us, as it is the time when humans have expanded and thrived throughout the planet, there is still a poor understanding of the ranges of climatic variability during this geological period (Mayewski et al., 2004). The Holocene is considered to have developed in three phases or chronozones, which started about 116000, 9000 and 5000-6000 years BP to pre-industrial times. These phases are also called “Preboreal and Poreal”, “Hypsithermal” and “Subboreal and Subatlantic”, respectively, and they correspond to times with different degrees of orbital forcing (Wanner et al., 2008). The Milankovitch theory that the insolation variations on the Earth are responsible for large climatic changes proposed an idea that the orbital forcing is the only one that can be calculated precisely (Milankovich, 1941; Berger, 1978; Laskar et al., 2004). For paleoclimate studies, the most widely used orbital solution in nowadays is either the averaged solution (Laskar et al., 1993) or the most numerical solution (Laskar et al., 2004). In addition, a number of

paleoclimatic records provide some evidence for a link between climate changes and solar activity changes (Bond et al., 2001; Neff et al., 2001). However, a clear link between solar activity and solar forcing based on physical processes is still missing (Wanner et al., 2008). Nevertheless, cosmogenic radionuclides that are generated due to the effect of Sun radiation on the atmosphere, such as ^{10}Be and ^{14}C, have provide a mean to establish a link between the solar variability and climate variability over at least the past 10,000 years (Vonmoos et al., 2006).

Despite significant progress over the last two decades, we still do not completely understand the detailed interactions between regional climate forcing, internal variability, system feedbacks, and the responses of surface climate, land cover, biosphere and hydrosphere that determine local climate variations (PAGES, 2009). In the Western Mediterranean area, the locations of the Azores High and the Icelandic Low pressure centers determine the latitudinal position and intensity of the North Atlantic westerlies and the storm tracks, which largely govern rainfall in the region (Greatbatch, 2000; Marshall et al., 2001). This atmospheric pressure system is known as the North Atlantic Oscillation (NAO) (Fig. 1-2). A change from persistent autumn NAO negative mode during the 19th century towards a dominant positive autumn NAO index during the 20th could be responsible for lower total annual precipitation in NE Iberian Peninsula, which was recorded by Lake Montcortés sediments (Corella et al., 2014; Luterbacher et al., 2002).

In general, the climate of western Mediterranean region is dominated by planetary scale forcing. However, the situation becomes complex under the synergetic effects of global patterns and regional features such as orography and land-use distribution, which may contribute to inter variability to a large extent beyond the global climate trend (Oliver & Morecroft, 2014). Moreover, the recent variations on different spatial-temporal scales are particularly important in modern and future climate change. Therefore, the spatial complexity and heterogeneity require more study using continental archives on a regional

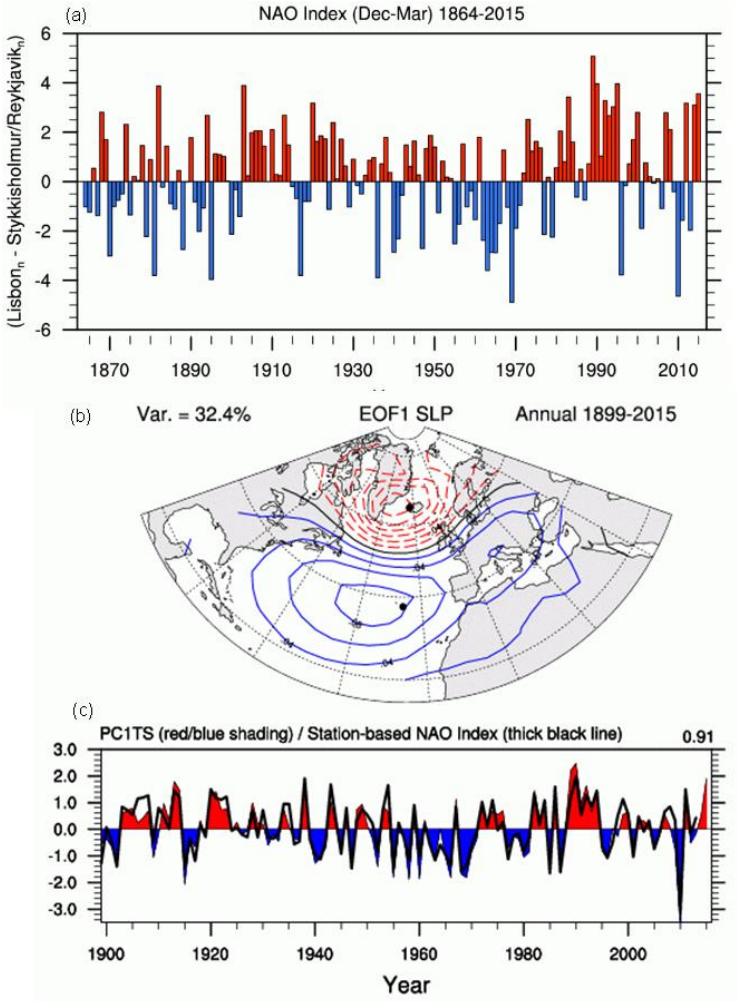

Figure 1-2 (a) Winter (December-March) index of the NAO based on the difference of normalized sea level pressure (SLP) between Lisbon, Portugal and Stykkisholmur/Reykjavik, Iceland since 1864. The SLP values at each station were normalized by removing the long-term mean and by dividing by the long-term standard deviation. Both the long-term means and standard deviations are based on the period 1864-1983. Normalization is used to avoid the series being dominated by the greater variability of the northern station. (b) The principal component (PC) time series of the leading EOF of annual SLP anomalies over the Atlantic sector (20-80 °N, 90°W-40°E) serves as an alternative index (see Hurrell et al. (2003) and Hurrell et al. (1995)). (c) The annual PC timeseries is shown below in color, and the station based index is given by the thick black line. The correlation between the two is 0.91 over the period 1899-2014. The black dots on the EOF panel show the location of the stations used in the annual station-based index (Phillips, 2016).

scale. Among continental archives, lakes are widely distributed and studied to provide a number of proxies (such as phytoplankton composition, inorganic element) for high-temporal (seasonally/annually to decadal scale) resolution paleoenvironmental reconstruction (Castañeda & Schouten, 2011). However, each proxy has its own limitation and bias. Thus, the combination of independent proxies have been performed to interpret

paleoclimate in recent years. Especially the molecular composition of organic matter (biomarker) has been used for paleoenvironment reconstruction, which we will discuss in the following section.

1.2. Biomarkers

1.2.1. Introduction to biomarkers

Biomarkers are organic molecules that are preserved in geologic materials, such as marine or lacustrine sediments but also soils, and fossil fuels. Besides their role as input markers of specific organisms, they also provide information of past environmental conditions at the time of synthesis in deposits spanning from tens to millions of years (Meyers, Edwards, & Eadie, 1980; Otto & Simpson, 2005). One basic conditions that a molecule must meet also to be considered a biomarker is that they must be sufficiently resilient to chemical and biological degradation to be preserved in the fossil record (e.g. Huang et al., 2004; Sachse et al., 2012). A number of available biomarkers have been discovered over the last decades due the improvement of analytical techniques in the separation, detection and charactering of organic compounds (Castañeda et al., 2011 and literature therein). In the following sections we concentrate on two families of biomarkers, the *n*-alkyl lipids and the glycerol dialkyl glycerol tetraethers (GDGTs).

1.2.2. *n*-Alkyl lipids

This class of compounds comprises the straight-chain *n*-alkanes, *n*-alcohols and *n*-alkanoic acids. They are hydrocarbons produced by many organisms, and their dominant chain lengths (i.e. number of carbon atoms in the chain), carbon number distributions and isotopic compositions vary depending on the source organism (Castañeda et al., 2011). Odd-over-even long-chain *n*-alkanes (C_{27}-C_{35}) and even-over-odd long-chain *n*-alkanoic acids (C_{26}-C_{34}) are major components of the epicuticular waxes of terrestrial vascular plants (Eglinton and Hamilton, 1967), and are relatively resistant to biodegradation during deposition in soils and sediments (Ho & Meyers, 1994). In contrast, shorter-chain *n*-alkanes (C_{17}-C_{21}) are preferentially produced

by aquatic algae/cyanobacteria (Giger et al., 1980; Cranwell et al., 1987), while the mid length-chain *n*-alkanes (C_{23}-C_{25}) are a dominant component of submerged aquatic macrophytes (Ficken et al., 2000). In this thesis, we focus only on mid and long chain *n*-alkanes.

A number of ratios based on *n*-alkyl lipids of distinct chain lengths have been used to examine the relative inputs of these components from their various putative sources, or even environmental conditions in the localities of the source organisms. For instance, the average chain length (ACL; *eq.1.1*) of plant leaf waxes are argued to vary with aridity, temperature, rainfall and vegetation changes. Thus, a relationship between ACL and temperature was found in arid environments (Bush & Mcinerney, 2015). In contrast, *n*-alkanes in herbaceous species are mainly dominated by C_{31} or C_{33} *n*-alkane, resulting in higher ACL values than in woody plants (Rommerskirchen et al., 2006). In addition, a change in vegetation types seems to be reflected in ACL values, as terrestrial higher plants synthesize longer *n*-alkanes than aquatic macrophytes (Ficken et al., 2000).

$$ACL = (25\times C_{25}+27\times C_{27}+29\times C_{29}+31\times C_{31}+33\times C_{33})/(C_{25}+ C_{27}+C_{29}+C_{31}+C_{33}) \quad (eq.1.1)$$

The carbon preference index (CPI), introduced by Bray & Evans (1961) (*eq.1.2*) of *n*-alkanes is used to examine the odd-over-even carbon number predominance in these compounds distributions, which allows to distinguish contributions of terrestrial plants from bacterial or petroleum sources (Clark & Blumer, 1967). Thus, the CPI index of *n*-alkanes from natural sources, such as plants, usually shows high values (>>1.0) in immature sediments. However *n*-alkanes in fossil fuels products have no odd over even carbon number preference and consequently the CPI index is relatively low, with values around 1.0, which in recent sediments are attributed to inputs of petroleum related products, and interpreted as evidence of pollution (Bray & Evans, 1961; Killops & Killops, 2005).

$$CPI=0.5\times[(C_{25}+C_{27}+C_{29}+C_{31}+C_{33})/(C_{24}+C_{26}+C_{28}+C_{30}+C_{32})+(C_{25}+C_{27}+C_{29}+C_{31}+C_{33})/(C_{26}+C_{28}+C_{30}+C_{32}+C_{34})] \quad (eq.1.2)$$

The P_{aq} index (*eq.1.3*) was proposed to differentiate aquatic inputs of *n*-alkanes in freshwater body from those of terrestrial vegetation, based on the observations that mid

length-chain *n*-alkanes are more abundant in macrophyte plates than in terrestrial higher plants (Ficken et al., 2000). If P_{aq} values are higher than 0.4, more contributions are assumed from submerged/floating macrophytes to the total *n*-alkane pool, and if the P_{aq} values are lower than 0.1, only a little contribution from the freshwater body is expected. If the values are between 0.1-0.4, more contributions are considered from emergent macrophytes.

$$P_{aq}=(C_{23}+C_{25})/(C_{23}+C_{25}+C_{29}+C_{31}) \quad (eq.1.3)$$

Compound specific isotopic analyses of leaf waxes are also a valuable mean to reveal information about the original sources of *n*-alkyl lipids. Stable carbon isotopic composition ($\delta^{13}C$) and long-chain *n*-alkyl molecules, especially C_{27}, C_{29}, C_{31} *n*-alkanes and C_{28}, C_{30} alkanoic acids are widely used as potentially powerful biomarkers in hot springs, soils and lake sediments for estimation past vegetation changes (Chikaraishi et al., 2004; Wang et al., 2015; Zhang et al., 2004). The $\delta^{13}C$ signatures are not much influenced by diagenesis, differential preservation of compound classes, and changes in the sources of organic matter that otherwise complicate interpretations of bulk $\delta^{13}C$ values (Pancost & Boot, 2004). Vegetation that uses one of three photosynthetic pathways (C3, C4 and CAM) can be identified from their *n*-alkane $\delta^{13}C$ values (Freeman et al., 1990). C3 plants have lower $\delta^{13}C$ values (e.g. trees, shrubs, temperate grasses; mean $\delta^{13}C$ = -27 ‰) than those using the C4 pathway (most tropical grasses; mean $\delta^{13}C$ = -13 ‰). CAM plants are uncommon except in arid regions and their $\delta^{13}C$ values are intermediate between C3 and C4 plants. In C3 and C4 plants, variations of several per mil in $\delta^{13}C$ may also be controlled by environmental factors such as water availability and light (Ehleringer et al., 1991). Some studies have also suggested that $\delta^{13}C$ signatures can be correlated with environmental parameters such as mean annual precipitation and aridity (Miller, 2001; Van de Water et al., 2002; Vogts et al., 2012).

1.2.3. Glycerol dialkyl glycerol tetraethers (GDGTs)

GDGTs were thought for decades to be unusual membrane lipids synthesized exclusively by extremophilic Archaea (reviewed by DeRosa & Gambacota, 1988).

However, since hopanoids and branched isoprenoids were first discovered in sediments by organic geochemists (Ourisson & Albrecht, 1992) and the discovery of 'non-extremophilic' Arhaea (DeLong, 1992), GDGTs, including crenarchaeol and GDGTs with branched carbon skeletons have been found to occur ubiquitously in a wide range of environments, such as soils (Weijers et al., 2006; 2007), peatlands (Coffinet et al., 2015; Weijers et al., 2006), marine sediments (Ge et al., 2014; Kim et al., 2008), water column (Loomis et al., 2014; Schouten et al., 2012; Blaga et al., 2009; Turich et al., 2007) and hot springs (Schouten et al., 2007; Zhang et al., 2013).

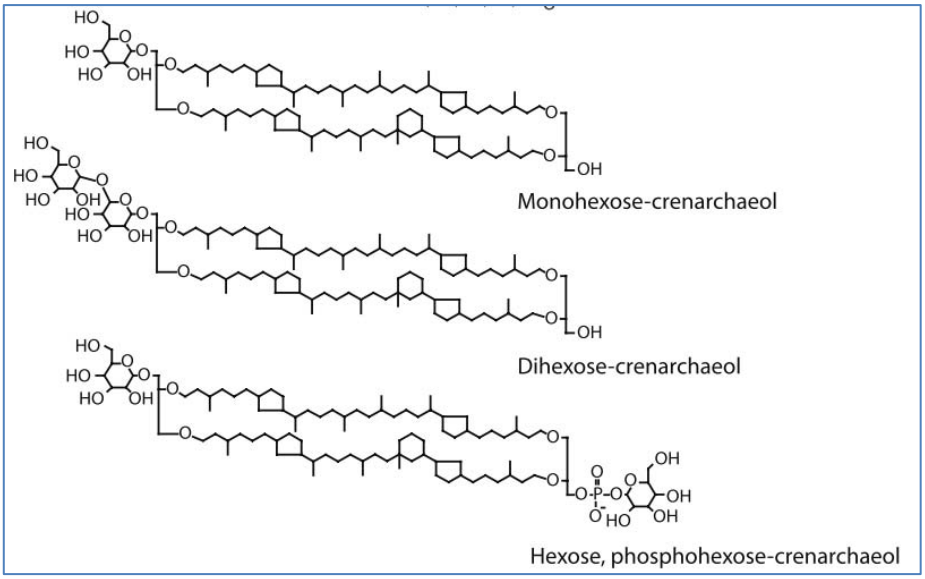

Figure 1-3 Structures of crenarchaeol-based IPLs (Lengger et al., 2012)

GDGTs can be detected as intact polar lipids (IPLs) or core lipids (CLs) in the environment. IPLs are the predominant form of lipids in the living cells (Pitcher et al., 2011; Wörmer et al., 2013) and correspond to CLs with polar head groups attached to glycerol moieties (Fig.1-3). The polar head group of the IPLs can be rapidly decreased after cell lysis (White et al., 1996), leading to the persistence of CLs in the environment. Thus, in this thesis, we only focus on core GDGTs, which could be classified into two types: isoprenoid GDGTs (isoGDGTs) and branched GDGTs (brGDGTs).

1.2.4. Structures and sources of isoGDGTs

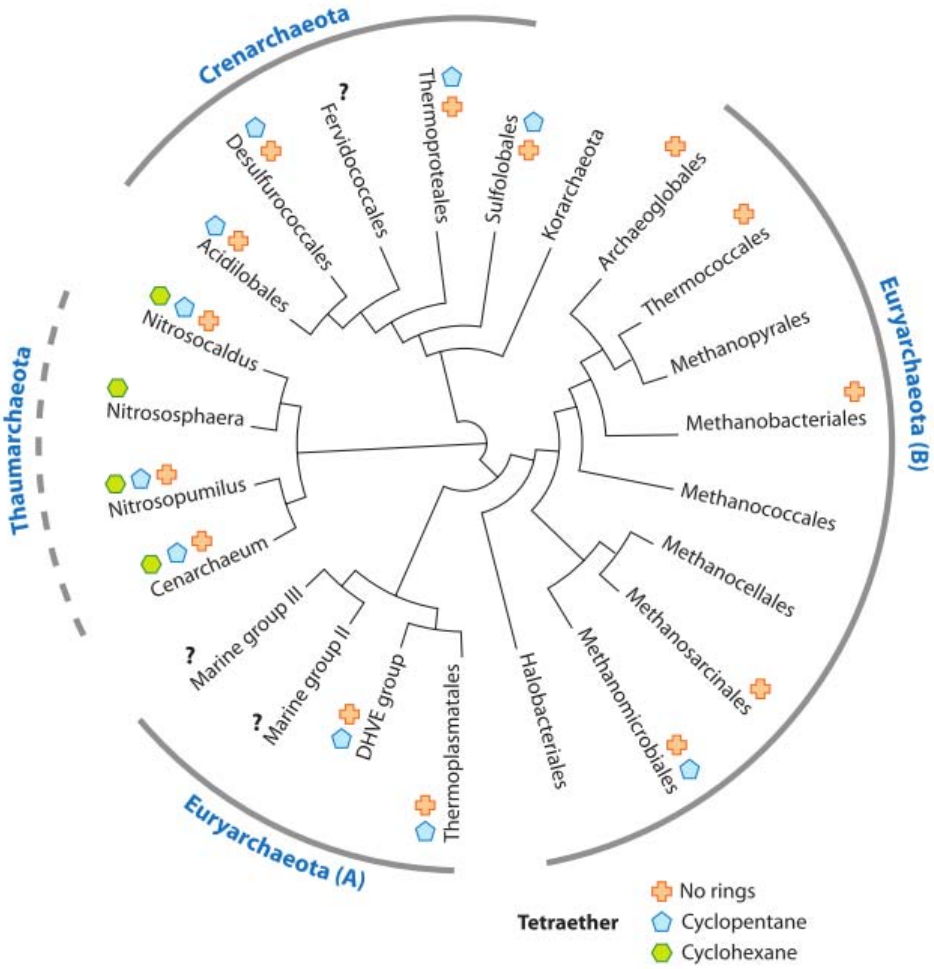

Figure 1-4 Phylogenetic tree showing the topology of relationships between orders of Archaea based on 16S rRNA sequences. The major kingdoms of Archaea are the Korarchaeota, Crenarchaeota, Thaumarchaeota, and Euryarchaeota.Within the Euryarchaeota, the euryarchaeal group comprising Thermoplasmatales and their relatives (A), as well as all Thaumarchaeota and Crenarchaeota studied to date, are known for synthesizing GDGT(glycerol dialkyl glycerol tetraether) lipids containing cyclopentane rings. Only the Thaumarchaeota are known to make crenarchaeol. Abbreviation: DHVE, deep-sea hydrothermal vent Euryarchaeota (Pearson and Ingalls, 2013).

Many types of membrane adaptations, including cyclization as well other structural variations, help Archaea (Fig. 1-4) to occupy Earth's diverse range of habitats (Koga & Morii, 2005). The isoGDGTs consist of two head to head C_{40} isoprenoid chains with a varying number of cyclopentane and cyclohexane rings, connected by ether bonds to two terminal glycerol groups (Koga & Morii, 2005; Tierney, 2012). The structures of the main isoGDGTs are shown (Fig.1-5), differing by the number of cyclopentane moieties in their

alkyl chains. GDGT-0 without a cyclopentane, also called as caldarcheol, is the most common isoGDGT that was detected in all the archaeal phyla (Turich et al., 2007). IsoGDGTs containing 1 to 4 cyclopentane rings (abbreviated as GDGTs-0, 1, 2, 3, 4 and 4') are produced by Thaumarchaeota, Crenarchaeota and some Euryarchaeota (Pearson & Ingalls, 2013). While GDGT-4 containing a cyclohexane group, as called crenarchaeol, has been found in all cultures of ammonia-oxidizing Thaumarchaeota and thus thought to be originated in this phylum (Sinninghe et al., 2012), even though a recent study suggested that it could also be produced by Marine Group II Euryarchaeota (Lincoln et al., 2014). Moreover, Thaumarchaeota also produce a small amount of crenarchaeol regioisomer at high temperature, as GDGT-4', which has been found in significant amounts in natural environment (Sinninghe Damsté et al., 2002; Schouten et al., 2002).

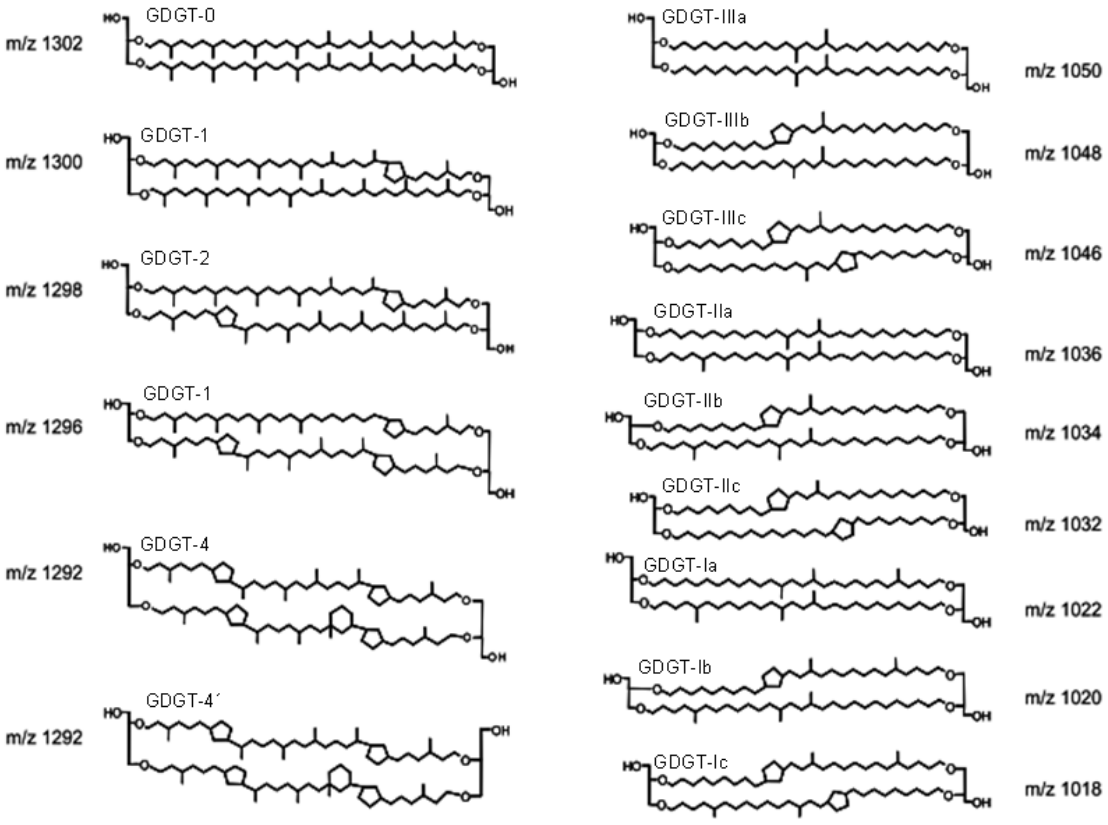

Figure 1-5 Structures of isoprenoid GDGTs and branched GDGTs (modified from Weijers et al., (2011)

1.2.4.1 Structures and sources of brGDGTs

In contrast to isoGDGTs, the brGDGTs have branched C_{30} alkyl chains containing 4-6 methyl groups instead of the C_{40} isoprenoid chains (Tierney, 2012) (Fig. 1-5). The group of bacteria that synthesize branched GDGTs has not been identified, except that Sinninghe Damsté et al. (2011) found two species of Acidobacteria producing one type of brGDGT (brGDGT-I). These GDGTs are widely observed in soils, peats, lakes and marginal environments, suggesting terrestrial origin (Niemann et al., 2012; Peterse et al., 2010; Weijers et al., 2007). In addition, in situ production of branched GDGTs has been found in lacustrine sediments and coastal marine sites (De Jonge et al., 2014; Sun et al., 2011; Tierney & Russell, 2009; Zhu et al., 2011).

1.2.4.2 Proxy development and calibration

TEX_{86}

For isoGDGTs, the most important is that their structural dependence on temperature, the number of rings had been observed to increase as temperature increases (De Rosa et al., 1980). Thus, TEX_{86}, a palaeotemperature proxy, based on the distinct distribution of isoprenoidal GDGTs in the extent of cyclic moieties, has been calibrated and applied for core-top and marine sediments (Huguet et al., 2007; Kim et al., 2008; Rueda et al., 2009; Schouten et al., 2002), lake sediments (Blaga et al., 2009; Naeher et al., 2014; L. Powers et al., 2010). In lakes, most of studies suggest that TEX_{86} should be applied only for those with sufficient production of GDGTs by aquatic Crenarchaeota relative to isoGDGTs derived from soil in the watershed or other sources like methanotrophs (Bechtel et al., 2010). Additionally, the TEX_{86} has been applied to reconstruct temperatures at different time scales, from seasonal to multimillennial (Blaga et al., 2011; Huguet et al., 2007; Sinninghe Damsté et al., 2012). The index is defined as (Schouten et al., 2002):

$$TEX_{86} = \frac{[GDGT-2]+[GDGT-3]+[GDGT-4\prime]}{[GDGT-1]+[GDGT-2]+[GDGT-3]+[GDGT-4\prime]} \qquad \textit{(eq. 1.4)}$$

The TEX_{86} index was first proposed as paleotemperature for surface sea temperature (SST) reconstruction (SST= (TEX_{86} – 0.28)/0.015, R^2 = 0.92) based on 43 surface

sediment samples (Schouten et al., 2002). Later, Kim et al. (2008) studied upper mixed layer of water column to suggest that TEX_{86} index is highly correlated to SST in the temperature range 5-30 °C (SST = 56.2 × TEX_{86} -10.8, R^2 = 0.94). Powers et al. (2005) selected a set of lakes to measure GDGTs and made a conclusion that only large lakes (15 out of 22 lakes) are suitable for TEX_{86} application because terrestrially-derived GDGTs may bias the TEX_{86} index in small-sized lakes. Thus, the reconstruction of mean annual lake surface temperature (LST) was considered to be suitable when sufficient GDGT signals exist (LST= (TEX_{86} -0.21)/0.019, R^2 = 0.94). In addition, another study from 47 European lakes confirmed that TEX_{86} could be only applicable in a small set of lakes (9 out 47 lakes) because isoGDGTs produced by methanogenic Archaea would result in a large bias of the reconstructed temperatures besides large terrestrial inputs. Thus, a ratio of GDGT-0/GDGT-4 was proposed to distinguish whether TEX_{86} is applicable or not based on the assumption that GDGT-4 is only derived from Thaumarchaeota (Blaga et al., 2009). If the ratio is not >2, the Thaumarchaeota could be considered as the primary producer of isoGDGTs, otherwise, methanogenic-derived isoGDGTs are predominant. Moreover, in the lacustrine systems, the TEX_{86} was assumed to reflect mean annual lake surface temperature (Powers et al., 2004), however slightly better correlation of TEX_{86} with winter than annual surface lake temperatures (Powers et al., 2005). Furthermore, a study from Lake Kivu in Africa revealed that crenarchaeol phylotypes were distributed throughout the epipelagic waters (0-100 m depth), which was consistent with vertical distribution of both nitrite and nitrate maxima in the water column (Llirós et al., 2010). Auguet et al. (2012) furtherly unveiled that ammonium oxidation zones in the water column of Lake Redon from central Pyrenees changing vertically with seasons.

MBT/CBT

According to Weijers et al.(2007), the relative extent of methyl branches (methylation index of branched tetraethers-MBT) is correlated with the mean annual air temperature (MAT) and soil pH, while the relative extent of cyclopentane moieties (cyclisation ratio of branched tetraethers-CBT) is only related to the soil pH. Thus, a combination of MBT and CBT index can give information for MAT.

MBT = (Ia+Ib+Ic)/(Ia+Ib+Ic+IIa+IIb+IIc+IIIa+IIIb+IIIc) (Weijers et al., 2007) *(eq.1.5)*

CBT = -Log((Ib+IIb)/(Ia+IIa)) = 3.33-0.38×pH (n=114; R^2=0.70) (Weijers et al., 2007) *(eq.1.6)*

The calibration of temperature was established based on Weijers et al.(2007):

MAT=*0.122+0.187×CBT+0.02×MAT (R^2=0.77)* *(eq.1.7)*

Even though the correlation between MBT, CBT and MAT is statistically significant, the distribution of samples is scattered to obtain an accurate reconstructed temperature with a root mean square error (RMSE) of 4.8 °C. Later, more brGDGT calibrations were developed, e.g. Peterse et al. (2012) modified a simpler equation MBT'

MBT' = (Ia+Ib+Ic)/(Ia+Ib+Ic+IIa+IIb+IIc+IIIa) *(eq. 1.8)*

MAT = 0.81-5.67×CBT+31.0×MBT' *(R^2=0.59)* (Peterse et al., 2012) *(eq. 1.9)*

This calibration equation based on soil dataset decreased the correlation coefficient to R^2=0.59 but with a similar RMSE (5 °C). The high scatter could be due to inherent heterogeneity of global soils, offset between MAT and mean annual soil temperature as well as soil parameter variations (Peterse et al., 2012; Weijers et al., 2007). In lacustrine system, a number of specific calibrations were developed, e.g. Zink et al. (2010) found relationships between MBT vs. MAT (*R^2=0.74*) CBT vs. MAT *(R^2=0.72)* and closer correlation between CBT vs. MST (mean summer temperature, *R^2=0.82*) in New Zealand freshwater lakes. Tierney et al. (2010) has improved the RMSE (3.0 °C) and proposed another formula as:

MAT=11.84+32.54×MBT-9.32×CBT (R^2=0.89) *(eq.1.10)*

Moreover, Loomis et al. (2012) developed a new brGDGT calibration equation based on fractional abundance of GDGT-III, II, IIc and Ib to obtain a smaller RMSE of 1.9 °C. Furthermore, the progress of advanced analytical methods brings more details of brGDGT proxies, e.g. the good separation of 5-methyl and 6-methyl brGDGTs, improving the calibration of MBT/CBT indices (De Jonge et al., 2014; Yang et al., 2015). Clearly, the applicability of the MBT/CBT proxies needs to be accessed for individual site depending

on better separation.

1.3. Thesis objectives and outline

The aim of the project is to validate the use of biomarker proxies to obtain high resolution (i.e. multidecadal) records of temperature and precipitation in the Iberian Peninsula for the late Holocene. The ultimate aim of the project is to establish links between decadal Iberian continental climate variations and North Atlantic variability, which may have caused environmental changes similar to current developments in the region. In order to achieve the main aim, the project has focused on the monitoring of modern sedimentation processes and of the putative sources of the targeted biomarkers in lake Montcortés, in NW Spain, and the study of laminated sedimentary sequences recovered from the lake.

The specific objectives addressed are:

- To identify the likely sources of terrigenous biomarkers in the sediment in the catchement of lake Montcortés and their spatial and temporal (monthly/seasonal) variability (Chapter 3).
- To determine the temporal (i.e. seasonal) and spatial (i.e. with depth) variability in the composition of suspended and settling particulate matter in the water column (Chapters 4 and 5).
- To relate the composition of biomarkers in the lake's particulate matter and sediments, and their ratios and carbon isotopic composition, to environmental parameters, such as temperature, precipitation and wind speed (Chapters 4-6).
- To appraise the fidelity of multidecadal proxy biomarker records to reconstruct quantitative climatic variability by contrasting them against instrumental meteorological records spanning 110 years across the XX to XIX centuries (chapter 6)
- To apply the biomarker proxies to establish if modern patterns of climate variability were in operation during the Spörer minimum, in the 15th to 17th centuries (Chapter 6).

1.4. References

Auguet, J.-C., Triadó-Margarit, X., Nomokonova, N., Camarero, L., & Casamayor, E. O. (2012). Vertical segregation and phylogenetic characterization of ammonia-oxidizing Archaea in a deep oligotrophic lake. *International Society for Microbial Ecology*, *6*(9), 1786–1797. doi:10.1038/ismej.2012.33

Bechtel, A., Smittenberg, R. H., Bernasconi, S. M., & Schubert, C. J. (2010). Distribution of branched and isoprenoid tetraether lipids in an oligotrophic and a eutrophic Swiss lake: Insights into sources and GDGT-based proxies. *Organic Geochemistry*, *41*(8), 822–832. doi:10.1016/j.orggeochem.2010.04.022

Berger, A. L. (1978). Long-term variations of caloric insolation resulting from the Earth´s orbital Elements. *Quaternary Research*, *9*, 139–167.

Blaga, C. I., Reichart, G. J., Vissers, E. W., Lotter, A. F., Anselmetti, F. S., & Sinninghe Damsté, J. S. (2011). Seasonal changes in glycerol dialkyl glycerol tetraether concentrations and fluxes in a perialpine lake: Implications for the use of the TEX86 and BIT proxies. *Geochimica et Cosmochimica Acta*, *75*(21), 6416–6428. doi:10.1016/j.gca.2011.08.016

Blaga, C. I., Reichart, G.-J., Heiri, O., & Sinninghe Damsté, J. S. (2009). Tetraether membrane lipid distributions in water-column particulate matter and sediments: a study of 47 European lakes along a north–south transect. *Journal of Paleolimnology*, *41*(3), 523–540. doi:10.1007/s10933-008-9242-2

Bond, G., Kromer, B., Beer, J., Muscheler, R., Evans, M. N., Showers, W., … Bonani, G. (2001). Persistent solar influence on North Atlantic climate during the Holocene. *Science (New York, N.Y.)*, *294*(5549), 2130–2136. doi:10.1126/science.1065680

Bray, E. ., & Evans, E. . (1961). Distribution of *n*-paraffins as a clue to recognition of source beds. *Geochimica et Cosmochimica Acta*, *22*(1), 2–15. doi:10.1016/0016-7037(61)90069-2

Brohan, P., Kennedy, J. J., Harris, I., Tett, S. F. B., & Jones, P. D. (2006). Uncertainty estimates in regional and global observed temperature changes: A new data set from 1850. *Journal of Geophysical Research Atmospheres*, *111*(12), 1–21. doi:10.1029/2005JD006548

Bush, R. T., & Mcinerney, F. a. (2015). Influence of temperature and C4 abundance on *n*-alkane chain length distributions across the central USA. *Organic Geochemistry*, *79*, 65–73. doi:10.1016/j.orggeochem.2014.12.003

Castañeda, I. S., & Schouten, S. (2011). A review of molecular organic proxies for examining modern and ancient lacustrine environments. *Quaternary Science Reviews*, *30*(21-22), 2851–2891. doi:10.1016/j.quascirev.2011.07.009

Chikaraishi, Y., Naraoka, H., & Poulson, S. R. (2004). Hydrogen and carbon isotopic fractionations of lipid biosynthesis among terrestrial (C3, C4 and CAM) and aquatic plants. *Phytochemistry*, *65*(10), 1369–81. doi:10.1016/j.phytochem.2004.03.036

Clark, R. C., & Blumer, M. (1967). Distribution of *n*-paraffins in marine organisms and sediment. *Limnology and Oceanography*, *12*(1), 79–87. doi:10.4319/lo.1967.12.1.0079

Coffinet, S., Huguet, A., Williamson, D., Bergonzini, L., Anquetil, C., Majule, A., & Derenne, S. (2015). Occurrence and distribution of glycerol dialkanol diethers and glycerol dialkyl glycerol tetraethers in a peat core from SW Tanzania. *Organic Geochemistry*, *83-84*, 170–177. doi:10.1016/j.orggeochem.2015.03.013

Corella, J. P., Benito, G., Rodriguez-Lloveras, X., Brauer, a., & Valero-Garcés, B. L. (2014). Annually-resolved lake record of extreme hydro-meteorological events since AD 1347 in NE Iberian Peninsula. *Quaternary Science Reviews*, *93*, 77–90. doi:10.1016/j.quascirev.2014.03.020

De Jonge, C., Stadnitskaia, A., Hopmans, E. C., Cherkashov, G., Fedotov, A., & Sinninghe Damste, J. S. (2014). In situ produced branched glycerol dialkyl glycerol tetraethers in suspended particulate matter from the Yenisei River, Eastern Siberia. *Geochimica et Cosmochimica Acta*, *125*, 476–491. doi:10.1016/j.gca.2013.10.031

De Rosa, M., Esposito, E., Gambacorta, A., Nicolaus, B., & Bu'Lock, J. D. (1980). Effects of temperature on ether lipid composition of Caldariella acidophila. *Phytochemistry*, *19*(5), 827–831. doi:10.1016/0031-9422(80)85120-X

Ehleringer, J. R., Sage, R. F., Flanagan, L. B., & Pearcy, R. W. (1991). Climate change and the evolution of C4 photosynthesis. *Trends in Ecology & Evolution*, *6*(3), 95–9. doi:10.1016/0169-5347(91)90183-X

Ficken, K. J., Li, B., Swain, D. L., & Eglinton, G. (2000). An *n*-alkane proxy for the sedimentary input of submerged/floating freshwater aquatic macrophytes. *Organic Geochemistry*, *31*, 745–749.

Freeman, K. H., Hayes, J. M., Trendel, J.-M., & Albrecht, P. (1990). Evidence from carbon isotope measurements for diverse origins of sedimentary hydrocarbons. *Nature*, *343*, 254–256.

Ge, H., Zhang, C. L., Li, J., Versteegh, G. J. M., Hu, B., Zhao, J., & Dong, L. (2014). Tetraether lipids from the southern Yellow Sea of China: Implications for the variability of East Asia Winter Monsoon in the Holocene. *Organic Geochemistry*, *70*, 10–19. doi:10.1016/j.orggeochem.2014.02.011

Gleixner, G., & Mügler, I. (2007). Compound-Specific Hydrogen Isotope Ratios of Biomarkers: Tracing Climatic Changes in the Past. *Terrestrial Ecology*, *1*, 249–265. doi:10.1016/S1936-7961(07)01016-0

Greatbatch, R. J. (2000). The North Atlantic Oscillation. *Stochastic Environmental Research and Risk Assessment*, *14*(4), 0213–0242. doi:10.1007/s004770000047

Ho, E. S., & Meyers, P. A. (1994). Variability of early diagenesis in lake sediments: Evidence from the sedimentary geolipid record in an isolated tarn. *Chemical Geology*, *112*(3-4), 309–324. doi:10.1016/0009-2541(94)90031-0

Huang, Y., Shuman, B., Wang, Y., & Iii, T. W. (2004). Hydrogen isotope ratios of individual lipids in lake sediments as novel tracers of climatic and environmental change: a surface sediment test. *Journal of Paleolimnology*, *31*, 363–375.

Huguet, C., Smittenberg, R. H., Boer, W., Sinninghe Damsté, J. S., & Schouten, S. (2007). Twentieth century proxy records of temperature and soil organic matter input in the

Drammensfjord, southern Norway. *Organic Geochemistry*, *38*(11), 1838–1849. doi:10.1016/j.orggeochem.2007.06.015

Hurrell, J. W. (1995). Decadal Trends in the North Atlantic Oscillation: Regional Temperatures and Precipitation. *Science (New York, N.Y.)*, *269*(5224), 676–9. doi:10.1126/science.269.5224.676

Hurrell, J. W., Kushnir, Y., Otterson, G., & Visbeck, M. (2003). An Overview of the North Atlantic Oscillation. *The North Atlantic Oscillation: Climatic Significance and Environmental Impact*, *134*, 263. doi:10.1029/GM134

Killops, S., & Killops, V. (2005). *Introdution to Organic Geochemistry* (2nd ed.). Blackwell Science Ltd. doi:10.1002/9781118697214

Kim, J.-H., Schouten, S., Hopmans, E. C., Donner, B., & Sinninghe Damsté, J. S. (2008). Global sediment core-top calibration of the TEX86 paleothermometer in the ocean. *Geochimica et Cosmochimica Acta*, *72*(4), 1154–1173. doi:10.1016/j.gca.2007.12.010

Koga, Y., & Morii, H. (2005). Recent advances in structural research on ether lipids from archaea including comparative and physiological aspects. *Bioscience, Biotechnology, and Biochemistry*, *69*(11), 2019–34. doi:10.1271/bbb.69.2019

Laskar, J., Joutel, F., & Boudin, F. (1993). Orbital, precessional, and isolation quantities for the Earth from -20Myr to +10Myr. *Astronomy and Astrophysics*.

Laskar, J., Robutel, P., Joutel, F., Gastineau, M., Correia, a. C. M., & Levrard, B. (2004). A long-term numerical solution for the insolation quantities of the Earth. *Astronomy and Astrophysics*, *428*(1), 261–285. doi:10.1051/0004-6361:20041335

Lengger, S. K., Hopmans, E. C., Reichart, G.-J., Nierop, K. G. J., Sinninghe Damsté, J. S., & Stefan, S. (2012). Intact polar and core glycerol dibiphytanyl glycerol tetraether lipids in the Arabian Sea oxygen minimum zone: I. Selective preservation and degradation in the water column and consequences for the TEX86. *Geochimica et Cosmochimica Acta*, *98*(July 2016), 244–258. doi:10.1016/j.gca.2012.05.003

Lincoln, S. A., Wai, B., Eppley, J. M., Church, M. J., Summons, R. E., & DeLong, E. F. (2014). Planktonic Euryarchaeota are a significant source of archaeal tetraether lipids in the ocean. *Proceedings of the National Academy of Sciences of the United States of America*, *111*(27), 9858–63. doi:10.1073/pnas.1409439111

Llirós, M., Gich, F., Plasencia, A., Auguet, J. C., Darchambeau, F., Casamayor, E. O., … Borrego, C. (2010). Vertical distribution of ammonia-oxidizing crenarchaeota and methanogens in the epipelagic waters of lake kivu (rwanda-democratic republi of the congo). *Applied and Environmental Microbiology*, *76*(20), 6853–6863. doi:10.1128/AEM.02864-09

Loomis, S. E., Russell, J. M., Heureux, A. M., D'Andrea, W. J., & Sinninghe Damsté, J. S. (2014). Seasonal variability of branched glycerol dialkyl glycerol tetraethers (brGDGTs) in a temperate lake system. *Geochimica et Cosmochimica Acta*, *144*, 173–187. doi:10.1016/j.gca.2014.08.027

Luterbacher, Xoplaki, Dietrich, Rickli, Jacobeit, Beck, … Wanner. (2002). Reconstruction of sea level pressure fields over the Eastern North Atlantic and Europe back to 1500. *Climate*

Dynamics, *18*(7), 545–561. doi:10.1007/s00382-001-0196-6

Marshall, J., Johnson, H., & Goodman, J. (2001). A Study of the Interaction of the North Atlantic Oscillation with Ocean Circulation. *Journal of Climate*, *14*(7), 1399–1421. doi:10.1175/1520-0442(2001)014<1399:ASOTIO>2.0.CO;2

Mayewski, P. A., Rohling, E. E., Stager, J. C., Karlén, W., Maasch, K. A., Meeker, L. D., … Steig, E. J. (2004). Holocene climate variability. *Quaternary Research*, *62*(3), 243–255. doi:10.1016/j.yqres.2004.07.001

Meyers, P. ., Edwards, S. J., & Eadie, B. J. (1980). MEYERS ET AL 1980.pdf. *Journal of Great Lakes Research*, *6*(4), 331–337.

Meyers, P. A., & Lallier-vergès, E. (1999). Lacustrine sedimentary organic matter records of Late Quaternary paleoclimates. *Journal of Paleolimnology*, *21*, 345–372.

Miller, J. M. (2001). Carbon isotope discrimination by a sequence of Eucalyptus species along a subcontinental rainfall gradient in Australia. *Functional Ecology*, 222–232.

Naeher, S., Peterse, F., Smittenberg, R. H., Niemann, H., Zigah, P. K., & Schubert, C. J. (2014). Organic Geochemistry Sources of glycerol dialkyl glycerol tetraethers (GDGTs) in catchment soils , water column and sediments of Lake Rotsee (Switzerland) – Implications for the application of GDGT-based proxies for lakes. *Organic Geochemistry*, *66*, 164–173.

Neff, U., Burns, S. J., Mangini, a, Mudelsee, M., Fleitmann, D., & Matter, a. (2001). Strong coherence between solar variability and the monsoon in Oman between 9 and 6 kyr ago. *Nature*, *411*(6835), 290–293. doi:10.1038/35077048

Niemann, H., Stadnitskaia, a., Wirth, S. B., Gilli, a., Anselmetti, F. S., Sinninghe Damsté, J. S., … Lehmann, M. F. (2012). Bacterial GDGTs in Holocene sediments and catchment soils of a high Alpine lake: application of the MBT/CBT-paleothermometer. *Climate of the Past*, *8*(3), 889–906. doi:10.5194/cp-8-889-2012

Otto, A., & Simpson, M. J. (2005). Degradation and Preservation of Vascular Plant-derived Biomarkers in Grassland and Forest Soils from Western Canada. *Biogeochemistry*, *74*(3), 377–409. doi:10.1007/s10533-004-5834-8

Pancost, R. D., & Boot, C. S. (2004). The palaeoclimatic utility of terrestrial biomarkers in marine sediments. *Marine Chemistry*, *92*(1-4), 239–261. doi:10.1016/j.marchem.2004.06.029

Pearson, A., & Ingalls, A. E. (2013). Assessing the Use of Archaeal Lipids as Marine Environmental Proxies. *Annual Review of Earth and Planetary Sciences*, *41*(1), 359–384. doi:10.1146/annurev-earth-050212-123947

Peterse, F., Nicol, G. W., Schouten, S., & Sinninghe Damsté, J. S. (2010). Influence of soil pH on the abundance and distribution of core and intact polar lipid-derived branched GDGTs in soil. *Organic Geochemistry*, *41*(10), 1171–1175. doi:10.1016/j.orggeochem.2010.07.004

Peterse, F., van der Meer, J., Schouten, S., Weijers, J. W. H., Fierer, N., Jackson, R. B., … Sinninghe Damsté, J. S. (2012). Revised calibration of the MBT–CBT paleotemperature proxy based on branched tetraether membrane lipids in surface soils. *Geochimica et Cosmochimica Acta*, *96*, 215–229. doi:10.1016/j.gca.2012.08.011

Pitcher, A., Wuchter, C., Siedenberg, K., Schouten, S., & Sinninghe Damsté, J. S. (2011). Crenarchaeol tracks winter blooms of ammonia-oxidizing Thaumarchaeota in the coastal North Sea. *Limnology and Oceanography*, *56*(6), 2308–2318. doi:10.4319/lo.2011.56.6.2308

Powers, L. A., Johnson, T. C., Werne, J. P., Castañeda, I. S., Hopmans, E. C., Sinninghe Damsté, J. S., & Schouten, S. (2005). Large temperature variability in the southern African tropics since the Last Glacial Maximum. *Geophysical Research Letters*, *32*(8), 1–4. doi:10.1029/2004GL022014

Powers, L. A., Werne, J. P., Johnson, T. C., Hopmans, E. C., Damsté, J. S. S., & Schouten, S. (2004). Crenarchaeotal membrane lipids in lake sediments: A new paleotemperature proxy continental paleoclimate reconstruction? *Geology*, *32*(7), 613–616. doi:10.1130/G20434.1

Powers, L., Werne, J. P., Vanderwoude, A. J., Sinninghe Damsté, J. S., Hopmans, E. C., & Schouten, S. (2010). Applicability and calibration of the TEX86 paleothermometer in lakes. *Organic Geochemistry*, *41*(4), 404–413. doi:10.1016/j.orggeochem.2009.11.009

Rommerskirchen, F., Plader, A., Eglinton, G., Chikaraishi, Y., & Rullkötter, J. (2006). Chemotaxonomic significance of distribution and stable carbon isotopic composition of long-chain alkanes and alkan-1-ols in C4 grass waxes. *Organic Geochemistry*, *37*(10), 1303–1332. doi:10.1016/j.orggeochem.2005.12.013

Rueda, G., Rosell-Melé, A., Escala, M., Gyllencreutz, R., & Backman, J. (2009). Comparison of instrumental and GDGT-based estimates of sea surface and air temperatures from the Skagerrak. *Organic Geochemistry*, *40*(2), 287–291. doi:10.1016/j.orggeochem.2008.10.012

Sachse, D., Billault, I., Bowen, G. J., Chikaraishi, Y., Dawson, T. E., Feakins, S. J., … Kahmen, A. (2012). Molecular Paleohydrology: Interpreting the Hydrogen-Isotopic Composition of Lipid Biomarkers from Photosynthesizing Organisms. *Annual Review of Earth and Planetary Sciences*, *40*(1), 221–249. doi:10.1146/annurev-earth-042711-105535

Schouten, S., Hopmans, E. C., Schefuß, E., & Sinninghe Damsté, J. S. (2002). Distributional variations in marine crenarchaeotal membrane lipids: A new tool for reconstructing ancient sea water temperatures? *Earth and Planetary Science Letters*, *204*(1-2), 265–274. doi:10.1016/S0012-821X(02)00979-2

Schouten, S., Rijpstra, W. I. C., Durisch-Kaiser, E., Schubert, C. J., & Sinninghe Damsté, J. S. (2012). Distribution of glycerol dialkyl glycerol tetraether lipids in the water column of Lake Tanganyika. *Organic Geochemistry*, *53*, 34–37. doi:10.1016/j.orggeochem.2012.01.009

Schouten, S., Van Der Meer, M. T. J., Hopmans, E. C., Rijpstra, W. I. C., Reysenbach, A. L., Ward, D. M., & Damsté, J. S. S. (2007). Archaeal and bacterial glycerol dialkyl glycerol tetraether lipids in hot springs of Yellowstone National Park. *Applied and Environmental Microbiology*, *73*(19), 6181–6191. doi:10.1128/AEM.00630-07

Sinninghe Damsté, J. S., Ossebaar, J., Schouten, S., & Verschuren, D. (2012). Distribution of tetraether lipids in the 25-ka sedimentary record of Lake Challa: extracting reliable TEX86 and MBT/CBT palaeotemperatures from an equatorial African lake. *Quaternary Science Reviews*, *50*, 43–54. doi:10.1016/j.quascirev.2012.07.001

Sinninghe Damsté, J. S., Rijpstra, W. I. C., Ellen, C., Prahl, F. G., Wakeham, S. G., Hopmans, E. C.,

& Schouten, S. (2002). Distribution of Membrane Lipids of Planktonic Crenarchaeota in the Arabian Sea Distribution of Membrane Lipids of Planktonic Crenarchaeota in the Arabian Sea †. *Applied and Environmental Microbiology*, *68*(6), 2997–3002. doi:10.1128/AEM.68.6.2997

Sinninghe Damsté, J. S., Rijpstra, W. I. C., Hopmans, E. C., Weijers, J. W. H., Foesel, B. U., Overmann, J., & Dedysh, S. N. (2011). 13,16-Dimethyl octacosanedioic acid (iso-Diabolic Acid), a common membrane-spanning lipid of Acidobacteria subdivisions 1 and 3. *Applied and Environmental Microbiology*, *77*(12), 4147–4154. doi:10.1128/AEM.00466-11

Sun, Q., Chu, G., Liu, M., Xie, M., Li, S., Ling, Y., … Lü, H. (2011). Distributions and temperature dependence of branched glycerol dialkyl glycerol tetraethers in recent lacustrine sediments from China and Nepal. *Journal of Geophysical Research: Biogeosciences*, *116*(1), 1–12. doi:10.1029/2010JG001365

Tierney, J. E. (2012). Gdgt Thermometry : Lipid Tools for Reconstructing Paleotemperatures. *The Paleontological Society Papers*, *18*, 115–131.

Tierney, J. E., & Russell, J. M. (2009). Distributions of branched GDGTs in a tropical lake system: Implications for lacustrine application of the MBT/CBT paleoproxy. *Organic Geochemistry*, *40*(9), 1032–1036. doi:10.1016/j.orggeochem.2009.04.014

Tierney, J. E., Russell, J. M., Eggermont, H., Hopmans, E. C., Verschuren, D., & Sinninghe Damsté, J. S. (2010). Environmental controls on branched tetraether lipid distributions in tropical East African lake sediments. *Geochimica et Cosmochimica Acta*, *74*(17), 4902–4918. doi:10.1016/j.gca.2010.06.002

Turich, C., Freeman, K. H., Bruns, M. A., Conte, M., Jones, a. D., & Wakeham, S. G. (2007). Lipids of marine Archaea: Patterns and provenance in the water-column and sediments. *Geochimica et Cosmochimica Acta*, *71*(13), 3272–3291. doi:10.1016/j.gca.2007.04.013

Van de Water, P. K., Leavitt, S. W., & Betancourt, J. L. (2002). Leaf δ13C variability with elevation, slope aspect, and precipitation in the southwest United States. *Oecologia*, *132*(3), 332–343. doi:10.1007/s00442-002-0973-x

Vogts, A., Schefuß, E., Badewien, T., & Rullkötter, J. (2012). *n*-Alkane parameters from a deep sea sediment transect off southwest Africa reflect continental vegetation and climate conditions. *Organic Geochemistry*, *47*, 109–119. doi:10.1016/j.orggeochem.2012.03.011

Vonmoos, M., Beer, J., & Muscheler, R. (2006). Large variations in Holocene solar activity: Constraints from 10Be in the Greenland Ice Core Project ice core. *Journal of Geophysical Research: Space Physics*, *111*(10), 1–14. doi:10.1029/2005JA011500

Wang, Y., Yang, H., Zhang, J., Gao, W., Huang, C., & Xie, B. (2015). Characterization of *n*-alkanes and their carbon isotopic composition in sediments from a small catchment of the Dianchi watershed. *Chemosphere*, *119*, 1346–1352. doi:10.1016/j.chemosphere.2014.01.085

Wanner, H., Beer, J., Bütikofer, J., Crowley, T. J., Cubasch, U., Flückiger, J., … Widmann, M. (2008). Mid- to Late Holocene climate change: an overview. *Quaternary Science Reviews*, *27*(19-20), 1791–1828. doi:10.1016/j.quascirev.2008.06.013

Weijers, J. W. H., Bernhardt, B., Peterse, F., Werne, J. P., Dungait, J. A. J., Schouten, S., &

Sinninghe Damsté, J. S. (2011). Absence of seasonal patterns in MBT-CBT indices in mid-latitude soils. *Geochimica et Cosmochimica Acta*, *75*(11), 3179–3190. doi:10.1016/j.gca.2011.03.015

Weijers, J. W. H., Schouten, S., Hopmans, E. C., Geenevasen, J. A. J., David, O. R. P., Coleman, J. M., … Sinninghe Damsté, J. S. (2006). Membrane lipids of mesophilic anaerobic bacteria thriving in peats have typical archaeal traits. *Environmental Microbiology*, *8*(4), 648–657. doi:10.1111/j.1462-2920.2005.00941.x

Weijers, J. W. H., Schouten, S., Spaargaren, O. C., & Sinninghe Damsté, J. S. (2006). Occurrence and distribution of tetraether membrane lipids in soils: Implications for the use of the TEX86 proxy and the BIT index. *Organic Geochemistry*, *37*(12), 1680–1693. doi:10.1016/j.orggeochem.2006.07.018

Weijers, J. W. H., Schouten, S., van den Donker, J. C., Hopmans, E. C., & Sinninghe Damsté, J. S. (2007). Environmental controls on bacterial tetraether membrane lipid distribution in soils. *Geochimica et Cosmochimica Acta*, *71*(3), 703–713. doi:10.1016/j.gca.2006.10.003

White, G. F., Russell, N. J., & Tidswell, E. C. (1996). Bacterial scission of ether bonds. *Microbiological Reviews*, *60*(1), 216–232.

Wörmer, L., Lipp, J. S., Schröder, J. M., & Hinrichs, K.-U. (2013). Application of two new LC–ESI–MS methods for improved detection of intact polar lipids (IPLs) in environmental samples. *Organic Geochemistry*, *59*, 10–21. doi:10.1016/j.orggeochem.2013.03.004

Yang, H., Lü, X., Ding, W., Lei, Y., Dang, X., & Xie, S. (2015). The 6-methyl branched tetraethers significantly affect the performance of the methylation index (MBT') in soils from an altitudinal transect at Mount Shennongjia. *Organic Geochemistry*, *82*, 42–53. doi:10.1016/j.orggeochem.2015.02.003

Zhang, C. L., Fouke, B. W., Bonheyo, G. T., Peacock, A. D., White, D. C., Huang, Y., & Romanek, C. S. (2004). Lipid biomarkers and carbo*n*-isotopes of modern travertine deposits (Yellowstone National Park, USA): Implications for biogeochemical dynamics in hot-spring systems. *Geochimica et Cosmochimica Acta*, *68*(15), 3157–3169. doi:10.1016/j.gca.2004.03.005

Zhang, C. L., Wang, J., Dodsworth, J. A., Williams, A. J., Zhu, C., Hinrichs, K. U., … Hedlund, B. P. (2013). In situ production of branched glycerol dialkyl glycerol tetraethers in a great basin hot spring (USA). *Frontiers in Microbiology*, *4*(181). doi:10.3389/fmicb.2013.00181

Zhu, C., Weijers, J. W. H., Wagner, T., Pan, J. M., Chen, J. F., & Pancost, R. D. (2011). Sources and distributions of tetraether lipids in surface sediments across a large river-dominated continental margin. *Organic Geochemistry*, *42*(4), 376–386. doi:10.1016/j.orggeochem.2011.02.002

Zink, K. G., Vandergoes, M. J., Mangelsdorf, K., Dieffenbacher-Krall, A. C., & Schwark, L. (2010). Application of bacterial glycerol dialkyl glycerol tetraethers (GDGTs) to develop modern and past temperature estimates from New Zealand lakes. *Organic Geochemistry*, *41*(9), 1060–1066. doi:10.1016/j.orggeochem.2010.03.004

Chapter 2
The study site and methods

This chapter contains a general description of the study area and the fieldwork undertaken to obtain the samples analyzed in this thesis, and the analytical methods employed to characterize and quantify the targeted biomarkers as well as to obtain ancillary data. All samples are from Lake Montcortés, and its catchment, in the Catalan pre-Pyrenees. Samples obtained for this thesis were analyzed for their biomarker contents at ICTA-UAB (Institut de Ciència i Tecnologia Ambientals, Universitat Autònoma de Barcelona), and at the SAQ-UAB (Servei d'Anàlisi Química, Universitat Autònoma de Barcelona). The fieldwork was undertaken in close collaboration with Dr Teresa Vegas (Dept. of Ecology at the Universitat de Barcelona) and her collaborators in the project MINECO-MONTCORTÈS-500. They provided access to sediment trap samples and facilitated the logistics of the monitoring program. They have also provided access to the ancillary unpublished water column data on temperature and oxygen contents (part of the thesis of M. Carme Trapote), as well as meteorological parameters from Pobla de Segur (compiled by Dr Javier Sigró and collaborators from the Centre for Climate Change and the Universitat Rovira i Virgili), which are discussed in chapters 4 and 5. In addition, the samples and meteorological data in chapter 6 were provided by Dr Juan Pablo Corella (Museo Nacional de Ciencias Naturales of the Consejo Superior de Investigaciones científicas-CSIC) and obtained during the projects MINECO-GLOBALKARST in collaboration as well with the group of Dr Blas Valero-Garcés at the Instituto Pirenaico de Ecología belonging to the CSIC.

2.1. Study site

Lake Montcorès is located at 42°19´50´´N, 0°59´46´´E, on the southern side of the Pre-Pyrenees, at an altitude of 1027 m (Fig. 2-1). It is kidney-shaped with the longest diameter of 525 m, and the shortest of 450 m, and a maximum depth of 30 m (Camps et al. 1976). The lake is recharged mainly by groundwater (precipitation) via ephemeral creeks that drain directly into the lake. The main water losses in the lake occur through evaporation and seasonal runoff in an outlet at the northern end of the lake (Corella et al., 2010).

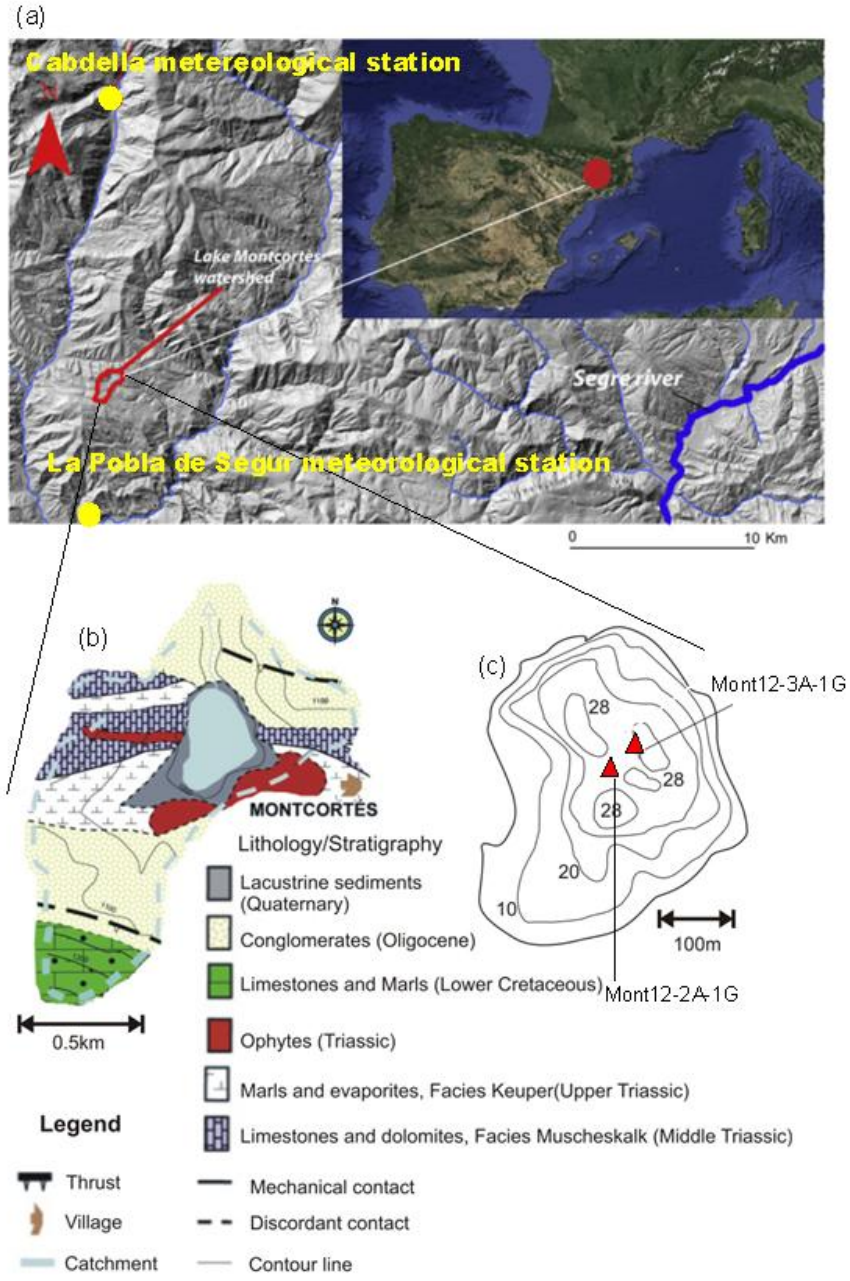

Figure 2-1 Location of Lake Montcortès in the Iberian Peninsula and Digital Terrain Model (5 m resolution) of the Pallars Sobira region and location of Lake Montcortès, Cabdella and La Pobla de Segur meteorological station (Corella et al., 2014). (b) Geologic map of Lake Montcorès catchment and (c) locations of the sediment core (modified from Corella et al., 2012)

The lake was formed on bedrock of Quaternary lacustrine depositions, Oligocene conglomerates and Triassic calcite, dolomite (MUSCHELKALK facies); pelites and evaporites with some intrusive ophites (KEUPER facies). The origin of the lake is attributed to interstratal dissolution and collapse of Keuper evaporites (Rosell, 1994; Corella et al., 2012).

The mineral composition of the lake water is dominated by HCO_3^-, Ca^{2+} and Mg^{2+}. Alkalinity values range from 2.5 to 3.5 meq/L, and pH values have a range of 7.0 to 8.5 (Camps et al. 1976). The lake is oligotrophic and meromictic. In summer, the lake is vertically stratified. Consequently, dissolved oxygen (DO) generally decreases from the top and is depleted at the bottom. However, DO may become homogenous throughout the water column if vertical mixing reaches the lake bottom in winter. When the bottom waters become anoxic, sulfide becomes also abundant due to the occurrence of sulfate-reducing bacteria (Camps et al. 1976). This situation favors the preservation of finely laminated sediments in central-distal areas of the lake basin, while littoral sediments are composed of massive carbonate silts with abundant plant remains and ostracods.

The region where lake Montcortés is located is within the margins of the Mediterranean Alpine climate, with mean annual precipitation of 860mm and mean annual air temperature of 10.6 °C. Heavy rainfall events in the region mostly occur in autumn and winter, which are related to mesoscale convective systems fed by Mediterranean moisture and intensified by the orography of the eastern Pre-Pyrenean mountains. These events may be also influenced by negative phases of North Atlantic Oscillation (NAO); and, to a lesser extent, by frontal Atlantic systems which may also contributes to persistent rainfall in autumn and winter (Llasat & Puigcercer, 1994; Martin-Vide et al., 2008; Vicente-Serrano et al., 2009). Monthly mean temperatures range from 1.9 °C in January (the coldest month) to 20.3 °C in July (the warmest month) (Corella et al., 2012).

The lake's catchment vegetation has 534 different species of plants located within the Sub-Mediterranean and Middle Montane belt. Major forest formations include evergreen oaks represented by *Quercus rotundifolia Lam.* woods, deciduous oak woodlands of *Quercus pubescens Willd* and *Q. subpyrenaica Villar*, as well as conifer forests dominated by *Pinus sylvestris L*., (Rull et al., 2010). In addition, the lake shoreline is surrounded by a belt of littoral vegetation dominated by *Juncus, Scirpus, Phragmites, Typha* and *Sparganium* (Camps et al. 1976).

The study area is located in the Pallars region of the Catalan Pyrenees, which has a

long history of human habitation. It was under the influence of the Roman Empire before 410 A.D., and then under the governance of Visigoths and Muslims until 8th century. Subsequently, and until present times three historical periods have been defined: Medieval Ages (8th -15th), Modern Ages (16th -18th) and Post-modern Ages (19th-present) (Marugan and Rapalino, 2005; Rull et al., 2010). During the Modern Ages, agriculture and cattle raising expanded and diversified, like the use of animals for plowing. The land use that is affected by human in the watershed is mainly dominated by cereal crops, meadows and pastures (Bringué, 2005; Rull et al., 2010). At the beginning and the middle of the 20th century, a general agricultural crisis and the onset of a period of industrialization in Catalonia led to a depopulation of the region. Today the main economic activities of the Pallars region are tourism and related services (Farrás, 2005). For exploring the effects of nature climate change and local anthropogenic activities on the lake sediment, a number of studies have argued that periods of lower clastic input into the lake occurred during the Iberian-Roman Humid Period, the Little Ice Age (LIA) and the last 50 years; whereas, periods of higher sediment input into the lake occurred from 690-1460 A.D. and the end of LIA, in parallel to an intensification of farming and human activities in the lake (Corella et al., 2011).

2.2. Fieldwork sampling

2.2.1. Plant leaves

A total of 14 specimens representative of major plants in the Montcortés lake catchment were collected in September, 2015. The plants chosen for this study and their locations are shown in Table 2-1. Plant identification was based on the work in (Mercadé et al., 2013), and the support of colleagues at the Department of Ecology at the Universitat de Barcelona. Leaves of six species of woodland trees, two species of bushes, three species of grassland vegetation and two species of emergent aquatic plants, and a species of submerged aquatic plant were collected from three different individuals. Once samples were in the laboratory, about 0.1-0.9 g of fresh leaves of each species were cleaned with distilled water and dried at 60 °C for 24 hours, and then ground with a pestle

and mortar.

Table 2-1 List of selected plants and types

No.	Plant genera and species	Plant family	Vegetation types
P1	*Salix alba*	Salicaceae	Woodland
P2	*Quercus pubescens*	Fagaceae	Forests
P3	*Quercus rotundifolia Lam.*	Fagaceae	Forests
P4	*Pinus nigra J. F. Arnold subsp. salzmannii (Dunal) Franco*	Pinaceae	Forests
P6	*Mesophile aspen stands*	Salicaceae	Forests
P13	*European ash*	Oleaceae	Forests
P7	*Buxus sempervirens*	Buxaceae	Shrubbery vegetation
P8	*Genista scorpius*	Fabaceae	Shrubbery vegetation
P5	*Cereal*	Poaceae	Crop fields
P9	*Medicago sativa*	Fabaceae	Pastures
P14	*Cirsium monspessulanum*	Asteraceae	Grasslands
P10	*Typha domingensis*	Typhaceae	Emergent macrophytes
P11	*Phragmites australis*	Poaceae	Emergent macrophytes
P12	*Myriophyllum spicatum*	Haloragaceae	Submerged macrophytes

2.2.2. Soils

Three topsoils (Ms1-Ms3) were sampled monthly (September 2013-November 2014) from three different locations around Lake Montcortés. These locations were selected to account for the variations in topography, sun exposure and vegetation types in the catchment (Fig.2-2). One site was in a pastureland close to the lake shore and had grasses dominated by *Cirsium monspessulanum*, *Molinia coerulea* and *Plantago serpentin*. Another was in an oak forest dominated by *Quercus pubescens and Q. subpyrenaica*. While the third one was on a stony slope at the eastern part of the lake catchment and had a mixture of low shrubbery vegetation and calcicolous grasses (such as *Aphyllanthes*). In addition, three topsoils (Ms4-Ms6) were sampled in January 2016 in three different locations, which were in a crop field (cereal), a grassland (*Plantago serpentin*), and evergreen oak woodland (*Quercus rotundifolia*) (Fig.2-2). For each soil sampling, after removing overlying leaf litter and loose gravel, three replicates were taken, each spanning an area of 20 x 20 cm^2 and from a 5 cm depth, separated approximately 5 m from each other. Soil samples were collected using a metal gardening hoe and a shovel, and placed

in pre-combusted (450 °C) aluminum trays. These were then wrapped in aluminum foil and put in zip-closure plastic bags and stored in a portable icebox. Once in the lab the three samples from each site were homogenized in a metallic container and about 400 g subsample was taken out, and stored in the freezer before being lyophilized. The metallic container was rinsed with water, distilled water, acetone and dichloromethane:methanol (2:1, v/v) prior to its use.

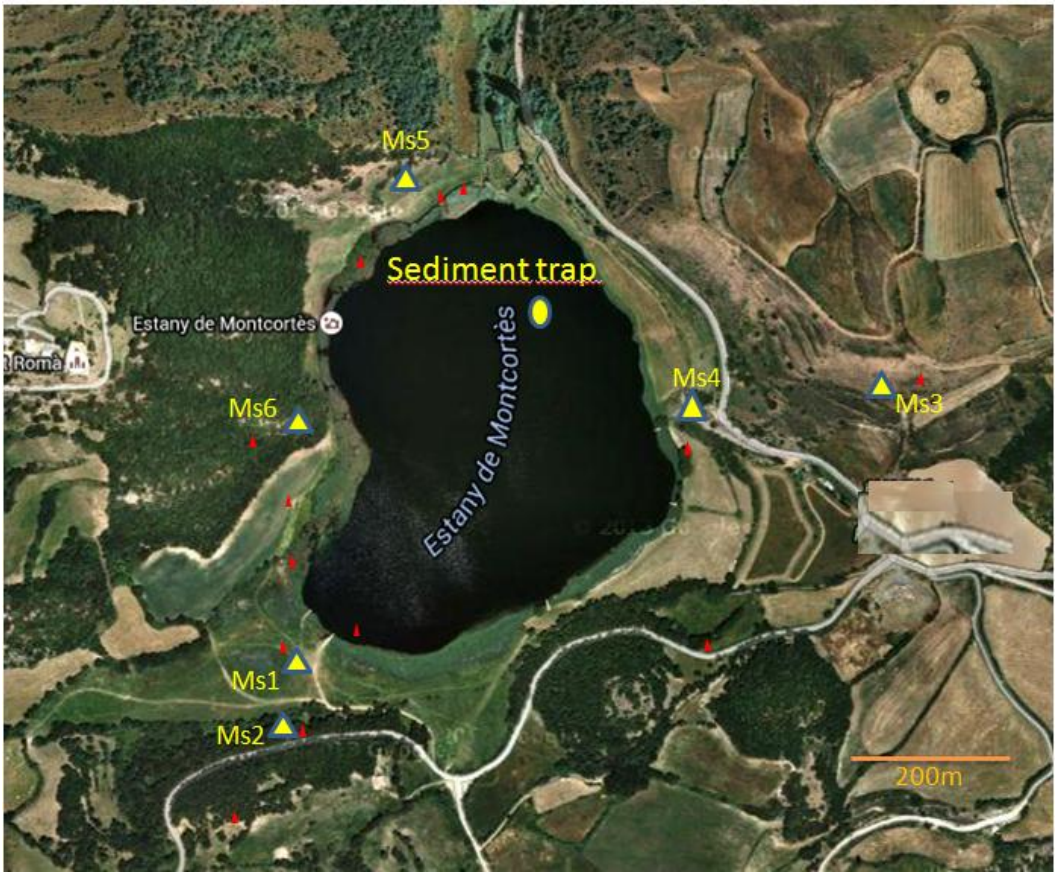

Figure 2-2 General location of soil sampling sites (Ms1-Ms6, yellow triangle) and plants (red triangle) as well as sediment trap (yellow dot) in Lake Montcortés, Catalan Eastern Pyrenees.

2.2.3. Suspended particulate matter (SPM)

From September 2013, on a monthly basis using a rubber dinghy with an electric off board motor, we collected lake water at three different depths: surface water (0 m), at the thermocline (5-12 m (thermocline depth changed seasonally) and above the lake floor (20-22 m). The surface water was collected by submerging manually from a dinghy ca. 20 cm below the surface a 20 L pre-cleaned polyethylene carboy. Before the final collection of 40 L of water, each carboy was rinsed three times with the lake water. To retrieve water

below the surface, the dinghy was moored to the sediment trap array at the northern part of the lake. From the dinghy a tube was immersed to the desired depth with a weight at its end. Water was retrieved using a sailboat bilge pump left just below the water surface, connected to a 12 V battery in the dinghy, with the long underwater tube plugged to the bottom suction end which was modified accordingly (Fig.2-3). A shorter 2 m tube plugged in the bilge pump vent allowed collecting water from the required depth into the carboys in the dinghy. Before collection, the long underwater tube was purged by pumping water through it for about 1 minute, and the polyethylene carboys were rinsed three times with the water from the required depth. Once in the laboratory, waters were immediately filtered through 0.7 μm glass fiber prefilters (GF/F, Merck Millipore Ltd. Ref APFF04700; precombusted at 450 °C) using a continuous filter system (Fig.2-3). The filters containing sample particles were then stored in the freezer until analysis.

Figure 2-3 Photos of pumping and filtering samples from water

2.2.4. Sediment trap

Collaborators from the University of Barcelona led by Dra Teresa Vegas deployed monthly a sediment trap array to collect settling particulate matter. The traps were placed at 20m water depth and anchored in one of the depocenters of the lake (Fig. 2-1). The trap array had 4 PVC tubes of 1 m length and a diameter of 6 cm. One of the tubes was dedicated to the biomarker analyses. After retrieving the trap, the uppermost water in the tube was discarded through a small hole at the side of the tube until approximately 1 L

water remained at the bottom. After stirring, the remaining water was then transferred into a 2 L polyethylene bottle. In the laboratory, the sediment trap water was stirred to resuspend the particulate matter and filtered through 0.7 μm glass fiber filters (GF/F, see properties above) using pump on a glass platform that overlying on a filtering flask with a side-arm. The sampling campaign lasted from October 2013 to April 2015. In total, 18 pieces of sediment trap samples were collected as trap water was collectedly monthly except that one sample was not retrieved in January 2015.

2.2.5. Sediment cores and surface sediments

Members of the Instituto Pirenaico de Ecologia (IPE-CSIC) led by Dr. Blas Valero-Garcés retrieved in 2012 two UWITEC gravity cores (MON12-3A-1G, 78 cm in length, and MON12-2A-1G, 106 cm in length) from the deepest area (~30 m depth) of the lake, where the seismic profiles displayed parallel reflections indicating undisturbed sediments. The sediment cores were carefully transported to the lakeshore and stored there for five days to favor sediment consolidation before being transported to the IPE cold room (Corella et al. 2014). Sections of these two cores were chosen to study the high-resolution records of climate changes in the last 110 years (1902-2012 A.D.) and the Spörer Minimum (1410-1585 A.D.). In February 2013, our team from ICTA-UAB collected five surface sediment cores from water-sediment interface using an Uwitec gravity corer with PVC liners. The top 2 cm of each sediment core was used to characterize the surface lake sediments.

The age model for the core spanning time was provided by Corella et al. (2010, 2014), by combining calcite varve counting, ^{210}Pb dating according to Arnaud's method (2002) and radiocarbon AMS ^{14}C dates. Since organic and detrital layers are not always present, each varve has been identified from the calcite layer and the good correlation of the varve counting with the four ^{14}C AMS dates verifies the annual nature of the laminations (Corella et al., 2012).

2.3. Analytical procedures

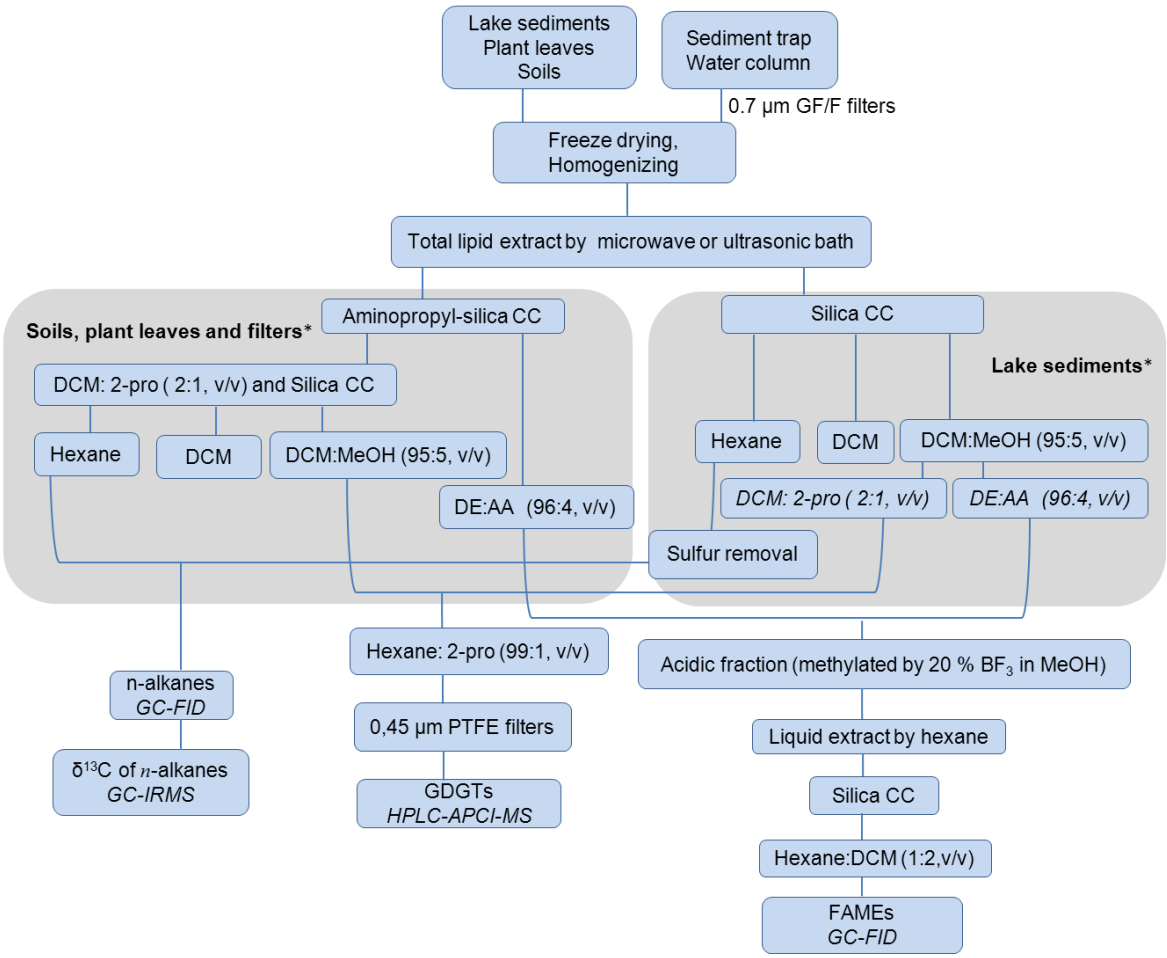

Figure 2-4 Schematic chart of analytical methods in the laboratory (* see abbreviations at the end of the thesis)

2.3.1. Preparation of glassware

New glassware used in the laboratory procedures were generally combusted at 450 °C in a muffle furnace for 8 hours prior to their use. This practice prevented contamination of the samples with compounds that could interfere with the instrumental analysis of biomarkers. Furthermore, utensils that could interact with the samples at any point of the laboratory procedure, such as syringes or recipients, were also cleaned by rinsing with solvent prior to use.

Glassware that had been previously used was rinsed with tap water, soaked in a 1% HNO_3 solution for 24 h, and rinsed with tap water again. Then, it was soaked in a 2%

BioSel solution (a phosphate-free alkaline detergent) during 24 h and rinsed with tap water, deionized water (Elix® Essential Water Purification System) and dried at 105 °C in the oven, before being fired in the muffle at 450 °C for 8 hours.

The volumetric glassware, such as measuring cylinder, was never heated. Prior to being used it was rinsed with acetone, a mix of dichloromethane and methanol (2:1, v/v) and wrapped in aluminum foil until use.

2.3.2. Freeze drying and sieving

Soils, filters and lake sediments were freeze-dried prior to extraction using a Telstar Cryodos device with the temperature of the cryogenic trap setting at -48~-52 °C, and vacuum around 2.0 mbar. The processes lasted for 24 to 60 h depending on the amount of water in the samples. After drying, we reweighed and ground the soils with a mortar and pestle, and sieved them (200 mesh). Small stones and roots of vegetation were removed with tweezers. Between samples, the mortar and pestle were rinsed with water, deionized water, acetone and dichloromethane:methanol (2:1, v/v).

2.3.3. Lipid extraction

Internal standards (Table 2-2) were added to the samples prior to their organic solvent extraction. *n*-Hexatriacontate (*n*-C_{36} alkane) (Aldrich, H1 255-2, 98%) was dissolved in isooctane. Compound GR standard was provided by Dr. Thierry Benvegnu (Ecole Nationale Supérieure de Chimie de Rennes, France), which is a synthetic tetraether with one cyclonpentane ring that presumably not exist in natural environment at 1208 m/z .

Table 2-2 Names and usage of internal standards

Item	Names of internal standards	Usage
n-alkanes	*n*-hexatriacontane	Internal standard
GDGTs	GR standards	Internal standard

Soil and plant samples were extracted using a CEM-MARS microwave accelerated reaction system which was equipped with 14 Greenchem pressure vessels (12 vessels for samples, the other two for a blank and a reference soil) with Teflon vessels of 100 mL capacity, according to the method appraised by (Kornilova and Rosell-Melé 2003; Ferrer

2013). The vessel with 10 mL dichloromethane:methanol 3:1 (v/v) and a teflon-coated magnetic stir bar inside were put to clean the vessels. The microwave increases its temperature to 70 °C in 2.5 minutes and held on at this temperature for 5 minutes and then cooled down to room temperature. About 6~8 g of soil were mixed in 25 mL dichloromethane:methanol (3:1, v/v) before being extracted by microwave using the same method as the cleaning procedure. After extract, solvent was poured slowly into a glass container with a funnel. The procedure was repeated for three times and the supernatant was transferred into a new pearl-shaped vessel which was then fitted to a rotary evaporator at 27 °C to make solvent dry.

Sediment samples and filters from the water column were analyzed in batches of 10 together with a blank and a reference sample. 1~2g of sediment was weighed in a GX-2000 precision balance with a weighting range of 0.01~2100g. The weighed sediment was added in a test tube. Internal standards and 10mL (4+3+3mL) dichloromethane:methanol (3:1,v/v) were added too. Each test tube containing solvent and samples was shaken using a rotational speed of 1800 for 30 seconds. The solvent and processes for extracting the total lipids on filters are the same but the amount was increased to 50mL (20+15+15mL) in a pearl-shaped vessel. All tubes or vessels were fixed in a rack in a sonication bath for 10 min before being centrifuged at 2000 rpm for 5 minutes using a Rotofix 32 centrifuge (Hettich Zentrifugen). For sediments, the supernatant was transferred into a new test tube before evaporating at room temperature in a miVac Duo concentrator coupled to a cold trap (Genevac) and a Thermo Savant vacuum pump unit, shortened as Centrivap. The processes were repeated for two more times. The supernatant of filters was transferred into pearl-shaped vessels and dried in a rotary evaporator at 27 °C.

2.3.4. Column chromatography

The method was adapted from (Huang et al., 1999) and (Schouten et al., 2002). Column chromatography is used for separating and purifying the liquids different compounds. Pasteur pipettes were combusted at 450 °C in the muffle furnace for 8 hours,

with cotton wool filled with 0.6 g silica (230-400 mesh) and Na_2SO_4 to be used for purification. Silica and cotton were previously cleaned with dichloromethane:methanol (2:1, v:v) during 24 hours using a Soxhlet. Then silica was heated in the oven at 105°C overnight and then deactivated with 1% deionized H_2O. The mobile phases for sediments were hexane (5 mL; F1, *n*-alkanes), dichloromethane (4 mL; F2, reserved), dichloromethane:methanol (95:5, v/v; 6 mL; F3, *n*-alkanoic acids and GDGTs) and methanol (5 mL; F4, reserved). Each fraction was collected in a new tube and dried in the centrifugal concentrator. F3 fraction was then dissolved in solvent dichromethane:isopropanol (2:1, v/v; 8 mL) through an aminopropyl-silica (40-60 μm) column chromatography. The total lipid extract of samples from sediment trap, water column and were separated into neutral and acid fraction using 8mL diclorometh ane:isopropanol (2:1, v/v; F1) and 10 mL diethyl ether:acetic acid (96:4, v/v; F2) using a Pasteur pipette plugged with a piece of cotton wool and filled with 0.8g of aminopropyl silica at the bottom and 0.5 g of sodium sulphate on top. The amino propyl silica and cotton were previously cleaned by a Soxhlet with dichloromethane:methanol (2:1, v/v) during 24 hours. Then aminopropyl and cotton were wrapped with aluminum foil and placed under the fume hood to dry before being stored in a desiccator. Before elution of the sample fraction, the column was conditioned with 3 mL dichloromethane:isopropanol (2:1, v/v). The columns for soil samples were larger and consumed more solvent. That is, 1.5g aminopropyl silica and 1g Na_2SO_4 upon it. The elution volumes for F1 and F2 were 12 mL and 15 mL, respectively. F1 fraction was separated into non-polar (F1-1; *n*-alkanes), slightly polar (F1-2, reserved) and polar fractions (GDGTs, F1-3) with 5mL hexane, 4 mL dichloromethane and 6mL methanol eluted through a silica column. The silica column was the same as the one for sediment cores. The *n*-alkane fraction was concentrated to 100 μL in an insert inside the 2 mL vial before instrumental analysis.

2.3.5. Sulphur removal

For desulphurization, copper turnings (99%, Sigma-Aldrich, approximately 40 mesh) were cut into small pieces and activated to metallic copper using a small amount of concentrated hydrochloric acid (analytical grade, 37%) for several minutes. When the copper reached its bright typical color, the acid was decanted and the copper was washed six times by deionized water. Acetone was used to remove water and hexane was used to clean the copper again before it was immersed in hexane in preparation for using. This method is according to (Brown et al., 1979).

The adequate copper was added into the tubes containing the apolar fraction and the mixture was shaken for 1 min. Blackening of the copper indicates elemental sulfur was present in the samples. The reaction lasted overnight and the tubes were centrifuged at 2000 rpm for 5 min and the supernatant was transferred into a new tube. The liquid-liquid extraction using hexane was repeated for three times and the total extract was filtered through a Pasteur pipette plugged with cotton wool to remove the copper turnings. The extract was then taken to dryness in the centrifugal concentrator at room temperature.

2.3.6. Instrumental analysis

2.3.6.1. Gas Chromatography Flame Ionization Detector (GC-FID)

The *n*-alkanes (F1) were analyzed using an Agilent gas chromatography fitted with a flame ionization detector in Agilent 7820A (GC-FID). The dry extracts were re-dissolved in isooctane and injected in splitless injection mode in the GC-FID using an autosampler. The injector and detector temperature were set at 320 °C. Hydrogen was used as carrier gas with a constant flux of 2 mL/min. Compounds were separated through an Agilent HP-1 capillary column of 60m length, 0.25 mm internal diameter connected to a guard column with a press-fit. For *n*-alkane fraction analysis, oven temperature was held at 80 °C during 1 min, increased to 120 °C at a rate of 30 °C per minute, then increased to 320 °C at 6 °C per minute and remained at 320 °C during 21 min. The detector is holding H_2 flow and air flow with a speed of 30 mL/min and 400 mL/min, respectively. Reference sediment

injected in gas chromatography mass spectrometry (GC-MS) was used identification of homologues of *n*-alkanes with different carbon chain lengths in GC-FID. Quantification of *n*-alkanes was based on internal standards.

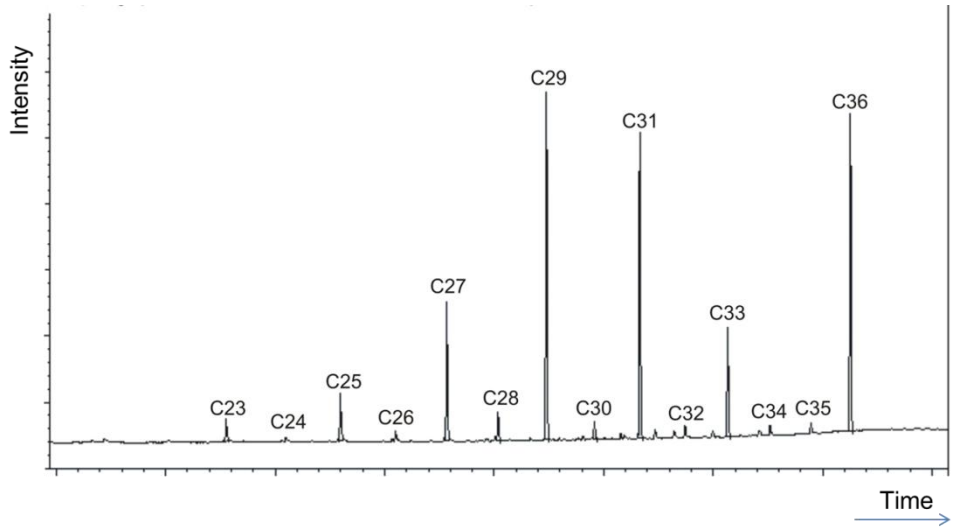

Figure 2-5 Chromatogram of C_{23}-C_{35} *n*-alkanes in the reference sediment from Lake Montcortés based on retention time.

2.3.6.2. Gas chromatography combustion isotope ratio mass spectrometry (GC-IRMS)

For the compound specific isotopic analysis, measurement of $\delta^{13}C$ ratio was performed by gas chromatography isotope ratio mass spectrometer Thermo Delta V Advantage (GC-IRMS). $\delta^{13}C$ are reported in per mil (‰) relative to the Vienna Peedee Beleminte (VPDB). Standard deviations of carbon isotope analyses were better than 0.5‰. Helium (UHP 5.5 grade) was used as the carrier gas operating at constant flow mode with a rate of 1.5 mL/min. Compounds separated by the GC column were converted to CO_2 and H_2O through the combustion furnace (0.5 mm i.d.× 1.5 mm o.d. × 34 cm) operated at 940 °C and loaded with CuO and Pt wires as oxidants and catalyst, respectively. The reproducibility and accuracy of the carbon was evaluated using laboratory isotopic standards which contain C_{20}, C_{28} and C_{36} *n*-alkanes. The precision of the GC-IRMS was checked by the injection of four isotopic standards after every five sample injections.

2.3.6.3. High Performance Liquid Chromatography Atmospheric Pressure Chemical Ionization Mass Spectrometry (HPLC-APCI-MS)

For GDGT analysis, the polar fraction containing GDGTs was dried and dissolved in 200-600 uL hexane:isopropanol (99:1,v/v) and filtered through a 0.45/0.22 PTFE filter. 5-20 µL sample was automatically injected in an Agilent Time-Off-Flight (TOF) mass spectrometer with an atmospheric pressure chemical ionization (APCI) interface set in positive mode. Following the methods (Escala et al., 2007; Huguet et al., 2013), the extracts were eluted through a Tracer Excel CN column (Teknokroma; 20 cm length, 0.4 cm diameter and 3 µm particle size) equipped with a precolumn filter and a guard column. The mobile phase was eluted with hexane:isopropanol (98.5:1.5) at a flow of 0.6 mL/min. The proportion of isopropanol was held at 1.5% for 4 minutes and increased gradually to 5% during 11 minutes, then increased to 10% for 1 minute and remained at this proportion for 4 minutes, then decreased back to 1.5% during 1 minute and held at 1.5% for 9 minutes until the end of the run. The parameters of the APCI interface were set as follows to generate positive ion spectra: corona discharge 3 µA, vaporizer temperature 400 °C, sheath gas pressure 49 mTorr, auxiliary gas (N_2) pressure 5 mTorr and capillary temperature 200 °C. GDGTs were detected in selected ion monitoring (SIM) mode of $[M+H]^+ \pm 0.5$ m/z units to increase signal to noise ratio at the following at m/z (Schouten et al., 2007): 1302, 1300, 1298, 1296, 1292, 1050, 1048, 1046, 1036, 1034, 1032, 1022, 1020, 1018 and the synthetic tetraether lipid at 1208 m/z (Fig. 2-6).

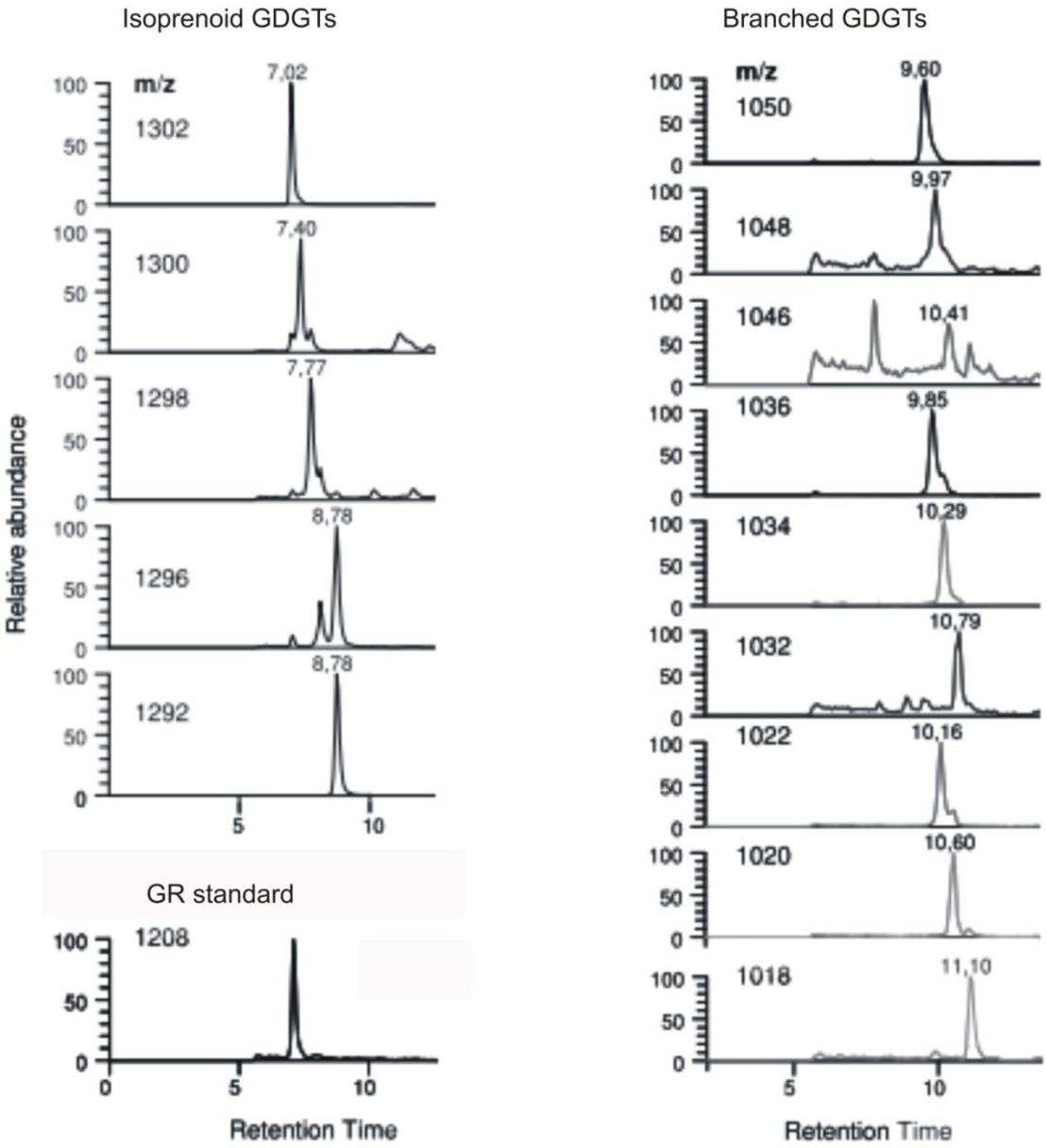

Figure 2-6 Chromatograms of the GDGT analysis in HPLC-APCI-MS system: isoprenoid, branched GDGTs and GR standard (Gemma, 2013)

Quantification of GDGTs was obtained using the GR internal standard. The average response factor of the standard GR versus the isolated isoprenoid GDGT-0 standard with a m/z of 1302 was 1.2±0.1(Escala, 2009). The linear range was calculated by injecting successive amount of the GR standard and monitoring the area of the peak. The linear range where the relationship between the concentration of the compound and the response of the detector is linear as follows:

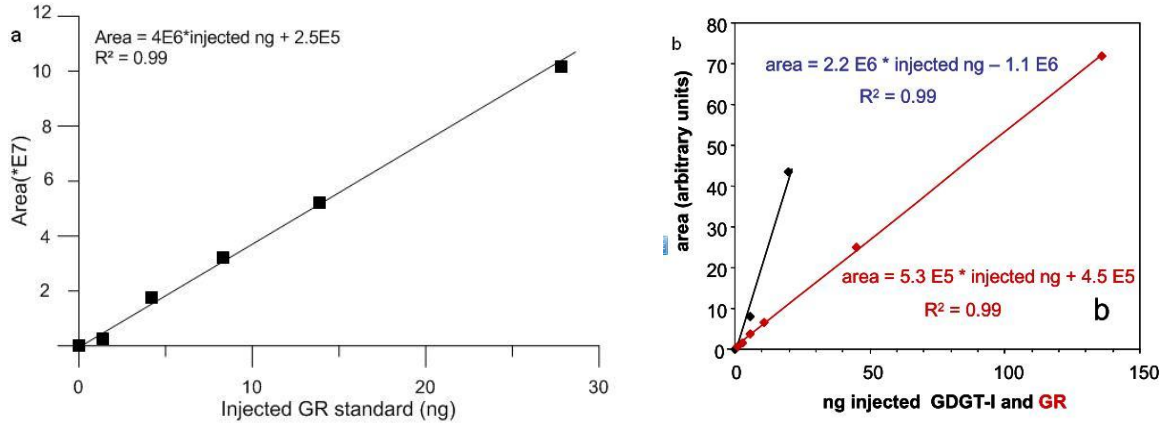

Figure 2-7 The injections of increasing concentrations of GR standard and peak area using Agilent HPLC-TOF-MS and Dionex HPLC –Thermo Finnigan TSQ-MS response to GDGT-0 (black dots) and to compound GR (red dots) (see details from Escala, 2009).

2.3.6.4. Analytical reproducibility and blank controls

The reproducibility of the analysis was obtained from a comparison of injections of the standard sediment when operating instrument. The precision of *n*-alkanes was assessed with triplicate injections of reference sediment, ranging from 0.001 to 0.05 (1σ). The reproducibility of biomarkers quantification showed an error below 0.078 (1σ). The precision of GDGTs was assessed with triplicate injections of reference sediment, ranging from 0.004 to 0.024 TEX_{86} units (1σ), and reference sediment injected during samples shows fairly stable TEX_{86} values.

2.3.7. Ancillary measurements

2.3.7.1. Loss on ignition of soils

The total amount of organic matter in soil samples was measured using the loss on ignition (LOI) method. Aluminium trays were combusted at 450 °C for 8 hour. 1g of newly-collected soil sample (triplicate) was deposited in a dry aluminium tray and dried for 18 hours at 105 °C in the oven. Afterwards the dry samples were weighted (DW_{105}) and heated at 550 °C for 4 hours. Afterwards, samples were taken out and cooled down in the desiccator until room temperature and weighted again (DW_{550}). The LOI value was calculated using the equation as follows (Heiri et al., 2001):

$LOI\ (\%) = (DW_{105} - DW_{550})/DW_{105} \times 100\%$

The total organic carbon (TOC) was calculated according to generally accepted TOC/LOI ratio of 0.58 (De Vos et al., 2005):

$TOC\ (\%) = 0.581 \times LOI \times 100\%$

2.3.7.2. pH analysis

The freeze-dried soils were homogenized and sieved (2 mm mesh size) to remove roots and small stones. The pH of the soil is potentiometrically measured in the supernatant suspension of a 1:2.5 soil:liquid (water) mixture (Protocol, 1975). About 10g of sieved soil was placed into a 100mL polythene wide-mouth bottle and mixed with 25 mL of deionized water. The bottle was capped and shaken for 1 hour with a reciprocating shaking machine. A pH meter (GLP22, Crison Instrument) with a glass-calomel combination electrode was calibrated by buffer solutions, pH 4.0 and 7.0. Shake the samples for about 5 seconds and open the bottle to immerse the sensing electrode inside and record the value when it is stabilized (1σ, 0.1 pH unit).

2.4. Instrumental data support

Long-time climatic instrumental data of temperature (1930-1992) and precipitation (1917-1994) at Cabdella meteorological station were provided by Juan Pablo Corella with a courtesy of the Spanish National Meteorological Agency (AEMET). The station (1200 m a.s.l.) is about 15 km north of the study lake (Corella et al., 2014).

Short-time climatic instrumental data (September 2013 to May 2015) of temperature and precipitation, wind velocity (Fig. 1-8) and wind direction, humidity were obtained at La Pobla de Segur meteorological station by a favor of Javier Sigró. This station (585 m a.s.l.) is about 10km south of the study lake.

The temperatures and DO at three depths of the water column from Lake Montcortés were obtained by Vegas-Vilarrúbia, Trapote and colleagues in her research team by means of a CTD probe once per month (unpublished data).

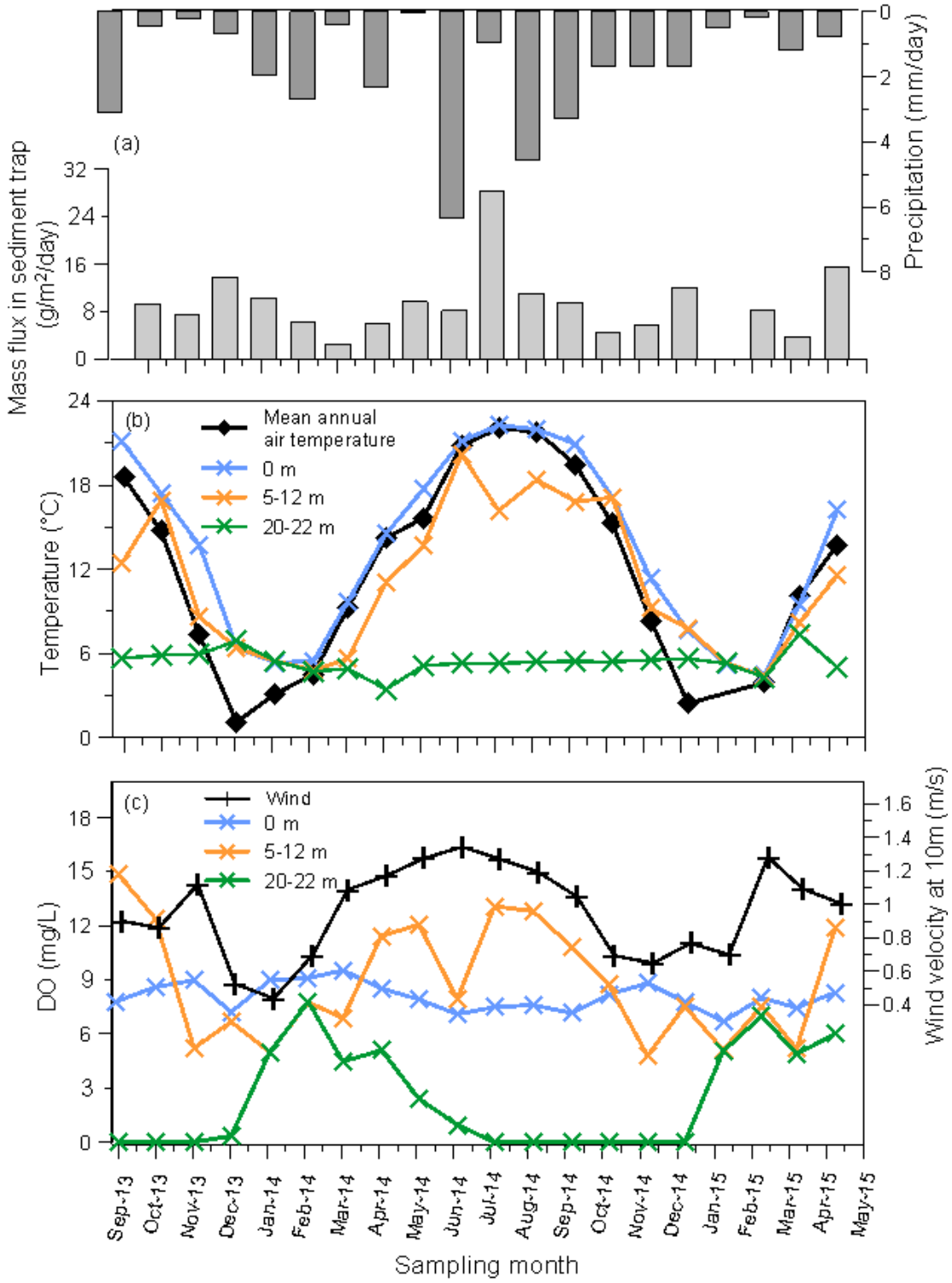

Figure 2-8 Meteorological data from September 2013 to April 2015 were from a weather station at La Pobla de Segur (a) daily accumulated precipitation (dark grey bar), (b) mean monthly air temperatures (MMAT, solid diamond), and (c) wind velocity (hollow diamond). In here we show CTD values at the depths where water samples were taken once per month; blue, orange and green crosses stand for samples from the surface (0m), thermocline (5-12m) and the bottom (20-22m) for (b) water temperature and for (c) dissolved oxygen (DO). Bulk sediment mass fluxes in the sediment trap in Lake Montcortés are shown as grey bars in the upper most graph (a).

2.5. Reference

Bringué, J.M. (2005). L'edat moderna. In: Marugan CM, Rapalino V (eds) Història del Pallars. Dels orígens als nostre dies. Pagès Editors, Lleida, pp 87–120.

Brown, D. W., Friedman, A. J. Burrows, D.G., Snyder, G. R., … MacLeod, W. D. (1979). Investigation of petroleum in the marine environs of the Strait of Juan de Fuca and Northern Puget Sound. Interagency energy/environment R&D program report. pp. 83.

Camps, J., Gonzalvo, I., Güell, J., Lópiz, P., Tejero, A., Toldrá, X., Vallespinos F., & Vicens.M. (1976). El lago de Montcortés, descripción de un ciclo anual. Oecol. Aquat., 2: 99-110.

Corella, J. P., Benito, G., Rodriguez-Lloveras, X., Brauer, a., & Valero-Garcés, B. L. (2014). Annually-resolved lake record of extreme hydro-meteorological events since AD 1347 in NE Iberian Peninsula. *Quaternary Science Reviews*, *93*, 77–90. doi:10.1016/j.quascirev.2014.03.020

Corella, J. P., Brauer, A., Mangili, C., Rull, V., Vegas-Vilarrúbia, T., Morellón, M., & Valero-Garcés, B. L. (2012). The 1.5-ka varved record of Lake Montcortès (southern Pyrenees, NE Spain). *Quaternary Research*, *78*(2), 323–332. doi:10.1016/j.yqres.2012.06.002

Corella, J. P., Moreno, A., Morellón, M., Rull, V., Giralt, S., Rico, M. T., … Valero-Garcés, B. L. (2010). Climate and human impact on a meromictic lake during the last 6,000 years (Montcortès Lake, Central Pyrenees, Spain). *Journal of Paleolimnology*, *46*(3), 351–367. doi:10.1007/s10933-010-9443-3

De Vos, B., Vandecasteele, B., Deckers, J., & Muys, B. (2005). Capability of loss-on-ignition as a predictor of total organic carbon in non-calcareous forest soils. *Communications in Soil Science and Plant Analysis*, *36*(19-20), 2899–2921. doi:10.1080/00103620500306080

Escala Pascual, M. (2009). Application of tetraether membrane lipids as proxies for continental climate reconstruction in Iberian and Siberian lakes Application of tetraether membrane lipids as proxies for continental climate reconstruction. *PhD Proposal*.

Escala, M., Rosell-Melé, A., & Masqué, P. (2007). Rapid screening of glycerol dialkyl glycerol tetraethers in continental Eurasia samples using HPLC/APCI-ion trap mass spectrometry. *Organic Geochemistry*, *38*(1), 161–164. doi:10.1016/j.orggeochem.2006.08.013

Heiri, O., Lotter, A. F., & Lemcke, G. (2001). Loss on ignition as a method for estimating organic and carbonate content in sediments : reproducibility and comparability of results, 101–110.

Huguet, C., Fietz, S., & Rosell-Melé, a. (2013). Global distribution patterns of hydroxy glycerol dialkyl glycerol tetraethers. *Organic Geochemistry*, *57*, 107–118. doi:10.1016/j.orggeochem.2013.01.010

Kornilova, O., & Rosell-Melé, A. (2003). Application of microwave-assisted extraction to the analysis of biomarker climate proxies in marine sediments. *Organic Geochemistry*, *34*(11), 1517–1523. doi:10.1016/S0146-6380(03)00155-4

Martin-Vide, J., Sanchez-Lorenzo, A., Lopez-Bustins, J. A., Cordobilla, M. J., Garcia-Manuel, A., & Raso, J. M. (2008). Torrential rainfall in northeast of the Iberian Peninsula: synoptic patterns

and WeMO influence. *Advances in Science and Research*, *2*, 99–105.

Mercadé, A., Vigo, J., Rull, V., Vegas-Vilarrúbia, T., Garcés, S., Lara, A., & Cañellas-Boltà, N. (2013). Vegetation and landscape around Lake Montcortès (Catalan pre-Pyrenees) as a tool for palaeoecological studies of lake sediments. *Collectanea Botanica*, *32*, 87–101. doi:10.3989/collectbot.2013.v32.008

Rueda, G. (2013). Reconstructing Climate Variability in the North Atlantic during the Late Holocene : an Integrated Biomarker Approach Reconstructing climate variability in the North Atlantic during the late Holocene : an integrated biomarker approach. *Universitat Autònoma de Barcelona*, (March).

Rull, V., González-Sampériz, P., Corella, J. P., Morellón, M., & Giralt, S. (2010). Vegetation changes in the southern Pyrenean flank during the last millennium in relation to climate and human activities: the Montcortès lacustrine record. *Journal of Paleolimnology*, *46*(3), 387–404. doi:10.1007/s10933-010-9444-2

Schouten, S., Hopmans, E. C., Schefuß, E., & Sinninghe-Damste, J. S. (2002). Distributional variations in marine crenarchaeotal membrane lipids: A new tool for reconstruting ancient sea-surface temperatures? *Earth and Planetary Science Letters*, *204*, 265–274.

Schouten, S., Huguet, C., Hopmans, E. C., Kienhuis, M. V. M., & Damste, J. S. S. (2007). Analytical Methodology for TEX 86 Paleothermometry by High-Performance Liquid Chromatography / Atmospheric Pressure Chemical Ionization-Mass Spectrometry. *Analytical Chemistry*, *79*(7), 2940–2944. doi:10.1029/2004PA001110.This

Vicente-Serrano, S. M., Beguería, S., López-Moreno, J. I., El Kenawy, A. M., & Angulo-Martínez, M. (2009). Daily atmospheric circulation events and extreme precipitation risk in northeast Spain: Role of the North Atlantic Oscillation, the Western Mediterranean Oscillation, and the Mediterranean Oscillation. *Journal of Geophysical Research Atmospheres*, *114*(8), 1–19. doi:10.1029/2008JD011492

Yong song Huang. F.Alayne Street-Perrott, R. Alan Perrott, Pierre Metzger, and G. E. (1999). Glacial – interglacial environmental changes inferred from molecular and compound-specific δ^{13}C analyses of sediments from Sacred Lake , Mt . Kenya, *63*(9), 1383–1404.

Chapter 3

Heterogeneity and seasonality of biomarkers in the plant-soil system of Lake Montcortés catchment

Abstract

Long chain (C_{23}-C_{35}) *n*-alkanes are widely used as terrestrial plant biomarkers, which were used for past climate change in the lake sediment. However, *n*-alkane abundance and variations of *n*-alkane chain length in modern plants and soils are still important in a given catchment. We collected 14 samples of plant specimens in September 2015 and 44 soil samples from 3 sites covered by different vegetation spanning over a year from September 2013 in the Lake Montcortés catchment. Our results suggest that particular plant groups: woody plants, grasses, emergent and submerged macrophytes present unequal abundance, distinguishable distributions of *n*-alkanes. The combination of C_{23}/C_{29}, C_{29}/C_{31}, ACL and P_{aq} indices might be a useful proxy for terrestrial/aquatic inputs in the lake sediment based on modern plants and soil formations. Stable $\delta^{13}C$ values of *n*-alkanes remained constant throughout the year in soils to faithfully preserve the $\delta^{13}C$ signals of dominant higher plants. In contrast, the abundance of glycerol dialkyl glycerol tetraethers (GDGTs) varied largely in different soils as well as throughout the year while the GDGT-derived TEX_{86}, and mean annual air temperature estimates were generally unchangeable on a short-time scale (monthly or seasonally). In addition, the MBT and CBT indices to some extent at a specific scale are dominated by pH values. Thus, our study does not provide evidence for seasonal effects on the abundance and proxies of *n*-alkanes and GDGTs in soils.

3.1. Introduction

Biomarkers proxies in sedimentary settings have been shown particular promise to reconstruct past variations in some key climatic parameters, such as temperature and precipitation. Their accurate interpretation in sediments requires, however, a thorough understanding of their putative sources and of the processes that have mediated in their transport to a sedimentary basin. Terrigenous biomarkers in lacustrine systems may have a variety of origins, such as higher plants or soil bacteria, and transported to the sedimentary basin by fluvial and eolian processes.

In here we characterize some of the likely sources of some terrigenous biomarkers in the sediments of Lake Montcortés. The lake sediments have highly laminated sequences and it is the target of a number of paleoclimatic reconstruction studies. In particular we characterize the signatures of biomarkers of recognized paleoclimatic interest in the soils and vegetation of the lake catchment. These are the long-chain alkyl lipids from higher plants, and the so-

called GDGTs (i.e. isoprenoid glycerol dialkyl glycerol tetraethers), which are biomarkers of recognized paleoclimatic interest..

Long chain *n*-alkanes are derived from higher plants and have been increasingly applied in biogeochemical studies of past global change (Eglinton and Hamilton, 1967; Huang et al., 2004; Makou et al., 2007; Bush and McInerney, 2013). Higher plant *n*-alkanes have typically carbon chain-lengths with a strong predominance of odd-carbon-number homologues, the C_{25}-C_{33} being the most common. Recent studies in living plants and modern soils have demonstrated that *n*-alkane chain-length ratios are driven by temperature or aridity, and are not specific to plant types, with the exception of those from aquatic plants and Sphagnum moss (Bush & Mcinerney, 2015; Pancost & Boot, 2004; Tipple & Pagani, 2013). With the advent of compound specific isotopic analysis (CSIA), it has become possible to measure isotopic ratios of carbon ($\delta^{13}C$) and hydrogen (δD) in *n*-alkanes. $\delta^{13}C$ signatures are less influenced by diagenesis, differential preservation of compound classes, and changes in the sources of organic matter that otherwise complicate interpretations of bulk $\delta^{13}C$ values (Pancost & Boot, 2004). Vegetation that uses one of three photosynthetic pathways (C3, C4 and CAM) can be identified from their *n*-alkane $\delta^{13}C$ values (Freeman et al., 1990). C3 plants have lower $\delta^{13}C$ values (e.g. trees, shrubs, temperate grasses; mean $\delta^{13}C$ = -27 ‰) than those using the C4 pathway (most tropical grasses; mean $\delta^{13}C$ = -13 ‰). CAM plants are uncommon except in arid regions and their $\delta^{13}C$ values are intermediate between C3 and C4 plants. In C3 and C4 plants, variations of several per mil in $\delta^{13}C$ may also be controlled by environmental factors such as water availability and light (Ehleringer et al., 1991), and some studies have also suggested that $\delta^{13}C$ signatures can be correlated with environmental parameters such as mean annual precipitation and aridity (Miller, 2001; Van de Water et al., 2002; Vogts et al., 2012).

The GDGTs are organic compounds occurring in membranes of archaea and bacteria, which have been recently used due to their potential as biomarkers and proxies (Schouten et al., 2000; Smith et al., 2012; Taylor et al., 2013). The isoprenoid GDGTs (isoGDGTs) have been widely found in the marine environment (Kim et al., 2008; Schouten et al., 2002), peat bogs (Pancost et al., 2000; Schouten et al., 2000) as well as in lake sediments (Powers et al., 2010; Woltering et al., 2012). The branched GDGTs (brGDGTs), have been identified in peat bogs (Stefan Schouten et al., 2000; Weijers et al., 2006), soils (Weijers et al., 2007), coastal sediments (Hopmans et al., 2004; Huguet et al., 2015) and lake sediments (Loomis et al., 2011; Tierney & Russell, 2009). However, the exact biological sources of brGDGTs

remain enigmatic, although there are indications that they may be sourced by Acidobacteria (Sinninghe Damsté et al., 2011, 2014). The study of the GDGT distributions in sediments has led to the development of the TEX_{86} index to reconstruct past sea surface temperature (SST) (Schouten et al., 2002) or lake surface temperature (LST) (Powers et al., 2010),and the MBT/CBT indices to estimate mean annual air temperature (MAT) and soil pH (Peterse et al., 2012; Weijers et al., 2007).

3.2. Material and Methods

3.2.1. The study area and sample collection

Lake Montcortés is located in the Pre-Pyrenees in northern Spain, a boundary climatic region under the influence of Mediterranean and sub-montane belt climates (Vigo and Ninot, 1987). The lake's catchment is small and characterized mainly by Triassic limestones, marls and evaporites and Oligocene calcareous conglomerates (Corella et al., 2010). Woodland formations, herbaceous vegetation and shrubbery lands are present in the catchment (Rull and Vegas, 2015).

From September 2013 to November 2014, 44 soil samples were monthly obtained from three locations (Ms1-Ms3) with different land use and vegetation covers in the lake Montcortés catchment (Fig. 2-8). In January 2015, three more soils (Ms4-Ms6) were collected to study the heterogeneity of the biomarker signatures in the catchment. For each soil sample, three replicates were collected at least 2m apart from each other within a 10m radius area from an area of 20cm × 20cm and a depth of 5cm, after removing leaf litter and clearing the surface from any visible traces of vegetation. The soils were placed in an pre-combusted aluminium tray within zig-closure plastic bags and stored at ambient temperature. Once in the lab, the samples were homogenized, freeze-dried, ground, and sieved through a mesh size of 2 mm. Then the dry samples were stored in a cupboard in a basement storage room (ICTA, UAB). For details on the measurement of soil pH and TOC see Chapter 2.

The locations of plant sampling are marked in Fig. 2-8. A total of 14 specimens of major plant leaves in the catchment were collected in September 2015. For each species, the sample was taken from three different individuals which were 5 m apart from each other. The leaves were obtained from 1.5 m height in the shadow and sunny areas. Once in the lab, the leaves were cleaned with deionized water, freeze dried, and ground into a fine powder.

Five surface sediment cores were retrieved in February 2013 by a gravity core sampler and the surface 2 cm were taken to characterize the lake's surface sediments signatures.

3.2.2. Sample preparation

Lipids were extracted from 2-8 g prepared soil samples or from 0.1-0.9 g plant leaves by microwave extraction with a mixture of 30 mL of dichloromethane:methanol (3:1, v/v, ×3) using a CEM-MARS microwave accelerated solvent extractor at 70 °C for 5 minutes. After cooling to room temperature, the total extract was evaporated to near dryness using a rotary evaporator and then was fractionated over an aminopropyl silica column using 12 mL dichloromethane:isopropanol (2:1, v/v; F1) and 15mL diethyl ether:acetic acid (96:4, v/v; F2). F1 fraction was then eluted through a silica column using hexane (6 mL, *n*-alkanes), dichloromethane (4mL, alketone) and dichloromethane:methanol (95:5, v/v, 6mL, GDGTs)(see more details in Chapter 2). The *n*-alkane fraction was dried and redissolved in isooctane before injection. The GDGT fraction was dried using centrifugal concentrator at 27 °C, and redissoved in a mixed solution of hexane:isopropanol (99:1, v/v), and filtered with a 0.45 μm PTFE filters before injection.

3.2.3. *n*-Alkane and GDGT analyses

The *n*-alkane extract was injected in splitless injection mode using an autosampler into an Agilent 7820A GC using hydrogen as a carrier gas with a constant flux of 2 mL/min. Quantification of *n*-alkanes was calculated with an internal standard (hexatriacontane, C_{36}) (see details in Chapter 2). The compound specific $\delta^{13}C$ was measured using a gas chromatography coupled to an isotopic ratio mass spectrometer (Thermo Delta V), and the $\delta^{13}C$ values are reported in per mil (‰) relative to the Vienna Peedee Beleminte (V-PDB). The standard deviations of carbon isotope are better than 0.5‰.

GDGTs were quantified by injecting 5-20 μL aliquots in an HPLC (Agilent) hyphenated to an Agilent Time-off-Flight (TOF) mass spectrometer with an atmospheric pressure chemical ionization (APCI) interface set in positive mode. Following the methods (Escala et al., 2007; Huguet et al., 2013), the extracts were eluted through a Tracer Excel CN column (Teknokroma; 20 cm length, 0.4 cm diameter and 3 μm particle size) equipped with a precolumn filter and a guard column. The mobile phase was eluted with hexane:n-propanol (98.5:1.5) at a flow of 0.6 ml/min and the parameters of the APCI interface were set as follows to generate positive ion spectra: corona discharge 3 μA, vaporizer temperature 400

°C, sheath gas pressure 49 mTorr, auxiliary gas (N_2) pressure 5 mTorr and capillary temperature 200 °C. GDGTs were detected in selected ion monitoring (SIM) mode of $[M+H]^+$ ± 0.5 m/z units to increase signal to noise ratio at the following at m/z (Schouten et al., 2007): 1302, 1300, 1298, 1296, 1292, 1050, 1048, 1046, 1036, 1034, 1032, 1022, 1020, 1018 and the synthetic tetraether lipid (GR) at 1208 m/z, which was used as the internal standard (see details in Chapter 2).

3.2.4. Biomarker ratios

A number of indices based in *n*-alkanes and GDGTs relative abundances are described in the literature, and oftimes purporte to relate to environmental variations of temperature, humidity and source inputs (e.g. Bush and McInerney, 2013). In here, the following have been used:

The average chain length (ACL) of *n*-alkanes was calculated according to Eglinton and Hamilton (1967):

$$ACL = (25\times C_{25}+27\times C_{27}+29\times C_{29}+31\times C_{31}+33\times C_{33})/(C_{25}+ C_{27}+C_{29}+C_{31}+C_{33}) \quad (eq.3.1)$$

The carbon preference index (CPI) was calculated according to Bray and Evans (1961):

$$CPI=0.5\times [(C_{25}+ C_{27}+C_{29}+C_{31}+C_{33})/(C_{24}+ C_{26}+C_{28}+C_{30}+C_{32})+(C_{25}+ C_{27}+C_{29}+C_{31}+C_{33})/(C_{26}+C_{28}+C_{30}+C_{32}+C_{34})] \quad (eq.3.2)$$

P_{aq} was first proposed by Ficken et al. (2000) to separate submerged/floating aquatic macrophyte inputs from emergent and terrestrial plant input to lake sediments. It is defined as follows:

$$P_{aq}=(C_{23}+C_{25})/(C_{23}+C_{25}+C_{29}+C_{31}) \quad (eq.3.3)$$

The following isoGDGTs ratio has also been calculated as defined by (Schouten et al., 2002):

$$TEX_{86}=(GDGT\text{-}2+GDGT\text{-}3+GDGT\text{-}4')/(GDGT\text{-}1+GDGT\text{-}2+GDGT\text{-}3+GDGT\text{-}4') \quad (eq.3.4)$$

When TEX_{86} are analyzed for reconstructing Sea surface temperature (SST), the relationship between the TEX_{86} and SST was defined as following:

$$SST = 81.5 \times TEX_{86} - 26.6 \text{ (standard error (s.e.) = 1.7 °C)} \quad (eq.3.5)$$

The lake surface water (LST) calibration equation is as following with the removal of some lakes with cren/brGDGT ratio >0.5, showing a mean square error of 0.058, resulting in a mean error of 3.6 °C:

$LST = -14 + 55.2 \times TEX_{86}$, $R^2 = 0.86$ *(eq.3.6)*

The ratios derived from brGDGTs were defined as:

MBT=(Ia+Ib+Ic)/(Ia+Ib+Ic+IIa+IIb+IIc+IIIa+IIIb+IIIc) (Weijers et al., 2007) *(eq.3.7)*

MBT' = (Ia+Ib+Ic)/(Ia+Ib+Ic+IIa+IIb+IIc+IIIa) (Peterse et al., 2012) *(eq.3.8)*

CBT=-Log((Ib+IIb)/(Ia+IIa)) =3.33-0.38×pH (n=114; R^2=0.7) (Weijers et al., 2007) *(eq.3.9)*

The two calibration equations based on global soil dataset were defined as: *MAT=0.122+0.187×CBT+0.02×MAT (R^2=0.77) (Weijers et al., 2007) (eq.3.10)*

MAT=0.81-5.67×CBT+31×MBT´ (R^2=0.59) (Peterse et al., 2012) (eq.3.11)

The former (eq.10) is with the calibration error <5°C and the latter gives lower correlation coefficient but more absolute values to the instrumental temperature (Peterse et al., 2012).

3.3. Results and discussion

3.3.1. Environmental parameters in soils

In our study catchment, soils had a variety of water content ranging from 13.1% (Ms1) to 66.3% (Ms6) with a mean of 30.6±6.7%. The mean soil organic carbon (SOC or TOC) varied from 5.4% to 31.7% (mean 14.0±3.2%) (Table 3-1). Soil pH ranged from 6.6 to 8.1, which is from near neutral to moderately alkaline (Appendix 2). Soil pH seems to be affected by climatic variables (dry/humid or cold/warm conditions), original bedrocks (granitic areas or calcareous parent material) soil textures (such as sand or clay) as well as land use patterns (ESDAC, 2010), while soil water content relates to precipitation, soil texture and structure and covers.

Table 3-1 Water content, TOC, pH and distribution of GDGTs in soils and surface sediment ("-" no data)

Soils	Water content %	TOC %	pH
Ms1	34,2	15,0	7,2
Ms2	27,8	10,8	7,0
Ms3	13,7	8,4	7,9
Ms4	13,1	5,4	-
Ms5	28,3	12,8	-
Ms6	66,3	31,7	-

3.3.2. *n*-alkanes

3.3.2.1. Spatial heterogeneity of *n*-alkane signatures in soils

The concentration and distribution of *n*-alkanes homologues are shown in Table 3-2. Concentrations of *n*-alkanes varied between 57 and 259 µg/g TOC in soils. It appears that shrubbery grassland had the highest concentration of *n*-alkanes in soils (Ms3), followed by woodland (Ms2 and Ms6) and cropland/sparse grassland (Ms4 and Ms5), suggesting that the *n*-alkanes abundance in the soils might be highly related to overlying vegetation (Schäfer et al., 2016). It is noticeable that low reported *n*-alkanes concentrations are from Ms4 and Ms5, which we interpret that is due to the effects of human plowing (Ms4) and lack of sufficient vegetation cover (Ms5), respectively. All n-alkane distributed within the range from nC_{25} to nC_{35}, just a few contributions from the short chain *n*-alkanes, reflected by C_{23}/C_{29} ratios within 0.04-0.08 for all soils. Besides, all grass soils exhibited maximum abundance at nC_{31} and woodland soils at nC_{29} except Ms4 which showed nearly the same abundance at nC_{29} or nC_{31} alkanes. The average chain length (ACL) ranged from 28.5 to 30.1 and the carbon preference index (CPI) values for nC_{25}~nC_{33} alkanes ranged from 4.2 to 11.4 (Table 3-2), indicating *n*-alkanes in the catchment soils are mainly from terrestrial higher plants. The two lowest CPI values from Ms4 and Ms5 were due to the higher abundance of nC_{28} alkane, which might be related to tractor plowing or aeolian oil contamination .

Table 3-2 Relative abundance of odd chain n-alkane homologues and ratios in soils and surface sediments

	C_{23}	C_{25}	C_{27}	C_{29}	C_{31}	C_{33}	**Total weight of *n*-alkanes**	CPI_{22-34}	ACL_{25-33}	C_{23}/C_{29}	P_{aq}
Soils	%	%	%	%	%	%	µg/g $_{TOC}$				
Ms1	1,0	2,3	8,0	25,7	39,4	14,6	167	9,9	30,1	0,04	0,05
Ms2	1,9	11,1	22,3	32,8	19,1	4,5	164	11,4	28,5	0,06	0,20
Ms3	0,9	2,0	9,3	23,2	35,2	18,1	259	7,9	30,1	0,04	0,05
Ms4	0,8	2,6	18,4	24,3	24,4	12,1	57	4,2	29,6	0,06	0,05
Ms5	1,2	3,2	14,7	24,5	30,4	10,7	75	5,2	29,7	0,08	0,06
Ms6	0,7	4,0	15,9	47,2	22,2	2,0	154	11,1	29,1	0,06	0,05
Surface sediment											
S1-5	11,5	11,5	16,4	23,9	18,4	5,4	1	8,9	28,8	0,15	0,35

3.3.2.2. Seasonality of *n*-alkane signatures in soils

In order to study the seasonality of *n*-alkanes in soils we explored the concentrations and ratios of *n*-alkanes within Ms1-Ms3 during one year (Fig. 3-1). The concentration of *n*-alkanes did not vary by much between months in any of the soils. Clearly, carbon annualy fixed by plants does not change by much the mean seasonal values of the soil carbon pool. i.e. the leaf wax *n*-alkanes contents. The standard deviation (SD) of ACL was 0.13, 0.46 and 0.18, in Ms1, Ms2 and Ms3, respectively. These values are larger than the seasonal change range (0.12) of leaf wax *n*-alkanes ACL observed in evergreen oak tree during its growing period (Sachse et al., 2015). We think that the ACL variability in Ms1 and Ms3 were due to heterogeneity of *n*-alkanes in soils while the ACL values in Ms2 might be related to new inputs of plants because the maximum ACL in April was consistent with the lowest *n*-alkanes concentration and the smallest P_{aq} index, which was highly correlated to ACL values in this soil without the April one (R^2 =-0.95, data not shown). For this month, we think the soil sample might be from another specie of tree that sheds leaves in April , showing low *n*-alkanes production and abundant in longer-chain homologues. Therefore, given the relative constant trends of *n*-alkanes concentrations, ACL and P_{aq} indices in each soil site during the

sampling period it does appear that the effect of seasonality in driving *n*-alkanes distributions could be considered negligible, or too subtle to be revealed from our data.

A study of 150-year soil records from Rothamsted Classical Experiment showed that the lipids components of the soil appear to reflect an input of *Quercus* derived organic matter combined with extant lipids possibly derived from vegetation which grew previously at the site, indicating molecular signals from the earlier vegetation could be still apparent 118 years after reversion (Evershed et al., 1998). Later, results from three sites in Germany and France growing different maize suggested that turnover times for long *n*-alkanes (such as C_{29}, C_{31}) were on average 60 years in silage-maize cropped soils but 35 years in grain-maize cropped soils (Wiesenberg et al., 2004). We think that in our study, the relatively stable ACL values in soils Ms1 and Ms3 could be due to the presence of high quantities of refractory fossil organic matter which might result from the occurrence of very long turnover times of *n*-alkanes (Wiesenberg et al., 2004). Arguably, in soil Ms2, the *n*-alkanes turnover times may be shorter due to a higher plant biomass inputs from deciduous trees, leading to more changeable ACL on a seasonal basis than in the other two soils. However, at this stage we can only speculate on the size of the fossil *n*-alkane pool in the soils, in the absence of radiocarbon ages of these components.

The CPI values were more variable than other indices. However, there were no consistent trends for the three soil. Ms1 showed the lowest values in October and March-June but the highest in September and December. Ms2 presented low values in December/July (with the exception of April that we discussed above) but highest values in September/November/February. Ms3 showed generally lower values than other two soils throughout the year, which was against observations from China that aridity is a dominating climate factor in controlling soil CPI value (negatively) with a large gradient of regional aridity (Luo et al., 2012) because Ms3 showing lowest CPI values is located on the slope with least soil water content. In Ms3 itself, low values were apparent in November and slightly higher values from May to October, which might be dependent on temperature.

Thus, we interpret that the inter annual variability of both *n*-alkanes concentration and distribution patterns in our study soils are not capable to reflect environmental parameters on a short-time scale (monthly or seasonally) together. Therefore, the soil samples taken each month during one year are likely to be replicates of the soils that accumulate over a long time (20 years) (Weijers et al., 2011). However, slight changes of ACL or CPI values between three soils or variations within a specific soil itself seemed to reveal some climatic effects on

n--alkanes, but how fast *n*-alkanes replace in the catchment soils have to be determined, which may give evidence to that CPI values of leaf wax long-chain *n*-alkanes have/not potential to be used as paleoclimatic indicator only turnover times of *n*-alkanes in soils are within the resolution scales that depend on targeted geological time scales.

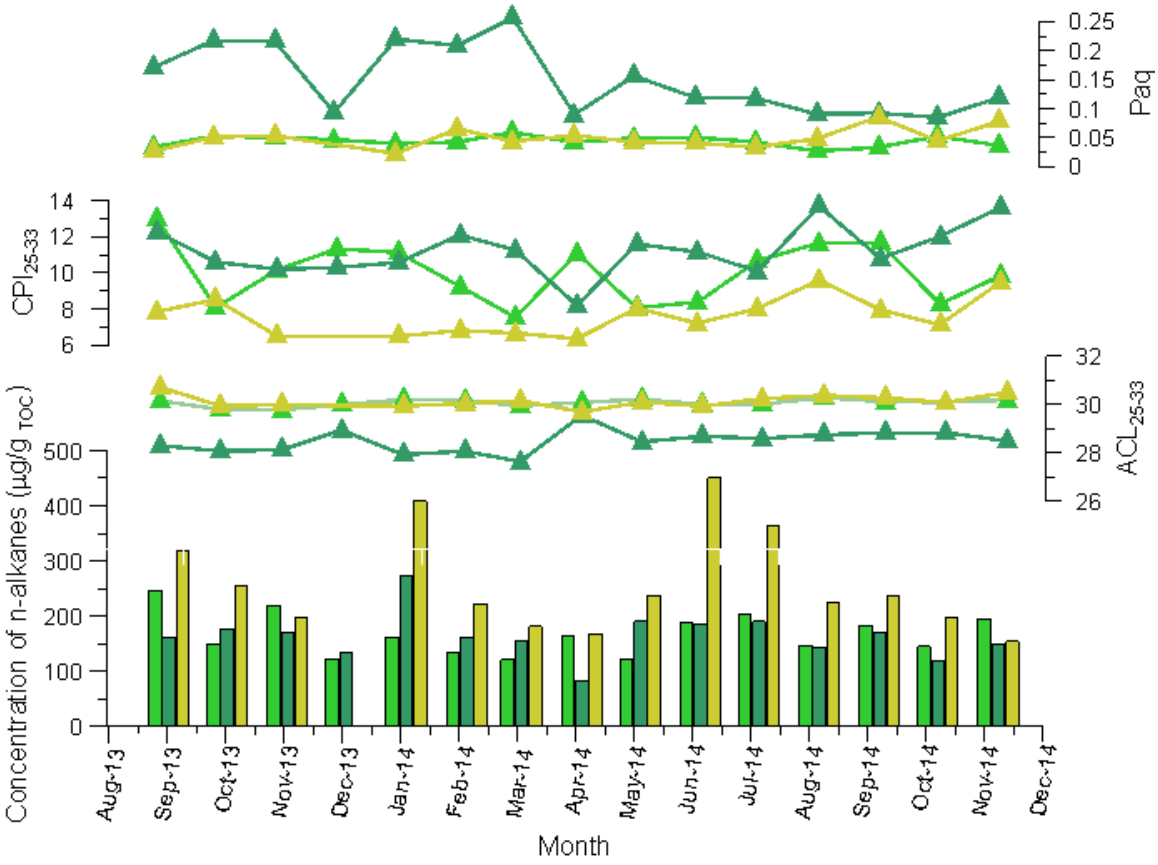

Figure 3-1 Concentration of *n*-alkanes, average chain length (ACL) and Carbon preference index (CPI) from three soils in the Lake Montcortés catchment from September 2013 to November 2014

3.3.2.3. Heterogeneity of *n*-alkane signatures in plants

The plant material is an important composition of soil lipids. The plant names and types collected in the catchment are shown in Table 3-2. The samples could be divided into woodland plants, grasses, emergent macrophytes and submerged macrophytes (Table 3-1). Moreover, the woodland samples can be separated into angiosperms species and gymnosperms species. The magnitude in the variability of n-alkanes concentrations for each species was strikingly different, ranging from 12 to 691µg/g dry leaf (Table 3-3), which is in the range of literature studies (Ficken et al, 2000; Diefendorf et al., 2011a; Schäfer et al., 2016). It is notable that *Pinus nigra J. F. Arnold subsp. salzmannii (Dunal) Franco*, the only

gymnosperms species we collected, presented the lowest concentration of *n*-alkanes. This difference in *n*-alkane production means that angiosperms are likely to be the main potential source of the local soil organic matter as conifer needles generally produce lower *n*-alkane abundance (Bush & McInerney, 2013; Diefendorf et al, 2011; Schäfer et al., 2016). There were also clear variations of *n*-alkane concentration within the same vegetation family, such as Salicaceae (*Salix spp. and Mesophile aspen stands*) and Fagaceae (*Quercus pubescens and Quercus rotundifolia Lam.*) (Table 3-3, Table 2-1). Moreover, the abundances between two *Quercus* types in the same plant family support former results that evergreen vegetation is likely to produce more amount of *n*-alkanes than those of deciduous plant (Diefendorf et al., 2011).

Table 3-3 The *n*-alkane concentration, ratios and carbon isotopes of different vegetation specimens in the Lake Montcortés catchment

No.	n-alkane concentration	ACL	CPI	C_{23}/C_{29}	P_{aq}	C_{25}	C_{27}	C_{29}	C_{31}
	µg/g dry leaf					$\delta^{13}C$ values of n-alkanes (‰)			
P1	365	27,7	27,84	0,03	0,09	-31,5	-30,6	-30,6	n.d.
P2	126	29,0	11,95	0,01	0,05	-32,7	-33,1	-33,7	-34,3
P3	395	28,5	10,16	0,03	0,12	-32,4	-32,8	-33,8	-35,2
P4	12	28,3	3,64	0,19	0,20	-34,0	-31,4	-30,9	n.d.
P6	260	26,3	13,15	0,77	0,41	-37,1	-36,2	-32,4	n.d.
P13	409	30,8	12,83	0,05	0,02	n.d.	-39,8	-39,9	-39,0
P7	152	27,9	8,44	0,02	0,07	n.d.	n.d.	-29,0	n.d.
P8	691	30,5	17,38	0,02	0,01	n.d.	-32,6	-31,6	-31,2
P5	49	31,6	28,30	0,16	0,19	-34,0	-33,8	-36,6	-37,2
P9	296	29,6	13,37	0,02	0,05	-36,3	-36,9	-38,5	-38,0
P14	19	29,1	13,27	0,04	0,07	-33,1	-33,0	-33,5	-33,5
P10	142	27,5	15,43	0,27	0,29	-34,9	-36,1	-36,0	-36,1
P11	86	27,7	5,65	0,14	0,20	-32,3	-32,2	-32,9	-33,1
P12	25	25,5	6,85	3,96	1,06	-24,8	-29,3	-32,8	-33,6

"n.d." indicates data not detected

The *n*-alkane distribution profiles were used to trace their various putative sources. Thus, short chain *n*-alkanes (C_{15}-C_{19}) are derived from algae (Gelpi, Schneider, Mann, & Oró, 1970), submerged/floating macrophytes have increased abundances of middle chain *n*-alkanes (C_{21}-C_{25}) (Ficken et al., 2000), while emergent macrophytes (Mead et al., 2005) and terrestrial higher plants (Eglinton and Hamilton, 1963) have higher carbon number *n*-alkanes, i.e. at carbon numbers nC_{27} and nC_{29} , while grasses have as most abundant the nC_{31} or nC_{33} alkanes (Bush & McInerney, 2013). In this study, most terrestrial woody plants *n*-alkane distributions maximize at nC_{29}, except two *Salicaceae* family plants maximizing at nC_{27}, while

Ash tree and *Genista scorpius* were dominated by nC_{31} alkane (Table 3-3). And grasses maximize at longer chain *n*-alkanes, such as nC_{31} or nC_{33} and only a little contribution from shorter chains (≤ nC_{23}). Emergent macrophytes around the lake fringe maximized at nC_{29}, and also abundant at nC_{27}. The submerged macrophyte (*Myriophyllum spicatum*) are dominated by nC_{25} and nC_{23}, yielding only slight abundance to long chain length *n*-alkanes.

Regarding to composition of *n*-alkanes, ACL values for emergent and submerged macrophytes were shortest, around 27.6 and 25.5, respectively. But ACL values for woody plants and grasses ranged between 26.3-30.8 and 29.1-31.6, respectively. There were overlaps between each end of woodland ACL. However, the distribution of overlapped parts (e.g. *Ash trees* or *Salix spp.*) only occupy very small area according to the investigation of vegetation cover in Lake Montcortés catchment (Mercadé et al., 2013), indicating that ACL combined with nC_{29}/nC_{31}, nC_{23}/nC_{29} for distinguishing woodland trees and grasses might be applicable in our study area.

Long-chain *n*-alkanes from lower organisms (such as green algae) have short-chain lengths and do not have odd-over-even carbon number predominance (i.e. CPI<1) (Martí et al., 1987), while terrestrial higher plants produce longer chain *n*-alkanes with a marked odd-over-even carbon number predominance (CPI>5) (Eglinton and Hamilton, 1967). In addition, CPI values close to 1 are thought to indicate greater inputs from petrogenic inputs (Killops & Killops, 2005) or marine microorganisms and/or recycled organic matter (Kennicutt et al., 1987). CPI values in our plant samples varied from 3.6 to 27.8 (Table 3-3), showing a large variability of CPI index between different plants, which confirms that it might be difficult to use CPI index as a climatic indicator due to the extreme variability and overlap in its values in modern plants (Bush & McInerney, 2013). However, smaller ranges of CPI values in soils suggest that CPI index might be useful in a given catchment that dominated by special plant specimens that leave dominant plant markers in the soils.

3.3.2.4. Comparison of sediments signatures with those from soils and plants

The average *n*-alkane distributions (from nC_{23} to nC_{33}) of different plant species, soils and surface sediment are shown in Fig. 3-2. The distribution of *n*-alkanes in each soil type showed similar patterns to those in the dominant plants that grow on the corresponding soils. It is apparent that the distribution of *n*-alkanes in the surface sediment was affected by aquatic macrophytes and terrestrial higher plants (directly or through soils) from the

catchment (Fig. 3-2). Even though aquatic macrophytes might produce less *n*-alkanes (Table 3-3), they could still make considerable contribution to the sedimentment due to their location within the lake. The surface sediment mean ACL values of *n*-alkanes are 28.8, which may indicate mixed sources (soils 28.6-30.3, and aquatic plants ≤ 27.6), but the main n-alkanes might be dominated by terrestrial woodland plants (i.e. oak tree) as the ACL values were closer to Ms2. Regarding to the variable values of CPI in plants, even though CPI of *n*-alkanes might decrease from raw leaves to soils as biomarker distribution is affected by diagenetic processes in plant-soil systems (Chikaraishi & Naraoka, 2006), the relative high CPI values indicate that effects from diagenetic processes on CPI values are not significant in our catchment soils. While in the surface sediment, the mean CPI value was 8.9, very close to the mean from sampled soils (8.3). We think that CPI values from plants (directly) or soils to lake sediments never decreased or the decrease was subtle. Some effects on CPI from contaminations from the anthropogenic activity, such as tractor plowing or petrogenic inputs might be negligible in the large pool of leaf wax derived *n*-alkanes.

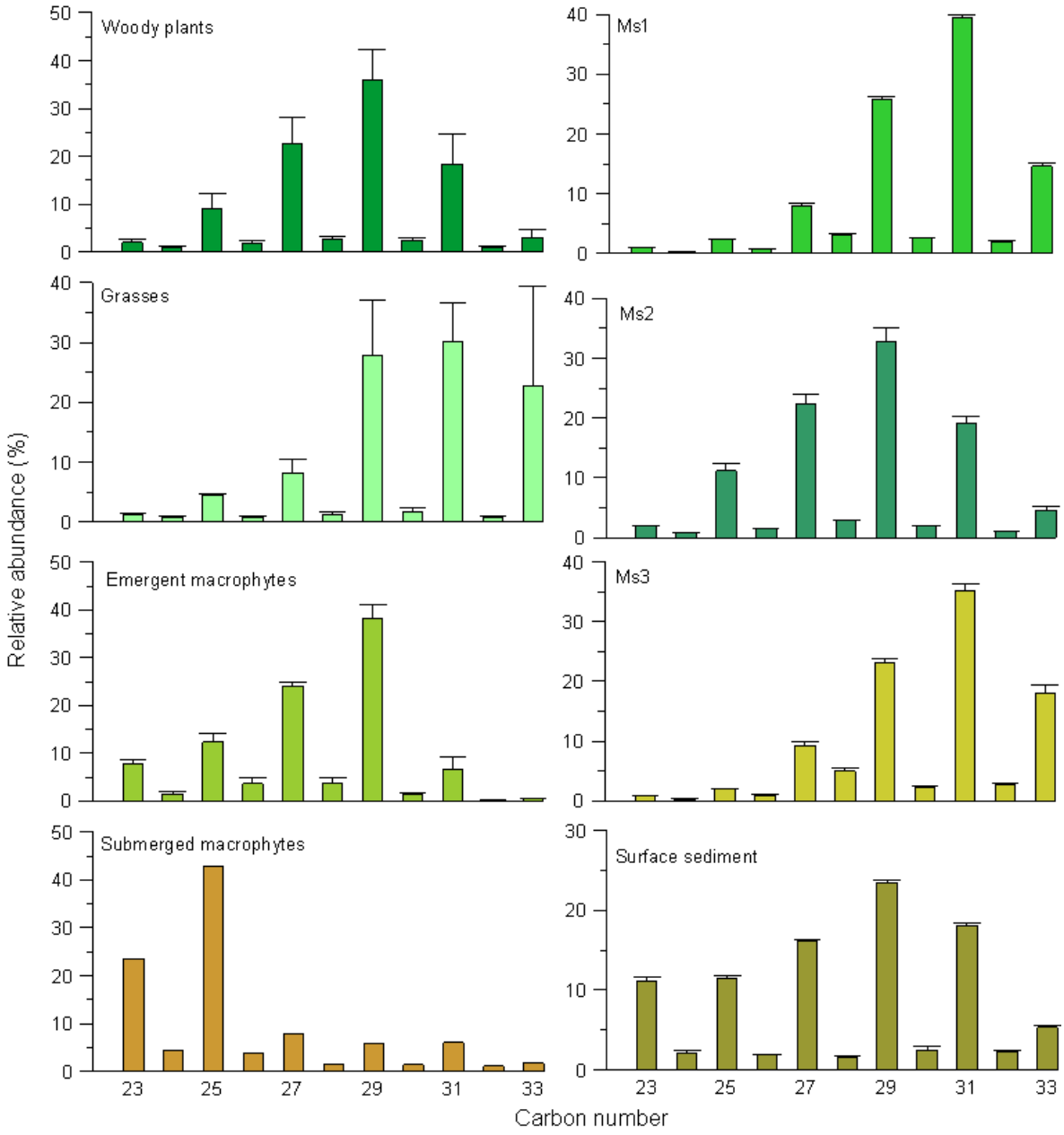

Figure 3-2 Distribution of *n*-alkanes in plants, soils and surface sediments

3.3.2.5. Implications of n-alkane chain length ratios for paleoecology

In the Montcortés lake, the emergent aquatic plants (e.g. typha) have abundant *n*-alkanes at C_{27} and C_{29}, similar to woody plants, in addition to lower carbon chain homologues (Fig. 3-2). A ratio between the abundance of It might be practicable if we apply a proxy combined with short-chain and long-chain *n*-alkanes might allow to discriminate between contributions

to the sediment from aquatic plants and terrestrial plants. This was already assayed using the P_{aq} index (*see eq.3.3*) by Ficken et al. (2000) to separate submerged/floating aquatic macrophytes input from emergent and terrestrial plant input to lake sediment. In Montcortés soils, the P_{aq} values from terrestrial woody plants and grasses were below 0.25 and 0.2, respectively, except for *Mesophile aspen stands* containing a value of 0.84. By comparison, *submerged macrophytes* had a P_{aq} index of 0.85 and emergent aquatic plants held values between 0.26 and 0.35. Therefore, P_{aq}<0.25 corresponds to the end member of terrestrial woody or grass inputs, 0.26-0.35 mostly to contributions from emergent aquatic plants and >0.85 might be ascribed to the end member of submerged macrophytes. This ratio was 0.35 in surface sediment, which can be interpreted as indicating a mixing from contributions of various aquatic end members with those from terrestrial sources. Nonetheless, it discards a dominant contribution of *n*-alkanes from submerged macrophytes (Table 3-2). Thus, a given value of P_{aq} will reflect a particular mixture of inputs from two or more sources (Ficken et al., 2000), making it difficult to disentangle whether the observed changes in *n*-alkane distributions through time are due to the direct influence of climate or climate-driven shifts in the local plant community or species turnover in plant communities (Bush & McInerney, 2013). However, according to the discussion above, it might be feasible to use a combination of different chain length ratios to track *n*-alkane inputs in the lake sediments based on modern vegetation formations and soils. In addition, a more complete understanding of the surrounding vegetation could increase the reliability of applying these ratios to paleoclimatic study.

3.3.2.6. Compound specific $\delta^{13}C$ of *n*-alkanes in plants and soils

Besides the concentration and distribution of *n*-alkanes, we found that most compound specific $\delta^{13}C$ of alkanes from the plant biomarkers were consistent with the general $\delta^{13}C$ distribution of lipid molecules from C3 higher plants (Table 3-3), except for submerged *Myriophyllum spicatum* which showed characteristics of C3 and C4 plants in spite of more similarity to C3 plants (Van & Haller., 1976). As carbon isotope from different plant specimens showed large differences within vegetation type (Table 3-3), we only presented the $\delta^{13}C$ values of major plant species of each vegetation group to show the general $\delta^{13}C$ characteristics (Fig. 3-3). Compound specific $\delta^{13}C$ values of *n*-alkanes from different fresh leaves of plant species record significant covariations along carbon chain. $\delta^{13}C$-depleted values appeared with increasing chain length of *n*-alkanes from -31.0‰ to -34.7‰ for the *Quercus, Phragmites australis* and *Cirsium monspessulanum*. It appears that they have both

similarity in $\delta^{13}C$ values and changing trends from nC_{23}-nC_{31}. *Myriophyllum spicatum* showed $\delta^{13}C$ values varying from -24‰ to -32‰ (Fig. 3-3). Thus, the $\delta^{13}C$ values of plants in our study do not allow distinguishable characteristics among different C3 plants. Our results agree with that increasing $\delta^{13}C$ depletion with increasing chain length that has been frequently reported for specific *n*-alkanes within a given plant sample (Huang et al., 1995; Lichtfouse et al., 1994).

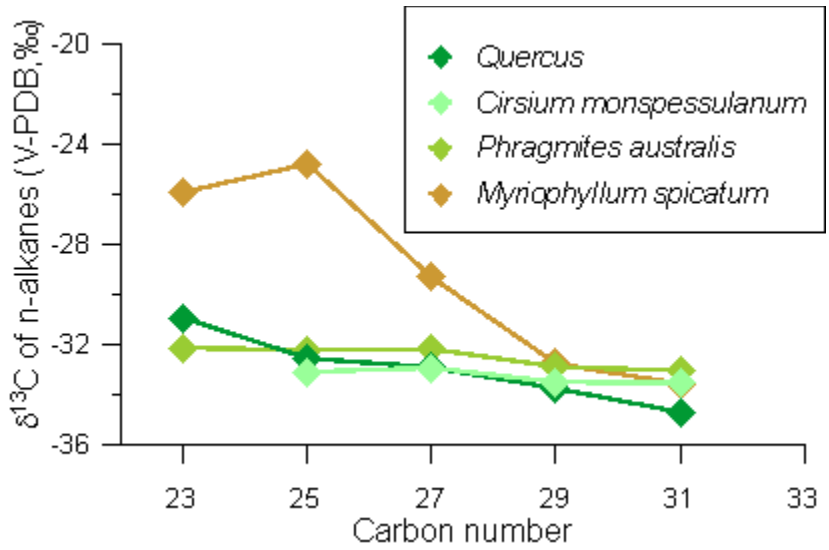

Figure 3-3 The compound specific $\delta^{13}C$ values of different plants

Our results of soils showed that the $\delta^{13}C$ variation during different seasons for individual molecule was very small among three soil samples, especially for nC_{27}, nC_{29}, nC_{31} alkanes (Fig. 3-4). The three compound specific $\delta^{13}C$ of nC_{27}, nC_{29}, nC_{31} alkanes presented values in a range of -33.0‰ to -35.5‰ with mean values about -33.8‰, -34.3‰ and -34.8‰ for Ms1, Ms2 and Ms3 respectively. Ms2 exhibited $\delta^{13}C$ values ranging from -31.2 to -34.0‰ (mean -32.4‰) for the nC_{27} alkane, from -33.1 to -34.5‰ (mean -34.2‰) for nC_{29} alkane and from -34.2 to -35.9‰ (mean -35.2‰) for C_{31} alkane. Ms3 exhibited $\delta^{13}C$ values ranging from -33.2 to -34.3‰ (mean -33.6‰) at nC_{27} alkane, from -33.7 to -34.6‰ (mean -34.2‰) at nC_{29} alkane and from -34.0 to -35.2‰ (mean -34.6‰) at C_{31} alkane. $\delta^{13}C$ of all soil samples yield slight negative values towards increasing carbon chain lengths. These values are very close to $\delta^{13}C$ values from plants (Fig. 3-3), indicating that soils preserve the original $\delta^{13}C$ characteristics of *n*-alkanes of dominant terrestrial plants growing on the soils. Average values of $\delta^{13}C$ at three sites are very similar throughout one year, especially the $\delta^{13}C$ of nC_{29} alkane only varied within 0.1 ‰. Interestingly, the $\delta^{13}C$ difference between different carbon chain length of *n*-alkanes was larger within Ms2 (*Quercus*), about 2.8‰ compared with a

variable value of 1.0‰ in Ms1 and Ms3. This result is consistent with $\delta^{13}C$ features of *Quercus* as well as previous studies on $\delta^{13}C$ of *n*-alkanes during biodegradation that degradative removal of *n*-alkanes is not accompanied with significant stable carbon isotope fractionation (Chikaraishi & Naraoka, 2006; Huang et al., 1997; Pond et al., 2002).

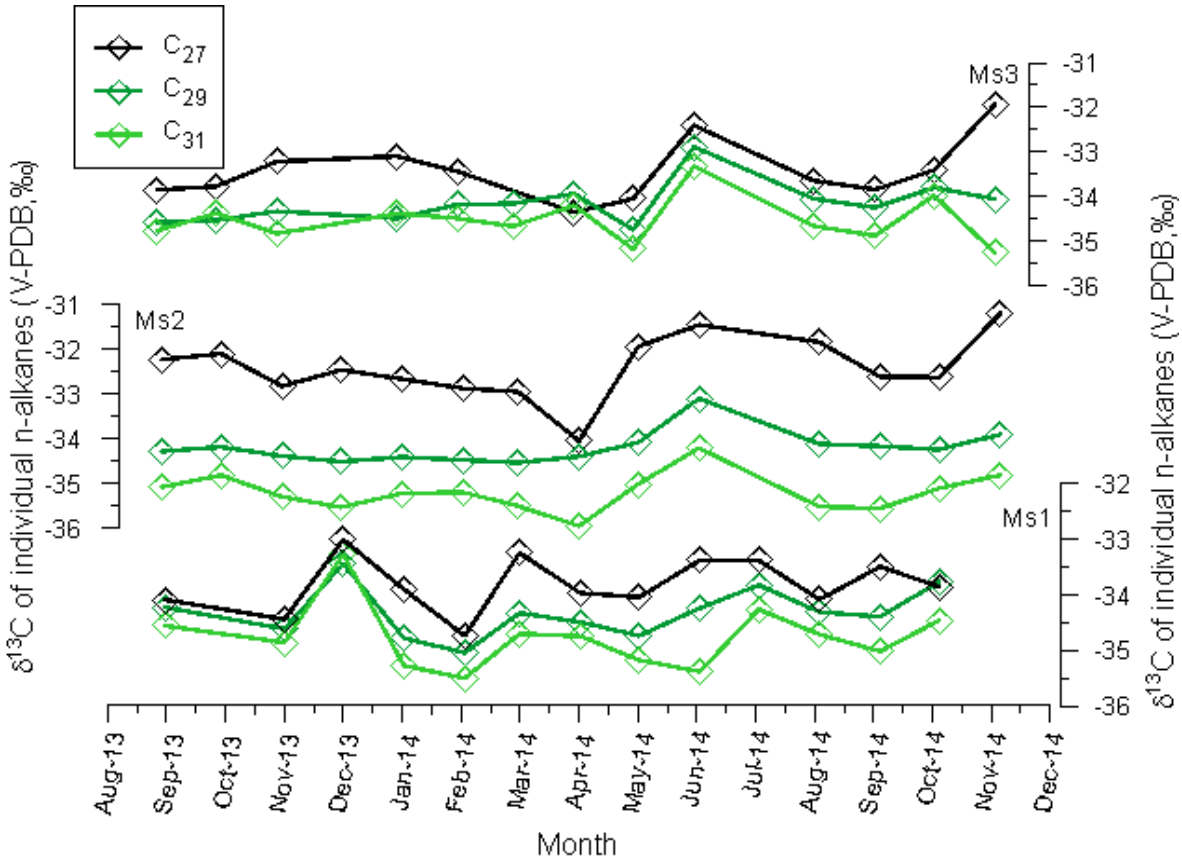

Figure 3-4 Carbon isotopic compositions of *n*-alkanes in soils in lake Montcortés catchment from September 2013 to November 2014

3.3.3. GDGTs

3.3.3.1. Spatial heterogeneity of GDGTs in catchment soils

Soils from six locations (Fig. 2-8) were analyzed to study heterogeneity in GDGT distribution in the Montcortés catchment. Samples from different sites showed variable concentrations of GDGTs, from 0.2 to 31.2 µg/g TOC. The average concentrations of brGDGTs and isoGDGTs were 11.0±4.3 and 0.9±0.3 µg/g TOC in respective (Table 3-4), showing brGDGTs were dominant in soil GDGTs. These values (especially brGDGTs) were

within the range of middle latitude soils reported by Weijers et al.(2010; 2011) and close to the mean values of Pyrenees soils (Rueda, 2013).

Table 3-4 GDGT concentration and ratios in soils and surface sediment

	isoGDGTs	**brGDGTs**	**III**	**II**	**I**	**TEX_{86}**	**CBT**	**MBT**	**MBT´**	**MAT 1**	**MAT2**
Soils	μg/g $_{TOC}$	μg/g $_{TOC}$	(%)	(%)	(%)					°C	°C
Ms1	1,6	17,2	19,9	50,7	29,4	0,66	0,11	0,29	0,30	7,6	9,3
Ms2	0,1	13,2	18,9	49,7	31,4	-	0,45	0,31	0,32	5,4	8,0
Ms3	2,0	2,9	33,0	51,4	15,6	0,75	0,48	0,14	0,16	-3,3	2,6
Ms4	0,1	0,2	35,4	50,0	14,6	0,77	0,28	0,15	0,15	-1,4	3,7
Ms5	0,4	2,5	16,3	50,7	33,0	0,70	0,38	0,33	0,33	6,9	8,9
Ms6	1,0	30,2	28,3	51,3	20,4	-	0,35	0,20	0,21	0,9	5,2
S1-S5	7,3	41,1	31,7	47,1	21,2	0,54	0,41	0,22	0.21	0,6	5,3

"-"data not be calculated

It has been observed that brGDGTs abundance is significantly correlated with mean annual precipitation (MAP) in Iberian soils (Menges et al., 2014). Considering that the local precipitation of multi-year mean is the same for each soil in the catchment, the fact that the brGDGT concentration in soils were variable even in such a small catchment, it indicates that precipitation is not a controlling factor for brGDGT abundance in our soils. While soil content affected by precipitation, soil texture, soil structure might be responsible. In Montcortés, the brGDGT concentrations seemed to be related to soil water content (R^2=0.43, Fig. 3-5a), which is particularly clear when the average brGDGT concentrations and soil water content of the 6 soil sites are considered (R^2=0.87, Fig. 3-5b). This can be interpreted as an indication that humid conditions are more favorable for brGDGT production than dry conditions in soils, which perhaps is not surprising given that the putative producers are bacteria.

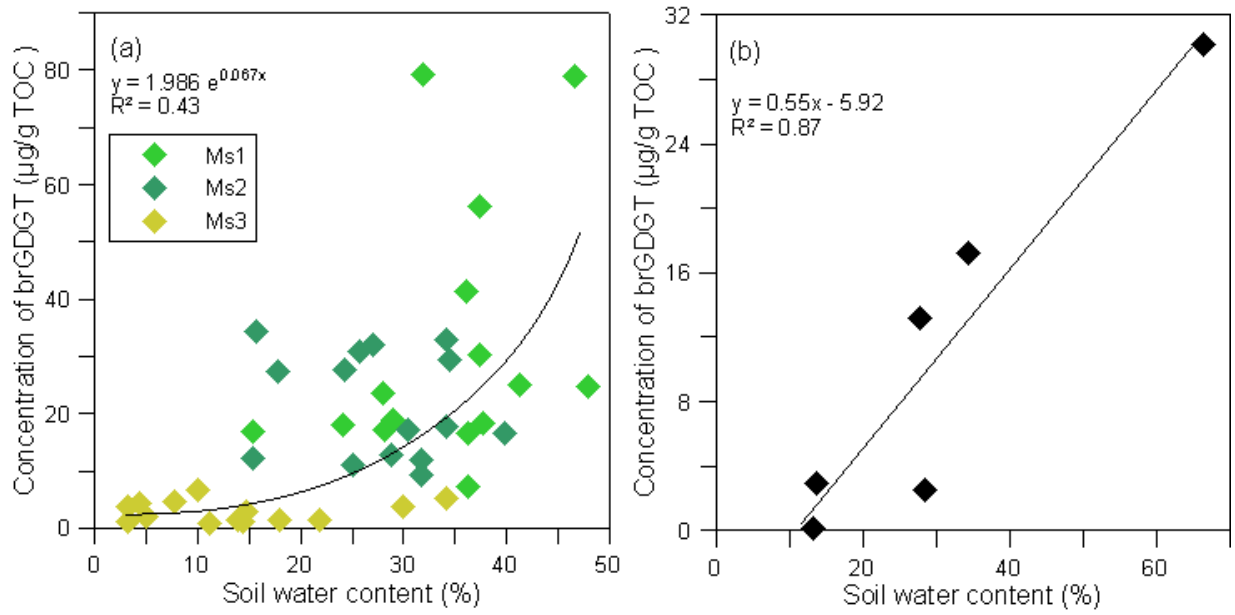

Figure 3-5 The relationship between (a) soil water content and concentration of brGDGTs from three sampling sites throughout the year (September 2013-November 2014), (b) soil water content and brGDGT concentration from 6 sampling sites (Ms1-Ms3 on average).

According to the distribution of brGDGTs in the soils. Two distinctive groups (A and B) can be sorted out (Fig. 3-6). The group A (Ms1, Ms2 and Ms5) was dominated by GDGT-II and GDGT-I, while group B was featured by GDGT-II and GDGT-III. Distribution of brGDGT abundance in the soils seemed not to be affected by vegetation covers as Ms1 and Ms3 was covered by grasses, Ms2 and Ms6 were covered by different types of woodlands. Thus, brGDGT distribution might be partly explained by soil properties (such as soil structure) as group A is located in south-north direction and group B in east-west direction in the catchment which might be controlled by the original geological formation (Fig. 2-8).

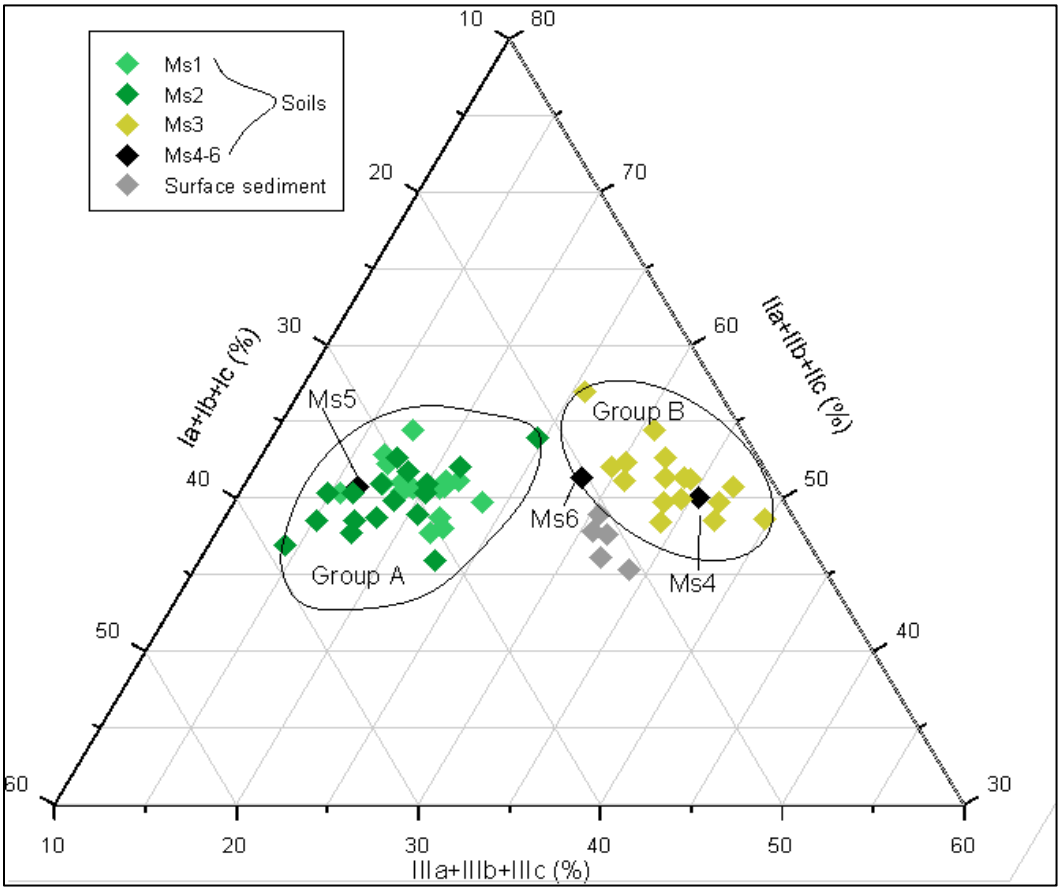

Figure 3-6 Ternary diagrams with relative abundance of GDGT-I, GDGT-II and GDGT-III

In our samples, GDGT-0 and/or GDGT-4 (crenarchaeol) were dominant in the isoGDGTs. In general, GDGT-0 (caldarchaeol) is more abundanct than crenarchaeol in terrestrial soils (Weijers et al., 2006). Crenarchaeol is a specific biomarker for the group 1.1 Crenarchaeota (Sinninghe Damsté et al., 2002), which exists in all study soils and its abundance relative to the total GDGT content was from 0.3% to 17.5% (more alkaline soils) in our soils. This observation is in good agreement with reports by Weijers et al.(2006) that the abundance of crenarchaeol in soils is higher with increasing pH. Besides, crenarchaeol abundance tends to be lower in forest soils (Ms2 and Ms6) than in grass soils (Table 3-1).

3.3.3.2. Seasonality of GDGT concentrations and indices

Samples from three sites in the catchment soil were analyzed to explore the seasonality of GDGT concentrations (Fig.3-7). It is apparent that all three types of soils showed no seasonality and the variability in each soils did not follow a fixed rule, which is likely to be heterogeneous. On a monthly scale, the concentration of brGDGTs varied largely within each soil, e.g. from 4.0 to 43.3 μg/g TOC for Ms1.

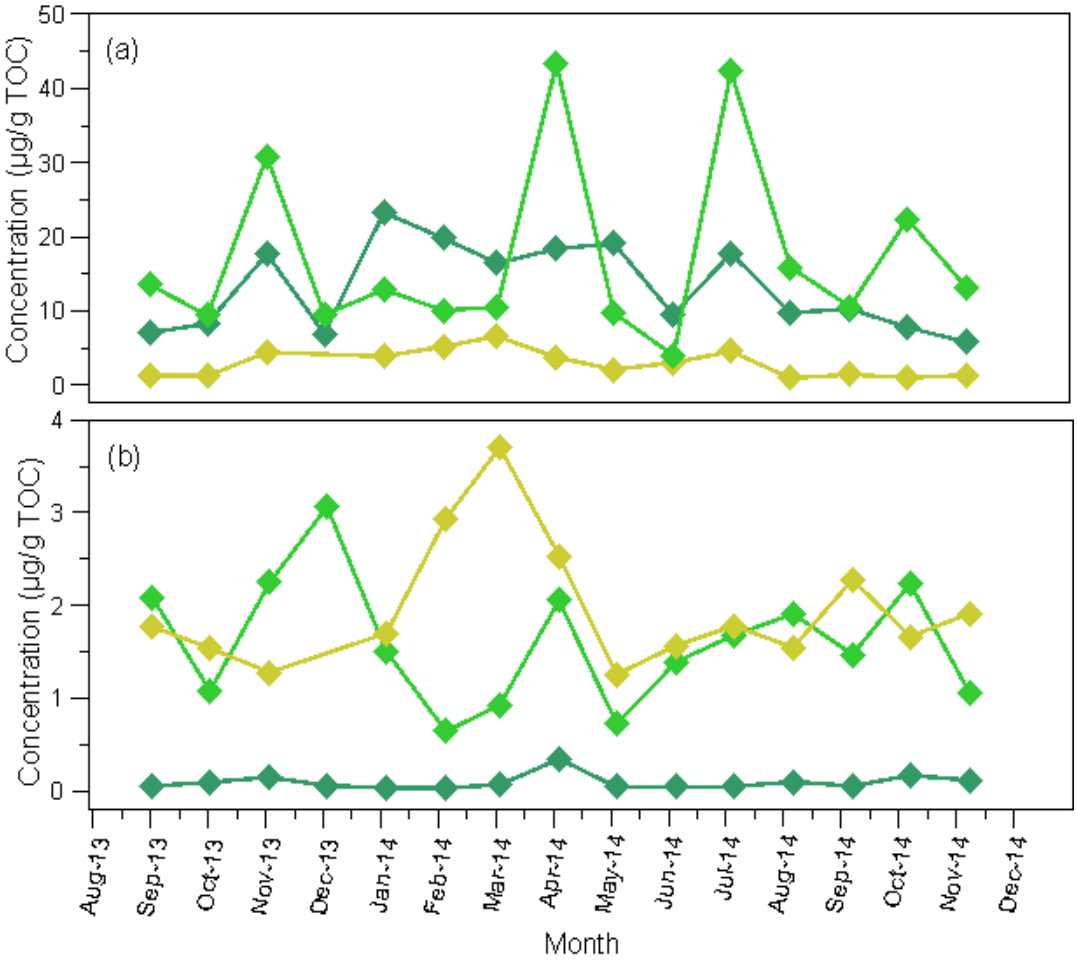

Figure 3-7 Concentrations of brGDGTs (a) and isoGDGTs (b) analyzed in the different soils from September 2013 to November 2014 in the Lake Montcortés catchment. Light green, dark green and yellow diamonds indicate soils from Ms1, Ms2 and Ms3, separately

In a year around, The CBT values ranged from -0.53 to 0.48, from 0.18 to 0.57 and from 0.23 to 0.60 for Ms1, Ms2 and Ms3, separately. Whereas MBT varied slightly within 0.1-0.2 for Ms1 and 0.2-0.4 for Ms3 throughout the year. It is apparent that during the sampling period CBT index varied largely while MBT stayed more constantly (Fig. 3-8).

TEX_{86} was calculated based on isoGDGTs (*eq.3.5*), having values within 0.6 and 0.8 for Ms1 and Ms3 (Fig. 3-8), while TEX_{86} index for Ms2 was not available as specific homologues of isoGDGTs were undetectable. It seems that dry and alkaline soils (such as Ms3) tend to exhibit higher TEX_{86} index. The seasonality of TEX_{86} is small and not be able to reveal seasonal signals (Fig. 3-8).

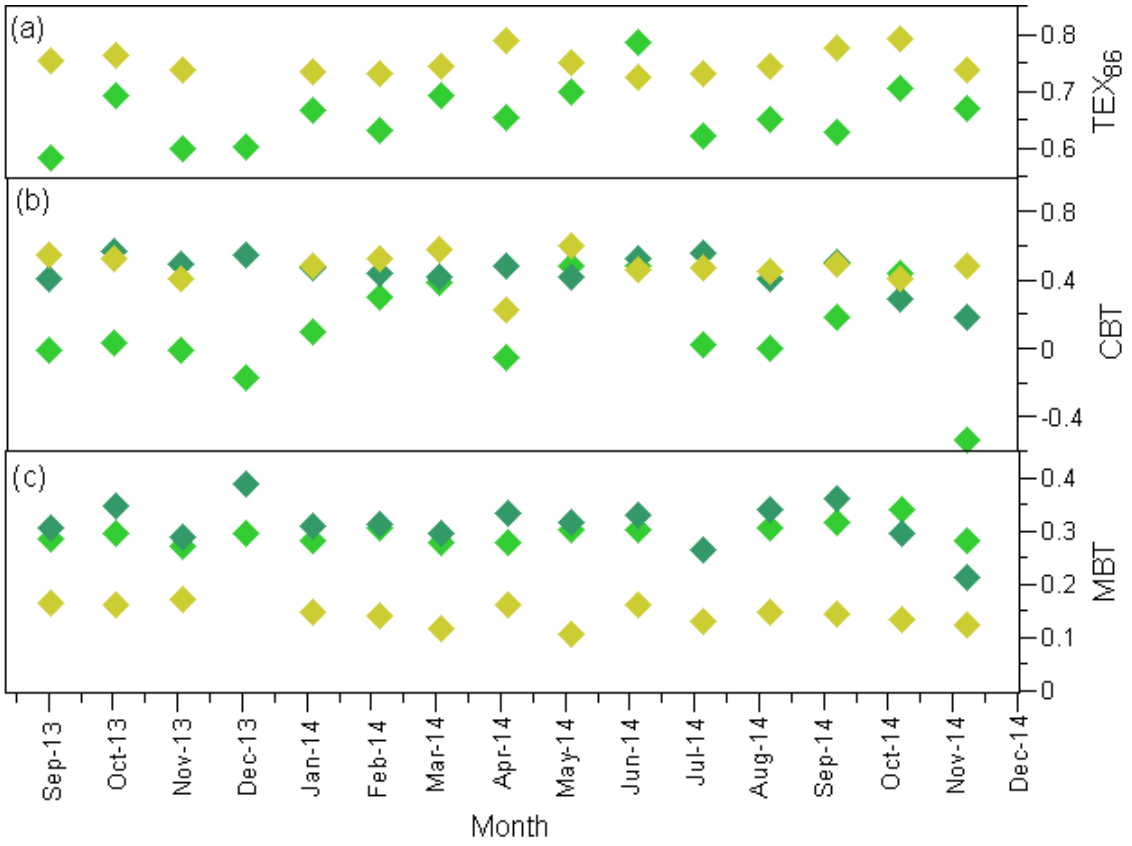

Figure 3-8 Variations of MBT, CBT and TEX_{86} proxies derived from GDGTs in soils during the sampling period (September 2013 to November 2014), the light green, dark green and yellow diamonds indicate for Ms1, Ms2 and Ms3, separately.

3.3.3.3. Comparison of GDGT signatures in surface sediments and soils

The brGDGT distributions in the surface sediment were more similar to the group A soils (Ms3, Ms4 and Ms6) than the group B soils (Ms1, Ms2 and Ms5) (See Fig. 3-6), suggesting that lake sediments got mixed sources of group A and B, but group B soils make more contributions to the brGDGTs in the lake sediment because their closer distributions. Another possibility is that the lake-produced brGDGTs had similar brGDGT distribution patterns as group B soils. The mean MBT and CBT indices were 0.22 and 0.41 in the surface sediment, indicating a mixed signature from soils too (Fig. 3-8).

In the surface sediment, the isoGDGTs were dominated by GDGT-0, followed by GDGT-1, GDGT-2, but with less crenarchaoel, suggesting that addional GDGT-0, 1, 2 were produced in situ in the lake rather than soils derived. Thus in the surface sediment, TEX_{86} index seem to record in situ changes in the lake rather than represent signals from the catchment soils.

However, as crenarchaeol abundance in some soils (such as Ms3) is very high, it can makes a significant contribution to the isoGDGTs sediment pool, which could potentially bias the lake TEX_{86} signals towards warmer signals which are apparent in the soils.

3.3.3.4. Implication of brGDGT-derived index

Previous studies have reported that brGDGTs producers adjust their membrane lipid distributions to soil temperature and pH variations, which were reflected by CBT and MBT indices (Hopmans et al., 2004; Peterse et al., 2012). However, soil temperature is not available in global scale, so mean annual air temperature in the specific region was used for the global soils calibration dataset. Thus a large part of the scatter in the calibration could be attributed to offset between air temperature and soil temperature as well as to the heterogeneity of soils (Peterse et al., 2012; Peterse et al, 2010; Weijers et al., 2007).

MBT/CBT reconstructed temperatures remained constant throughout one year in all soils, and did not follow seasonal changes in temperature in the study area (Table 3-3). MBT/CBT estimates (MAT estimates) based on *eq.3.10* presented mean values from -3.3 to 7.6 °C (mean 2.7±1.7°C) for the catchment soils. MBT/CBT estimates based on *eq.3.11* ranged from 2.6 to 9.3 °C (mean 6.3±1.1°C) in the catchment soils (Table 3-3). It is apparent that the MBT/CBT estimates from Peterse (eq.3.11) are better matching the actual mean annual air temperature (10.6 °C, Corella et al., 2010)) and show smaller errors than MBT/CBT estimates from Weijers's global calibration dataset (eq.3.10). Here, we used eq. 3.11 to reconstruct temperatures (Table 3-3), the average MAT estimates (8.0-9.3 °C) from the group A soils (Ms1, Ms2 and Ms5) are much closer to average instrumental air temperatures than average MAT estimates (2.6-5.2 °C) from the group B soils (Ms3, Ms4 and Ms6). We discussed above that brGDGT distributions in the surface sediment were more similar to the group B soils rather than the group A soils. In this case, brGDGTs in the surface lake would record temperature signals similar to group B soils, which show larger offsets to the actual temperatures. According to the global calibration dataset, the standard error of reconstructed temperatures between group A soils and group B soils was no more than 2.4 °C, which is acceptable on a global scale, but it needs more attention if we use it in a regional/catchment scale where the errors would be amplified based on smaller variations of absolute temperatures. The heterogeneous variability of reconstructed temperature in the catchment soils also suggest that in our catchment, the offset differs with soil types rather than vegetation/water variations.

The estimated temperatures for Ms1-Ms3 soils throughout the year showed mean values of 9.5±0.4 °C, 8.1±0.3 °C and 3.1±0.3 °C, separately, suggesting that the observed variations in different soils were larger than seasonal variations in soil temperatures, which might be affected by soil water content. The absence of seasonal patterns in all three soils agrees with those observations from other mid altitude soils (Weijers et al., 2011) and also in previous study in Norway and the Pyrenees (Rueda, 2013), which they argued to be ascribed to a standing stock of core lipids whose abundance is much higher than new brGDGT productions over a seasonal cycle. It could be argued that brGDGT distributions in soils do not adapt to environmental changes on seasonal time scales and that MAT derived from brGDGTs is a time-integrated signal over several years (depending on turnover time of soil lipids) (Weijers et al., 2011). Therefore, absolute temperatures reconstructed using MBT/CBT index are unlikely to reflect the actual MAT on an interannual scale, but rather interdecadal means. Anyway, this proxy is able to provide reasonable estimates on a global scale, especially when the annual accumulated precipitation was above 500mm per year (Peterse et al., 2012; Weijers et al., 2007), because of a large scale (e.g. globally), the local mean annual air temperature changes even spanning decades could be very small in the same region. Thus, to study temperature changes in the geological time, calibrations based on a regional scale are very important.

Besides MAT, soil pH seems to have an effect on brGDGT distributions (Weijers et al., 2007). The CBT values are highly correlated (R^2=0.72) with in situ pH for each type of soils especially for Ms1 (R^2=0.94) (Fig. 3-9a). However, weaker correlation was found between CBT and measured pH together. We also compared our CBT-pH values with published data in regional and global calibration soil dataset, it shows that our CBT-pH data are generally consistent with regional and global soil dataset. It suggests that CBT was controlled by pH on a large scale (regional or global scale) as a wider pH gradient is needed to confirm the effect of pH on the CBT index (Weijers et al., 2007) and additional environmental parameters affect the degree of cyclisation or a different brGDGT producing community in the Iberian Peninsula soils (Menges et al., 2014). The lack of too high (above 1.5) CBT values in Iberian Peninsula soils might be due to the narrow cover of latitude variability (37-44°N). The significant effect of pH on the CBT index probably occurs within the same soil type, indicating that additional parameters besides pH might influence the CBT index in different soil types.

The MBT values and MBT´ values in our study soils are very similar (nearly at 1:1 line, not shown). A less significant correlation (R^2=0.56) between MBT´ and pH values was present in

the global soil dataset, but a more significant correlation was present for Iberian Peninsula soils (R^2=0.70) (Fig. 3-9b). Therefore, pH is an important factor affecting MBT´ variations of Iberian Peninsula soils containing lower MBT´ values compared with global soils (Menges et al., 2014). Our data confirms that variations of MBT´ index should be linked to pH variations on a regional scale or at least in Iberian soils.

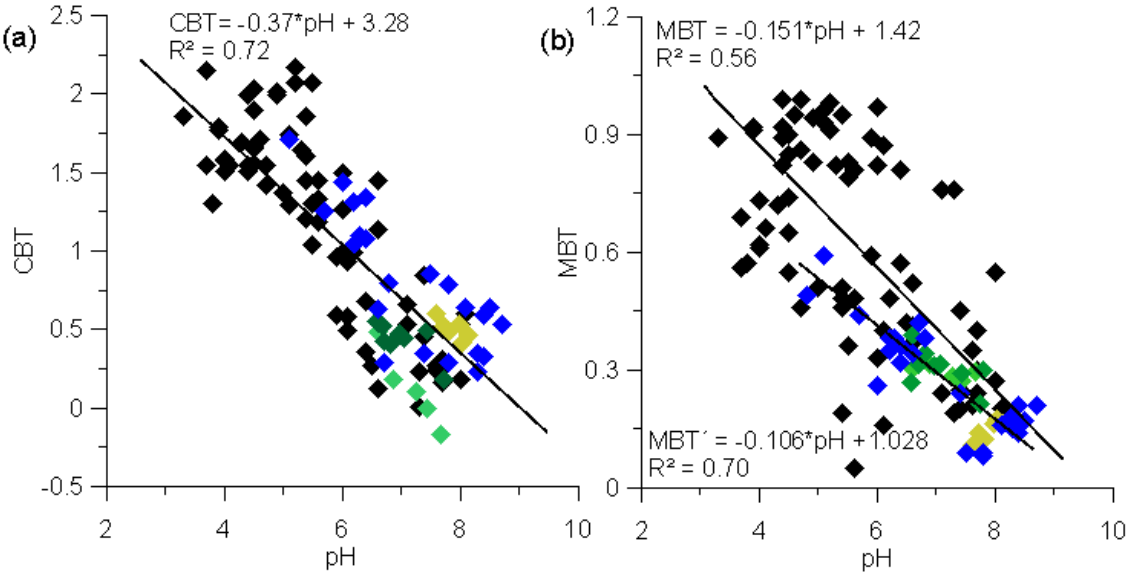

Figure 3-9 Linear regression plots of (a) measured soil pH vs. CBT, (b) measured soil pH vs. MBT. Data plotted in black and blue are from Weijers et al. (2007) and Menges et al. (2014), respectively, data plotted in other colors are from this study.

3.4. Conclusions

n-alkanes abundance in the soils are highly related to overlying vegetation, which is responsible for the heterogeneity of *n*-alkanes concentrations and ACL index, P_{aq} index changes in the catchment soils. No seasonal changes were found in *n*-alkanes concentration and distribution (ACL). While CPI index of plants and soils is too various, which might be related to water soil content, degradation processes as well as anthropogenic inputs. Angiosperms plants (*Quercus*) produce more *n*-alkanes than gymnosperms and should be responsible for long-chain *n*-alkanes signatures in soil and lake sediments. Different plant species showed different $\delta^{13}C$ features of *n*-alkanes, but major plants (*Quercus, Cirsium monspessulanum and Phragmites australis*) in the catchment showed very similar $\delta^{13}C$ values and distributions as C3 plants. *Myriophyllum spicatum* tends to show mixed features of C3 and C4 plants.

The concentrations of brGDGTs and isoGDGTs are various throughout the year. The brGDGTs are less abundant in alkaline and dry soil environments while forest soils seem to be unfavorable for isoGDGTs. Two soil groups were identified according to brGDGT distribution and the surface lake sediment has similar distribution pattern as group B, but the MBT-CBT derived temperatures of group A were much closer to the actual MAT rather than group A soils. The heterogeneity of MBT/CBT estimates in the catchment soil might be affected by soil water content. Besides, the MBT/CBT temperature estimates from the brGDGTs of soil samples do not reflect the air temperature seasonality. TEX_{86} indices in soils tend to show warmer signals, which would bias the signals in the lake sediment if transported into the lake. Soil pH has a significant effect on the CBT and MBT indices in a global scale and higher correlation between pH and CBT occurred in a single soil type.

3.5. Reference

Bush, R. T., & Mcinerney, F. a. (2015). Influence of temperature and C4 abundance on n-alkane chain length distributions across the central USA. *Organic Geochemistry*, *79*, 65–73. doi:10.1016/j.orggeochem.2014.12.003

Bush, R. T., & McInerney, F. A. (2013). Leaf wax n-alkane distributions in and across modern plants: Implications for paleoecology and chemotaxonomy. *Geochimica et Cosmochimica Acta*, *117*, 161–179. doi:10.1016/j.gca.2013.04.016

Chikaraishi, Y., & Naraoka, H. (2006). Carbon and hydrogen isotope variation of plant biomarkers in a plant–soil system. *Chemical Geology*, *231*(3), 190–202. doi:10.1016/j.chemgeo.2006.01.026

Corella, J. P., Moreno, A., Morellón, M., Rull, V., Giralt, S., Rico, M. T., … Valero-Garcés, B. L. (2010). Climate and human impact on a meromictic lake during the last 6,000 years (Montcortès Lake, Central Pyrenees, Spain). *Journal of Paleolimnology*, *46*(3), 351–367. doi:10.1007/s10933-010-9443-3

Diefendorf, A. F., Freeman, K. H., Wing, S. L., & Graham, H. V. (2011). Production of n-alkyl lipids in living plants and implications for the geologic past. *Geochimica et Cosmochimica Acta*, *75*(23), 7472–7485. doi:10.1016/j.gca.2011.09.028

Ehleringer, J. R., Sage, R. F., Flanagan, L. B., & Pearcy, R. W. (1991). Climate change and the evolution of C4 photosynthesis. *Trends in Ecology & Evolution*, *6*(3), 95–9. doi:10.1016/0169-5347(91)90183-X

Evershed, R. P., van Bergen, P. F., Nott, C. J., & Poulton, P. R. (1998). Tracing the origin and fate of lipids in soils from the Rothamsted Classical Experiment. *Tracing the Origin and Fate of Lipids in Soils from the Rothamsted Classical Experiment R.*, *62*, 430–431.

Ficken, K. J., Li, B., Swain, D. L., & Eglinton, G. (2000a). An n -alkane proxy for the sedimentary input of submerged / ¯ oating freshwater aquatic macrophytes, *31*.

Ficken, K. J., Li, B., Swain, D. L., & Eglinton, G. (2000b). An n-alkane proxy for the sedimentary input of submerged/floating freshwater aquatic macrophytes. *Organic Geochemistry*, *31*, 745–749.

Freeman, K. H., Hayes, J. M., Trendel, J.-M., & Albrecht, P. (1990). Evidence from carbon isotope measurements for diverse origins of sedimentary hydrocarbons. *Nature*, *343*, 254–256.

Gelpi, E., Schneider, H., Mann, J., & Oró, J. (1970). HYDROCARBONS OF GEOCHEMICAL

SIGNIFICANCE MICROSCOPIC ALGAE * IN. *Ph6ytochemistry*, *9*(1955), 603–612.

Hopmans, E. C., Weijers, J. W. ., Schefuß, E., Herfort, L., Sinninghe Damsté, J. S., & Schouten, S. (2004). A novel proxy for terrestrial organic matter in sediments based on branched and isoprenoid tetraether lipids. *Earth and Planetary Science Letters*, *224*(1-2), 107–116. doi:10.1016/j.epsl.2004.05.012

Huang, Y., Eglinton, G., Ineson, P., Latter, P. M., Bol, R., & Harkness, D. D. (1997). Absence of carbon isotope fractionation of individual n-alkanes in a 23-year field decomposition experiment with Calluna vulgaris. *Organic Geochemistry*, *26*(7-8), 497–501. doi:10.1016/S0146-6380(97)00027-2

Huang, Y., Murray, M., Eglinton, G., Chimie, L. De, Physique, O., & Cnrs, U. A. (1995). Sacredicene , a Novel Monocyclic C33 Hydrocarbon from Sediment of Sacred Lake , a Tropical Freshwater Lake , Mount Kenya, *36*(33), 5973–5976.

Huang, Y., Shuman, B., Wang, Y., & Iii, T. W. (2004). Hydrogen isotope ratios of individual lipids in lake sediments as novel tracers of climatic and environmental change: a surface sediment test. *Journal of Paleolimnology*, *31*, 363–375.

Huguet, A., Grossi, V., Belmahdi, I., Fosse, C., & Derenne, S. (2015). Archaeal and bacterial tetraether lipids in tropical ponds with contrasting salinity (Guadeloupe, French West Indies): Implications for tetraether-based environmental proxies. *Organic Geochemistry*, *83-84*, 158–169. doi:10.1016/j.orggeochem.2015.02.010

Killops, S., & Killops, V. (2005). *Introdution to Organic Geochemistry* (2nd ed.). Blackwell Science Ltd. doi:10.1002/9781118697214

Kim, J.-H., Schouten, S., Hopmans, E. C., Donner, B., & Sinninghe Damsté, J. S. (2008). Global sediment core-top calibration of the TEX86 paleothermometer in the ocean. *Geochimica et Cosmochimica Acta*, *72*(4), 1154–1173. doi:10.1016/j.gca.2007.12.010

Lichtfouse, ??ric, Derenne, S., Mariotti, A., & Largeau, C. (1994). Possible algal origin of long chain odd n-alkanes in immature sediments as revealed by distributions and carbon isotope ratios. *Organic Geochemistry*, *22*(6), 1023–1027. doi:10.1016/0146-6380(94)90035-3

Loomis, S. E., Russell, J. M., & Sinninghe Damsté, J. S. (2011). Distributions of branched GDGTs in soils and lake sediments from western Uganda: Implications for a lacustrine paleothermometer. *Organic Geochemistry*, *42*(7), 739–751. doi:10.1016/j.orggeochem.2011.06.004

Luo, P., Peng, P. A., Lü, H. Y., Zheng, Z., & Wang, X. (2012). Latitudinal variations of CPI values of long-chain n-alkanes in surface soils: Evidence for CPI as a proxy of aridity. *Science China Earth Sciences*, *55*(7), 1134–1146. doi:10.1007/s11430-012-4401-8

Makou, M. C., Hughen, K. a., Xu, L., Sylva, S. P., & Eglinton, T. I. (2007). Isotopic records of tropical vegetation and climate change from terrestrial vascular plant biomarkers preserved in Cariaco Basin sediments. *Organic Geochemistry*, *38*(10), 1680–1691. doi:10.1016/j.orggeochem.2007.06.003

Mead, R., Xu, Y., Chong, J., & Jaff??, R. (2005). Sediment and soil organic matter source assessment as revealed by the molecular distribution and carbon isotopic composition of n-alkanes. *Organic Geochemistry*, *36*(3), 363–370. doi:10.1016/j.orggeochem.2004.10.003

Menges, J., Huguet, C., Alca??iz, J. M., Fietz, S., Sachse, D., & Rosell-Mel??, A. (2014). Influence of water availability in the distributions of branched glycerol dialkyl glycerol tetraether in soils of the Iberian Peninsula. *Biogeosciences*, *11*(10), 2571–2581. doi:10.5194/bg-11-2571-2014

Mercadé, A., Vigo, J., Rull, V., Vegas-Vilarrúbia, T., Garcés, S., Lara, A., & Cañellas-Boltà, N. (2013). Vegetation and landscape around Lake Montcortès (Catalan pre-Pyrenees) as a tool for palaeoecological studies of lake sediments. *Collectanea Botanica*, *32*, 87–101. doi:10.3989/collectbot.2013.v32.008

Miller, J. M. (2001). Carbon isotope discrimination by a sequence of Eucalyptus species along a subcontinental rainfall gradient in Australia. *Functional Ecology*, 222–232.

Pancost, R. D., & Boot, C. S. (2004). The palaeoclimatic utility of terrestrial biomarkers in marine sediments. *Marine Chemistry*, *92*(1-4), 239–261. doi:10.1016/j.marchem.2004.06.029

Pancost, R. D., Damsté, J. S. S., Lint, S. De, Maarel, M. J. E. C. Van Der, Gottschal, J. C., & Party, T. M. S. S. (2000). Biomarker Evidence for Widespread Anaerobic Methane Oxidation in Mediterranean Sediments by a Consortium of Methaogenic Archaea and Bacteria. *Applied and Environmental Microbiology*, *66*(3), 1126–1132. doi:10.1128/AEM.66.3.1126-1132.2000.Updated

Peterse, F., Nicol, G. W., Schouten, S., & Sinninghe Damsté, J. S. (2010). Influence of soil pH on the abundance and distribution of core and intact polar lipid-derived branched GDGTs in soil. *Organic Geochemistry*, *41*(10), 1171–1175. doi:10.1016/j.orggeochem.2010.07.004

Peterse, F., van der Meer, J., Schouten, S., Weijers, J. W. H., Fierer, N., Jackson, R. B., … Sinninghe Damsté, J. S. (2012). Revised calibration of the MBT–CBT paleotemperature proxy based on branched tetraether membrane lipids in surface soils. *Geochimica et Cosmochimica Acta*, *96*, 215–229. doi:10.1016/j.gca.2012.08.011

Pond, K. L., Huang, Y., Wang, Y., & Kulpa, C. F. (2002). Hydrogen isotopic composition of individual n-alkanes as an intrinsic tracer for bioremediation and source identification of petroleum contamination. *Environmental Science & Technology*, *36*(4), 724–8. Retrieved from http://www.ncbi.nlm.nih.gov/pubmed/11878389

Powers, L., Werne, J. P., Vanderwoude, A. J., Sinninghe Damsté, J. S., Hopmans, E. C., & Schouten, S. (2010). Applicability and calibration of the TEX86 paleothermometer in lakes. *Organic Geochemistry*, *41*(4), 404–413. doi:10.1016/j.orggeochem.2009.11.009

Rueda, G. (2013). Reconstructing Climate Variability in the North Atlantic during the Late Holocene : an Integrated Biomarker Approach Reconstructing climate variability in the North Atlantic during the late Holocene : an integrated biomarker approach. *Universitat Autònoma de Barcelona*, (March).

Sachse, D., Dawson, T. E., & Kahmen, A. (2015). Seasonal variation of leaf wax n-alkane production and δ2H values from the evergreen oak tree, Quercus agrifolia. *Isotopes in Environmental and Health Studies*, *51*(1), 124–142. doi:10.1080/10256016.2015.1011636

Schäfer, I., Lanny, V., Franke, J., Eglinton, T. I., Zech, M., Vysloužilová, B., & Zech, R. (2016). Leaf waxes in litter and topsoils along a European transect. *SOIL Discussions*, (May), 1–18. doi:10.5194/soil-2016-37

Schouten, S., Hopmans, E. C., Pancost, R. D., & Sinninghe Damsté, J. S. (2000). Widespread occurrence of structurally diverse tetraether membrane lipids: evidence for the ubiquitous presence of low-temperature relatives of hyperthermophiles. *Proceedings of the National Academy of Sciences of the United States of America*, *97*(26), 14421–14426. doi:10.1073/pnas.97.26.14421

Schouten, S., Hopmans, E. C., Schefuß, E., & Sinninghe Damsté, J. S. (2002). Distributional variations in marine crenarchaeotal membrane lipids: A new tool for reconstructing ancient sea water temperatures? *Earth and Planetary Science Letters*, *204*(1-2), 265–274. doi:10.1016/S0012-821X(02)00979-2

Schouten, S., Hopmans, E. C., Schefuß, E., & Sinninghe-Damste, J. S. (2002). Distributional variations in marine crenarchaeotal membrane lipids: A new tool for reconstruting ancient sea-surface temperatures? *Earth and Planetary Science Letters*, *204*, 265–274.

Sinninghe Damsté, J. S., Rijpstra, W. I. C., Ellen, C., Prahl, F. G., Wakeham, S. G., Hopmans, E. C., & Schouten, S. (2002). Distribution of Membrane Lipids of Planktonic Crenarchaeota in the Arabian Sea Distribution of Membrane Lipids of Planktonic Crenarchaeota in the Arabian Sea †. *Applied and Environmental Microbiology*, *68*(6), 2997–3002. doi:10.1128/AEM.68.6.2997

Sinninghe Damsté, J. S., Rijpstra, W. I. C., Hopmans, E. C., Foesel, B. U., Wüst, P. K., Overmann, J., … Stott, M. B. (2014). Ether- and ester-bound iso-diabolic acid and other lipids in members of Acidobacteria subdivision 4. *Applied and Environmental Microbiology*, *80*(17), 5207–5218. doi:10.1128/AEM.01066-14

Sinninghe Damsté, J. S., Rijpstra, W. I. C., Hopmans, E. C., Weijers, J. W. H., Foesel, B. U., Overmann, J., & Dedysh, S. N. (2011). 13,16-Dimethyl octacosanedioic acid (iso-Diabolic Acid), a common membrane-spanning lipid of Acidobacteria subdivisions 1 and 3. *Applied and Environmental Microbiology*, *77*(12), 4147–4154. doi:10.1128/AEM.00466-11

Smith, R. W., Bianchi, T. S., & Li, X. (2012). A re-evaluation of the use of branched GDGTs as terrestrial biomarkers : Implications for the BIT Index. *GEOCHIMICA ET COSMOCHIMICA ACTA*, *80*, 14–29. doi:10.1016/j.gca.2011.11.025

Taylor, K. W. R., Huber, M., Hollis, C. J., Hernandez-Sanchez, M. T., & Pancost, R. D. (2013). Re-evaluating modern and Palaeogene GDGT distributions: Implications for SST reconstructions. *Global and Planetary Change*, *108*, 158–174. doi:10.1016/j.gloplacha.2013.06.011

Tierney, J. E., & Russell, J. M. (2009). Distributions of branched GDGTs in a tropical lake system: Implications for lacustrine application of the MBT/CBT paleoproxy. *Organic Geochemistry*, *40*(9), 1032–1036. doi:10.1016/j.orggeochem.2009.04.014

Tipple, B. J., & Pagani, M. (2013). Environmental control on eastern broadleaf forest species' leaf wax distributions and D/H ratios. *Geochimica et Cosmochimica Acta*, *111*, 64–77. doi:10.1016/j.gca.2012.10.042

Valentí Rull, T. V.-V. (2015). Crops and weeds from the Estany de Montcortès catchment, central Pyrenees, during the last millennium: a comparison of palynological and historical records, 699–710. doi:10.1007/s00334-015-0525-z

Van de Water, P. K., Leavitt, S. W., & Betancourt, J. L. (2002). Leaf δ13C variability with elevation, slope aspect, and precipitation in the southwest United States. *Oecologia*, *132*(3), 332–343. doi:10.1007/s00442-002-0973-x

Van, T. K., Haller, W. T., & Bowes, G. (1976). Comparison of the photosynthetic characteristics of three submersed aquatic plants. *Plant Physiology*, *58*, 761–768. doi:10.1104/pp.58.6.761

Vogts, A., Schefuß, E., Badewien, T., & Rullkötter, J. (2012). n-Alkane parameters from a deep sea sediment transect off southwest Africa reflect continental vegetation and climate conditions. *Organic Geochemistry*, *47*, 109–119. doi:10.1016/j.orggeochem.2012.03.011

Weijers, J. W. H., Bernhardt, B., Peterse, F., Werne, J. P., Dungait, J. A. J., Schouten, S., & Sinninghe Damsté, J. S. (2011). Absence of seasonal patterns in MBT-CBT indices in mid-latitude soils. *Geochimica et Cosmochimica Acta*, *75*(11), 3179–3190. doi:10.1016/j.gca.2011.03.015

Weijers, J. W. H., Schouten, S., Hopmans, E. C., Geenevasen, J. A. J., David, O. R. P., Coleman, J. M., … Sinninghe Damsté, J. S. (2006). Membrane lipids of mesophilic anaerobic bacteria thriving in peats have typical archaeal traits. *Environmental Microbiology*, *8*(4), 648–657. doi:10.1111/j.1462-2920.2005.00941.x

Weijers, J. W. H., Schouten, S., Spaargaren, O. C., & Sinninghe Damsté, J. S. (2006). Occurrence and distribution of tetraether membrane lipids in soils: Implications for the use of the TEX86 proxy and the BIT index. *Organic Geochemistry*, *37*(12), 1680–1693. doi:10.1016/j.orggeochem.2006.07.018

Weijers, J. W. H., Schouten, S., van den Donker, J. C., Hopmans, E. C., & Sinninghe Damsté, J. S. (2007). Environmental controls on bacterial tetraether membrane lipid distribution in soils. *Geochimica et Cosmochimica Acta*, *71*(3), 703–713. doi:10.1016/j.gca.2006.10.003

Weijers, J. W. H., Steinmann, P., Hopmans, E. C., Schouten, S., & Sinninghe Damsté, J. S. (2011). Bacterial tetraether membrane lipids in peat and coal: Testing the MBT–CBT temperature proxy for climate reconstruction. *Organic Geochemistry*, *42*(5), 477–486.

doi:10.1016/j.orggeochem.2011.03.013

Weijers, J. W. H., Wiesenberg, G. L. B., Bol, R., Hopmans, E. C., & Pancost, R. D. (2010). Carbon isotopic composition of branched tetraether membrane lipids in soils suggest a rapid turnover and a heterotrophic life style of their source organism(s). *Biogeosciences*, *7*(9), 2959–2973. doi:10.5194/bg-7-2959-2010

Wiesenberg, G. L. B., Schwarzbauer, J., Schmidt, M. W. I., & Schwark, L. (2004). Source and turnover of organic matter in agricultural soils derived from n-alkane/n-carboxylic acid compositions and C-isotope signatures. *Organic Geochemistry*, *35*(11-12 SPEC. ISS.), 1371–1393. doi:10.1016/j.orggeochem.2004.03.009

Woltering, M., Werne, J. P., Kish, J. L., Hicks, R., Sinninghe Damsté, J. S., & Schouten, S. (2012). Vertical and temporal variability in concentration and distribution of thaumarchaeotal tetraether lipids in Lake Superior and the implications for the application of the TEX 86 temperature proxy. *Geochimica et Cosmochimica Acta*, *87*, 136–153. doi:10.1016/j.gca.2012.03.024

Chapter 4

Seasonality of alkyl lipid signatures in the water column of Lake Montcortés

Abstract

In lakes sediment organic compounds are ubiquitous and are increasingly used as paleoenvironmental proxies. Their interpretations are however complex as they are derived from a variety of sources and undergo transformations during sedimentation. This paper describes the seasonal changes in the distribution and fluxes of alkyl lipids in suspended particulate matter (SPM) in the water column of Lake Montcortés, since October 2013 to May 2015. Monthly samples of SPM were taken at three depths in parallel with the deployment of a sediment trap near the lake bottom. The *n*-alkyl lipid concentrations (*n*-alkanes and *n*-alkanoic acids) in the water column increased from winter to summer. The *n*-alkyl lipid indices and $\delta^{13}C$ variations of *n*-alkanes showing distinctive seasonality (ACL, CPI, Paq index) in SPM of the water column and sediment trap to indicate terrestrial inputs (natural sources or petrogenic sources) or in situ production within the lake which provide different distribution patterns of *n*-alkane homologues that degrade along depth in a different rate in different seasons. The sediment trap flux of *n*-alkyl lipids (e.g. nC_{29} alkane and nC_{28} alkanoic acids) showing significant seasonality was dominated by terrestrial higher plant inputs which were transported by precipitation/runoff (especially the storm) or wind. However, the aquatic plant inputs and resuspension processes in water column also made contributions to variations of sediment trap flux. Our results suggest that *n*-alkyl lipids in the lake Montcortés are mainly from the catchment higher plants, which record the original environmental information in their formation processes and when transported into the lake their main distribution characteristics never changed, which could be useful in the paleoenvironmental.

4.1. Introduction

Organic matter in subaqueous sediments is derived from biological sources in the overlying and benthic water column, nearby land areas and detrital matter eroded from geological deposits (Meyers et a., 1980). In the pool of allochthonous organic materials in the sediments, significant components of paleoclimatic interest are mainly derived from higher plant waxes which are composed of long-chain *n*-alkanes, *n*-alkanols and *n*-alkanoic acids. The latter can be converted into *n*-alkanes or *n*-alkanols via enzymatic decarboxylation or reduction (Kunst and Samuels, 2003; Chikaraishi et al., 2004). These long chain cuticular waxes (C_{25}-C_{35}) are synthesized as protective coatings in higher plants, among other

functions, to preserve the water content in the leaves. And recent studies in living plants and modern soils have argued that *n*-alkane chain-length ratios are driven by temperature or aridity, and are not specific to plant types, with the exception of those from aquatic plants and *Sphagnum* moss (Nichols et al., 2009, 2010; Bush & Mcinerney, 2015).

In modern sediments, long chain acids with an even-over-odd carbon number predominance are commonly found, with a similar carbon-chain length occurrence (nC_{24}-nC_{32}) to what is also found in the higher plant waxes. The C_{14}-C_{20} *n*-alkanoic acids are also frequently found, but these are mostly derived from planktonic and benthonic algae (Tissot & Welte, 1984). Similarly, *n*-alkanes distribution patterns in sediments are equivalent to those found in plant waxes, including their range of chain lengths and the predominance of odd or even carbon atoms chain lengths. However, aquatic algae synthesize shorter chain *n*-alkanes (C_{15}-C_{21}) and bacteria produce *n*-alkanes covering a large carbon number range (C_{14}-C_{50}) albeit in very low concentrations (Eglington and Hamilton, 1967; Clark and Blumer, 1967; Goutx and Saliot, 1980). In comparison with their functionalized homologues, the *n*-alkanes are rather inert and bioresistant, and their degradation by aerobic bacteria is drastically retarded in low temperature and low oxygen conditions (Brassell et al., 1987). In fact, *n*-alkanes can survive for tens of millions of years in immature sediments (Pedentchouk et al., 2006). This results in their preferential accumulation in sediments, so they become much more abundant than their functionalized counterparts, despite these accounting for up to 95% of the *n*-alkyl lipids in leaf tissues in higher plants. *n*-Alkane in sediments, can also have petrogenic sources. such as oil, and coal, and their partially combusted products (Bray and Evans, 1961; Tissot and Welte 1984; Del Rio 1992; Rao et al. 2009). The relative contributions from natural and petrogenic sources can be gleaned using the odd-over-even carbon preference index (CPI).

Stable carbon isotopes can also be used to distinguish between sources of *n*-alkanes from various plant functional types. Thus, C3 plants have lower $\delta^{13}C$ values (e.g. trees, shrubs, temperate grasses; mean $\delta^{13}C$ = -27‰) than those using the C4 pathway (most tropical grasses; mean $\delta^{13}C$ = -13‰). CAM plants are uncommon except in arid regions and their $\delta^{13}C$ values are intermediate between C3 and C4 plants. A number of studies have shown that $\delta^{13}C$ signatures in *n-alkanes* from surface sediments reflect plants contribution (C3 *vs* C4) from the nearby continental areas (Vogts et al., 2012). In C3 and C4 plants, variations of several per mil in $\delta^{13}C$ may also be controlled by environmental factors such water availability and light (Ehleringer et al., 1991), and some studies have suggested that $\delta^{13}C$

signatures can be correlated with environmental parameters such as mean annual precipitation and aridity (Vogts et al., 2012).

The presence of *n*-alkyl lipids in sediments is typically attributed to transport of the lipids in leaf litter and soils by run-off or fluvial processes, and less so to aeolian transport in aquatic continental settings (Pancost & Boot, 2004). However, a mechanistic understanding of how the *n*-alkyl lipids accumulate in sediments after transport from their distal sources, and the relative importance of the plants and their debris vs soil sources is still lacking. For instance, *n*-alkanes in sediments or suspended particulate matter can be much older than the age of autochthonous organic matter, which indicates that long time lags can occur between their synthesis and their subsequent deposition in sediments(Kusch et al., 2010). This poses the question of which is the temporal constraint in the interpretation of terrigenous biomarker records in sediments, in comparison with those from autochthonous water column proxies, as the signals may be temporally decoupled. Another hypothetical complicating factor is that organic components are associated with particles of different size, and spatial fractionation of the various chemicals may take place according to the hydrodynamic properties of the carrier particles during fluvial transport, and in air according to meteorological conditions, season and particle ageing (Ladji et al., 2014). To gain some insights into these questions this study presents a one-year round observations of *n*-alkyl lipids in suspended particulate matter (SPM) in the water column of Lake Montcortés. Our primary objective was to investigate the seasonality of *n*-alkanes and *n*-alkanoic acids fluxes and relative ratios and compound specific $\delta^{13}C$ signatures to ascertain the variability in sources as well as the factors controlling the transport of these lipids into the lake.

4.2. Methods and Materials

4.2.1. Study area

Lake Montcortés (42°19’50’’N, 0°59’46’’E, 1027m a.s.l.) is one of the deepest karstic lakes (ca. 30m) in the Pre-Pyrenean Range of the Iberian peninsula (Alonso, 1998) (Fig. 2-1). Its watershed is on Triassic bedrock, comprising mainly carbonates, evaporites, claystones and shale formations (Rosell, 1994; Corella et al., 2012). The lake is roughly circular with a total diameter of 1320 m, meromictic and oligotrophic (Camps et al., 1976). Relatively high surface/depth ratio and steep margins (Fig.2-1) provide favorable environments for deposition and preservation of finely laminated facies (Corella et al., 2010). Surface water

has an average pH value of 8.4, whereas the pH is only 7.5 in the anoxic hypolimnion (Modamio, 1988; Corella et al., 2012). Episodes of holomixis during the winter have also been documented (Modamio et al, 1988).

Total mean annual rainfall is 860 mm with the most humid seasons in spring and autumn (Corella et al., 2012). The lake is recharged by precipitation (groundwater and runoff inputs) and loses water mainly by evaporation or through a temporal outlet in the northern end. Mean monthly air temperature ranges from 1.9 °C in the coldest month (January) to 20.3 °C in the warmest (July), showing a continental character of the regional Mediterranean alpine climate type (Corella et al., 2012).

The main vegetation formations in the lake catchment are woodlands of evergreen oak (e.g.*Quercus rotundifolia*), deciduous oak (e.g. *Quersus pubescens*), conifers (e.g. *Pinus nigra subsp. salzmanii*) and littoral vegetation (e.g. *Juncus Phragmites*) (Rull et al., 2010).

From September 2013 to April 2015, records of the rainfall, wind velocity and temperatures were obtained from the town of Pobla de Segur, the closest meteorological station from Lake Montcortés. During the study period it rained every month, and the most abundant precipitation occurred in August 2014, while by the period from December 2014 to February 2015 had the lowest rainfall. From March to September 2014 the weather was somewhat windy. The water column was completely mixed from December 2013 to February 2014, and was stratified from March to November 2014 as indicated by the lake temperatures and dissolved oxygen (DO) levels at different depths (Fig. 2-8).

4.2.2. Sample collection

A team led by Dra Teresa Vegas from the University of Barcelona deployed and retrieved monthly a sediment trap at 20 m within the lake to collect settling particulate matter (see section 2.2.4 for a full description). Data on water column parameters were obtained by Dra Teresa Vegas and her collaborators who undertook monthly CTD profiles in the same day when the sediment traps were retrieved from the Lake Montcortés, one day earlier than our water SPM sampling took place. This consisted retrieving 40 L of water at three depths: surface (0 m, 20 cm under water level), thermocline (5-12 m depth) and above the sea floor (20-22 m) from September 2013 to November 2014. All samples for *n*-alkyl lipid analysis were immediately filtered through pre-combusted GF/F filters with a pore size of 0.7 µm when transported to the lab at the Autonomous University of Barcelona. The filters were freeze-dried before analysis.

4.2.3. Analytical processes

SPM filters from the water column using *n*-C_{36} alkane as internal standard were immersed in 50 mL (20+15+15 mL) dichloromethane:methanol (3:1,v/v) in wide-month test tubes. An excess of activated copper was added to remove sulfur (if exists). Each tube containing solvent and filters were shaken using a rotational speed of 1800 for 30 seconds before ultrasonic solvent extraction. All tubes were fixed in rack in an ultrasonic bath for 10 min before being centrifuged at 2000 rpm for 5 minutes using a centrifuge. The supernatant of filters was transferred into pearl-shaped vessels and dried at 27 °C in a rotary evaporator.

The method of column chromatography for separating and purifying the liquids in different class compounds was adapted from (Huang et al., 1999) and (Schouten et al., 2002). Pasteur pipettes were combusted at 450 °C in the muffle furnace for 8 hours before being filled with 0.7 g of aminopropyl silica and 0.5 g Na_2SO_4 which were placed over a piece of cotton that plugged the narrow end of the pipette, The adsorbents and the cotton were previously cleaned using a Soxhlet with dichloromethane:methanol (2:1, v/v) during 24 hours. Before elution, 3 mL dichloromethane:isopropanol (2:1, v/v) was used to condition the columns. Sequentially, the eluting volumes for F1 (neutral fraction) and F2 (acid fraction) were 6 mL dichloromethane:isopropanol (2:1, v/v) and 8 mL diethyl ether:acetic acid (96:4, v/v), respectively. F1 fraction was then separated into non-polar (F1-1; *n*-alkanes), slightly polar (F1-2, reserved) and polar fractions (F1-3; GDGTs) with 5 mL hexane, 4 mL dichloromethane and 6 mL dichloromethane:methanol (95:5, v/v) eluted through a silica column. Prior to analyses, Fatty acids (F2) were reacted with BF3 (20% boron trifluoride in methanol, Merk) to form fatty acid methylesters (FAMES) at 90 °C for 1 hour and extracted by hexane followed by another purifying process using hexane:dichloromethane (1:2, v/v) over a silica column.

4.2.4. n-alkyl lipid analysis in GC-FID

The fractions were analyzed using a gas chromatograph fitted with a flame-ionization detector in Agilent 7820A (Agilent GC-FID). The dry extracts were re-dissolved in isooctane and injected in splitless injection mode in the GC-FID using an autosampler. The injector and detector temperature were set at 320 °C. Hydrogen was used as carrier gas with a constant flux of 2 mL/min. Compounds were separated through an Agilent HP-1 capillary column of 60 m length, 0.25 mm internal diameter connected to a guard column with a press-fit. For *n*-alkane fraction analysis, oven temperature was held at 80 °C during 1 min, increased to 120

°C at a rate of 30 °C per minute, then increased to 320 °C at 6 °C per minute and remained at 320 °C during 21 min. The detector was fed with H_2 and air with a flow of 30 mL/min and 400 mL/min, respectively. Reference sediment (Chapter 2) injected in gas chromatography coupled to mass spectrometry was reinjected to GC-FID for identification of homologues of *n*-alkanes with different carbon chain lengths. Quantification of *n*-alkanes was based on internal standards.

For the compound specific isotopic analysis, measurement of $\delta^{13}C$ ratios performed by a gas chromatography coupled to an isotope ratio mass spectrometer Thermo Delta V Advantage (GC-IRMS). $\delta^{13}C$ are reported in per mil (‰) relative to the Vienna Peedee Beleminte (V-PDB). Standard deviations of carbon isotope analyses were better than 0.5‰. Helium (UHP 5.5 grade) was used as the carrier gas operating at constant flow mode with a rate of 1.5 mL/min. Compounds separated by the GC column were converted to CO_2 and H_2O through the combustion furnace (0.5 mm i.d.× 1.5 mm o.d. × 34 cm) operated at 940 °C and loaded with CuO and Pt wires as oxidants and catalyst, respectively. The reproducibility and accuracy of the carbon was evaluated using laboratory isotopic standards which contain C_{20}, C_{28} and C_{36} *n*-alkanes. The precision of the GC-IRMS was checked by the injection of four isotopic standards after every five sample injections.

4.3. Results and discussion

4.3.1. Seasonal and vertical variability in the concentrations of SPM *n*-alkyl lipids in the water column

There are distinct seasonal variations in the concentrations of *n*-alkyl lipids in the SPM at three depths (Fig. 4-1, 4-2). It is apparent that the abundances of *n*-alkanes and *n*-alkanoic acids in the surface section of water column were higher in spring and summer (April-August, 2014) and this phenomenon was particularly significant for *n*-alkanoic acids. SPM samples from the thermocline layer only showed maximal concentrations of *n*-alkanes and *n*-alkanoic acids in August/September and July/August 2014, respectively. SPM from the deeper section of water column presented maximum concentrations of *n*-alkanes and *n*-alkanoic acids in October-January and September 2014 in respective, about two-month delay after the relative maximum values in the thermocline waters. The seasonal variations at each depth may reflect temporary blooms of different *n*-alkanes/*n*-alkanoic acids producers that were

controlled by temperature or seasonal nutrient dynamics influenced by the rainfall within the lake or soil runoff in the catchment.

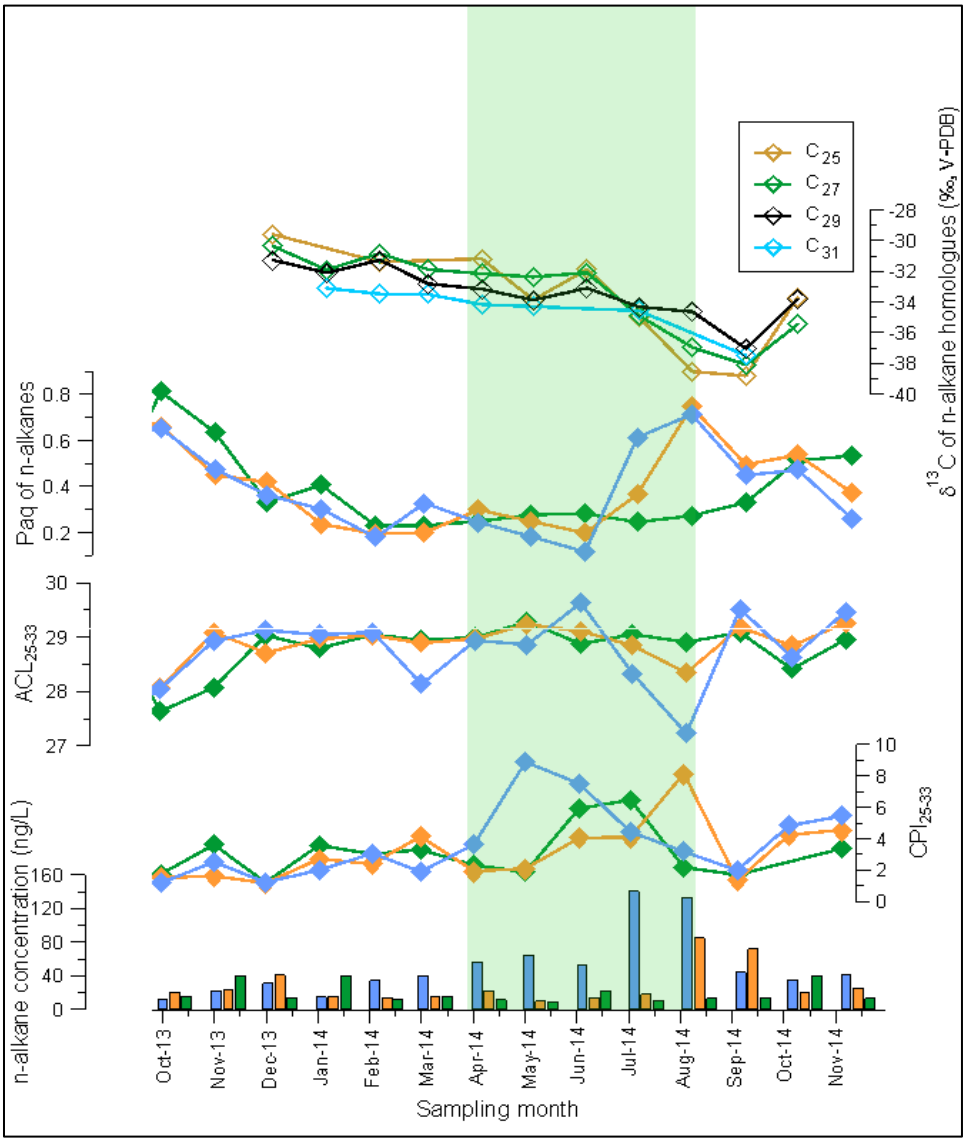

Figure 4-1 Concentration of *n*-alkanes from suspended particulate matter (SPM) in the water column from October 2013 to November 2014: blue bar/line, orange bar/line and green bar/line stand for SPM from the surface waters, the thermocline waters and bottom waters. Carbon preference index (CPI) and average chain length (ACL) with odd subscript means CPI/ACL for *n*-alkanes. P_{aq} index was calculated from the equation $P_{aq}=(C_{23}+C_{25})/(C_{25}+C_{27}+C_{29}+C_{31})$, subscripts indicate *n*-alkanes with same carbon number. The top is specific carbon isotopic composition of *n*-alkanes from SPM of surface waters

Table 4-1 *n-A*lkane concentrations and ratios in the water column from Sep. 2013 to Nov. 2014

	C_{23}	C_{25}	C_{27}	C_{29}	C_{31}	C_{33}	$Total_{23-33}$	ACL	CPI	P_{aq}
0m				ng/L						
Sep-13	3.9	5.2	4.2	3.8	3.5	2.3	37.5	27.4	1.36	0.59
Oct-13	1.8	1.8	1.4	1.2	1.1	0.5	13.1	28.1	1.18	0.65
Nov-13	3.9	1.2	1.8	2.8	2.1	0.9	15.9	28.9	2.51	0.48
Dec-13	2.4	2.8	3.5	4.1	4.5	3.0	34.6	29.1	1.24	0.36
Jan-14	1.1	1.0	1.5	2.4	2.0	0.9	12.8	29.0	1.99	0.30
Feb-14	1.0	2.3	4.1	7.4	6.1	1.8	30.5	29.1	3.06	0.18
Mar-14	1.8	2.7	4.7	6.6	0.8	1.2	26.3	28.1	1.90	0.33
Apr-14	3.1	4.2	6.8	11.4	8.6	2.8	46.5	28.9	3.63	0.24
May-14	2.8	4.7	10.4	16.5	11.7	2.5	53.8	28.9	8.88	0.18
Jun-14	0.6	2.9	1.3	15.2	12.5	2.7	39.4	29.6	7.52	0.12
Jul-14	21.4	7.4	8.2	9.9	7.4	1.9	64.5	28.3	4.44	0.61
Aug-14	82.8	11.3	37.2	11.2	0.6	2.0	180.1	27.2	3.17	0.71
Sep-14	8.5	2.6	4.4	5.4	6.5	4.7	43.7	29.5	1.99	0.45
Oct-14	6.9	2.8	4.2	5.4	4.0	1.2	28.1	28.6	4.83	0.47
Nov-14	4.5	1.8	3.7	8.0	8.0	2.4	32.4	29.5	5.45	0.26
5-12m										
Sep-13	4.2	4.0	2.7	2.2	1.8	0.7	24.9	27.7	1.52	0.75
Oct-13	4.0	2.5	2.4	1.9	1.6	0.8	20.2	28.1	1.51	0.66
Nov-13	3.8	1.8	2.5	3.2	3.1	1.8	23.4	29.1	1.63	0.45
Dec-13	3.6	3.7	4.7	4.7	4.4	2.4	40.8	28.7	1.17	0.42
Jan-14	1.2	1.0	2.4	3.2	2.5	0.9	15.0	29.0	2.71	0.24
Feb-14	0.9	0.7	2.3	2.9	2.2	0.8	13.7	29.0	2.40	0.19
Mar-14	0.9	1.1	2.6	3.8	2.8	0.7	14.8	28.9	4.14	0.20
Apr-14	1.4	2.0	2.8	3.9	3.3	1.6	22.4	29.0	1.94	0.30
May-14	0.5	0.8	0.7	2.3	1.7	0.6	9.5	29.2	2.10	0.25
Jun-14	0.8	0.9	2.0	3.2	2.7	0.9	13.0	29.1	4.05	0.20
Jul-14	3.1	1.4	2.9	3.6	2.9	1.0	17.9	28.8	4.10	0.37
Aug-14	48.4	5.9	8.8	8.8	6.5	1.8	85.1	28.3	8.15	0.75
Sep-14	13.4	4.9	6.9	7.9	8.7	5.5	71.7	29.2	1.35	0.50
Oct-14	6.5	1.5	2.3	3.4	2.7	0.9	20.1	28.8	4.24	0.54
Nov-14	5.0	1.5	2.8	5.1	4.7	1.6	24.5	29.3	4.56	0.37
20-22m										
Sep-13	2.1	2.6	1.4	1.2	1.0	0.5	15.5	27.6	1.30	0.81
Oct-13	6.6	5.5	4.4	4.4	3.6	1.4	39.9	28.1	1.74	0.64
Nov-13	1.9	1.0	1.8	2.9	2.3	0.8	13.2	29.0	3.62	0.33
Dec-13	2.9	3.9	4.4	4.9	4.5	2.7	40.2	28.8	1.22	0.41
Jan-14	1.1	0.8	2.1	2.7	2.2	0.8	12.2	29.0	3.58	0.23
Feb-14	1.2	1.0	2.5	3.2	2.5	0.9	14.8	28.9	3.02	0.23
Mar-14	0.9	0.9	1.6	2.6	2.0	0.7	11.1	29.0	3.30	0.25
Apr-14	0.7	0.6	1.0	1.6	1.5	0.8	8.7	29.3	2.31	0.28
May-14	1.2	1.9	3.2	3.6	3.2	1.5	21.9	28.9	1.88	0.28
Jun-14	1.0	0.9	1.6	2.9	2.3	0.7	10.9	29.1	5.91	0.25
Jul-14	1.2	1.2	2.0	3.1	2.5	0.7	12.8	28.9	6.48	0.27
Aug-14	1.5	1.1	1.9	2.5	1.9	1.3	14.2	29.1	2.17	0.33
Sep-14	6.9	4.0	4.9	5.3	4.2	1.5	39.6	28.4	1.70	0.51
Nov-14	4.2	0.9	1.4	2.2	1.8	0.6	13.3	29.0	3.38	0.53

The most abundant *n*-alkane in SPM of surface waters is the nC_{29} homologue, followed by the nC_{31} alkane. This is the case in most of months except from July to October 2014. This is likely to indicate the occurrence of new inputs containing abundant middle-chain *n*-alkanes, probably from aquatic plants in the lake (Table 4-1).The range of carbon chain lengths of the *n*-alkanoic acid distributions in the water column spanned from nC_{14} to nC_{32}, and never showed distinctive variations of the distribution pattern from month to month, having maxima at nC_{24} and strong even-over-odd predominance ($CPI_{24\text{-}30}$), which is typical of terrigenous higher plants inputs (Eglinton and Hamilton, 1967).

The SPM *n*-alkanes concentrations decrease with depth and vary between 12.8-180.1 ng/L, 9.5-85.1 ng/L and 8.7-40.2 ng/L from the upper waters to the deeper waters (Fig.4-1). Similarly, the *n*-alkanoic acid concentrations of water column SPM ranged between 0.1-1.5 µg/L, 0.1-1.7 µg/L and 0.1-0.3 µg/L from the upper waters to the deeper waters (Fig. 4-2). In general, our data suggest that concentrations of n-alkyl lipids of SPM showed decreasing seasonal variability with increasing depths.

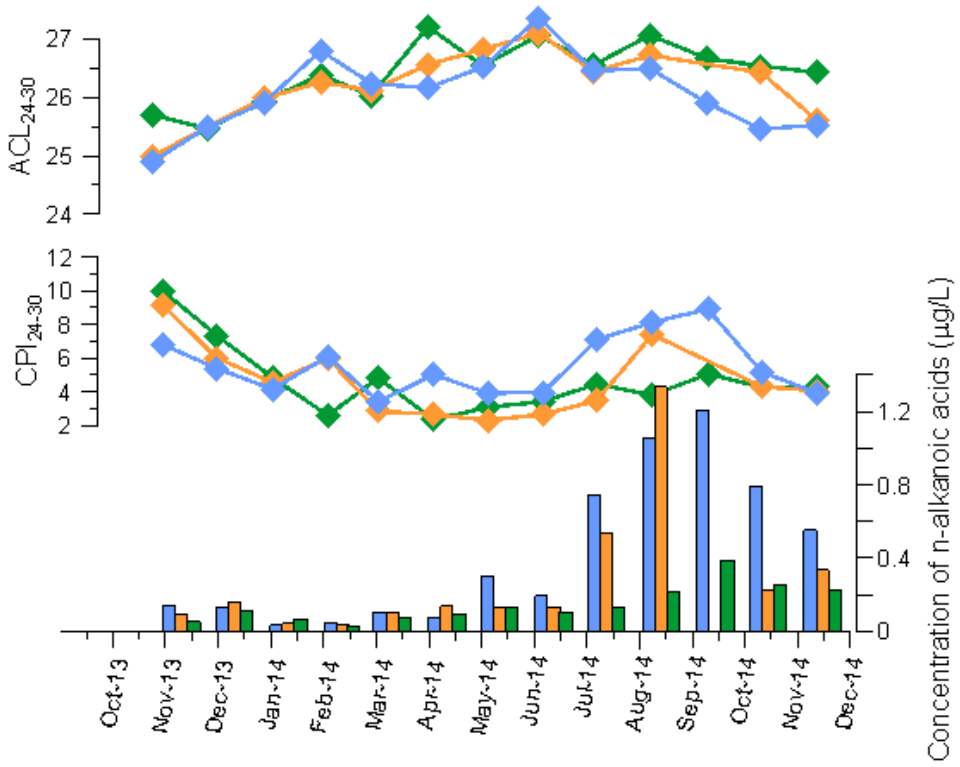

Figure 4-2 Concentration of *n*-alkanoic acids from suspended particulate matter (SPM) in the water column from October 2013 to November 2014: blue bar/line, orange bar/line and green bar/line stand for SPM from the surface waters, the thermocline waters and bottom waters. Carbon preference index (CPI) and average chain length (ACL) with even subscript means CPI/ACL for n-alkanoic acids.

Both similarities and differences exist in the concentration patterns of *n*-alkanes and *n*-alkanoic acids in the SPM of the water column. The concentration of *n*-alkanes and *n*-alkanoic acids of SPM generally decreased with increasing water depth, although some SPM samples from deeper sections of the water column interrupted this trend by having higher *n*-alkyl lipid concentrations during the mixing period (December 2013–February 2014) in the water column (Fig. 2-8, Fig. 4-1 and Fig. 4-2). This could have resulted largely from increasing resuspension of bottom sediment (Meyers & Takeuchi, 1979), which exert different effects on *n*-alkane and *n*-alkanoic acid concentrations that were shown in highest *n*-alkane values in October/November, January but continuous high values from August to December. Specifically, the *n*-alkanes and *n*-alkanoic acids of SPM did not show similar trends at three depths, which might be due to their different sources, residence times in soils and transport paths. The reasons for decreasing amount of *n*-alkyl lipids in the water column could also be related to degrading processes in the water column even though *n*-alkanes are reported to be less sensitive to degradation processes as the lack of oxygen-containing functional groups in the compounds and the double bonds that are susceptible to microbial attack (Meyers & Eadie, 1993). Nevertheless, we tried to calculate the degrading rates of *n*-alkyl lipids from the upper section to the deeper section of the water column. We develop a kind of ratio (Ri) between *n*-alkanes from the surface and the bottom waters considering a two-month delay of transporting downwards. The ratio is defined as:

$$Ri = nC(i\text{-}2)_e / (nCip + nC(i\text{-}2)_e) \quad (eq.4.1,\ 12 \geq i \geq 3)$$

$$Ri = nC(i+10)_e / (nCip + nC(i+10)_e) \quad (eq.4.2,\ i = 1 \text{ or } 2)$$

note: nC standards for concentration of n-alkane homologues (nC_{23}, nC_{29}) or alkanoic acid homologues (nC_{22}, nC_{28}), i stands for specific month (12≥ i ≥1). Subscript e and p indicate samples from the epilimnion or hypolimnion.

For *n*-alkanes, we compared degrading rates (Ri) of nC_{23} (middle chain) and nC_{29} (long chain) alkane concentrations in the upper and deeper sections of the water column (Fig. 4-3a). Ri of nC_{23} alkane ranged from 0.16 to 0.88 (mean 0.53±0.07) and nC_{29} alkane within 0.28-0.82 (mean 0.62±0.05). The Ri ratios of nC_{23} and nC_{29} alkane changed in a similar trend, e.g. a general decrease and increase in an annual cycle (Fig. 4-3a). However, if we check details: Ri of nC_{23} decreased continuously from 0.80 in December to below 0.2 in July and increased to nearly the initial values in November except that August 2014 presented a sharp increase. In contrast, Ri of nC_{29} alkane remained constant from December to March, followed by a sharp decrease in April, and stayed steady until June, followed by another

sharp decrease in July and increased values until October/November. The variations of Ri values in different *n*-alkanes suggest that nC_{23} alkane degraded a bit faster than nC_{29} alkane except in August. Moreover, both Ri in nC_{23} and nC_{29} seemed to be higher in summer and lower in winter, indicating that processes affecting degrading rates of *n*-alkanes might be related to temperature. In addition, the magnitude of varying rate of long-chain *n*-alkanes (nC_{29}) within seasons was relatively lower compared with intra-season dynamics.

The Ri of *n*-alkanoic acid homologues (nC_{22} and nC_{28}) varied between 0.2 and 1.0 (Fig. 4-3b), showing minimum values from March to June and relatively higher values in other months, which is not consistent with was observed for the *n*-alkanes. Moreover, the Ri trends of nC_{22} and nC_{28} alkanoic acids were very similar in an annual cycle except in August 2014 and there was no evidence to indicate that shorter chain (nC_{22}) *n*-alkanoic acids degrade faster than longer-chain (nC_{28}) homologues.

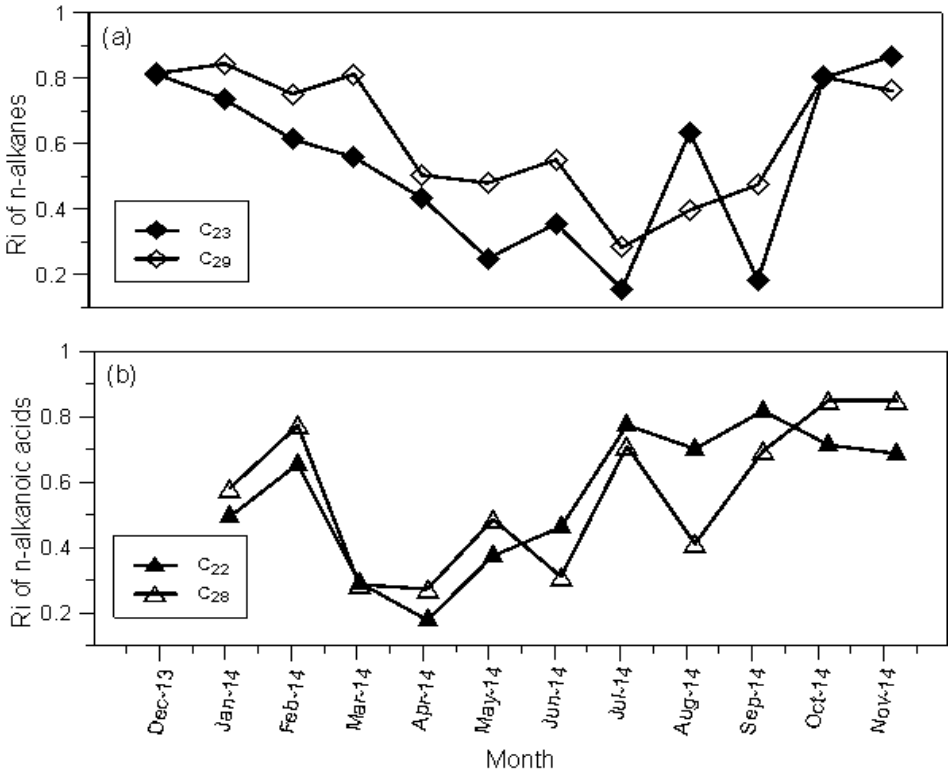

Figure 4-3 Degrading rate of nC_{23} and nC_{29} concentration from the epilimnion to the hypolimnion

Therefore, we conclude that both *n*-alkanes and *n*-alkanoic acids decrease from the upper section to the deeper section in the water column and the degrading rates for the same homologue showed seasonal changes. The higher temperature might be favorable factor to degradation of *n*-alkyl lipids. Whereas some sufficient inputs of specific compounds could

interfere the general trends, e.g. in August 2014, abundant inputs of shorter-chain alkyl lipids (nC_{23} alkane and nC_{22} alkanoic acid) in the water column yielded very low degrading rates.

4.3.2. Seasonal and vertical variability in the ratios of *n*-alkyl lipids in SPM

The average chain length of *n*-alkanes (ACL_{25-33}) from SPM of the upper section in the water column showed lowest values (ACL_{25-33}=27) in August and relatively higher values (ACL_{25-33}=29) in other seasons (Fig. 4-1). ACL_{25-33} of SPM from in the thermocline waters followed this trend but varied to less extent. The SPM from deeper waters presented a similar trend except in October/November 2013, showing lowest values. It indicates that SPM *n*-alkane in most of months might be mainly derived from soils that had stable ACL values throughout the year. The ACL_{24-30} values of *n*-alkanoic acids increased from 25 (November 2013) to 27 (June 2014) followed by a decrease to 25 November 2014 (Fig. 4-2). All ACL values of SPM samples at three depths in the water column showed no significant vertical variability, indicating ACL values are stable in the water column. In our study area, the seasonal variations of SPM ACL_{25-33} seem to indicate variations of source inputs rather than influence from temperature because the lowest ACL values presenting in July/August and October, which were consistent with blooming of aquatic plants that have shorter ACL values.

We try to clarify the possible sources of *n*-alkyl lipids between natural or anthropogenic sources in Lake Montcortés through the ratios, such as carbon preference index (CPI). For both *n*-alkanes and *n*-alkanoic acids from terrestrial higher plants, CPI values are normally higher than 5 (Eglintaon and Hamilton, 1967; Rieley et al., 1991). In contrast, values of CPI ≤ 1 indicate contributions from anthropogenic sources (Cranwell., 1973; Meyers & Takeuchi, 1979). The CPI values (CPI_{25-33}) of *n*-alkanes in SPM from the surface waters ranged from 1.2 to 8.9, showing the maximum in May (8.9) and minimum (around 1.0) in September-December (Fig. 4-1). The thermocline SPM CPI_{25-33} index presented its maximum value (8.1) in August, and the CPI_{25-33} exhibited the maximum of 6.5 in July, suggesting natural plant inputs. In the whole water column, it seems that CPI_{25-33} kept relative low values from October 2013 to April 2014 (within 2.0-3.0), indicating oil-originated sources (Killops & Killops, 2005; Reddy et al., 2000) that were probably from remote eolian transportation and deposition of *n*-alkanes in the lake. The relationship between CPI values and SPM nC_{29} alkane concentration were different at three depths (the figure not shown, see original data in

Table 4-1), showing linear correlations at the surface water (R^2 =0.72) and the thermocline water (R^2 =0.62) and no correlation at the bottom water. Besides, the mean annual CPI_{25-33} values at three depths were 3.5, 3.0 and 2.9, a slight decrease from the upper section to the deeper section of the water column, indicating some processes (such as microbial influence) may also modify CPI values in the water column. Thus, to discuss outside-lake inputs, we take SPM of the surface water as an example, a general increase of CPI_{25-33} from April to May followed a decrease until August (still relatively higher values), which we interpret as natural source inputs that include deposition of organic aerosols containing higher CPI values derived from terrestrial plants as well as production of local emergent aquatic plants during this period. While in low-natural *n*-alkane production seasons (October-March), especially in winter, dry and wet deposition of organic aerosols influenced by human emissions of petroleum (low CPI) could might make more contributions to the lake.

n-alkanoic acid CPI_{24-30} values decreased from 9.9 to 2.3 in an annual cycle, likely to be the opposite trend of the ACL_{24-30} in the water column (Fig. 4-2). CPI_{24-30} of *n*-alkanoic acids showed lower values from January to June and slightly higher values in summer and autumn. The increase of CPI_{24-30} values in the surface might be due to the new natural inputs showing more significant odd-over-even characteristics of *n*-alkanoic acids. The mean annual CPI_{24-30} values at three depths were 5.5, 4.6 and 4.6 from the upper to the deeper waters, separately, indicating new inputs or degradation of even-chain *n*-alkanoic acid homologues in the upper section of water column. Especially from March to June the thermocline SPM showed significant lower CPI values, it could be due to bloom of some *n*-alkanoic acid producers that contributed no CPI preference to the water column.

The P_{aq} index (% of aquatic plants) of the SPM in the water column varied from 0.12 to 0.80 in a one-year round (Fig.4-1). Specifically, P_{aq} values at three depths were similar and decreased from 0.8 in December 2013 to the lowest in June 2014 followed a sharp increase in July/August for the upper sections (the surface and the thermocline) but a slight increase during September and December for the deeper one. A value of P_{aq} above 0.4 indicates inputs of submerged/floating macrophytes; below 0.1 corresponds to terrestrial inputs and 0.1-0.4 indicates inputs of emergent macrophytes or a mixture of emergent macrophytes and terrestrial higher plants (Ficken et al., 2000). This suggests that significant inputs of submerged/floating macrophytes were dominant in *n*-alkanes from July to November (summer/autumn) in the upper water column and from September to November (autumn) in the bottom water when the water column was stratified. The mixing period (starting from

December) and residence time lag of *n*-alkanes in the water column may be responsible for the shorter appearing time of higher P_{aq} values in the bottom water. The variations of P_{aq} indices in the water column were seasonal, which might be consistent with the life cycle of specific aquatic plants in the upper sections of the lake.

4.3.3. Seasonality in the fluxes and ratios of *n*-alkyl lipids of in the sediment trap

According to the observed data from the sediment trap, the flux of *n*-alkanes presented the minimum value (43.5 ng/m^2/day) in February, and the maximum values in September (232.8 ng/m^2/day) and December (221.9 ng/m^2/day). Flux of *n*-alkanoic acids in the sediment trap are one order of magnitude higher than those of *n*-alkanes but show similar trends, ranging from a minimum in February 2014 (0.39 µg/m^2/day) to maxima in September 2014 (2.49 µg/m^2/day) and December 2014 (2.46 µg/m^2/day) (Fig. 4-4). It is apparent that fluxes of *n*-alkyl lipids in the sediment trap showed more distinctive seasonality than those concentrations of SPM at the three depths of the water column. The reason could be that sediment trap collected lipids per month to provide typically accumulated information while the water column only recorded the current conditions when we were sampling.

The *n*-alkanes were dominated by the nC_{29} homologue followed by nC_{27} and nC_{31} except in September to November 2014, when nC_{23} was much abundant, indicating an increase of nC_{23}-containing inputs of submerged/floating macrophytes (Fig. 4-4, Fig. 4-5). In an annual cycle, the two maxima of total *n*-alkanes (both December) seem to follow seasonal cycles. Moreover, from December to March in 2013/2014, all *n*-alkane homologues declined, which was consistent with variations of mass fluxes in the sediment trap that seemed not to be correlated with variations of precipitation or wind forces during this period (Fig. 2-8). The co-increase of *n*-alkanes at nC_{29}, nC_{31} and nC_{27} in the sediment trap indicates a terrestrial vascular inputs rather than emergent aquatic plants, because those from emergent aquatic plants showed maximum *n*-alkanes at nC_{29}, nC_{27} and $nC_{25.}$ Thus, we interpret these increasing fluxes to be driven by resuspension processes rather than life cycle of emergent aquatic plants as December is coupled with the onset of mixing events in the water column. However, this trend did not occur in SPM of the water column for the reason that SPM sampling just provided a short snapshot of the lake dynamics, whereas the sediment trap integrated the monthly signals. Notably, a new-production period appear in the water column SPM and sediment trap from April/May to August/September. The increasing fluxes could be

due to terrestrial higher plant inputs (probably through soil runoff) as well as wind according to more precipitation and higher wind velocity in this period.

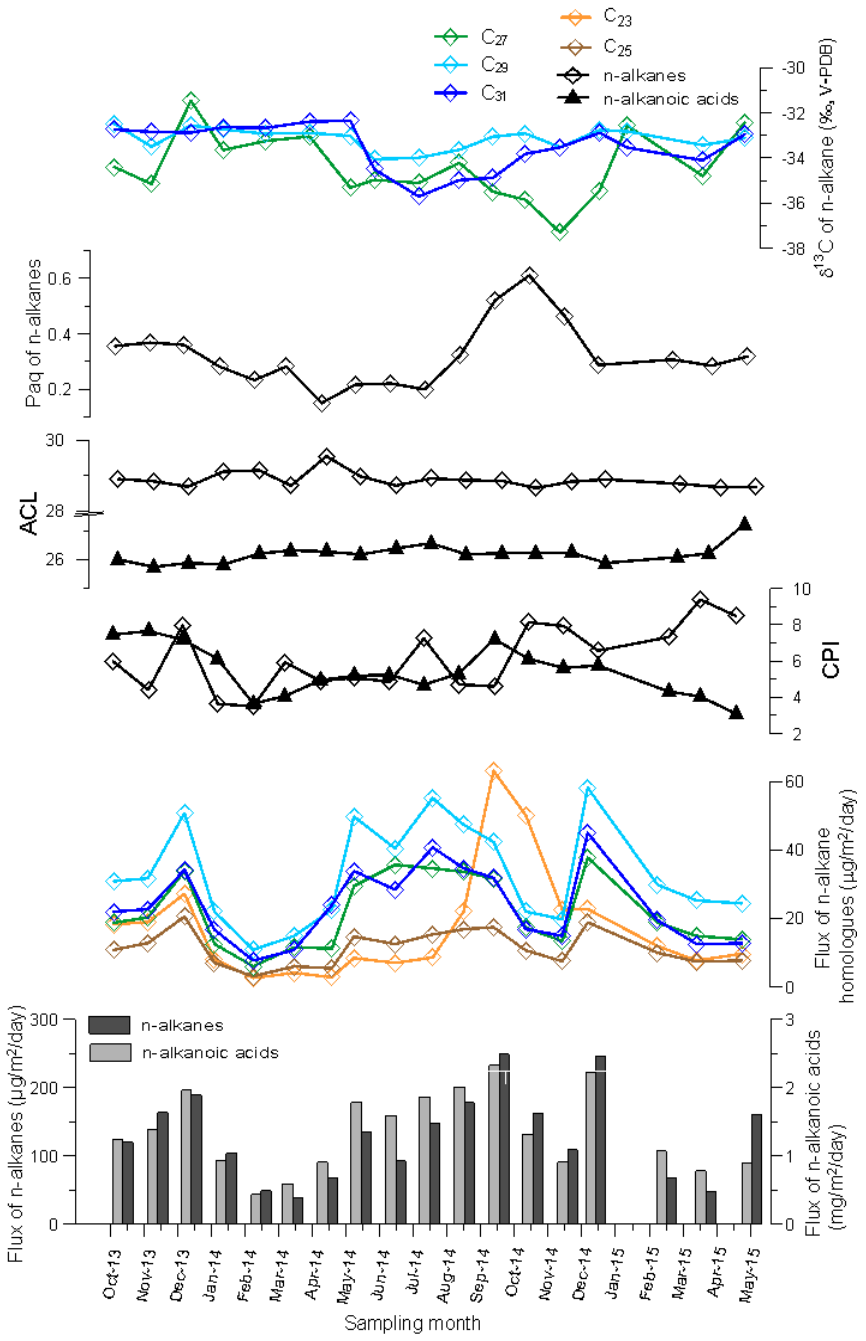

Figure 4-4 Sediment trap flux of *n*-alkanes (black bar) and *n*-alkanoic acids (grey bar) and *n*-alkyl lipid-related proxies. Carbon preference index (CPI) and average chain length (ACL) with odd/even subscript means CPI/ACL for *n*-alkanes and *n*-alkanoic acids. P_{aq} index was calculated from the equation $P_{aq} = (C_{23}+C_{25})/(C_{25}+C_{27}+C_{29}+C_{31})$, subscripts indicate *n*-alkanes with same carbon number. The top is compound specific $\delta^{13}C$ of *n*-alkane homologues (nC_{25}-nC_{31}) from the sediment trap from October 2013 to April 2015

In the sediment trap, ACL_{25-33} values of *n*-alkanes and ACL_{24-30} of alkanoic acids in the sediment trap were very steady and close to 29 and 26, respectively, throughout the sampling period (Fig. 4-4). The absence of seasonality in ACL_{25-33} values, in spite of changing fluxes, would lend support to the notion that put forward above that *n*-alkanes in Lake Montcortés are mainly derived from soils inputs, not directly plant debris. CPI index of *n*-alkyl lipids in the sediment trap did not follow the same trend for *n*-alkanes and *n*-alkanoic acids throughout the year (Fig. 4-4). CPI of *n*-alkanes showed an increasing trend while CPI_{24-30} index of *n*-alkanoic acid decreased from October 2013 to April 2014 followed by an increase to October 2014 and then decreased, which was consistent with CPI_{24-30} variations of SPM in the water column.

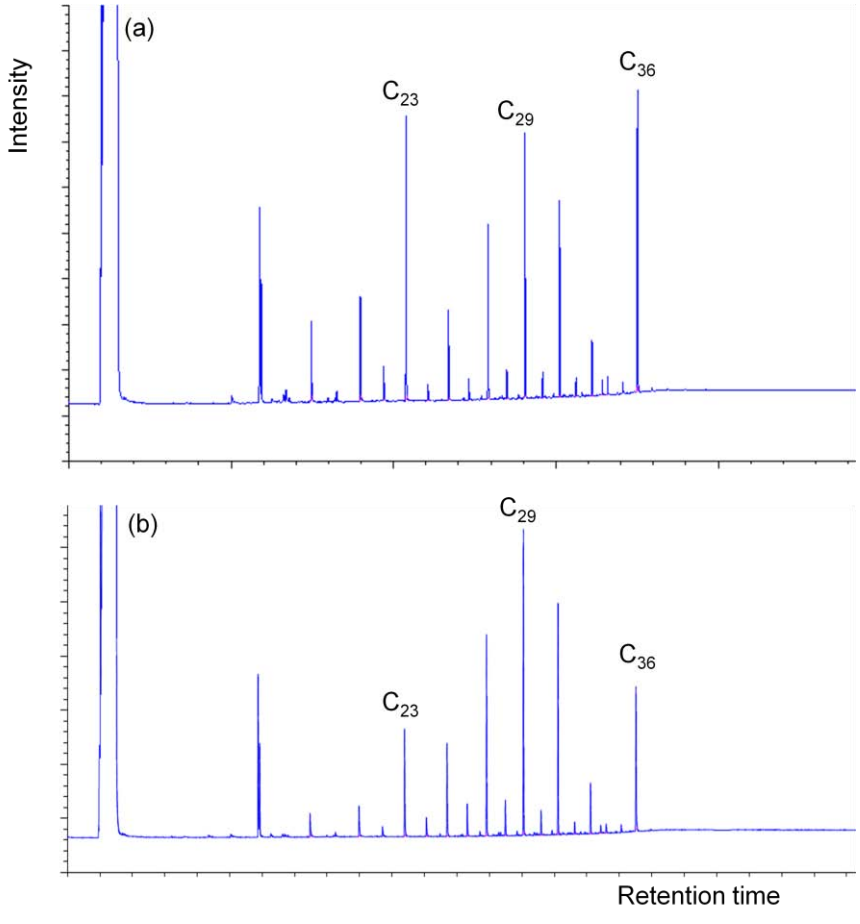

Figure 4-5 Chromatography of *n*-alkane distribution in the sediment trap, (a) November 2014, dominated by C_{23} alkane ; (b) December 2014, dominated by C_{29} alkane.

4.3.4. Compound-specific $\delta^{13}C$ values of n-alkanes

The $\delta^{13}C$ of *n*-alkanes could not be measured in samples from the two deeper sections as the concentration of *n*-alkanes was too low for accurate isotopic measurements, so we just present the carbon isotope data from the surface water and from the sediment trap. Throughout one year, $\delta^{13}C$ of all *n*-alkane homologues varied significantly (i.e. larger variation that the analytical error) in the surface waters, ranging from –30.3‰ in December 2013 to -38.1‰ in September 2014. The overall values typical of C3 plants, as it could be expected given the absence of C4 plants in the study area (Fig. 4-1, Table 4-2). Specifically, the $\delta^{13}C$ values for nC_{29} alkane declined 1.8‰ from December 2013 to June 2014, and 3.9‰ from June to September 2014. The trends for other long-chain *n*-alkanes were similar, but the magnitude of decreasing was larger for nC_{25} and nC_{27} alkane. This trend is consistent with new production in the water column that should be responsible for the variations of $\delta^{13}C$ in *n*-alkanes.

Table 4-2 Compound specific $\delta^{13}C$ values (‰) of long odd chain n-alkanes in SPM and sediment trap

	Sediment trap			**SPM 0 m**	
Month	**C_{27}**	**C_{29}**	**C_{31}**	**C_{27}**	**C_{29}**
Oct-13	-34.4	-32.5	-32.7	n.d	n.d
Nov-13	-35.2	-33.5	-32.8	n.d	n.d
Dec-13	-31.5	-32.6	-32.9	-30.4	-31.3
Jan-14	-33.6	-32.7	-32.6	n.d	n.d
Feb-14	-33.2	-32.9	-32.7	-30.8	-31.3
Mar-14	-33.0	-32.9	-32.4	-31.9	-32.8
Apr-14	-35.3	-33.0	-32.3	-32.2	-33.2
May-14	-35.0	-34.0	-34.5	-32.4	-33.9
Jun-14	-35.1	-34.0	-35.7	-32.1	-33.1
Jul-14	-34.2	-33.6	-35.0	-34.9	-34.3
Aug-14	-35.5	-33.0	-34.9	-37.0	-34.6
Sep-14	-35.8	-32.9	-33.8	-38.1	-37.0
Oct-14	-37.3	-33.5	-33.5	-35.5	-33.8
Nov-14	-35.4	-32.7	-32.9	n.d	n.d
Dec-14	-32.5	-32.8	-33.5	n.d	n.d
Feb-15	-34.8	-33.4	-34.1	n.d	n.d
Mar-15	-32.4	-33.1	-32.9	n.d	n.d

"n.d" indicates not detectable

The sediment traps showed more variable $\delta^{13}C$ variations between specific *n*-alkanes (Fig. 4-3, Table 4-2). The $\delta^{13}C$ variations of nC_{27} were largest, followed by nC_{31} and nC_{29} alkane even though they had similar mean values of -32.4‰, -33.1‰ and -33.5‰, respectively,

more depleted in longer chain homologues, such as the nC_{31} alkane. The values of $\delta^{13}C$ in nC_{29} alkane were the most stable and only dropping from June to August 2014. A number of factors might explain the $\delta^{13}C$ of *n*-alkane changes in the sediment trap, e.g. different sources of plant waxes, seasonality of the same species, soil fungi, insects and microbes as well as isotopic fraction (Chikaraishi & Naraoka, 2006). The experiment of carbon isotopic dynamics by Wang et al. (2014) showed that the $\delta^{13}C$ value of long chain *n*-alkanes changed only 0.6-1.7‰, which is less lower than the difference values between C3 and C4 plants even though 90% of initial organic matter was degraded. Thus, we think that $\delta^{13}C$ variations of *n*-alkanes in the sediment trap could be mainly driven by different sources of *n*-alkanes, just in the range of $\delta^{13}C$ values of *n*-alkanes in soils (Chapter 3) except that $\delta^{13}C$ of nC_{27} in November 2014.

4.3.5. Transport mechanism of alkyl lipids from higher plants

Certain environmental processes affect the patterns of *n*-alkanes eventually embedded in the sediments. The processes taking place are transportation, deposition and diagenesis (Brassell, 1987) and these processes depend on the aquatic environment itself (Morris and Culkin, 1975). Terrigenous organic matter is generally transported to lake sediments by winds and fluvial processes. We discussed above that the inputs of long chain *n*-alkanes in the water column are from April to August, which must be transported somehow by runoff or wind, from the point of generation on land to the site of deposition in the lake sediments. Therefore we try to look into the relationship between the precipitation/wind and concentrations/fluxes of *n*-alkyl lipids in the water column/sediment trap.

The variations of *n*-alkyl lipid fluxes were controlled by terrestrial as well as lacustrine processes. We think that most contributions of long chain *n*-alkanes/*n*-alkanoic acids could be attributed to terrestrial sources (dominated by nC_{29} and nC_{31} alkane) in the lake catchment. Here we compared nC_{29} alkane concentration and nC_{28} alkanoic acid concentration in the water column with mean daily accumulated precipitation during the sampling intervals. Positive relationships were found between precipitation and related alkyl lipid homologues of SPM in the water column (Fig. 4-6). All SPM samples showed that large uncertainty occurred at the lower end of precipitation, especially in May 2014, only 1.2 mm rainfall (R^2=0.47, Fig. 4-6a). The relationship between precipitation and nC_{28} alkanoic acids was weaker (R^2=0.37) than nC_{29} alkanes (Fig. 4-6b). It suggests that the long chain *n*-

alkanes were always transported to the water column by runoff which makes a large contribution to concentration of *n*-alkyl lipids in the water column when there was sufficient precipitation. However, the alkanes from the terrestrial plants or soils might be also transported by wind. We found that there were positive correlations between the nC_{29} alkane/nC_{28} alkanoic acid concentration from the surface water and the wind velocity (R^2=0.42 and R^2=0.18, respectively, Fig. 4-6c, d). Moreover, the effects of wind on nC_{29} alkane and nC_{28} alkanoic acid were different in different month. For example, nC_{29} alkane and nC_{28} alkanoic acid concentrations were highly correlated to wind velocity from January to July (R^2=0.80 and R^2=0.57, respectively). Therefore, long chain *n*-alkyl lipids derived from terrestrial higher plants were transported into the water column to some extent by runoff or wind and the controlling factor was changed depending on distinctive meteorological conditions. In addition, the effects of precipitation/wind on *n*-alkanes were more significant than *n*-alkanoic acids.

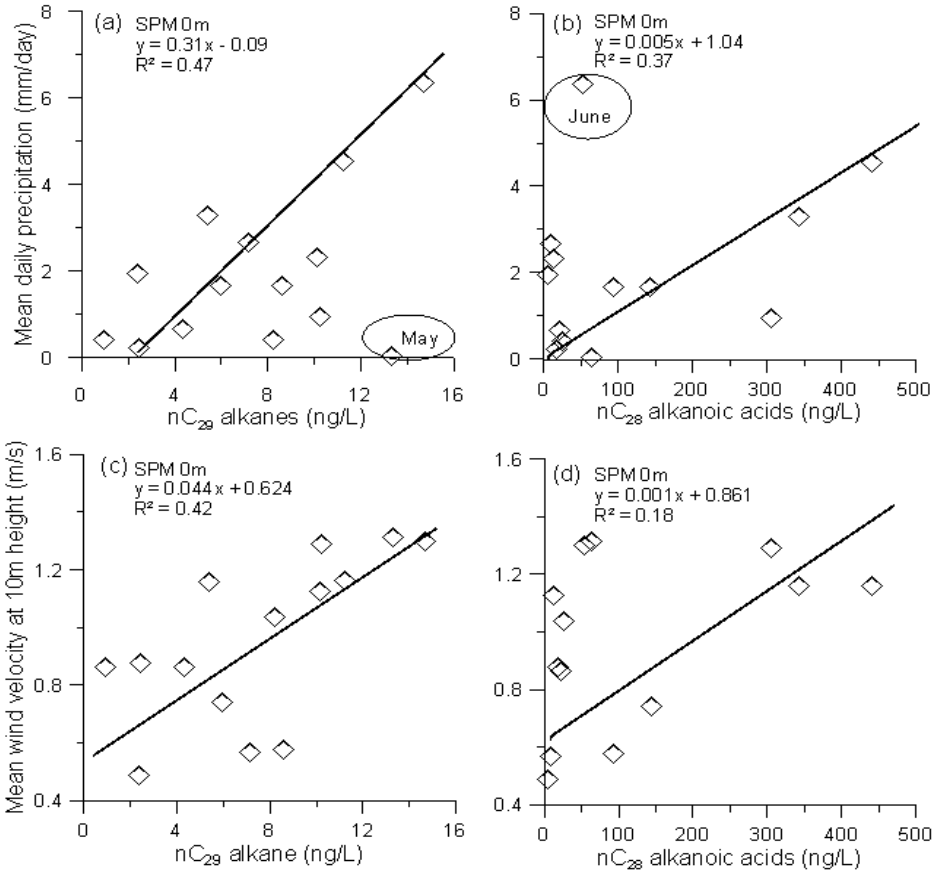

Figure 4-6 Suspended particulate matter (SPM) of water column containing *n*-alkanes and *n*-alkanoic acids correlated with the mean daily accumulated precipitation from the meteorological station: (a, c) *n*-C_{29} alkane concentration of SPM from the surface waters; (b, d) nC_{28} alkanoic acid concentration of SPM from the surface water

SPM needs two months to get into the deeper section, but the main particulates could sink faster and get to the lake bottom. The relationships between mean daily precipitation and *n*-alkyl lipids in the sediment trap were not significant (Fig. 4-7a, b). We also explore the relationships between sediment trap recovery rates of nC_{29} alkane/nC_{28} alkanoic acids and wind velocity. There was a positive relationship (R^2=0.45) between wind velocity and flux of nC_{29} alkane in the sediment trap (Fig. 4-7c), indicating that the flux of nC_{29} alkane in the sediment trap was affected by wind velocity except in December when the flux might be increased by resuspension processes in the lake. The relationship between the flux of nC_{29} alkanoic acid and wind velocity was also weak (Fig. 4-7d).

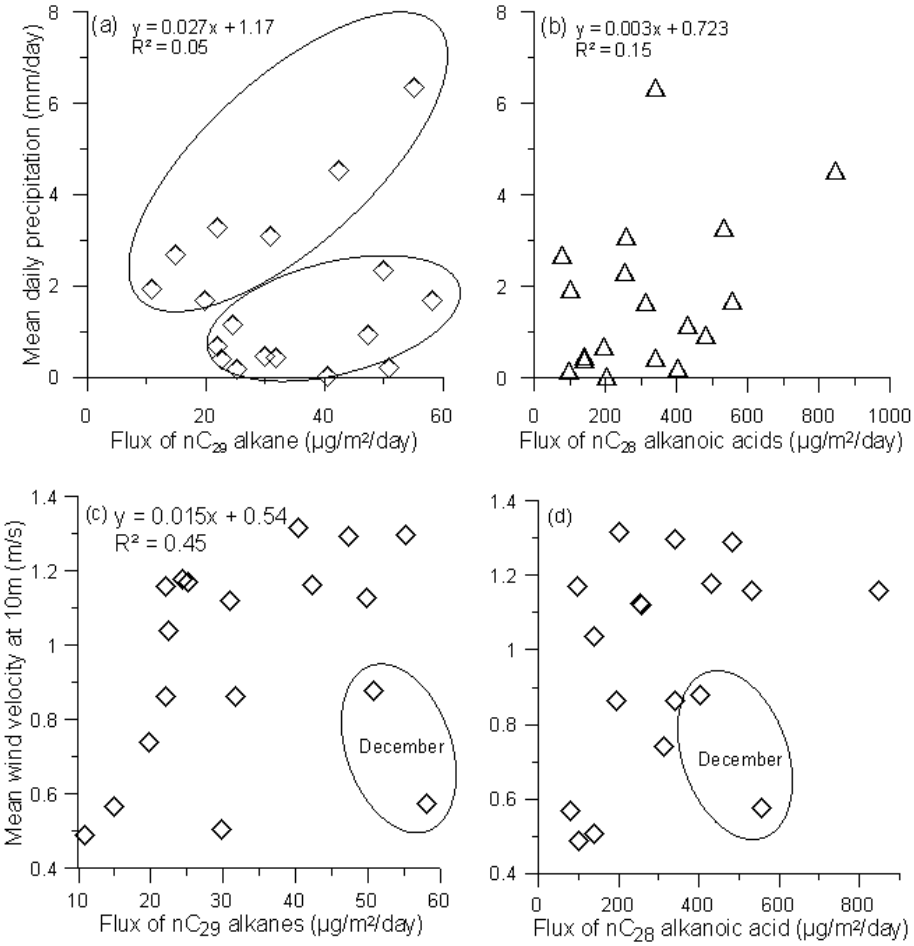

Figure 4-7 The relationship between mean daily precipitation /wind velocity and sediment trap flux of *n*-alkanes (a, c)/*n*-alkanoic acids (b, d) in Lake Montcortés

4.4. Conclusion

Here, we have a preliminary conclusion that the long chain *n*-alkyl lipids (nC_{29} alkane or nC_{28} alkanoic acids) in the water column of Lake Montcortés are mainly from the terrestrial higher plant inputs and their transport into the lake was to some extent due to precipitation and wind. In general, the *n*-alkane flux in the sediment trap was affected by runoff, wind condition, aquatic plants bloom and resuspension.

1) *n*-alkyl lipid concentration of SPM in the water column showed a clear seasonal pattern, with maxima in summer and minima in winter. With depth, *n*-alkyl lipids concentrations decreased towards the deeper sections. The fastest degrading rates of *n*-alkanes and *n*-alkanoic acids occurred in summer and spring, respectively. Fluxes of *n*-alkyl lipids in the sediment trap also showed seasonal changes, depicting the lowest values in February/March and the highest values in September/December.

2) P_{aq} of *n*-alkanes, which is used for indicating aquatic inputs, showed inputs of submerged/floating macrophytes in summer and autumn every year. SPM ACL of *n*-alkyl lipids in the water column seemed to indicate immediately mixing sources from the terrestrial plants or aquatic plants in the catchment. While ACL values and compound specific $\delta^{13}C$ of *n*-alkanes in the sediment trap stayed in the same level in an annual cycle, indicating that alkyl lipids in the sediment trap were from the surrounding soils by runoff rather than from the plant debris directly. CPI values in the water column recorded anthropogenic inputs in the lake in winter (probably by eolian transport).

4.5. References

Brassell et al., (1987). Natural background of alkanes in the aquatic environment. *Aquatic Pollutants: Transformation and Biological Effects.* 69-86.

Bush, R. T., & Mcinerney, F. a. (2015). Influence of temperature and C4 abundance on n-alkane chain length distributions across the central USA. *Organic Geochemistry*, *79*, 65–73. doi:10.1016/j.orggeochem.2014.12.003

Chikaraishi, Y., & Naraoka, H. (2006). Carbon and hydrogen isotope variation of plant biomarkers in a plant–soil system. *Chemical Geology*, *231*(3), 190–202. doi:10.1016/j.chemgeo.2006.01.026

Chikaraishi, Y., Naraoka, H., & Poulson, S. R. (2004). Hydrogen and carbon isotopic fractionations of lipid biosynthesis among terrestrial (C3, C4 and CAM) and aquatic plants. *Phytochemistry*, *65*(10), 1369–81. doi:10.1016/j.phytochem.2004.03.036

Corella, J. P., Brauer, A., Mangili, C., Rull, V., Vegas-Vilarrúbia, T., Morellón, M., & Valero-Garcés, B. L. (2012). The 1.5-ka varved record of Lake Montcortès (southern Pyrenees, NE Spain).

Quaternary Research, *78*(2), 323–332. doi:10.1016/j.yqres.2012.06.002

Corella, J. P., Moreno, A., Morellón, M., Rull, V., Giralt, S., Rico, M. T., … Valero-Garcés, B. L. (2010). Climate and human impact on a meromictic lake during the last 6,000 years (Montcortès Lake, Central Pyrenees, Spain). *Journal of Paleolimnology*, *46*(3), 351–367. doi:10.1007/s10933-010-9443-3

Del Rio, J. C., Gonzalez-Vila, F. J., & Martin, F. (1992). Variation in the content and distribution of biomarkers in two closely situated peat and lignite deposits. *Organic Geochemistry*, *18*(1), 67–78. doi:10.1016/0146-6380(92)90144-M

Ehleringer, J. R., Sage, R. F., Flanagan, L. B., & Pearcy, R. W. (1991). Climate change and the evolution of C(4) photosynthesis. *Trends in Ecology & Evolution*, *6*(3), 95–9. doi:10.1016/0169-5347(91)90183-X

Ficken, K. J., Li, B., Swain, D. L., & Eglinton, G. (2000). An n-alkane proxy for the sedimentary input of submerged/floating freshwater aquatic macrophytes. *Organic Geochemistry*, *31*, 745–749.

Killops, S., & Killops, V. (2005). *Introdution to Organic Geochemistry* (2nd ed.). Blackwell Science Ltd. doi:10.1002/9781118697214

Kunst, L., & Samuels, a L. (2003). Biosynthesis and secretion of plant cuticular wax. *Progress in Lipid Research*, *42*(1), 51–80. Retrieved from http://www.ncbi.nlm.nih.gov/pubmed/12467640

Kusch, S., Rethemeyer, J., Schefuß, E., & Mollenhauer, G. (2010). Controls on the age of vascular plant biomarkers in Black Sea sediments. *Geochimica et Cosmochimica Acta*, *74*(24), 7031–7047. doi:10.1016/j.gca.2010.09.005

Ladji, R., Yassaa, N., Balducci, C., & Cecinato, a. (2014). Particle size distribution of n-alkanes and polycyclic aromatic hydrocarbons (PAH_S) in urban and industrial aerosol of Algiers, Algeria. *Environmental Science and Pollution Research*, *21*(3), 1819–1832. doi:10.1007/s11356-013-2074-2

Meyers, P. A., & Eadie, B. J. (1993). Sources, degradation and recycling of organic matter associated with sinking particles in Lake Michigan. *Organic Geochemistry*, *20*(1), 47–56. doi:10.1016/0146-6380(93)90080-U

Meyers, P. A., Maring, H. B., & Bourbonniere, R. A. (1980). Alkane and alkanoic acid variations with depth in modern sediments of Pyramid Lake. *Physics and Chemistry of the Earth*, *12*(C), 365–374. doi:10.1016/0079-1946(79)90119-8

Meyers, P. A., & Takeuchi, N. (1979). Fatty acids and hydrocarbons in surficial sediments of Lake Huron. *Organic Geochemistry*, *1*(3), 127–138. doi:10.1016/0146-6380(79)90001-9

Nichols, J., Booth, R. K., Jackson, S. T., Pendall, E. G., & Huang, Y. (2010). Differential hydrogen isotopic ratios of Sphagnum and vascular plant biomarkers in ombrotrophic peatlands as a quantitative proxy for precipitation-evaporation balance. *Geochimica et Cosmochimica Acta*, *74*(4), 1407–1416. doi:10.1016/j.gca.2009.11.012

Pancost, R. D., & Boot, C. S. (2004). The palaeoclimatic utility of terrestrial biomarkers in marine sediments. *Marine Chemistry*, *92*(1-4), 239–261. doi:10.1016/j.marchem.2004.06.029

Pedentchouk, N., Freeman, K. H., & Harris, N. B. (2006). Different response of δD values of n-alkanes, isoprenoids, and kerogen during thermal maturation. *Geochimica et Cosmochimica Acta*, *70*(8), 2063–2072. doi:10.1016/j.gca.2006.01.013

Rao, Z., Zhu, Z., Wang, S., Jia, G., Qiang, M., & Wu, Y. (2009). CPI values of terrestrial higher plant-derived long-chain n-alkanes: A potential paleoclimatic proxy. *Frontiers of Earth Science in China*, *3*(3), 266–272. doi:10.1007/s11707-009-0037-1

Reddy, C. M., Eglinton, T. I., Pali??, R., Benitez-Nelson, B. C., Stojanovi??, G., Pali??, I., … Eglinton, G. (2000). Even carbon number predominance of plant wax n-alkanes: A correction. *Organic Geochemistry*, *31*(4), 331–336. doi:10.1016/S0146-6380(00)00025-5

Rull, V., González-Sampériz, P., Corella, J. P., Morellón, M., & Giralt, S. (2010). Vegetation changes in the southern Pyrenean flank during the last millennium in relation to climate and human activities: the Montcortès lacustrine record. *Journal of Paleolimnology*, *46*(3), 387–404. doi:10.1007/s10933-010-9444-2

Schouten, S., Hopmans, E. C., Schefuß, E., & Sinninghe-Damste, J. S. (2002). Distributional variations in marine crenarchaeotal membrane lipids: A new tool for reconstruting ancient sea-surface temperatures? *Earth and Planetary Science Letters*, *204*, 265–274.

Tipple, B. J., & Pagani, M. (2013). Environmental control on eastern broadleaf forest species' leaf wax distributions and D/H ratios. *Geochimica et Cosmochimica Acta*, *111*, 64–77. doi:10.1016/j.gca.2012.10.042

Tissot, B. P., & Welte, D. H. (1984). *Petroleum Formation and Occurrence*. *Second Revised and Enlarged Edition* (Vol. 66). doi:10.1029/EO066i037p00643

Vogts, A., Schefuß, E., Badewien, T., & Rullkötter, J. (2012). n-Alkane parameters from a deep sea sediment transect off southwest Africa reflect continental vegetation and climate conditions. *Organic Geochemistry*, *47*, 109–119. doi:10.1016/j.orggeochem.2012.03.011

Wang, G., Zhang, L., Zhang, X., Wang, Y., & Xu, Y. (2014). Chemical and carbon isotopic dynamics of grass organic matter during litter decompositions: A litterbag experiment. *Organic Geochemistry*, *69*(April 2016), 106–113. doi:10.1016/j.orggeochem.2014.02.012

Yong song Huang. F.Alayne Street-Perrott, R. Alan Perrott, Pierre Metzger, and G. E. (1999). Glacial – interglacial environmental changes inferred from molecular and compound-specific $\delta^{13}C$ analyses of sediments from Sacred Lake , Mt . Kenya, *63*(9), 1383–1404.

Chapter 5

Seasonal variations of glycerol dialkyl glycerol tetraether lipids (GDGTs) contents in the water column of a southern European lake

Abstract

To determine where and when the glycerol dialkyl glycerol tetraether (GDGT) distribution and the potential application in paleoclimate reconstruction in lakes, we collected samples of suspended particulate matter from the water column at three depths every month from October in 2013 to November 2014 and using sediment traps for 18 months to monitor the seasonal variations of GDGTs and implications of GDGT-based proxies in a oligotrophic karst lake (Lake Montcortés). The fluxes and concentrations of brGDGTs and isoGDGTs in sediment traps and SPM from the water column presented similar seasonal variations, showing high values in summer and autumn. The distribution of isoGDGTs in the lake system (water column, sediment trap and surface sediment) showed a typical pattern, indicating an aquatic origin for isoGDGTs in the lake. Concentrations of isoGDGTs decreased from the upper water column to the deeper section, indicating that isoGDGTs are produced in the upper water column in Lake Moncortès. Our results showed that TEX_{86} recorded the absolute temperature in the thermocline layer rather than bottom water temperature. Besides, SPM from water column reflected the temperature signals closer to the CTD-measured temperature at the thermocline water than sediment trap. Moreover, the TEX_{86} –derived temperatures matched well with mean annual lake surface water temperature using a global lake calibration curve. MBT/CBT-estimated temperatures from monthly SPM in water column and sediment traps were changeless to indicate the mean annual temperature rather than seasonal temperature changes.

5.3.1. Introduction

Sedimentary organic matter provides a variety of biomarker proxies to be used in the reconstruction of marine and continental paleoenvironments and paleoclimates (Meyers, 1997). In recent years, glycerol dialkyl glycerol tetraethers (GDGTs, see structures in Fig. 2-5) ratios have shown significant promise as proxies of various climatic and environmental parameters. These biomarkers are found ubiquitously in the environment (Weijers et al., 2006; Schouten et al., 2013), and can be sorted into two types: isoprenoid and branched GDGTs. The former (isoGDGTs), are produced in mesophilic environments by Archaea of the phylum Thaumarchaeota and Euryarchaeota (Brochier et al., 2008; Schouten et al., 2008) or from planktonic (Sinninghe Damsté et al., 2002), methanogenic (Llirós et al., 2010) and methanotrophic sources (Schouten et al., 2003). They are found typically in aquatic settings (Damsté et al., 2009; Karner et al., 2001; Wakeham et al., 2003), but also in peat

soils (Leininger et al., 2006; Huguet et al., 2015) and dust (Fietz et al., 2013). Branched GDGTs (brGDGTs), with sn1,2 stereochemistry, and containing methyl branched alkyl chains are purported to have a bacterial source in terrestrial settings, like peat bogs and soils (Hopmans et al., 2004; Weijers et al., 2006a; Weijers et al., 2006b), possibly from Acidobacteria (Weijers et al., 2009). However, brGDGTs are also detected in the water column of lakes and oceans, including coastal settings and rivers (Walsh et al., 2008; Peterse et al., 2009; Tierney et al., 2009).

The relative distribution of various isoGDGTs and brGDGTs homologues is temperature dependent. This finding led to the application of isoGDGT or brGDGT-derived proxies, such as TEX_{86} and MBT/CBT index. The former is based on ratios between isoGDGTs (GDGT-1, 2, 3 and GDGT4´), whereas the latter is based on establishing the number of methyl branches (MBT) and the degree of cyclisation (CBT) in brGDGTs. TEX_{86} has been applied for reconstructing sea surface temperature (SST) and lake surface temperature (LST), while the MBT/CBT index is generally applied to estimate continental air temperature (MAT) (Kim et al., 2008; Rao et al., 2009; Peterse et al., 2014). In continental settings, the application of TEX_{86} is believed to be constrained to large lakes due to the fact that Crenarchaeota in small lakes are not present in sufficient abundance to produce detectable amounts of isoGDGTS (Powers et al., 2010). Inputs of allochthonous organic matter containing isoGDGTs to lakes may potentially hamper the straightforward application of TEX_{86} (Huguet et al., 2007; Tierney et al., 2010; Loomis et al., 2011). Some studies that determined the provenance and distribution of GDGTs in suspended particulate matter (SPM) from the water column and sediment traps reached the conclusion that TEX_{86}-based temperature derived from sedimenting particles corresponded well with water temperature (Blaga et al., 2008; Woltering et al., 2012).

The sources of brGDGTs in aquatic settings is hypothesized by some researchers to derive partly from in-situ production in the water column as well as soils (Blaga et al., 2011; Schouten et al., 2012; Buckles et al., 2014). Nevertheless, their use as a biomarker to track terrestrial inputs to sediments is common (Hopmans et al., 2004; Loomis et al., 2014b), partly because they degrade more slowly than lignin, a well acknowledged terrestrial carbon marker (Huguet et al., 2008). Moreover, the brGDGTs and their related proxies, derived on fractional indices, have been proposed to reflect temperature, pH and nutrient conditions in lakes, which make them a very attractive proxy in lake sediments (Loomis et al., 2014a). The

validation of brGDGT proxies in lakes has been assessed on local and global scales (Tierney et al., 2010; Weijers et al., 2011; Peterse et al., 2012; Hopmans et al., 2016).

Water or air temperature appears to be the primary control on the sedimentary distributions of GDGTS (Pearson et al., 2011; Loomis et al., 2014a). However, it is still debated the role of secondary parameters, the site of production in the water column and the spatiotemporal variations in driving the distributions and fluxes of GDGTs, and how all these affect the aforementioned indices to estimate surface lake or sea temperature (Blaga et al., 2011; Huguet et al., 2011; Woltering et al., 2012; Loomis et al., 2014b). It is very important to understand what temperature the TEX_{86} proxy represents in different lakes before it is applied for paleotempertuare reconstructions. In order to appraise the application of GDGTs proxies we have investigated their seasonal and depth variability in the water column of Lake Montcortés. We seek to establish if there is a seasonality in the production and fluxes of GDGTs in the lake water column and whether seasonality may influence the sedimentary values of the GDGTs proxies.

5.3.2. Methods and Material

5.3.3. Study area

Lake Montcortés (42°19'50''N, 0°59'46''E, 1027m a.s.l.), located in Pre-Pyrenean Range, is one of the deepest karstic lakes (about 30m) in the Iberian Peninsula (Alonso, 1998) (Fig. 2-1). Its watershed is on Triassic bedrock, comprising mainly carbonates, evaporites, claystones and shale formations (Rosell, 1994; Corella et al., 2012). The lake is roughly circular with a total diameter of 1320 m, and it is meromictic and oligotrophic (Camps et al., 1976). Relatively high surface/depth ratio and steep margins (Fig. 2-1) provide favorable environments for deposition and preservation of finely laminated facies (Corella et al., 2010). Surface water has an average pH value of 8.4, whereas the pH is only 7.5 in the anoxic hypolimnion (Modamio, 1988; Corella et al., 2012) and episodes of holomixis during the winter have also been documented (Modamio et al., 1988).

Total mean annual rainfall is 860 mm with the most humid seasons in spring and autumn (Corella et al., 2012). The lake is recharged by precipitation (groundwater and runoff inputs) and loses water mainly by evaporation or through a temporal outlet in the northern end. Mean monthly air temperature ranges from 1.9°C in the coldest month (January) to 20.3°C in

the warmest (July), showing a continental character of the regional Mediterranean alpine climate type (Corella et al., 2012).

The main vegetation formations in the lake catchment are evergreen oak forest, deciduous oak forests, conifer forests and littoral vegetation (Rull et al., 2010).

5.3.4. Sampling

A sediment trap was deployed and retrieved monthly at 20m within the lake to collect settling particulate matter (see section 2.2.4 for a full description). The SPM in 40 L water was collected every month at three depths: surface (0 m, 20 cm under water level), thermocline (5-12 m depth) and above the sea floor (20-22 m) from September 2013 to November 2014. Data on water column parameters were obtained by Dra Teresa Vegas from the University of Barcelona, and her collaborators, who undertook monthly CTD profiles in the same day when the sediment traps were retrieved from the Lake Montcortés, which generally was one day earlier than our water SPM sampling took place. All samples for core GDGT analyses were immediately filtered through pre-combusted glass fiber filters (GF/F filters) with a pore size of 0.7µm when transported to the laboratory. The filters were freeze-dried before analysis. The surface samples were collected in February 2013.

5.3.5. Extract clean up

SPM filters from the water column were added a GDGT (i.e. GR) internal standard, and were immersed in 50 mL (20+15+15 mL) of dichloromethane:methanol (3:1,v/v) in wide-mouth test tubes. Each tube containing solvent and filters were shaken using a rotational speed of 1800 rpm for 30 seconds before ultrasonic solvent extraction. All tubes were fixed in a rack in an ultrasonic bath for 10 min before, and subsequently centrifuged at 2000 rpm for 5 minutes. The supernatant was transferred into pearl-shaped vessels and dried at 27 °C in a rotary evaporator under vaccuum.

The method of column chromatography for separating and purifying the liquids different compounds is adapted from (Huang et al., 1999) and (Schouten et al., 2002), using pasteur pipettes (previously combusted at 450 °C/ hours) and amino propyl silica (cleaned by Soxhlet with dichloromethane:methanol (2:1, v/v) during 24 hours). About 0.7 g of aminopropyl silica and 0.5 g of Na_2SO_4 were placed over a piece of cotton that plugged the narrow end of the pipette. The column were conditioned with 3 mL of dichloromethane:isopropanol (2:1, v/v), and after placing the extract, they were eluted 6 mL dichloromethane:isopropanol (2:1, v/v;

F1 or neutral fraction) and 8 mL diethyl ether:acetic acid (96:4, v/v; F2 or acid fraction). The F1 fraction was further separated through a silica column into non-polar (F1-1; n-alkanes), slightly polar (F1-2, reserved) and polar fractions (F1-3; GDGTs) with 5 mL hexane, 4 mL dichloromethane and 6 mL dichloromethane:methanol (95:5, v/v).

5.3.6. Instrumental analysis

For GDGT analysis, fraction (F1-3) was dried and dissolved in 200-600 µL hexane:isopropanol (99:1,v/v) and filtered through a 0.45 PTFE filter. Between 5 to 20 µL solvent was injected in an Agilent Time-Off-Flight (TOF) mass spectrometer with an atmospheric pressure chemical ionization (APCI) interface set in positive mode. Following the methods in (Escala et al., 2007; Huguet et al., 2013), the extracts were eluted through a Tracer Excel CN column (Teknokroma; 20 cm length, 0.4 cm diameter and 3 µm particle size) equipped with a pre-column filter and a guard column. The mobile phase consisted of n-hexane:isopropanol (98.5:1.5) and was eluted at a flow of 0.6 mL/min. The proportion of isopropanol was held at 1.5% for 4 minutes and increased gradually to 5% during 11 minutes, then increased to 10% for another 1 minute, and remained at this proportion for another 4 minutes, to be finally decreased back to 1.5% during 1 minute and held at 1.5% for 9 minutes until the end of the run. The parameters of the APCI interface were set as follows to generate positive ion spectra: corona discharge 3 µA, vaporizer temperature 400 °C, sheath gas pressure 49 mTorr, auxiliary gas (N_2) pressure 5 mTorr and capillary temperature 200 °C. GDGTs were detected in selected ion monitoring (SIM) mode of $[M+H]^+$ ± 0.5 m/z units to increase signal to noise ratio at the following at m/z (Schouten et al., 2007): 1302, 1300, 1298, 1296, 1292, 1050, 1048, 1046, 1036, 1034, 1032, 1022, 1020, 1018 and the synthetic tetraether lipid (GR) at 1208 m/z (Fig. 2-7).

The GDGTs indices that were measured are defined as following:

TEX_{86} as defined by (Schouten et al., 2002):

$$TEX_{86} = \frac{[GDGT-2]+[GDGT-3]+[GDGT-4']}{[GDGT-1]+[GDGT-2]+[GDGT-3]+[GDGT-4']} \quad \text{(eq. 5.1)}$$

LST estimates were calculated using the lacustrine calibration by Powers et al. (2010):

$$LST = -14.0 + 55.2 \times TEX_{86} \quad \textit{(eq. 5.2)}$$

The number of methyl groups (MBT) and cyclisation ratio of branched tetraethers (CBT) as defined by Weijers et al. (2007):

$MBT = (Ia + Ib + Ic)/(all\ brGDGTs)$ *(eq. 5.3)*

$CBT = -log\ (\frac{Ib+IIb}{Ia+IIa})$ *(eq.5.4)*

MAT1 estimates were calculated by Weijers et al. (2007) and MAT2 was from (Peterse et al., 2012).

$MAT1 = (MBT - 0.122 - 0.187 * CBT)/0.02$ (eq. 5.5)

$MAT2 = 0{,}81 - 5{,}67 * CBT7 + 31 * MBT$ *(eq.5.6)*

5.3.7. Results and discussion

5.3.8. Environmental conditions

At three depths in the water column, water temperatures ranged from 4.5 to 22.3 °C (mean 14.6 °C) at the surface, from 4.4 to 20.2 °C (mean 12.4 °C) at the thermocline and from 3.5 to 7.4 °C (mean 5.4 °C) near the lake bed (Fig. 2-8b). Thus, the two upper water column temperatures show a marked seasonality which closely track the variability in the air temperatures in La Pobla de Segur, whereas the bottom water temperatures are much more stable, and rather constant throughout the sampling period. The water column was markedly stratified from spring to autumn, while the highest temperatures were reached in June and July in the metalimnion and epilimnion, respectively. The minimum temperatures at the three depths occurred in February, and the water column was mixed in winter (December to February) when the temperatures of the whole water column cooled down below 6°C. The occurrence of stratification led to a depletion in the dissolved oxygen (DO), with values near the sea floor of 0 to 7.8 mg/L, and the occurrence of anoxia in the hypolimnion lasted from July to December (Fig. 2-8c). In contrast, DO values were relatively constant at the surface, ranging from 6.7 to 9.5 mg/L, while waters in the thermocline showed DO values spanning a range of 4.8 to 14.9 mg/L. The higher DO values in the thermocline than at the surface, from April to October, was probably related to an increase in primary productivity in summer and early autumn. The seasonal variability in stratification and mixing of the water column seems to have been driven by changes in water temperature, rather than wind as the latter is weakest when DO starts increasing in the deepest waters, and water temperatures become homogeneous throughout the water column. Conversely, during the highest mean values of wind velocity, the lake was stratified and the bottom waters became oxygen depleted.

The period when the water column was well mixed for months, and had homogeneous temperatures at the three depths, coincided with the occurrence of the lowest sediment mass fluxes (the lowest value was 2.56 g/m^2/day in February 2014). Conversely, when the lake water column was stratified, sediment fluxes increased to the highest values in the study period (the highest value of 28.28 g/m^2/day in July). It does appear, thus, that biogenic production in the water column was one of the chief processes that drove total sediment fluxes. From April to September 2014, a gradual increase/decrease in the sediment fluxes occurred in parallel with the values of DO at the thermocline being higher than at the lake surface, which was likely related to biogenic production. At the onset of winter, in November/December 2014 and 2015, as the water column stopped being stratified, it also coincided with a period of relatively high sediment fluxes. These gradually decreased as the lake water column continued being well mixed until stratification gradually began (i.e. February 2014 and March 2015). The winter high sediment fluxes are not linked to increases in run off nor eolian transport, as the values of precipitation and wind velocity do not appear to be coupled to sediment mass fluxes. Instead they are likely to be caused by increases of production driven by nutrient supply to the surface with the onset of mixing in the lake.

5.3.9. Seasonal variability in the concentrations and fluxes of GDGT classes in the water column and the sediment trap

Changes in the concentrations of isoGDGTs from the SPM are likely to reflect the abundance of Thaumarchaeota over time and space. The surface waters of the lake experienced isoGDGT concentrations from 0.1 ng/L (February 2014) to 2.2 ng/L (November 2014). The thermocline waters showed values between 0.1 ng/L (April) and 2.20 ng/L (August 2014), and the bottom waters showed values in a range of 0.1 ng/L (April/May) and 1.1 ng/L (September) (Fig. 5-1a). It appears that there were distinctive low-high isoGDGT concentration periods at three depths in the water column. Low concentrations appeared from January to April/May for the upper sections of the water column and from March to June for the deeper section. The higher concentrations appeared in May/June to August/November for SPM from upper/deeper section of the water column, presenting a time-lag for the production of isoGDGTs towards deeper water colomn. It is apparent that the isoGDGTs in the SPM generally had higher concentrations in the upper sections of the water

column from April to August but showed an opposite trend from September 2014 to February 2015 except in November 2014.

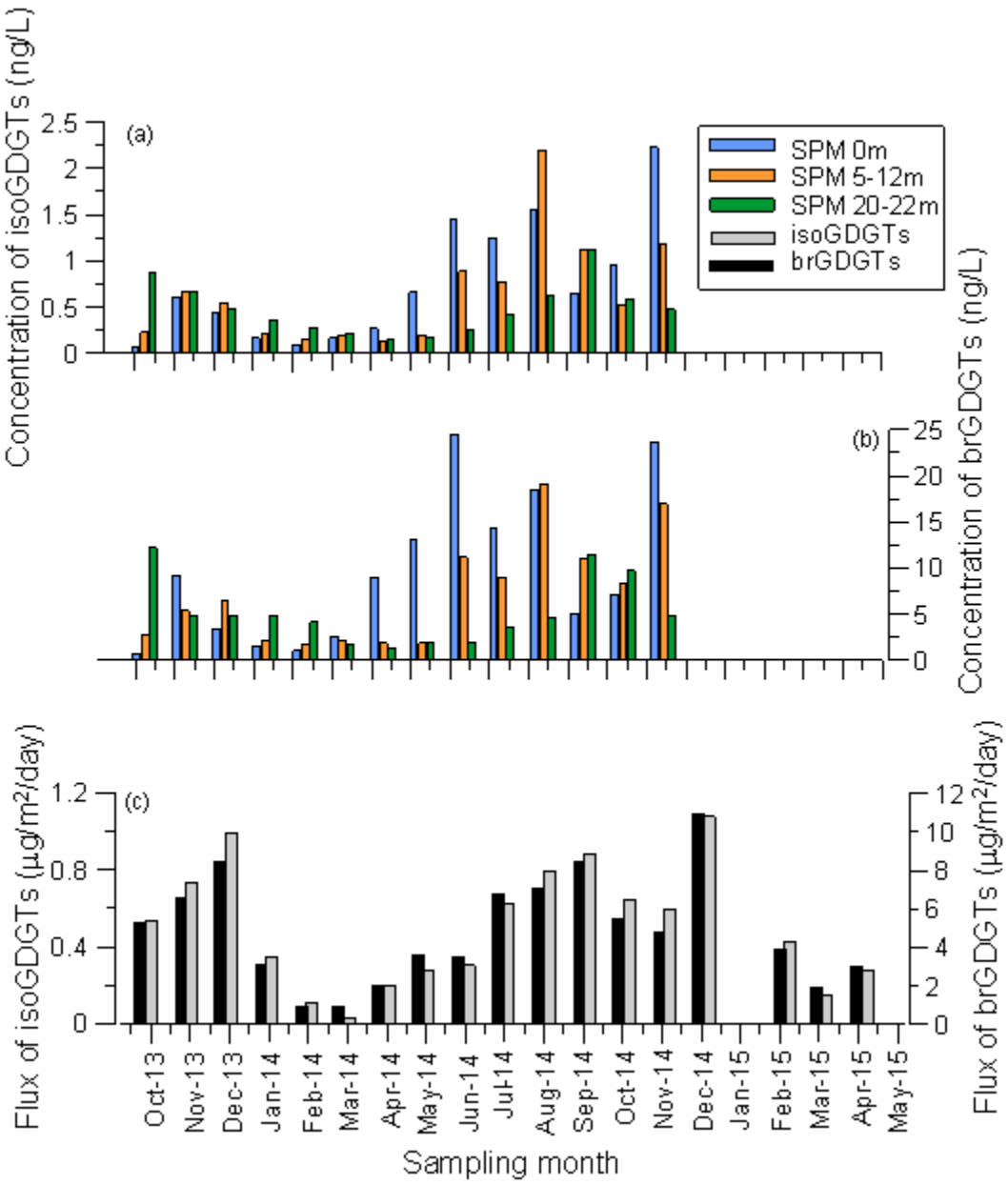

Figure 5-1 Concentrations of isoGDGTs (a) and brGDGTs (b) of SPM in the water column from September 2013 to November 2014, blue bar, orange bar and green bar stand for SPM at three depths: 0m, 5-12m and 20-22m, respectively; (c) isoGDGT flux (grey bar) and brGDGT flux (black bar) in the sediment trap from October 2013 to April 2015 in Lake Montcortés

The brGDGT concentrations in SPM from the surface water ranged from 1.1 ng/L (February) to 24.4/23.6 ng/L (June/November 2014). The thermocline water had brGDGT concentration in a range of 1.8 ng/L (February) and 19.1 ng/L (August) and the bottom water showed the concentration between 1.4 ng/L (April) and 12.2 (October) (Fig. 5-1b). The

concentration decreased from the upper to the deeper water column from April to August, but showed equal or higher values from September to February next year. Thus, the main production of brGDGTs was from April to August in the upper water column and from July to December in the bottom water. Some studies reported increasing brGDGTs concentrations in anaerobic environments (Huguet et al., 2010; Weijers, et al., 2006). The increased brGDGT concentration of SPM in the deep water from July to December corresponds to stratified water column with oxygen depletion (Fig. 2-2), suggesting that anaerobic conditions in the water column might favor brGDGT production. However, the variation of DO conditions in the water column could not explain the data from the upper water column that presented markedly different values throughout the year even though the DO was abundant all the year. Thus, more factors besides DO are responsible for increased brGDGT concentration in the water column.

The flux of isoGDGTs showed two maxima in both December (0.99/1.08 μg/m^2/day) and September 2014 (0.89 μg/m^2/day), and the minimum (0.03 μg/m^2/day) in February. Similarly, the flux of brGDGTs showed two maxima in both December (8.48/10.92 μg/m^2/day) and September (8.42 μg/m^2/day), and the minimum in February/March (0.92/0.88 μg/m^2/day). The flux data obviously suggest that the main input phase of isoGDGTs and brGDGTs to the sediments in Lake Montcortes is from July to December, and the maximum and minimum were consistent with the mass peaks (Fig. 2-2, Fig. 5-1c).

The abundant concentration (April to September) and flux in the water column and sediment trap were probably related to the bloom of phytoplankton in summer and autumn as well as delivery of nutrients from runoff in the catchment, as there were more rainfall from June to November 2014 (Fig. 2-2). The period of increasing concentration of isoGDGTs in May corresponds to the timing of great spring phytoplankton bloom (such as Cyclotella) in the surface waters of Lake Montcortés (Modamio et al., 1988). The onset of thermal stratification in the water column certainly strengthened the concentration difference of GDGTs at three depths (Fig. 5-1a, b). The phytoplankton bloom in the surface water could make contribution to the increasing amount of SPM in the water column and also settling particulate matter in the sediment traps by transporting isoGDGTs from the upper water column, which agreed with observed increasing fluxes of isoGDGTs in the sediment trap from spring. The seasonal changes can depend on the release of ammonium from the particulate organic nitrogen produced by phytoplankton communities in the lake surface waters (Blaga et al., 2011).

Table 5-1 Concentrations of isoGDGTs and brGDGTs, TEX_{86} (Schouten et al., 2002), MBT and CBT values, reconstructed MAT (Weijers et al., Peterse 2012) for SPM at three depths of water column from October 2013 to November 2014.

	brGDGT	isoGDGT	GDGT-0/ GDGT-4	MBT	CBT	TEX_{86}	LST	MAT1	MAT2
0 m	**µg/L**	**µg/L**					**ºC**	**ºC**	**ºC**
Dec-13	0.69	0.08	17.51	0.23	0.51	-	13.6	0.8	12.7
Jan-14	9.26	0.71	9.33	0.22	0.54	0.55	16.5	0.1	12.1
Feb-14	3.47	0.51	18.29	0.24	0.50	0.35	5.1	1.0	12.8
Mar-14	1.59	0.19	22.21	0.24	0.53	0.37	6.4	1.2	12.9
Apr-14	1.05	0.11	9.99	0.25	0.51	0.37	6.3	1.7	13.2
May-14	2.56	0.19	11.06	0.19	0.57	-	9.8	-2.1	10.6
Jun-14	9.01	0.32	33.25	0.14	0.62	0.48	12.8	-4.7	8.7
Jul-14	13.12	0.77	16.34	0.15	0.58	0.65	22.1	-4.2	9.2
Aug-14	24.42	1.70	17.16	0.18	0.62	0.47	11.8	-2.8	10.0
Sep-14	14.24	1.46	18.21	0.21	0.56	0.48	12.6	-1.0	11.3
Oct-14	18.43	1.81	16.75	0.22	0.57	0.48	12.4	-0.6	11.5
Nov-14	5.09	0.76	9.06	0.22	0.57	0.48	12.3	-0.3	11.8
Oct-14	7.16	1.12	13.47	0.15	0.74	0.45	10.7	-5.5	7.8
Nov-14	10.07	2.29	20.45	0.46	-0.08	0.44	10.2	17.7	25.5
5-12 m							11.6	0.1	12.2
Oct-13	0.44	0.22	13.91	0.25	0.53	0.53	15.2	1.4	13.2
Nov-13	5.36	0.67	12.33	0.23	0.48	0.45	11.0	0.8	12.9
Dec-13	6.50	0.55	11.65	0.20	0.62	0.47	11.7	-2.0	10.6
Jan-14	2.05	0.21	18.82	0.24	0.52	0.35	5.3	1.3	13.1
Feb-14	1.75	0.15	20.75	0.25	0.50	0.39	7.3	1.7	13.4
Mar-14	2.04	0.20	12.78	0.22	0.51	0.48	12.7	0.1	12.4
Apr-14	1.88	0.13	8.17	0.19	0.55	0.43	9.8	-1.5	11.2
May-14	1.87	0.19	9.36	0.21	0.47	0.50	13.7	-0.1	12.3
Jun-14	11.13	0.89	11.87	0.20	0.51	0.52	14.6	-0.9	11.7
Jul-14	9.02	0.77	11.72	0.22	0.56	0.48	12.6	-0.1	12.0
Aug-14	19.12	2.20	15.10	0.21	0.51	0.49	13.1	-0.6	11.8
Sep-14	10.93	1.12	12.84	0.25	0.53	0.54	16.1	1.2	13.0
Oct-14	4.37	0.52	8.97	0.37	0.01	0.53	15.4	12.3	24.7
Nov-14	7.50	1.27	13.96	0.34	0.15	0.60	19.1	9.5	20.2
20-22 m							12.7	1.7	13.7
Oct-13	1.29	0.88	17.73	0.25	0.48	0.47	11.8	1.8	15.4
Nov-13	4.85	0.66	15.63	0.22	0.45	0.50	13.5	0.8	15.0
Dec-13	4.92	0.47	15.25	0.20	0.54	0.51	14.0	-0.9	13.7
Jan-14	4.91	0.36	13.60	0.24	0.52	0.46	11.6	1.1	15.0
Feb-14	4.11	0.28	17.60	0.24	0.50	0.33	4.4	1.4	15.2
Mar-14	1.79	0.21	16.92	0.23	0.48	0.42	9.2	1.2	15.2
Apr-14	1.37	0.15	17.56	0.17	0.72	0.39	7.5	-4.6	10.5
May-14	1.98	0.16	9.89	0.21	0.47	0.47	12.0	-0.2	14.2
Jun-14	2.00	0.26	16.32	0.20	0.45	0.46	11.5	-0.4	14.2
Jul-14	3.54	0.42	19.05	0.19	0.44	0.40	8.0	-1.0	13.6
Aug-14	4.63	0.63	16.60	0.22	0.48	0.42	9.1	0.4	14.6
Sep-14	11.46	1.12	16.35	0.30	0.62	0.61	19.5	3.0	15.9
Oct-14	4.37	1.04	16.92	0.30	-0.22	0.49	12.8	3.0	15.9
Nov-14	2.77	0.76	19.32	0.30	0.41	0.48	12.5	3.0	15.9

It seems that isoGDGT and brGDGT concentrations varied in parallel over time and space in the water column. Even though there is no satisfying reason to explain the global pattern of strong correlations between brGDGTs and crenarchaeol, a mixed source for both GDGT types is commonplace (Fietz et al., 2012), which may indicate a common environment process, e.g. co-variance between nutrient inputs by run-off and aquatic productivity (Ge et al., 2014). The similar trends of seasonal patterns of brGDGTs and isoGDGTs may be attributed to diatom bloom-related brGDGTs or the same external processes that controls the production of brGDGTs in situ or transport of brGDGTs outside the lake. Moreover, the highest fluxes of isoGDGTs and brGDGTs in the sediment trap occurred in December when the lake started to present a mixed water column. This can be due to the resuspension or transport of settling particles towards the deeper water column from the sediment boundary layer when the water column started to be mixed since December (Baker & Eisenreich, 1989). Resuspension and transport of SPM towards the deeper water column could also be driven by external factors, such as rainstorms, which could have brought in allochthonous GDGTs from the surrounding soils and deposited them in the upper water column. This process could be explained by the highest amount of precipitation in August and November resulting in highest fluxes of isoGDGTs and brGDGTs in September and December (Fig. 5-1c).

5.3.10. Seasonal variability in GDGT distributions in the water column and sediment trap

The presence of GDGT-0, 1, 2, 3 and 4 (crenarchaeol), 4’ (regio-isomer crenarchaeol) in soils (Chapter 3) and water column (this study) indicates that isoGDGTs in the lake sediment can be derived from soil inputs into the lake or in situ Thaumarchaeota production in the water column. All SPM, sediment trap and surface sediment samples were dominated by GDGT-0, followed by GDGT-1, GDGT-2 and GDGT-4 (Fig. 5-2). However, isoGDGT distribution patterns in the SPM were different from those found in soils and similar to surface sediment (Chapter 3), which are dominated by GDGT-0 and/or GDGT-4. The increased abundance of GDGT-1 and GDGT-2 in the water column and sediment trap seemed to indicate that these GDGT homologues in the water column are mainly produced in situ in the lake environment. GDGT-0 is assumed to be produced by all major groups of Archaea except halophilic Archaea while crenarchaeol is mainly from Thaumarchaeota (Schouten et al., 2013). Thus, the ratio of GDGT-0/crenarchaeol is proposed to distinguish methanogen-

derived isoGDGTs: if this ratio is >2, it indicates a substantial methanogenic origin for GDGTs (Blaga et al., 2009), as in Group I Crenarchaeota this ratio is between 0.2 and 2 to be considered as temperature-dependent (Schouten et al., 2002). The GDGT-0/crenarchaeol ratio ranged from 0.2 to 4.4 in surrounding soils in Montcortés (Chapter 3). Whereas this ratio was between 13.0 and 16.7 in water column and sediment traps, and the values were 21.8 in surface sediment (Table 5-1). The ratios at three depths in water column were stable and never showed variations along depths or DO conditions, indicating some Archaea settings other than methanogenic sources and Group I Crenarchaeota should be responsible for high concentration of GDGT-0 in the water column (Blaga et al., 2009). Therefore, GDGT-0/crenarchaeol ratio >2 in the water column and sediment trap cannot be used to indicate methanogenic-derived GDGTs, but might be used as an endmember of soil input GDGTs.

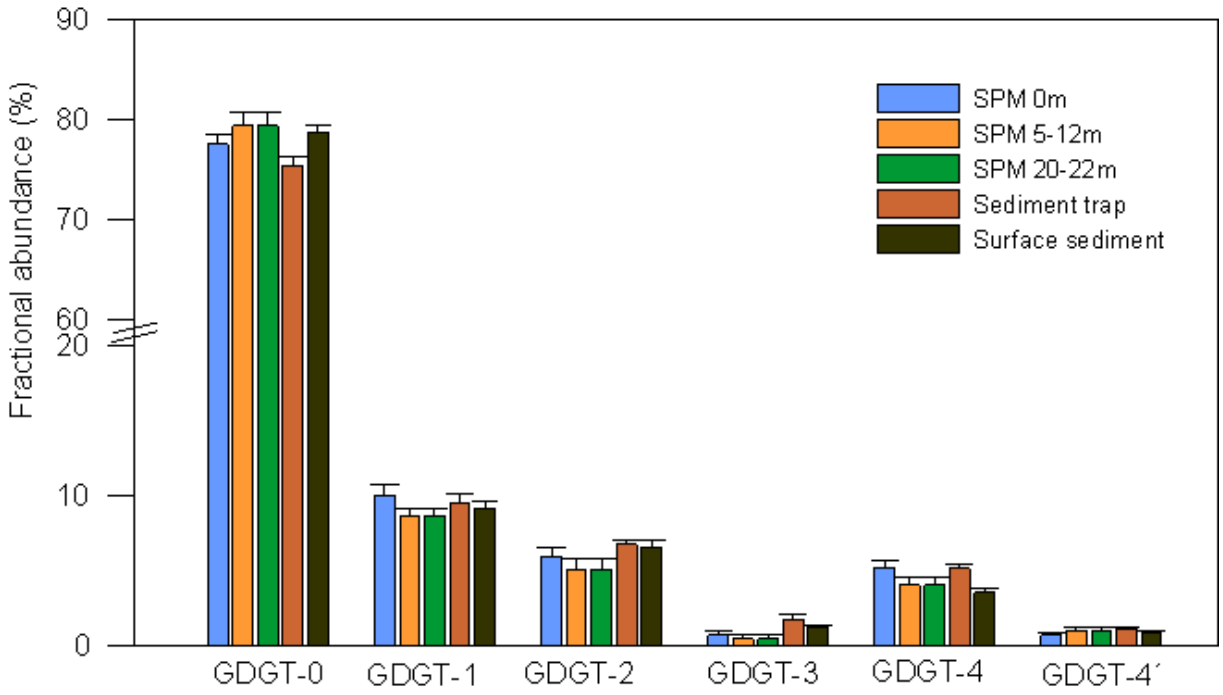

Figure 5-2 Fractional abundance of isoprenoid GDGTs in the water column (0 m, 5-12 m, 20-22 m), the sediment trap and surface sediment (0–2 cm).

The brGDGTs occupied a substantial fraction of GDGTs in the lake (>80%), which was consistent with the previous studies in lakes that brGDGTs are widely present (Blaga et al., 2009; Powers et al., 2010). brGDGT distribution in SPM, trap and surface sediments showed that the lake brGDGTs were dominated by GDGT-IIa, GDGT-IIIa, GDGT-Ia, followed by GDGT-IIb and GDGT-Ib (Fig. 5-3). This distribution and flux variations of GDGTs in the sediment trap supports the idea that erosion of catchment soil mainly delivers brGDGTs to the water column and finally sink into the sediment. However, in situ production of brGDGTs

for the surface sedimentary processes might contribute more GDGT-IIIa as its relative abundance was higher in the sediment than in the SPM and sediment trap (Fig. 5-3). The fractional abundance of GDGT-IIIa ranged between 20-40%, 17-32%, 23-36% and 24-31% for SPM from three depths of the water column and the sediment trap, presenting lower contributions in January/February and higher concentrations in April to August (Table 5-1), consistent with observed concentration or flux variations and to confirm the inputs of new production containing GDGT-IIIa.

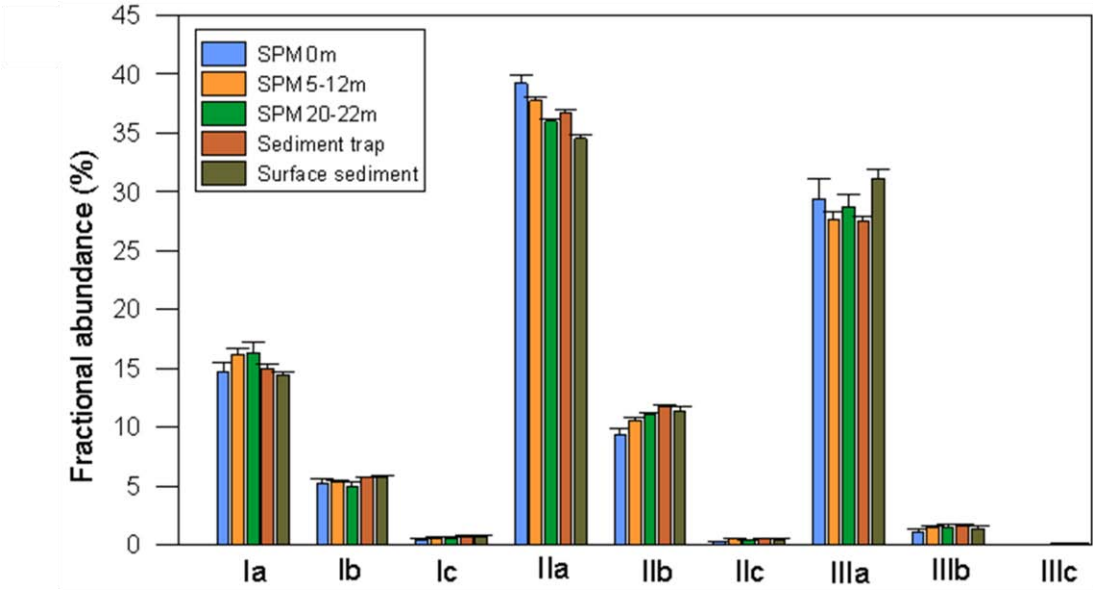

Figure 5-3 Fractional abundance of branched GDGTs in the water column (0 m, 5-12 m, 20-22 m), the sediment trap and surface sediment (0–2 cm).

5.3.11. TEX_{86} values and estimated temperatures in the water column and sediment trap

The application of TEX_{86} in the sediment needs more understanding of the ecology and patterns of in situ production of isoGDGTs derived from Thaumarchaeota living in the water column. We explained above that TEX_{86} related GDGTs in Lake Montcortes are mainly derived from in situ production in the water column. However, TEX_{86} values from soil-derived isoGDGTs are seasonally stable (Chapter 2), and a large input could modify the TEX_{86} signal from the isoGDGTs produced in situ towards the high-value end. Here we start to present the TEX_{86} values at three depths of the water column and sediment trap throughout the year and try to find whether they are biased by soil inputs or methanogenic sources.

TEX_{86} values of SPM ranged from 0.35 (December) to 0.65 (May) with a mean value of 0.46±0.02 for the surface water, from 0.35 (January) to 0.60 (November) with a mean value of 0.48±0.02 for the thermocline water, and from 0.33 (February) to 0.61 (September) with a mean value of 0.46±0.02 for the deep water (Table 5-1). It is apparent that TEX_{86} values varied in line with seasonal variations in temperature in the water column. Besides, there is a time lag for the minimum TEX_{86} present in the upper section to the deeper section. However, the maximum values appearing in different months showed that the warming signals may be related to soil inputs or processes in the lake. In the sediment trap, TEX_{86} values of settling particulates varied between 0.39 (February) and 0.63 (April), with a mean values of 0.51±0.02 that was consistent with TEX_{86} from surface sediments (0.54±0.01) that was higher than those from SPM. It seems to follow a seasonal change of temperature. The highest values in April are probably affected by new production of isoGDGTs within the lake rather than soil inputs that provide relatively high values and transported to the lake by runoff or wind, indicating that isoGDGTs in the sediment trap and surface sediment were not only from water column, which might be affected by other processes (such as methanogenic production) or older, allochthonous lipids were transported into the lake (Woltering et al., 2012). The significant seasonal trend of TEX_{86} values could be potentially used to reconstruct temperatures in the water column and sediment trap.

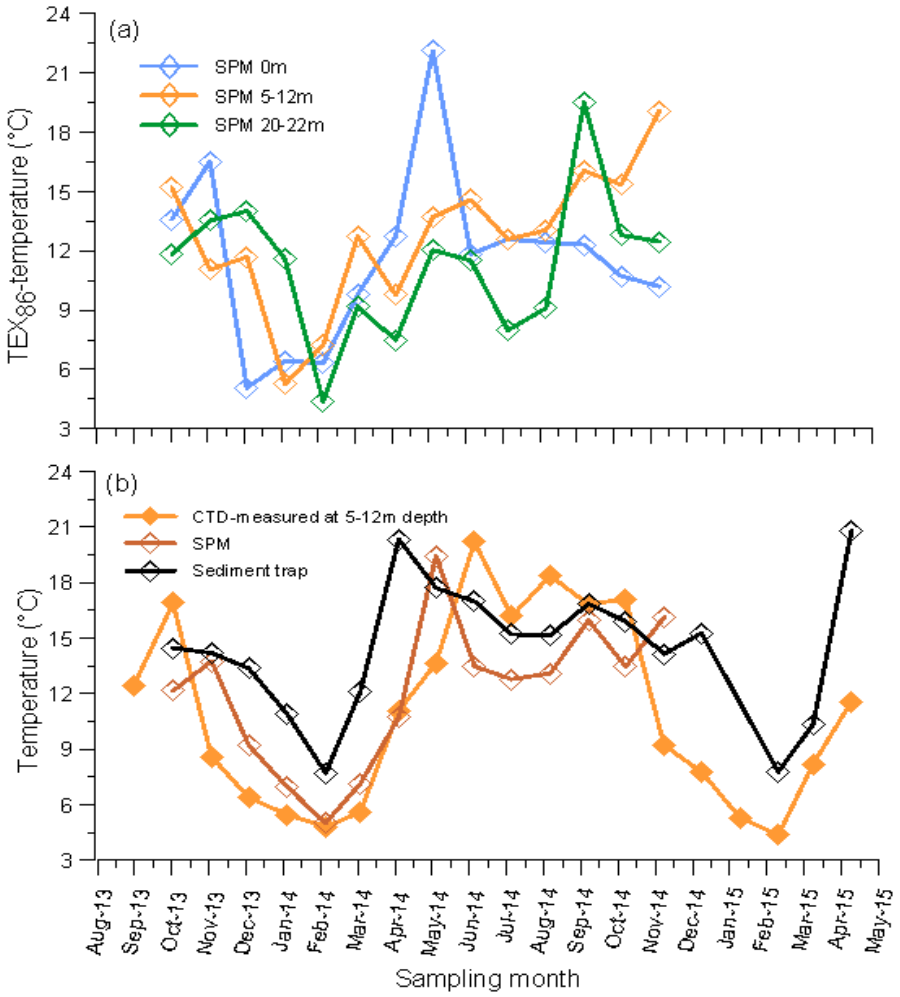

Figure 5-4 TEX_{86}-derived lake temperature from SPM at three depths of water column (a) and comparison of CTD-measured temperature at thermocline (5-12 m depth) and reconstructed temperatures from SPM in the water column and sediment trap

According to Schouten et al. (2002) (eq.2),TEX_{86}-estimated temperature of SPM from three depths of water column in Lake Montcortés showed a remarkable similarity to each other and within the range of CTD-measured temperatures in the upper water column when sampling (Fig. 5-4a). SPM at three depths of the water column confirmed that TEX_{86} index reflects upper water temperature with seasonal changes, which agreed with the observation in Lake Challa that Thaumarchaeota were present in the upper part of the water column and in Lake Kivu throughout the epipelagic waters (Sinninghe Damsté et al., 2009; Llirós et al., 2010).

The water column presented CTD-temperatures around 6.0 °C at three depths in the water column from December to February when the water column was not stratified in Lake Montcortés. However, for reconstructed temperature, SPM from the surface water showed

the minimum values in December, SPM from the thermocline water and bottom water showed minimum temperatures in January and February, respectively. TEX_{86} estimated temperatures ranged from 5.1 °C to 22.1 °C (mean 11.6±1.1 °C) for the surface water, from 5.3 °C to 19.1 °C (mean 12.7±0.9 °C) for the thermocline water and from 4.4 °C to 19.5 °C (mean 11.3±1.0 °C) for the bottom water (Fig. 5-4a). All TEX_{86} -estimated temperatures of SPM in the water column corresponded to air temperature variations (or upper lake water temperature). Even though the concentration of SPM from the deep waters was low, it still gives signals from the upper water column (Fig. 5-4a). This confirms that TEX_{86}-derived Thaumarchaeota occur in the upper section of the water column and are transported from the surface water to the sediment (Wakeham et al., 2003).

TEX_{86} -estimated temperatures matched better with CTD surface/thermocline water temperatures when the water column was mixed (Fig. 5-4a). The highest TEX_{86}-derived temperature occurred in May 2013 from the surface water, in November from the thermocline water and in September from the bottom water. These temperature biases would be also due to the phytoplankton bloom in an annual cycle and the temporary stratification from the bottom water of the lake, which was reflected by DO conditions at bottom waters.

Considering DO state as a constraint factor for TEX_{86} index in the bottom water, we calculated weighted $TEX_{86(w)}$ from SPM samples at three depths in the water column. The equation (8) presented as follows, and the contribution from deep water was calculated only when the water column was mixed.

$$GDGTw\text{-}i=0.3*(GDGT\text{-}i)_{0m}+0.5*(GDGT\text{-}i)_{5\text{-}12m}+0.2*(GDGT\text{-}i)_{20\text{-}22m}\ (i=1,2,3,4') \quad (8)$$

$$TEX_{86(w)} = \frac{[GDGTw-2]+[GDGTw-3]+[GDGTw-4']}{[GDGTw-1]+[GDGTw-2]+[GDGTw-3]+[GDGTw-4']} \quad (9)$$

* $TEX_{86(w)}$ indicates the TEX_{86} index calculated for the SPM in the water column and the inferred lake surface temperature (LST_w) was according to equation (2).

It suggests that both TEX_{86}(w)-derived temperature and TEX_{86}(trap)-derived temperature were well matched with the thermocline water temperature variability throughout the year (Fig. 5-4b). The maximum (5.0 °C) and minimum (19.5 °C) of TEX_{86}(w)-derived temperatures were nearly the same as the measured temperature in the thermocline layer (4.8-18.4 °C). While minimum TEX_{86}(trap)-estimated temperature was higher (7.7 °C) compared with the actual thermocline temperature, consistent with the trend that the estimated temperatures were also generally higher than the CTD-temperatures from November 2013 to May 2014.

And from June to October 2014, the estimated temperatures were nearly in line with the actual temperatures. This would be due to the seasonal changes of phytoplankton production in the lake, which might be depending on phytoplankton-derived resources, such as ammonium (Fietz et al., 2011), seasonal thermal stratification, DO variations in the lake.

The good correspondence between TEX_{86}(w)-derived temperatures vs. CTD-temperatures rather than TEX_{86}(trap)-derived temperatures vs. CTD-temperatures in November 2013 to April 2014 suggested that $TEX_{86(trap)}$-derived temperatures were affected mainly by TEX_{86}(w)-related Thaumarchaeota in the water column to present a seasonal variation. In addition, TEX_{86}(w)-derived temperatures were lower than the thermocline CTD-temperatures from June to October, indicating some contribution from isoGDGTs might be produced a little below the thermocline waters, but not the exact hypolimnetic waters during the period of stratification, which was consistent with Blaga et al.(2011)'s observation that TEX_{86} values tends to reflect sub-thermocline temperature from the position of the Thaumarchaeota in the sub-thermocline in Lake Lucerne. It suggests that the position of Thaumarchaeta in the water column may vary between seasons depending on variations of lake conditions, such as stratifying.

As discussed above, TEX_{86} values of sediment trap seemed to reflect thermocline water temperature in an annual cycle. However, the mean TEX_{86}-temperature of sediment trap (14.4±0.8 °C) tended to record the mean lake surface temperature (13.3±1.5°C) rather than the mean thermocline temperature (10.9±1.2 °C). We put our TEX_{86} values of sediment trap into the calibration of Powers et al. (2010). There are positive relationships between lake surface temperature (LST) vs. $TEX_{86(w)}$ (R^2=0.47) and LST vs.$TEX_{86(trap)}$ (R^2=0.47) (Fig. 5-5a, b). $TEX_{86(trap)}$ values in April were higher relative to the samples collected in other months, which gives a large bias of reconstructed surface or thermocline water temperature (Fig. 5-5b, c). Without the two samples from April, the correlation between $TEX_{86(trap)}$ and LST or thermocline temperature in the water column is more significant (R^2=0.61 and R^2=0.62, respectively). We also used the mean value of $TEX_{86(w)}$ and $TEX_{86(trap)}$ and some TEX_{86} from the literature to match the previous calibration curve (Powers et al., 2010), which showed a satisfying results (R^2=0.89) (Fig. 5-5d). It means that using TEX_{86} as a temperature proxy in the water column or sediment trap of Lake Montcortes could provide information about local temperature in short-time scale (monthly-seasonally), reflecting temperatures from the upper section of water column. And our TEX_{86} data reveal that TEX_{86} index in Lake Montcortes

could provide a robust temperature reconstruction in a global scale (in line with the global lake surface temperature calibration).

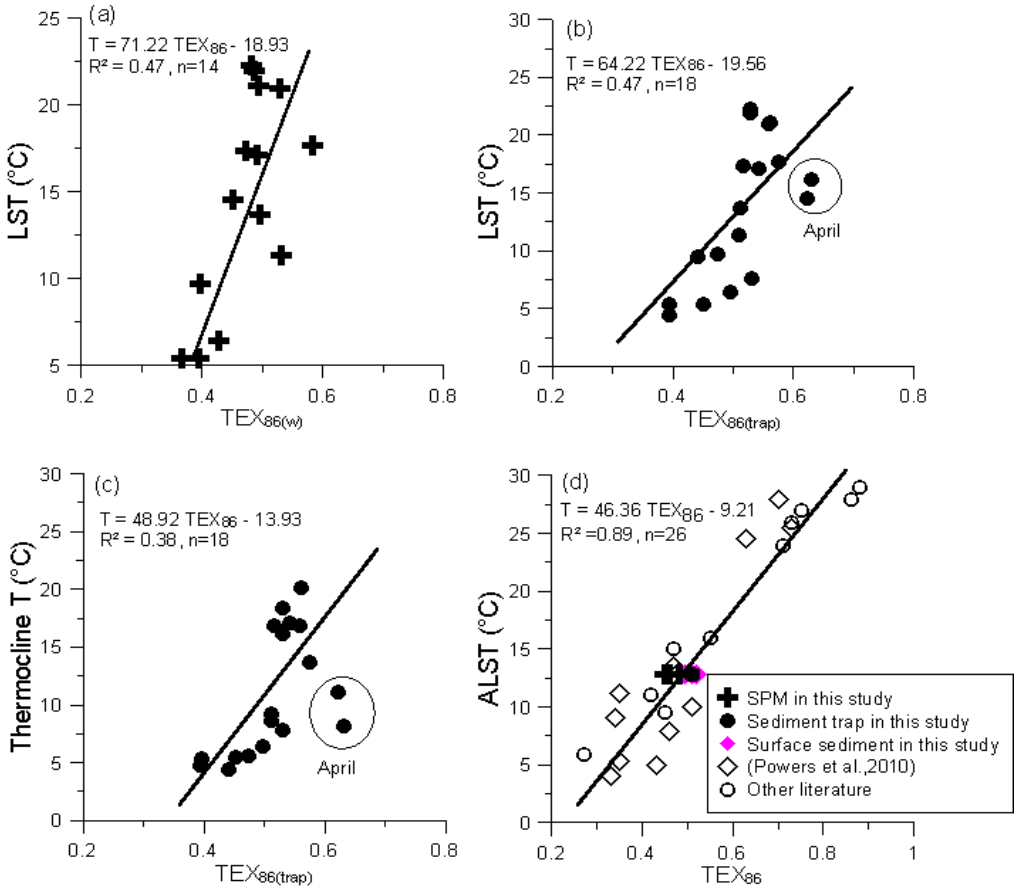

Figure 5-5 Linear regression and correlation of TEX_{86} in water column and sediment trap in Lake Montcortés. (a) CTD-measured lake surface temperature (LST) and TEX_{86} values of SPM in the water column, (b) CTD-measured lake surface temperature (LST) and TEX_{86} values of sediment trap, (c) CTD-measured thermocline temperature and TEX_{86} values of sediment trap, (d) global lake surface temperature and TEX_{86} (Powers et al., 2010; Tierney et al., 2010; Blaga et al., 2011; Yang et al., 2012)

5.3.12. MBT/CBT index as temperature proxy in the water column and sediment trap

The MBT/CBT index was calculated using equation (eq.5.3, eq.5.4) based on the distribution of branched GDGTs of presumably soil bacterial origin (Weijers et al., 2007). CBT index of SPM ranged from -0.08 to 0.74 (mean 0.52) for the surface water, from 0.01 to 0.62 (mean 0.46) for the thermocline water and from -0.22 to 0.72 (mean 0.45) for the deep water (Table 5-1). MBT values of SPM varied between 0.14-0.46 (mean 0.22), 0.19-0.37 (mean 0.24) and 0.17-0.30 (mean 0.23) at three depths of the water column, separately. We

used the calibration equation (eq.5.5) from global soils proposed by Weijers et al.(2007) to estimate temperatures in the water column SPM and sediment trap. The MBT/CBT-estimates from eq.5.5 were below 0 °C (Table 5-1), which means Weijers et al.(2007)´s calibration is not applicable in Lake Montcortés catchment soils as MBT/CBT index tended to largely underestimate the reconstructed temperatures (MAT1) (Table5-1). We also used Peterse et al. (2012)'s calibration (eq.5.6) to reconstruct temperature from the water column. The new MAT2-derived temperatures ranged from 1.3 to 15.5 °C (mean 4.7±0.9 °C) for the surface temperature, from 3.4 to 12.2 °C (mean 5.7±0.7 °C) for the thermocline water and from 1.9 to 11.3 °C (mean 5.5±0.5 °C) (Fig. 5-6). It seems that all reconstructed temperatures from the water column SPM changed within 5 °C during the period from October 2013 to September 2014. Besides, the reconstructed temperature from settling particulate in the sediment trap varied between 4.1 and 6.8 °C (mean 4.8±0.2 °C). These values were similar to CTD-measured temperature at 20m in the water column ranging from 3.5 to 6.9°C (mean 5.4±0.2 °C). It indicates that brGDGTs could be produced at the deeper water column in the lake. However, the relatively high concentration brGDGTs in the upper water column and nearly unchangeable reconstructed MAT2 at three depths did not support this idea. As seasonal variations of concentration and flux from SPM in the water column and sediment trap, brGDGTs in Lake Montcortes derived from soils and in situ production. This could explain that the distributions of brGDGTs and MAT were nearly stable in water column because of absence of seasonal changes in soil-derived brGDGTs over the annual cycle due to a large pool of residual GDGTs (Weijers, et al., 2011) (see our data of catchment soils in Chapter 3). Considering the soil inputs of brGDGTs, the average MAT2 estimated from catchment soils were 6.3±1.1 °C, a little higher that MAT2 values from the SPM and sediment trap. As we discussed in Chapter 2, the MBT/CBT variability of different soils are larger than that within annual scale. Therefore, even though brGDGTs in the lake are mainly from the catchment soils, the contributions from different soil types are different, which reflected temperature signals predominantly from specific soil types. Autochthonous GDGTs would obviously change the primary, soil-derived GDGT signals (Blaga et al., 2009; Tierney & Russell, 2009; Tierney et al., 2010). Our data of MAT2 (Fig. 5-6) from the sediment trap suggests that soil-derived brGDGTs might be responsible for the relatively stable temperature signals in the lake throughout the year. However, abnormally higher reconstructed MAT2 in the water column in October and November could be driven by brGDGTs produced in the lake because the values were too high (from 11.3-15.5 °C) to outrange the soil endmember.

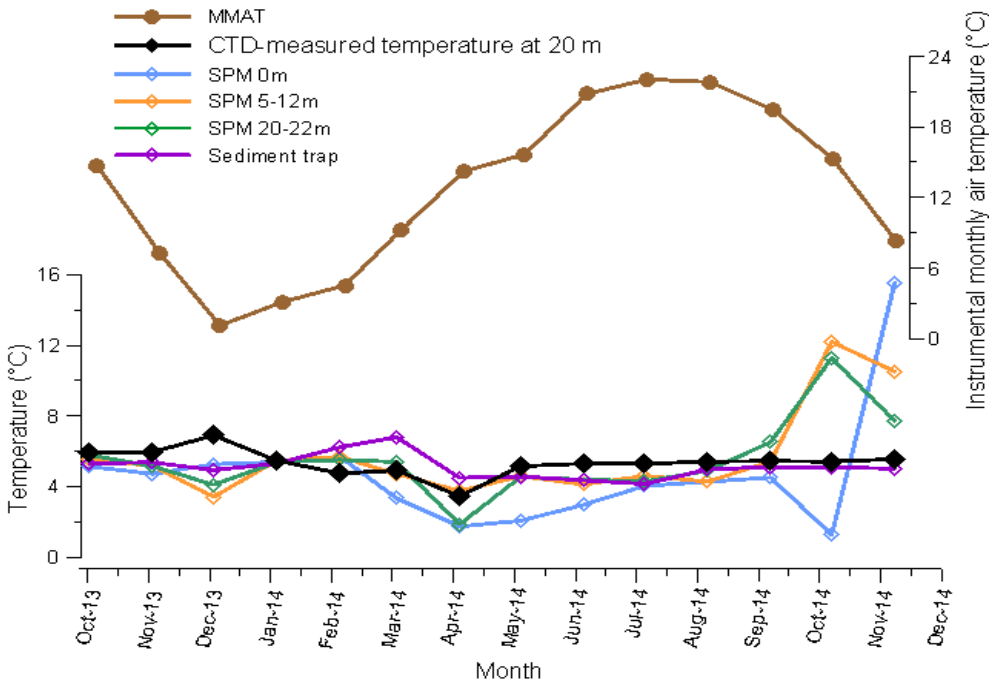

Figure 5-6 MBT/CBT estimated temperature from SPM at three depths of water column and sediment trap vs. the instrumental mean monthly air temperature and CTD-measured lake bottom water temperature

5.3.13. Conclusions

We explored temporal (monthly) variability of isoGDGTs and brGDGTs in Lake Montcortés.

1) Our study shows that in Lake Montcortés, isoGDGTs are primarily occur at the water column, which show higher concentrations in summer and autumn in the epilimnion and thermocline, but are also abundant in autumn in the hypolimnion. The isoGDGTs reflect seasonal variations of upper water temperatures over the annual cycle.
2) TEX_{86}-estimated temperatures from SPM of the water column and sediment trap matched better with observed lake temperature at thermocline rather than the surface layer and TEX_{86} temperatures for water column show a closer correlation to the CTD-measured temperatures at the thermocline water than those from the sediment trap. The mean TEX_{86}-derived temperatures from SPM in the water column and sediment trap, surface sediments suggest that TEX_{86} is a reliable tool for temperature reconstruction in short-time scales (monthly/seasonally) in Lake Montcortés.

3) The brGDGTs show similar concentration and flux patterns in the water column and sediment trap. Our data of sediment trap suggest that brGDGTs are mainly deposited during the summer season and the starting of mixing water column.
4) MBT/CBT values from the sediment trap seemed to be stable throughout the year, close to mean values from catchment soils but much closer to group B soils (Chapter3). Reconstructed MAT from SPM and sediment trap varies a little with depth and lack of seasonal changes. The bias of MBT/CBT estimates in October and November in the water column might be due to in situ production of brGDGTs or eolian transport outside the catchment. Nevertheless, they made only a little contribution to the sediment brGDGT pool which can be neglected in the paleoclimatic reconstruction.

5.3.14. Reference

Baker, J. E., & Eisenreich, S. J. (1989). PCBs and PAHs as Tracers of Particulate Dynamics in Large Lakes. *Journal of Great Lakes Research*, *15*(1), 84–103. doi:10.1016/S0380-1330(89)71464-7

Blaga, C. I., Reichart, G. J., Vissers, E. W., Lotter, A. F., Anselmetti, F. S., & Sinninghe Damsté, J. S. (2011). Seasonal changes in glycerol dialkyl glycerol tetraether concentrations and fluxes in a perialpine lake: Implications for the use of the TEX86 and BIT proxies. *Geochimica et Cosmochimica Acta*, *75*(21), 6416–6428. doi:10.1016/j.gca.2011.08.016

Blaga, C. I., Reichart, G.-J., Heiri, O., & Sinninghe Damsté, J. S. (2009). Tetraether membrane lipid distributions in water-column particulate matter and sediments: a study of 47 European lakes along a north–south transect. *Journal of Paleolimnology*, *41*(3), 523–540. doi:10.1007/s10933-008-9242-2

Brochier-Armanet, C., Boussau, B., Gribaldo, S., & Forterre, P. (2008). Mesophilic Crenarchaeota: proposal for a third archaeal phylum, the Thaumarchaeota. *Nature Reviews. Microbiology*, *6*(3), 245–252. doi:10.1038/nrmicro1852

Buckles, L. K., Weijers, J. W. H., Tran, X. M., Waldron, S., & Sinninghe Damst??, J. S. (2014). Provenance of tetraether membrane lipids in a large temperate lake (Loch Lomond, UK): Implications for glycerol dialkyl glycerol tetraether (GDGT)-based palaeothermometry. *Biogeosciences*, *11*(19), 5539–5563. doi:10.5194/bg-11-5539-2014

Corella, J. P., Brauer, A., Mangili, C., Rull, V., Vegas-Vilarrúbia, T., Morellón, M., & Valero-Garcés, B. L. (2012). The 1.5-ka varved record of Lake Montcortès (southern Pyrenees, NE Spain). *Quaternary Research*, *78*(2), 323–332. doi:10.1016/j.yqres.2012.06.002

Corella, J. P., Moreno, A., Morellón, M., Rull, V., Giralt, S., Rico, M. T., … Valero-Garcés, B. L. (2010). Climate and human impact on a meromictic lake during the last 6,000 years (Montcortès Lake, Central Pyrenees, Spain). *Journal of Paleolimnology*, *46*(3), 351–367. doi:10.1007/s10933-010-9443-3

Damsté, J. S. S., Ossebaar, J., Abbas, B., Schouten, S., & Verschuren, D. (2009). Fluxes and distribution of tetraether lipids in an equatorial African lake: Constraints on the application of the TEX86 palaeothermometer and BIT index in lacustrine settings. *Geochimica et Cosmochimica Acta*, *73*(14), 4232–4249. doi:10.1016/j.gca.2009.04.022

Escala, M., Rosell-Melé, A., & Masqué, P. (2007). Rapid screening of glycerol dialkyl glycerol tetraethers in continental Eurasia samples using HPLC/APCI-ion trap mass spectrometry. *Organic Geochemistry*, *38*(1), 161–164. doi:10.1016/j.orggeochem.2006.08.013

Fietz, S., Huguet, C., Bendle, J., Escala, M., Gallacher, C., Herfort, L., … Rosell-Melé, A. (2012). Co-variation of crenarchaeol and branched GDGTs in globally-distributed marine and freshwater sedimentary archives. *Global and Planetary Change*, *92-93*, 275–285. doi:10.1016/j.gloplacha.2012.05.020

Fietz, S., Martínez-Garcia, A., Rueda, G., Peck, V. L., Huguet, C., Escala, M., & Rosell-Melé, A. (2011). Crenarchaea and phytoplankton coupling in sedimentary archives: Common trigger or metabolic dependence? *Limnology and Oceanography*, *56*(5), 1907–1916. doi:10.4319/lo.2011.56.5.1907

Fietz, S., Prahl, F. G., Moraleda, N., & Rosell-Melé, A. (2013). Eolian transport of glycerol dialkyl glycerol tetraethers (GDGTs) off northwest Africa. *Organic Geochemistry*, *64*, 112–118. doi:10.1016/j.orggeochem.2013.09.009

Ge, H., Zhang, C. L., Li, J., Versteegh, G. J. M., Hu, B., Zhao, J., & Dong, L. (2014). Tetraether lipids from the southern Yellow Sea of China: Implications for the variability of East Asia Winter Monsoon in the Holocene. *Organic Geochemistry*, *70*, 10–19. doi:10.1016/j.orggeochem.2014.02.011

Hopmans, E. C., Schouten, S., & Sinninghe Damsté, J. S. (2016). The effect of improved chromatography on GDGT-based palaeoproxies. *Organic Geochemistry*, *93*, 1–6. doi:10.1016/j.orggeochem.2015.12.006

Hopmans, E. C., Weijers, J. W. ., Schefuß, E., Herfort, L., Sinninghe Damsté, J. S., & Schouten, S. (2004). A novel proxy for terrestrial organic matter in sediments based on branched and isoprenoid tetraether lipids. *Earth and Planetary Science Letters*, *224*(1-2), 107–116. doi:10.1016/j.epsl.2004.05.012

Huguet, A., Grossi, V., Belmahdi, I., Fosse, C., & Derenne, S. (2015). Archaeal and bacterial tetraether lipids in tropical ponds with contrasting salinity (Guadeloupe, French West Indies): Implications for tetraether-based environmental proxies. *Organic Geochemistry*, *83-84*, 158–169. doi:10.1016/j.orggeochem.2015.02.010

Huguet, C., de Lange, G. J., Gustafsson, ??rjan, Middelburg, J. J., Sinninghe Damsté, J. S., & Schouten, S. (2008). Selective preservation of soil organic matter in oxidized marine sediments (Madeira Abyssal Plain). *Geochimica et Cosmochimica Acta*, *72*(24), 6061–6068. doi:10.1016/j.gca.2008.09.021

Huguet, C., Fietz, S., & Rosell-Melé, a. (2013). Global distribution patterns of hydroxy glycerol dialkyl glycerol tetraethers. *Organic Geochemistry*, *57*, 107–118. doi:10.1016/j.orggeochem.2013.01.010

Huguet, C., Fietz, S., Stockhecke, M., Sturm, M., Anselmetti, F. S., & Rosell-Melé, a. (2011). Biomarker seasonality study in Lake Van, Turkey. *Organic Geochemistry*, *42*(11), 1289–1298. doi:10.1016/j.orggeochem.2011.09.007

Huguet, C., Smittenberg, R. H., Boer, W., Sinninghe Damsté, J. S., & Schouten, S. (2007). Twentieth century proxy records of temperature and soil organic matter input in the Drammensfjord, southern Norway. *Organic Geochemistry*, *38*(11), 1838–1849. doi:10.1016/j.orggeochem.2007.06.015

Huguet, C., Urakawa, H., Martens-Habbena, W., Truxal, L., Stahl, D. a., & Ingalls, A. E. (2010). Changes in intact membrane lipid content of archaeal cells as an indication of metabolic status. *Organic Geochemistry*, *41*(9), 930–934. doi:10.1016/j.orggeochem.2010.04.012

Karner, M. B., DeLong, E. F., & Karl, D. M. (2001). Archaeal dominance in the mesopelagic zone of the Pacific Ocean. *Nature*, *409*(6819), 507–510. doi:10.1038/35054051

Kim, J.-H., Schouten, S., Hopmans, E. C., Donner, B., & Sinninghe Damsté, J. S. (2008). Global sediment core-top calibration of the TEX86 paleothermometer in the ocean. *Geochimica et Cosmochimica Acta*, *72*(4), 1154–1173. doi:10.1016/j.gca.2007.12.010

Leininger, S., Urich, T., Schloter, M., Schwark, L., Qi, J., Nicol, G. W., … Schleper, C. (2006). Archaea predominate among ammonia-oxidizing prokaryotes in soils. *Nature*, *442*(August), 806–809. doi:10.1038/nature04983

Llirós, M., Gich, F., Plasencia, A., Auguet, J. C., Darchambeau, F., Casamayor, E. O., … Borrego, C. (2010). Vertical distribution of ammonia-oxidizing crenarchaeota and methanogens in the epipelagic waters of lake kivu (rwanda-democratic republi of the congo). *Applied and Environmental Microbiology*, *76*(20), 6853–6863. doi:10.1128/AEM.02864-09

Loomis, S. E., Russell, J. M., Eggermont, H., Verschuren, D., & Sinninghe Damsté, J. S. (2014). Effects of temperature, pH and nutrient concentration on branched GDGT distributions in East African lakes: Implications for paleoenvironmental reconstruction. *Organic Geochemistry*, *66*, 25–37. doi:10.1016/j.orggeochem.2013.10.012

Loomis, S. E., Russell, J. M., Heureux, A. M., D'Andrea, W. J., & Sinninghe Damsté, J. S. (2014). Seasonal variability of branched glycerol dialkyl glycerol tetraethers (brGDGTs) in a temperate lake system. *Geochimica et Cosmochimica Acta*, *144*, 173–187. doi:10.1016/j.gca.2014.08.027

Loomis, S. E., Russell, J. M., & Sinninghe Damsté, J. S. (2011). Distributions of branched GDGTs in soils and lake sediments from western Uganda: Implications for a lacustrine paleothermometer. *Organic Geochemistry*, *42*(7), 739–751. doi:10.1016/j.orggeochem.2011.06.004

Meyers, P. a. (1997). Organic geochemical proxies of paleoceanographic, paleolimnologic, and paleoclimatic processes. *Organic Geochemistry*, *27*(5-6), 213–250. doi:10.1016/S0146-6380(97)00049-1

Modamio xavier; vicente pérez; francesc Samarra. (1988). Limnología del lago de Montcortes (Pallars Jussa, Lleida). *Oecologia Aquatica*, *9*, 9–17.

Pearson, E. J., Juggins, S., Talbot, H. M., Weckström, J., Rosén, P., Ryves, D. B., … Schmidt, R. (2011). A lacustrine GDGT-temperature calibration from the Scandinavian Arctic to Antarctic: Renewed potential for the application of GDGT-paleothermometry in lakes. *Geochimica et Cosmochimica Acta*, *75*(20), 6225–6238. doi:10.1016/j.gca.2011.07.042

Peterse, F., Kim, J.-H., Schouten, S., Kristensen, D. K., Koç, N., & Sinninghe Damsté, J. S. (2009). Constraints on the application of the MBT/CBT palaeothermometer at high latitude environments (Svalbard, Norway). *Organic Geochemistry*, *40*(6), 692–699. doi:10.1016/j.orggeochem.2009.03.004

Peterse, F., Martínez-garcía, A., Zhou, B., Beets, C. J., Prins, M. A., Zheng, H., & Eglinton, T. I. (2014). Molecular records of continental air temperature and monsoon precipitation variability in East Asia spanning the past 130 , 000 years. *Quaternary Science Reviews*, *83*, 76–82. doi:10.1016/j.quascirev.2013.11.001

Peterse, F., van der Meer, J., Schouten, S., Weijers, J. W. H., Fierer, N., Jackson, R. B., … Sinninghe Damsté, J. S. (2012). Revised calibration of the MBT–CBT paleotemperature proxy based on branched tetraether membrane lipids in surface soils. *Geochimica et Cosmochimica Acta*, *96*, 215–229. doi:10.1016/j.gca.2012.08.011

Powers, L., Werne, J. P., Vanderwoude, A. J., Sinninghe Damsté, J. S., Hopmans, E. C., & Schouten, S. (2010). Applicability and calibration of the TEX86 paleothermometer in lakes. *Organic Geochemistry*, *41*(4), 404–413. doi:10.1016/j.orggeochem.2009.11.009

Rao, Z., Zhu, Z., Jia, G., Henderson, A. C. G., Xue, Q., & Wang, S. (2009). Compound specific δD values of long chain n-alkanes derived from terrestrial higher plants are indicative of the δD of meteoric waters: Evidence from surface soils in eastern China. *Organic Geochemistry*, *40*(8), 922–930. doi:10.1016/j.orggeochem.2009.04.011

Rull, V., González-Sampériz, P., Corella, J. P., Morellón, M., & Giralt, S. (2010). Vegetation changes in the southern Pyrenean flank during the last millennium in relation to climate and human activities: the Montcortès lacustrine record. *Journal of Paleolimnology*, *46*(3), 387–404.

doi:10.1007/s10933-010-9444-2

Schouten, S., Hopmans, E. C., Baas, M., Boumann, H., Standfest, S., K??nneke, M., … Sinninghe Damst??, J. S. (2008). Intact membrane lipids of “Candidatus Nitrosopumilus maritimus,” a cultivated representative of the cosmopolitan mesophilic group I crenarchaeota. *Applied and Environmental Microbiology*, *74*(8), 2433–2440. doi:10.1128/AEM.01709-07

Schouten, S., Hopmans, E. C., Schefuß, E., & Sinninghe-Damste, J. S. (2002). Distributional variations in marine crenarchaeotal membrane lipids: A new tool for reconstruting ancient sea-surface temperatures? *Earth and Planetary Science Letters*, *204*, 265–274.

Schouten, S., Hopmans, E. C., & Sinninghe Damsté, J. S. (2013). The organic geochemistry of glycerol dialkyl glycerol tetraether lipids: A review. *Organic Geochemistry*, *54*, 19–61. doi:10.1016/j.orggeochem.2012.09.006

Schouten, S., Huguet, C., Hopmans, E. C., Kienhuis, M. V. M., & Damste, J. S. S. (2007). Analytical Methodology for TEX 86 Paleothermometry by High-Performance Liquid Chromatography / Atmospheric Pressure Chemical Ionization-Mass Spectrometry. *Analytical Chemistry*, *79*(7), 2940–2944. doi:10.1029/2004PA001110.This

Schouten, S., Rijpstra, W. I. C., Durisch-Kaiser, E., Schubert, C. J., & Sinninghe Damsté, J. S. (2012). Distribution of glycerol dialkyl glycerol tetraether lipids in the water column of Lake Tanganyika. *Organic Geochemistry*, *53*, 34–37. doi:10.1016/j.orggeochem.2012.01.009

Schouten, S., Wakeham, S. G., Hopmans, E. C., Damsté, J. S. S., & Damste, J. S. S. (2003). Biogeochemical Evidence that Thermophilic Archaea Mediate the Anaerobic Oxidation of Methane Biogeochemical Evidence that Thermophilic Archaea Mediate the Anaerobic Oxidation of Methane, *69*(3), 1680–1686. doi:10.1128/AEM.69.3.1680

Sinninghe Damsté, J. S., Rijpstra, W. I. C., Ellen, C., Prahl, F. G., Wakeham, S. G., Hopmans, E. C., & Schouten, S. (2002). Distribution of Membrane Lipids of Planktonic Crenarchaeota in the Arabian Sea Distribution of Membrane Lipids of Planktonic Crenarchaeota in the Arabian Sea †. *Applied and Environmental Microbiology*, *68*(6), 2997–3002. doi:10.1128/AEM.68.6.2997

Tierney, J. E., & Russell, J. M. (2009). Distributions of branched GDGTs in a tropical lake system: Implications for lacustrine application of the MBT/CBT paleoproxy. *Organic Geochemistry*, *40*(9), 1032–1036. doi:10.1016/j.orggeochem.2009.04.014

Tierney, J. E., Russell, J. M., Eggermont, H., Hopmans, E. C., Verschuren, D., & Sinninghe Damsté, J. S. (2010). Environmental controls on branched tetraether lipid distributions in tropical East African lake sediments. *Geochimica et Cosmochimica Acta*, *74*(17), 4902–4918. doi:10.1016/j.gca.2010.06.002

Toney, J. L., Huang, Y., Fritz, S. C., Baker, P. a., Grimm, E., & Nyren, P. (2010). Climatic and environmental controls on the occurrence and distributions of long chain alkenones in lakes of the interior United States. *Geochimica et Cosmochimica Acta*, *74*(5), 1563–1578. doi:10.1016/j.gca.2009.11.021

Wakeham, S. G., Lewis, C. M., Hopmans, E. C., Schouten, S., & Sinninghe Damsté, J. S. (2003). Archaea mediate anaerobic oxidation of methane in deep euxinic waters of the Black Sea. *Geochimica et Cosmochimica Acta*, *67*(7), 1359–1374. doi:10.1016/S0016-7037(02)01220-6

Walsh, E. M., Ingalls, A. E., & Keil, R. G. (2008). Sources and transport of terrestrial organic matter in Vancouver Island fjords and the Vancouver-Washington Margin: A multiproxy approach using d13Corg, lignin phenols, and the ether lipid BIT index. *Limnology and Oceanography*, *53*(3), 1054–1063. doi:10.4319/lo.2008.53.3.1054

Weijers, J. W. H., Bernhardt, B., Peterse, F., Werne, J. P., Dungait, J. A. J., Schouten, S., & Sinninghe Damsté, J. S. (2011). Absence of seasonal patterns in MBT-CBT indices in mid-latitude soils. *Geochimica et Cosmochimica Acta*, *75*(11), 3179–3190. doi:10.1016/j.gca.2011.03.015

Weijers, J. W. H., Panoto, E., van Bleijswijk, J., Schouten, S., Rijpstra, W. I. C., Balk, M., … Damsté,

J. S. S. (2009). Constraints on the Biological Source(s) of the Orphan Branched Tetraether Membrane Lipids. *Geomicrobiology Journal*, *26*(6), 402–414. doi:10.1080/01490450902937293

Weijers, J. W. H., Schouten, S., Hopmans, E. C., Geenevasen, J. A. J., David, O. R. P., Coleman, J. M., … Sinninghe Damsté, J. S. (2006). Membrane lipids of mesophilic anaerobic bacteria thriving in peats have typical archaeal traits. *Environmental Microbiology*, *8*(4), 648–657. doi:10.1111/j.1462-2920.2005.00941.x

Weijers, J. W. H., Schouten, S., Spaargaren, O. C., & Sinninghe Damsté, J. S. (2006). Occurrence and distribution of tetraether membrane lipids in soils: Implications for the use of the TEX86 proxy and the BIT index. *Organic Geochemistry*, *37*(12), 1680–1693. doi:10.1016/j.orggeochem.2006.07.018

Weijers, J. W. H., Schouten, S., van den Donker, J. C., Hopmans, E. C., & Sinninghe Damsté, J. S. (2007). Environmental controls on bacterial tetraether membrane lipid distribution in soils. *Geochimica et Cosmochimica Acta*, *71*(3), 703–713. doi:10.1016/j.gca.2006.10.003

Weijers, J. W. H., Steinmann, P., Hopmans, E. C., Schouten, S., & Sinninghe Damsté, J. S. (2011). Bacterial tetraether membrane lipids in peat and coal: Testing the MBT–CBT temperature proxy for climate reconstruction. *Organic Geochemistry*, *42*(5), 477–486. doi:10.1016/j.orggeochem.2011.03.013

Woltering, M., Werne, J. P., Kish, J. L., Hicks, R., Sinninghe Damsté, J. S., & Schouten, S. (2012). Vertical and temporal variability in concentration and distribution of thaumarchaeotal tetraether lipids in Lake Superior and the implications for the application of the TEX 86 temperature proxy. *Geochimica et Cosmochimica Acta*, *87*, 136–153. doi:10.1016/j.gca.2012.03.024

Yong song Huang. F.Alayne Street-Perrott, R. Alan Perrott, Pierre Metzger, and G. E. (1999). Glacial – interglacial environmental changes inferred from molecular and compound-specific 13 C analyses of sediments from Sacred Lake , Mt . Kenya, *63*(9), 1383–1404.

Chapter 6

Biomarker proxies in two high-resolution records in a Pyrenean lake spanning the last 110 years and the Spörer Minimum

Abstract

Climate warming has received more and more attention as the increasing temperatures have affected our ecosystem and economic society. Reliable methods for reconstructing past temperature in the continental terrestrial environments are becoming more important. Herein, a combination of alkyl lipids data from Lake Montcortés and instrumental climatic data (precipitation and temperature) explains the environmental changes spanning last 110 years and the Spörer Minimum. Our result shows that nC_{17}/nC_{29} is to some extent consistent with hydrological changes in the history. Warmer temperature since the mid XX century (1949-2012) is strikingly significant, which is revealed by TEX_{86}, CBT or F(IIa) index derived from glycerol diethyl glycerol tetraethers. Moreover, on a 5-year scale, these proxies could be used as a potential paleotemperature proxy in the lacustrine system considering the contributions of sources of isoGDGTs or brGDGTs. However, MBT/CBT proxy could not work properly in our lake compared with other proxies. In despite of the fact like this, the root mean squared error is no more than 1°C. Thus, we suggest that TEX_{86}, CBT or F(IIa) index calibration could be used for reconstruction in the lakes showing similar characteristics with our study lake but with caution.

6.1. Introduction

The Pyrenees are located in the northern Iberian Peninsula and are under the influence of both Atlantic and Mediterranean climates, which makes them highly sensitive to current global warming trends (Lionello et al., 2006; Gottfried et al., 2012).Many proxies from different type of archives, e.g. tree rings (Büntgen et al., 2007; Dorado et al., 2012), lake sediments (Corella et al., 2010), stalagmites (Spötl et al., 2010), have been used to reconstruct past climate conditions in this mountain range. However, we still lack quantitative proxies to reconstruct past changes in air temperature and the hydrological cycle (Corella et al., 2014) on a decadal scale in this region. In here we appraise further the application of biomarkers that have shown particular promise to reconstruct past climate changes, related to temperature and precipitation, in lake sediments.

Biomarkers are organic compounds in geological sample that can be structurally related to their precursor molecules, whose distributions reflect source signals, maturity of organic matter or possible migration pathways (Meyers et al., 1980; Otto & Simpson, 2005). *n*-alkanes and glycerol dialkyl glycerol tetraether (GDGTs) are two of the most widely reported

classes of biomarkers used in lake sediments for paleoenvironmental reconstructions (Mügler et al., 2008; Sachse et al., 2004) and continental temperature reconstruction (i.e. Loomis et al., 2012; Powers et al., 2010).

GDGTs including the two classes: the isoprenoid GDGTs (isoGDGTs) and branched GDGTs (brGDGTs), are membrane-spanning lipids (Fig. 1-5). The isoGDGTs are thought to be derived from Archaea (Schouten et al., 2002), one proxy based on them is the TEX_{86} index (eq.1.4), which has been applied to reconstruct lake surface temperature (LST) (Escala et al, 2009; Powers et al., 2010). Another proxy, derived from the degree of cyclisation of branched tetraethers (CBT) and/or methylation extent of branched tetraethers (MBT) has been used to estimate past mean annual air temperature (MAT) (Peterse et al., 2012; Tierney & Russell, 2009; Weijers et al., 2007). brGDGTs are assumed to originate from bacteria while which kind of bacteria are more uncertain, and so far linked to some type of bacteria (Hopmans et al., 2004; Sinninghe-Damsté et al., 2000). Presently, there are a number of calibrations for TEX_{86} application and the Powers et al. (2010)'s calibration for LST was the most common for lake calibration. Whereas, brGDGT-derived proxies result in more calibrations, e.g. Weijers et al. (2007) studied the global topsoils and presented a regression equation (e.q.1.7) with MAT and MBT, CBT. The estimates using this equation leaded to a temperature of 10 °C or larger difference from the observed MAT (Tierney & Russell, 2009). Peterse (2012) enlarged the surface soil dataset and proposed another calibration equation with CBT, MBT' (e.q.1.8-1.9). In lake environment, MBT/CBT index has been calibrated and applied in specific areas (Niemann et al., 2012; Sun et al., 2011). Single CBT or MBT were explored in New Zealand lakes (Zink et al., 2010). Moreover, the calibrations based on fractional abundance of all or several of GDGT homologues were established (Loomis et al., 2014; Pearson et al., 2011).

The use of *n*-alkane distribution as source and maturity indicators started decades ago, such as publications by (Bray & Evans, 1961; Clark & Blumer, 1967; Mango, 1997). Several proxies derived from the distribution of *n*-alkanes, such as the average chain length (ACL), carbon preference index (CPI) and Paq index (indicating aquatic inputs) or other chain length ratios have been developed to track the sources and forming environmental conditions (Poynter and Eglinton, 1990; Clark & Blumer, 1967; Ficken, 2000). Some researchers attempted to refine the relationship between environmental conditions with these proxies, e.g. However, until now no consistent agreement on these findings in the global scale.

Even though applications and calibrations of biomarker-derived proxies have been assayed in modern and geological times, the applicability and reliability of these proxies have been rarely compared with instrumental records for last 100 years at a decadal scale. In this paper, we will test whether or not the content and distribution/ratio of *n*-alkanes could record climatic variations, and distribution of GDGT could reflect the local temperature changes that can be compared with instrumental records (precipitation and temperature) to improve the accuracy of temperature reconstruction in Lake Montcortés sediment. We then applied the calibrated proxies to the sediment core that has similar resolution during XV-XVII century (covering the Spörer Minimum). The Spörer Minimum, is a period lasting from about 1420 to 1550 AD with the strongest reduction in incoming total solar irradiance during 1460–1550 AD (Eddy, 1976)).

6.2. Materials and methods

6.2.1. Study area

Montcortés is a small, oligotrophic karst lake with a maximal depth of 30m (Camps et al., 1976) (Fig. 2-1). It has a significant anoxic hypolimnion (Corella et al., 2012). The lake is mainly recharged by groundwater and runoff and discharged by evaporation and an outlet in the northern shore (Corella et al., 2012). The annual average air temperature is 10.6 °C with the minimum at 1.9 °C in January and 20.3 °C in July, while the annual accumulated precipitation is 860mm (Martin-Vide et al., 2008). The vegetation in the lake catchment is dominated by evergreen oak forest, deciduous oak forests and conifer forests (Rull et al., 2010). Llittoral vegetation, such as *Phragmites communis, Typha* occurs around the lake shore (Camps et al., 1976) and submerged/floating aquatic plants such as *Myrophyllum*, *Potamogeton crispus/pectinatus* and *Chara spp.* are also common in the lake.

The daily maximum precipitation during the period 1917-1994 and the temperature during 1930-1992 was obtained from Cabdella meteorological station (about 15 km north of the lake, 1200m a.s.l., just a little higher than the study lake which is located at 1027m a.s.l.), the nearest station with longest records of precipitation and temperature in this region (Corella et al., 2014).

6.2.2. Sediment coring and slicing

A high-resolution, single channel Edge-Tech sub-bottom profiling systems was used to determine optimal core location for undisturbed sediments. Two UWITEC gravity cores, namely Mont12-3A-1G (78cm) and Mont12-2A-1G (106cm) were retrieved for the study by collaborators from the Pyrenean Institute of Ecology (IPE-CSIC) from the deepest part of the Lake Montcortes in 2012. The sediment cores were kept on the lake shore for 5 days to get consolidated sediments before being transported to a cold room in the IPE-CSIC near Zaragoza. More details of physical and chemical properties about the core were described in the published paper by Corella et al. (2014). The samples were taken every 0.5 cm. The age model and calcite varve counting was performed by Corella et al.(2014; 2012) and an additional age model based on excess ^{210}Pb activity was established to determine the age and sediment accumulation rates for the past 100-150 years (Corella et al., 2014). In this study, only samples from the last 110 years and the AD 1410 to 1580 were selected for the analysis of *n*-alkanes and GDGTs.

6.2.3. Sample analysis

For each sample depth, ~2 g of dry sediment were extracted in 10 mL dichloromethane:methanol (3:1, v/v) by sonication three times and the sum of three extracts was fractionated using a Pasteur pipette filled with a piece of pre-cleaned cotton at the bottom, 0.6 g of silica (230-400 mesh particle size) and 0.5 g of sodium sulfate on the top. After conditioned by 3ml hexane, the solvents for mobile phases were hexane (5 ml; F1, *n*-alkanes), dichloromethane (4 ml; F2, reserved), dichloromethane:methanol (95:5, v/v; 6 ml; F3, *n*-alkanoic acids and GDGTs) and methanol (5 ml; F4, preserved). Each fraction was collected in a new tube and dried in the centrivap at 27 °C. The F3 fraction was then separated into GDGTs and *n*-alkanoic acids using 8 ml diclorometh ane:2-propanol (2:1, v/v; F3-1, GDGTs) and 10ml diethyl ether:acetic acid (96:4, v/v; F3-2, *n*-alkanoic acids) over an aminopropyl column. Each column consisted of 0.7 g aminopropyl at the bottom and 0.5g sodium sulfate on the top. Only F1 (*n*-alkanes) and F3-1 (GDGTs) were analyzed for this study. GDGT fraction was re-dissolved in hexane:isopropanol (99:1) and filtered through 0.45 μm GF/F filters before injection.

The dry extract of *n*-alkanes was dissolved in isooctane and injected in splitless injection mode using an autosampler in gas chromatography Agilent 7820A. An internal standard

(hexatriacontane, C_{36}) was used for quantification of *n*-alkanes. The compound specific carbon isotopic compositions was measured using a gas chromatography coupled with isotope ratio mass spectrometer (GC-IRMS) and the $\delta^{13}C$ values are reported in per mil (‰) relative to the Vienna Peedee Beleminte (V-PDB). The standard deviations of carbon isotope are better than 0.5‰.

Between 5-20 µL solvent was automatically injected in an Agilent Time-Off-Flight (TOF) mass spectrometer with an atmospheric pressure chemical ionization (APCI) interface set in positive mode. Following the methods by Escala et al. (2007) and Huguet et al. (2013), the extracts were eluted through a Tracer Excel CN column (Teknokroma; 20 cm length, 0.4 cm diameter and 3 µm particle size) equipped with a precolumn filter and a guard column. The mobile phase was eluted with hexane:*n*-propanol (98.5:1.5) at a flow of 0.6 ml/min and the parameters of the APCI interface were set as follows to generate positive ion spectra: corona discharge 3 µA, vaporizer temperature 400 ºC, sheath gas pressure 49 mTorr, auxiliary gas (N_2) pressure 5 mTorr and capillary temperature 200 ºC. GDGTs were detected in selected ion monitoring (SIM) mode of $[M+H]^+ \pm 0.5$ m/z units to increase signal to noise ratio at the following at m/z (Schouten et al., 2007): 1302, 1300, 1298, 1296, 1292, 1050, 1048, 1046, 1036, 1034, 1032, 1022, 1020, 1018 and the synthetic tetraether lipid (GR) at 1208 m/z. GDGTs were quantified by an internal standard (GR).

6.3. Results and discussion

6.3.1. Climate records from previous study in Montcortes or nearby lakes during XX century and XV-XVII century

Corella et al. (2014) found that there was a close relationship between detrital layers deposition and instrumental daily rainfall records from 1917 to 1994 (5-year return period), the period is similar to another period AD 1401-1592, featured by low or intermediate frequencies and thickness of detrital layers. He also clarified that the dominant detrital types were different in AD 1401-1444 (DL, 70%), 1509-1592 (DL, 60-86%), 1445-1508 (N-C DL, 50%; DL, 43%) and 1917-2012 (N-C33, %; DL, 33%; F-T, 33%)[1]. The Lake Montcortés records (Corella et al., 2014) were particularly related to lowest solar activity at around AD

[1] DL: Detrital layer,
N-C DL: Non-continuous detrital layer
F-T: Flood-induced turbites

1450 and a positive autumn NAO index during the 20th might be responsible for a lower total annual precipitation in NE Iberian Peninsula (Luterbacher et al., 2002). Low-resolution pollen record (4 samples) of sharp increase of conifer forests and minimum crops and weeds in 15th century suggested a moisture and colder climate and low human pressure (Rull et al., 2010; Rull, 2015). The TP decreased around AD 1500 due to the decreasing population and increased around AD 1660, leading to a vegetation shift in littoral plants (Scussolini et al., 2011). Here we present our biomarker records (GDGTs and *n*-alkanes) to see how informative they are compared with these records.

6.3.2. GDGTs

6.3.2.1. GDGT abundance and indices changed in the sediment core (the XX century and the XV-XVII century)

The concentration of isoGDGTs are relatively higher in the XX century than in the XV-XVII century (Fig. 6-2), ranging from 0.39 to 1.43 µg/g dw with mean values of 0.83±0.26 and 0.76±0.28 µg/g dw, respectively. GDGT-0 is the most abundant isoGDGTs, contributing above 80% of the total isoGDGTs pool. The concentration of brGDGTs was ranging from 2.60 to 17.39 µg/g dw with mean values of 5.90±2.03 and 7.30±4.32 µg/g for these two periods, in respective, accounting for 82.41-93.44% of the total GDGTs. The GDGT-Ia, IIa and IIIa are the main GDGTs and GDGT-IIa was predominant one. TEX_{86} values ranged between 0.41-0.54, with the mean value of 0.48±0.01 and 0.56±0.03 for the XX century and the XV-XVII century, respectively. MBT index ranged from 0.18 to 0.24 and CBT index ranged between 0.39 and 0.70.

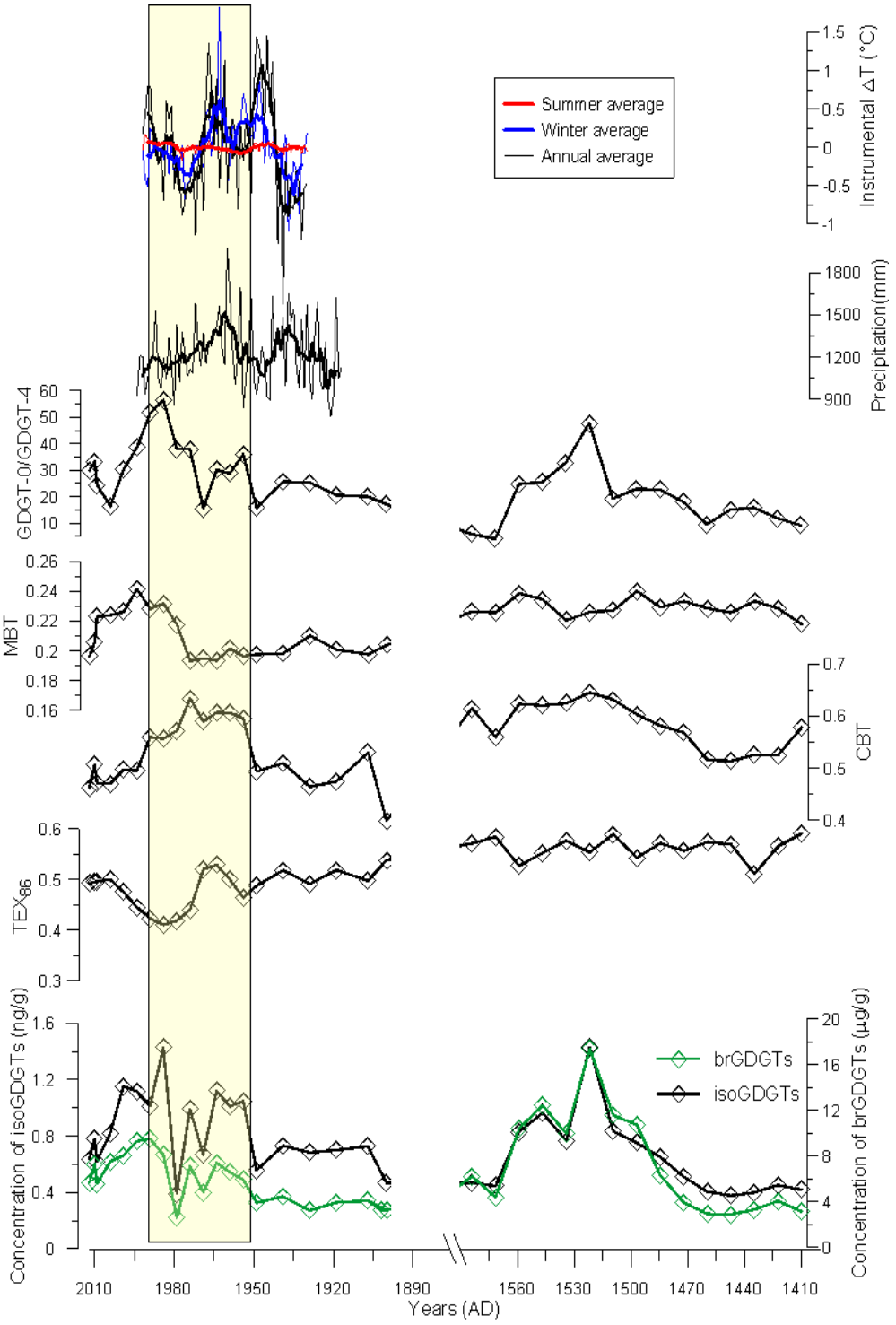

Figure 6-1 GDGT concentration and proxies in XX century and XV-XVII century

6.3.2.2. Validation of isoGDGT proxy with instrumental air temperature record

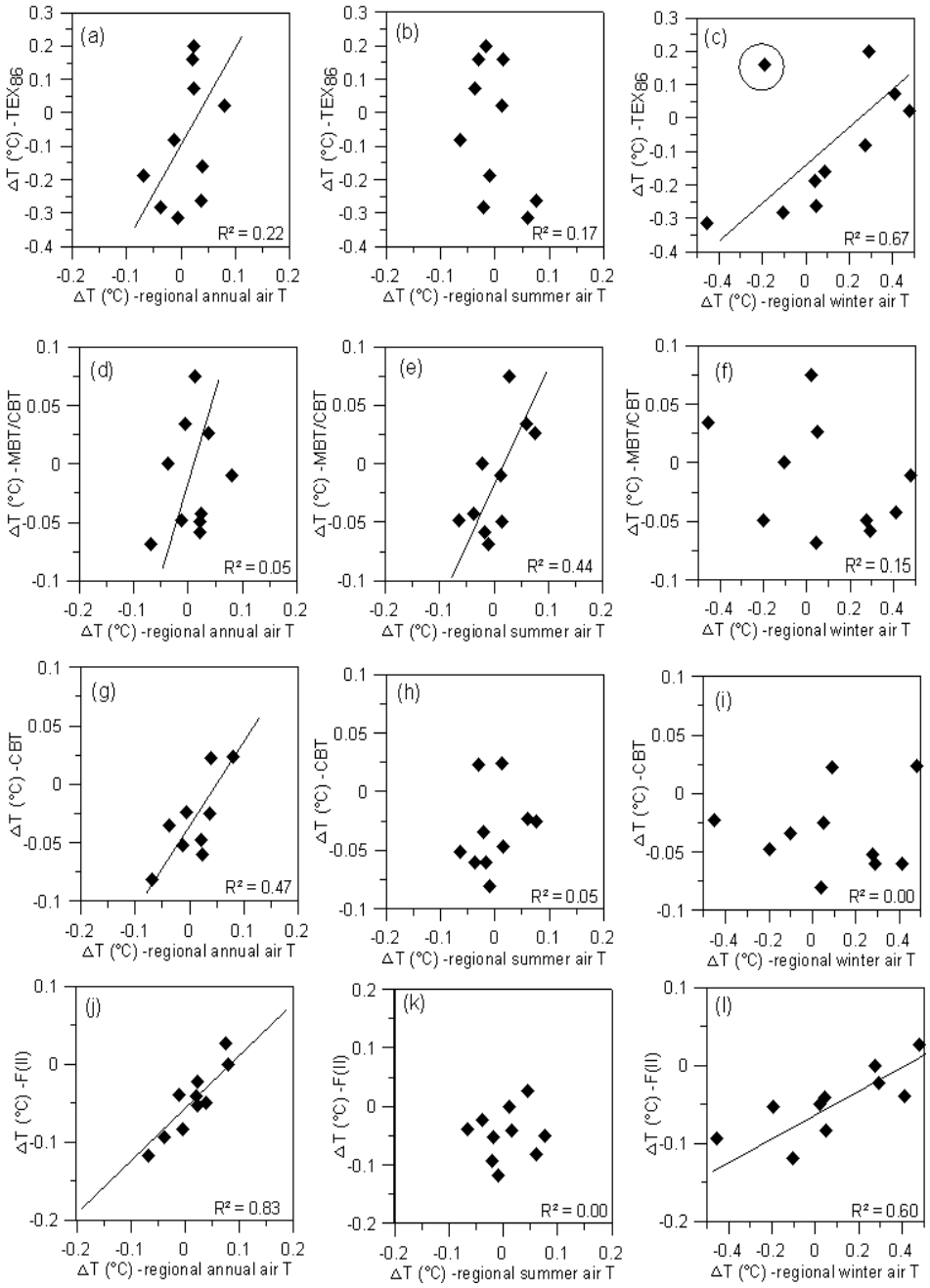

Figure 6-2 (a-c) The correlation between instrumental mean/summer/winter air temperature anomaly (5 years running average) and TEX_{86} temperature anomaly; (d-f) The correlation between instrumental mean/summer/winter air temperature anomaly (5 years running average) and MBT/CBT temperature anomaly; The correlation between instrumental mean/summer/winter air temperature anomaly (5 years running average) and CBT temperature anomaly; The correlation between instrumental mean/summer/winter air temperature anomaly (5 years running average) and F(IIa) temperature anomaly (1949-1992).

isoGDGT-derived TEX_{86} has been used to reconstruct paleotemperature in the lake (Powers et al., 2010; Tierney et al., 2010). We discussed isoGDGTs in the SPM in the water column and sediment trap in Chapter 5, which indicating a predominant production in situ from the upper water column of the lake as well as a few contributions from the catchment soils. Thus the isoGDGT-derived temperature could reflect the actual mean annual lake surface temperature. According to the calibration of Powers et al. (2010), the reconstructed temperature ranged from 9.8 °C to 15.7 °C (mean 13.2±0.4 °C) for the XX century, which was in agreement with the mean lake surface water temperatures (mean 14.7±1.8 °C) or thermocline water temperatures (12.0±1.6 °C) today (Chapter 5).

The water temperature in Lake Montortès quickly responds to air temperature changes. In this case, the water temperature variations seem to be comparable with air temperature variations on the geological time scale. In order to remove the error between the absolute temperatures in different places, we compared temperature anomaly (ΔT) between instrumental temperatures (1949-1992, 5-year running average) and reconstructed lake surface temperatures (LST). The mean annual ΔT and summer ΔT only changed between -0.1 and 0.1 °C, which was much less than TEX_{86} ΔT that ranged between -0.4 and 0.3 °C (Fig. 6-5a, b). Whereas, the TEX_{86} ΔT and winter air temperature ΔT seemed to be more correlated as the ranges of anomaly were similar (-0.4 and 0.4°C, R^2=0.27). Moreover, we found that 1969 was the year transforming from the warming to cooling with ΔT variation of 0.4°C, which was the sparsest sample from the calibration curve (Fig. 6-5c). In this case, we took it away and the correlation between TEX_{86} ΔT and instrumental winter ΔT was more significant (R^2=0.67). No matter TEX_{86} ΔT is more correlated with mean winter air temperature or mean annual air temperature, TEX_{86} in our sediment core seemed to provide convincible information of local temperature changes (1949-1992) based on a high resolution of 5-year temperature reconstruction. However, from the beginning to the middle of the XX century, reconstructed temperatures tended to show a cooling process and the averages during this period were relatively high compared with last 50 year (Fig. 6-7). These biases towards warming could be due to effects of isoGDGTs from soils that provide higher TEX_{86} values and lower GDGT-0/GDGT-4 ratios (Chapter 3). GDGT-0/GDGT-4 ratio was proposed to track the relative contributions or occurrence of Thaumarchaeota or methanogenic Archea in the environment as the ratios from Thaumarchaeota are always lower than 2 and the higher values are attributed to be from methanogenic archaea (Blaga et al., 2009). Thus, when the GDGT-0/GDGT-4 ratio is above 2, it indicating more methanogen-derived

isoGDGTs and the TEX_{86} was not reliable (Blaga et al., 2009; Naeher et al., 2014). However, in our data, the values of this ratio were relatively low in soils (below 5) and increased in the sediment core with reduced TEX_{86} values (Fig. 6-6), indicating an increasing effects from methanogenic Archaea, which could explain the low TEX_{86}-derived temperatures from 1974-1994 (Fig. 6-7). Nevertheless, TEX_{86} recorded the warming since 1970s, which was consistent with the regional instrumental records. GDGT-0/GDGT-4 ratio below 10, could be considered as significant effects from soil inputs, and it markedly biased the TEX_{86} values above 30 (Fig. 6-6). Thus, our data from the lake sediment core suggested that TEX_{86} values could reconstruct the mean annual lake surface temperatures, which might be biased by soil isoGDGTs (warming) and methanogenic production of isoGDGTs (cooling) and there were more methanogenic production in XX century than in XV-XVII century.

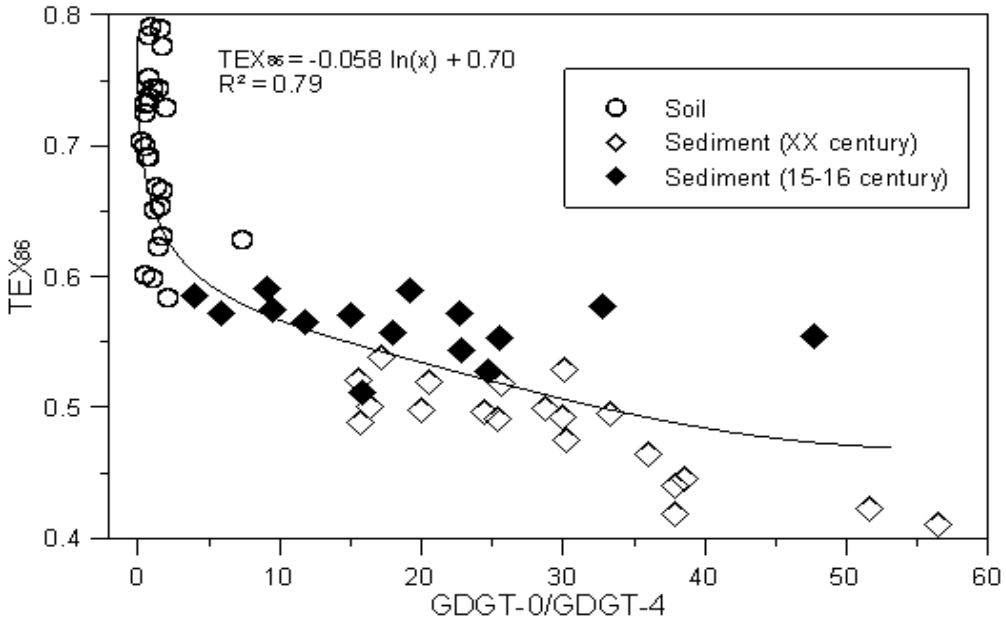

Figure 6-3 The relationship between TEX_{86} and GDGT-0/GDGT-4 ratios in lake sediment and soils (soil data from Chapter 3)

6.3.2.3. Validation of brGDGT estimates based on instrumental temperatures

The global soil MBT/CBTcalibration showed a cold bias and large heterogeneity in reconstructed MAAT (Chapter 5). Here we just used previously published lake temperature calibrations based on MBT/CBT by Peterse (2012) and based on CBT by Zink (2010) as well

as our newly proxy F(IIa) that is derived from abundance of GDGT-IIa in Lake Montcortés into the instrumental temperature variability.

F(IIa) = -38.077×(GDGT-IIa/total brGDGTs)+22.76

It is apparent that all calibrations to some extent are in response to instrumental temperature variability through time. Based on similar proxies (such CBT or MBT/CBT), all temperature trends reconstructed from different calibrations are similar, showing the minima at 1974 (Fig. 6-7). The instrumental MAT ranged from 7.6 to 10.5 °C with a mean value of 9.1±0.1 °C. Whereas, the reconstructed temperatures based on MBT/CBT yielded to cool values, ranging from 3.2 to 5.5 °C (mean 4.2±0.2 °C), the CBT-reconstructed temperature ranged from 9.1 to 10.5 °C (mean 9.7±0.1 °C) and the F(IIa)-reconstructed temperatures were from 8.5 to 10.1 °C with a mean value of mean 9.2±0.1 °C. Obviously, the former MBT/CBT index presented cooler signals for reconstructed MAT. The last two calibrations (based on CBT and F(IIa)) seemed to reflect the actual temperature variability on a 5-year scale (Fig. 6-7). Furthermore, we checked the relationship between reconstructed ΔT and instrumental mean annual, summer and winter ΔT on a 5-year average running basis. The result showed that our F(IIa) calibration could explain about most of mean annual temperature variability (R^2=0.80) during the period AD 1949-1992 (Fig. 6-5 j-l). MBT/CBT-based and CBT-based and reconstructions were followed but showing that estimated ΔT is less correlated with instrumental ΔT on an annual, a summer or a winter basis (Fig. 6-5 d-i). In this case, we think the F(IIa) calibration could be better used for temperature reconstruction in the sediment core from Lake Montcortés. According to the calibration equation F(IIa), the MAT decreased from 9.7 °C in 1900 to 8.5 °C in 1974 and from 1974 to present, the MAT varied between 8.5 °C and 10.6 °C with an increase of 2.1°C in recent 40 years (Fig. 6-7), which confirmed that the global warming occurred in the Lake Montcortés.

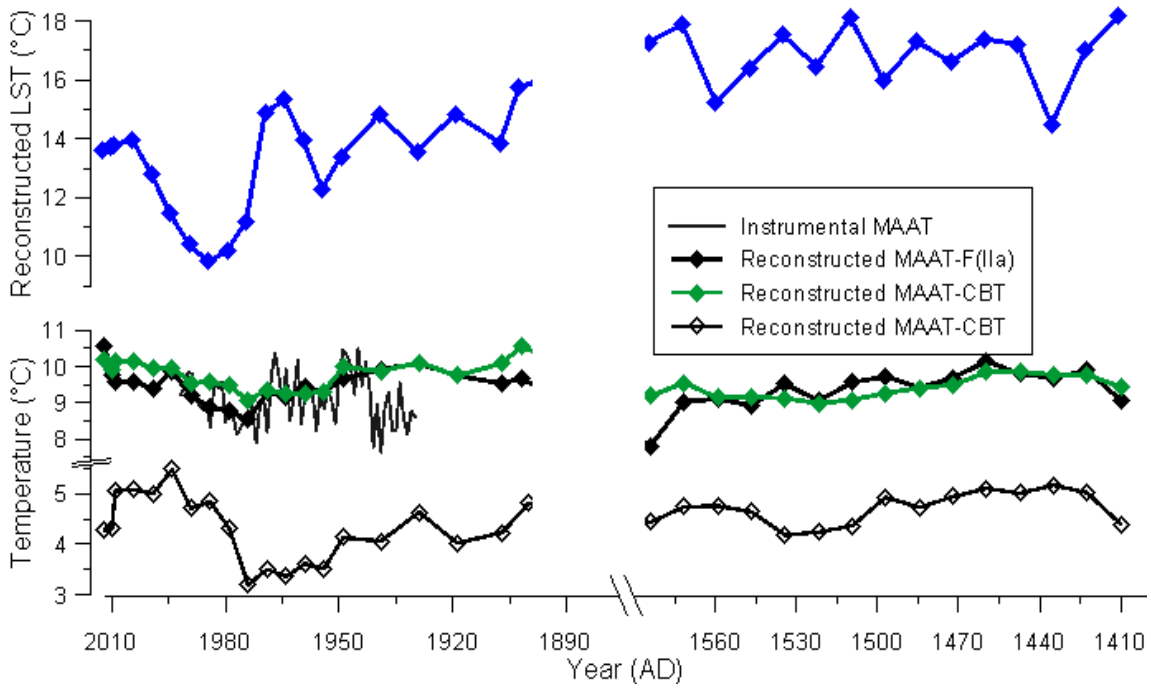

Figure 6-4 GDGT-reconstructed temperatures and instrumental mean air temperatures spanning last 110 years and the XV-XVII century

6.3.2.4. Application of validated proxies in Montcortés core during XV-XVII century (covering the Spörer Minimum)

According to our discussion above, TEX_{86} values for temperature reconstructions for lake surface temperature have biases depending on isoGDGT sources. While brGDGT-derived proxy, such as CBT or F(IIa) are more reliable for MAT reconstruction. Thus, combination of these proxies would suitabley explain temperature variability. Three groups of GDGT-derived indices (TEX_{86}, CBT and F(II)) spanning the sediment core were applied to characterize the mean climate changes during the Spörer Minimum (AD 1420-1550) and the decadal variability was investigated (AD 1410-1584).

The reconstructed lake temperature based on TEX_{86} ranged from 14.5 °C to 18.2 °C (mean 16.9±0.3 °C) in XV-XVII century, which was significantly higher than those in XX century, indicating bias was partly from soil isoGDGTs (Fig. 6-6). Thus the warming signals of TEX_{86} in 1410s and 1570s (Fig. 6-7) seem to be affected by large inputs of soil isoGDGTs through rainfall as these two periods are described with high frequency floods occurring during AD 1350-1400 (Corella et al., 2014) and AD 1580-1620 (Benito et al., 2008). However, other warming signals might be due to abundant production of isoGDGTs in

summer within the lake. Application of the F(IIa) and CBT calibration to sediment core spanning the XV-XVII century in the Lake Montcortés reflected slightly lower temperatures at the beginning and the end of the Sporer Minimum, ranging from 7.8 to 10.1 °C (mean 9.4±0.1 °C) and from 9.0 to 9.9 °C (mean 9.4±0.1 °C), respectively. Moreover, there was a cooling trend since 1450s and the slightly low temperatures during this period were consistent with previous sedimentary and pollen records in Montcortés that showed a cooling trend to indicate the onset of Little Ice Age (LIA) (Corella et al., 2012; Rull et al., 2010).

6.3.3. *n*-alkanes

6.3.3.1. *n*-alkane abundance and indices changed in the sediment core (the XX century and the XV-XVII century)

*n-A*lkane were present in all sediment samples from XX and XV-XVII century (Fig. 6-5), showing slightly higher values in the modern times (11.09±2.19 µg/g dw), corresponding to an increase in total organic carbon (TOC) (Corella et al., 2014).

Mid to long chain *n*-alkanes (>nC_{23}) were predominant in most of the samples. The average chain length (ACL_{25-33}) was in the range of 29-30, indicating land plant epicuticular waxes were the most important sources of *n*-alkanes in the sediment (Eglinton & Hamilton, 1950). In the same way, CPI values were >>1 in all samples, confirming the primary terrestrial higher plants. P_{aq} values were in the range of 0.1-0.3, suggesting that *n*-alkanes were mainly originated from a mix of terrestrial plants and emergent aquatic macrophytes rather than from submerged macrophytes (Chapter 4, Ficken et al., 2000).

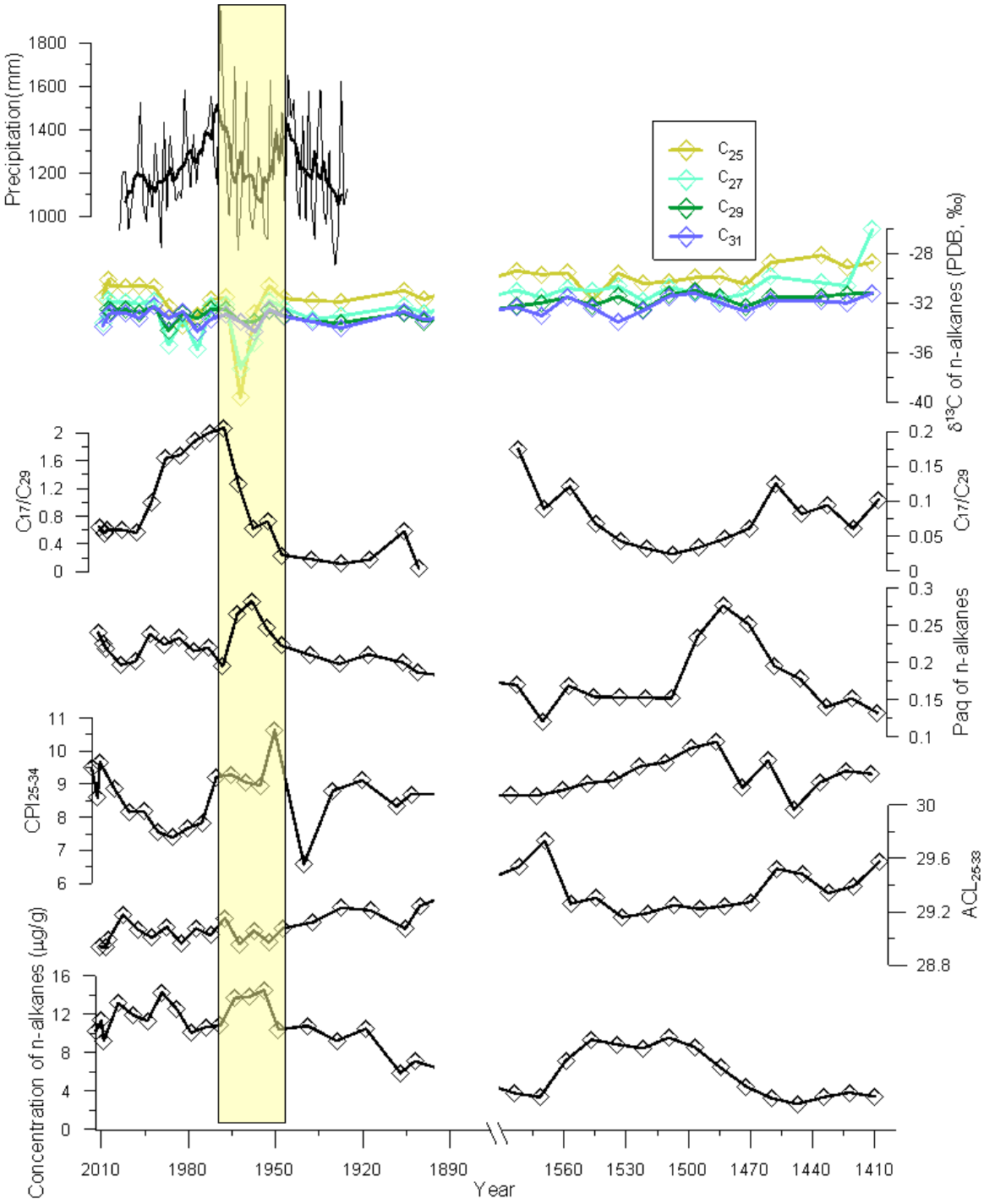

Figure 6-5 Concentration, ratios and carbon isotope of *n*-alkanes in XX century and XV-XVII century

6.3.3.2. Compound specific $\delta^{13}C$ values changed in the sediment core (the XX century and the XV-XVII century)

A slight decrease in the $\delta^{13}C$ values of the long-chain *n*-alkanes (nC_{27}, nC_{29}, nC_{31}) was observed in XX century sediments, the mean $\delta^{13}C$ values of nC_{25}-nC_{29} alkane were -32.0±2.0‰, -33.2±1.6 ‰, -33.0±0.5‰ and -33.2±0.6‰, separately. In contrast, during the XV-XVII century, all the $\delta^{13}C$ values tended to be more positive, -29.7±0.9‰ for nC_{25} alkane and -30.6±1.4‰, -31.7±0.5‰ and -32.1±0.7‰ for nC_{27}, nC_{29} and nC_{31} alkanes, separately. This represents a difference of 2.3‰ for nC_{25}, nC_{27} and a difference of 1.1‰ for nC_{29} and nC_{31} during the two periods, showing a more variable isotopic values and also much lighter values in the shorter chain *n*-alkanes (such as $\delta^{13}C$ of nC_{25} alkane).

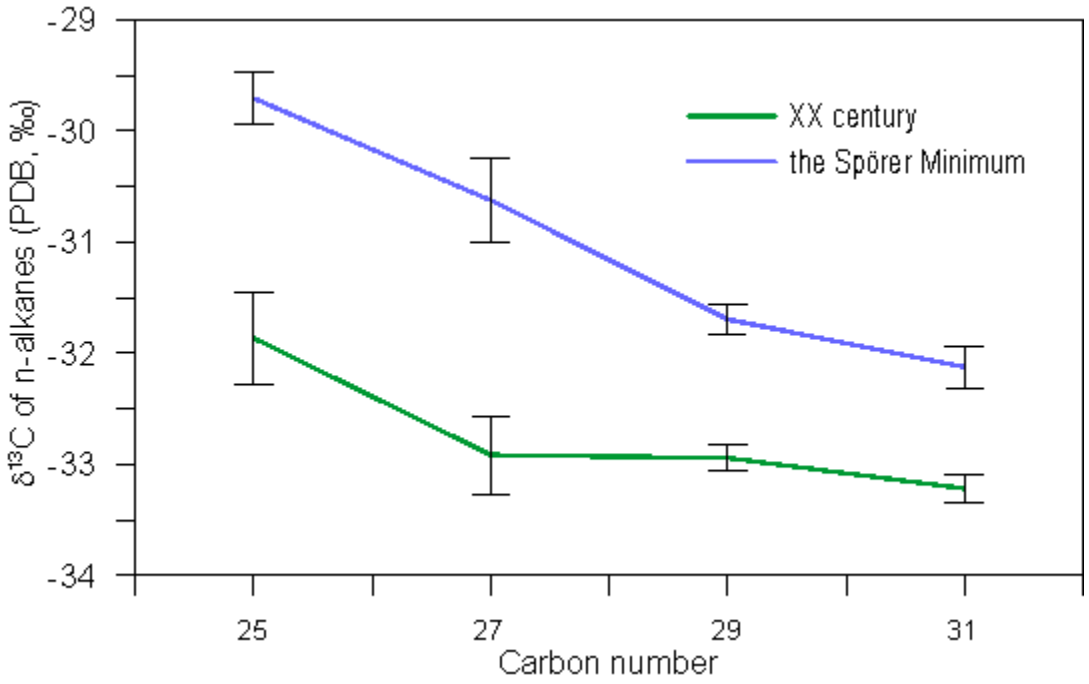

Figure 6-6 Mean $\delta^{13}C$ values of *n*-alkanes in XX century and XV-XVII century

6.3.3.3. Climatic implication of *n*-alkanes in the sediment core

The abundance of *n*-alkanes in the lake sediment increased with more rainfall from 1917 to 1954 AD. From 1954 to present, there was no correlation between them (Fig. 6-1). As we discussed in Chapter 4, the settling particulate particular flux in the lake water column was sensitive to precipitation/runoff and wind, especially the storm. However, there are also other factors controlling the abundance of *n*-alkanes in the sediment that is why the *n*-alkane abundance could not correspond to precipitation variability. ACL values of *n*-alkanes were

slightly decreasing in XX century, which was not corresponding to instrumental records of temperature or precipitation from 1930 to 1992 (Fig. 6-1, Fig. 6-5). In addition, the CPI values were not significantly lower than CPI in soils (Chapter 3), indicating less effect on CPI from biodegradation. Seen from Fig. 6-7, CPI values showed the maximum in 1949 and the minimum in1939 as well as an increasing trend since 1970s, which were consistent with regional instrumental temperature record. Here, we can assume that temperature might be an important climatic factor for controlling CPI changes.

The more abundant *n*-alkane concentration from 1470 to 1560 AD might indicate a more humid period than previous decades (1410-1470 AD) and CPI variability decreased since 1500, suggesting a cooling trend.

6.3.3.4. Other implication of *n*-alkane proxy in the sediment core

According to observations from modern plants and SPM/sediment trap, the distribution of *n*-alkanes in the sediment core was similar to mixing data of living plants and soil samples in the catchment (Chapter 3), indicating inputs from terrestrial higher plants, grasses, aquatic macrophytes and algae. However, the compositions of *n*-alkanes changed in different period of sedimentation processes (Fig. 6-7). A bimodal distribution maximizing at nC_{17} and nC_{29} was detected in some samples from XX century (1959-1994 AD), others only maximized at nC_{29} (Fig. 6-7). Bacteria and algae are potential sources of short-chain *n*-alkanes (such as nC_{17}) (Geger et al., 1980) while terrestrial higher plants only provide long-chain *n*-alkanes (especially nC_{27}-nC_{33}). C_{17}/C_{29} ratio could be used to assess proportional inputs of the aquatic algae and terrestrial higher plants. The increasing nC_{17}/nC_{29} ratio from 1959 to 1994 AD might indicate a large number of algae inputs. Moreover, the largest $\delta^{13}C$ variations of nC_{25} and nC_{27} alkane occurred in this period, confirming new *n*-alkane product depleted $\delta^{13}C$ from the other aquatic plants. Furthermore, nC_{17}/nC_{29} ratio peaked at 1970s, in line with more rainfall and warmer temperature, indicating that wet-warmer conditions were favorable for specific algae growth and thus resulted in more production of nC_{17} alkane.

It is also revealed that emergent aquatic plants *Typha/Sparganium* were abundant in littoral communities around AD 1660 (Scussolini et al., 2011), which could result in lower ACL values. In addtion, the P_{aq} ratio by Ficken et al. (2000) has been proposed to distinguish submerged aquatic macrophytes and terrestrial plants or emergent macrophytes. There were more *n*-alkane inputs of emergent aquatic macrophytes during AD 1950-1970 as well as last 20 years the higher P_{aq} index appeared, corresponding to less humidity and less terrestrial

inputs as instrument-recorded lower amount of rainfall. Furthermore, the temperature during AD 1950-1970 was warmer, which might be suitable for growing submerged macrophytes in the lake (Fig. 6-5). A significant peak of P_{aq} index during AD 1460-1500, coincided with an increase of conifer forests that grew in moisture and colder climate (Rull et al., 2010). The conifer forests produce fewer *n*-alkanes showing higher P_{aq} index (0.26 for *Pinus nigra*, see Chapter 3) compared with evergreen or deciduous *Quercus* forests. Therefore, we think the variation of P_{aq} index could not only reflect changes of submerged aquatic inputs and terrestrial/emergent aquatic inputs, but also indicate source variations within terrestrial inputs if the vegetation shift was sufficiently significant.

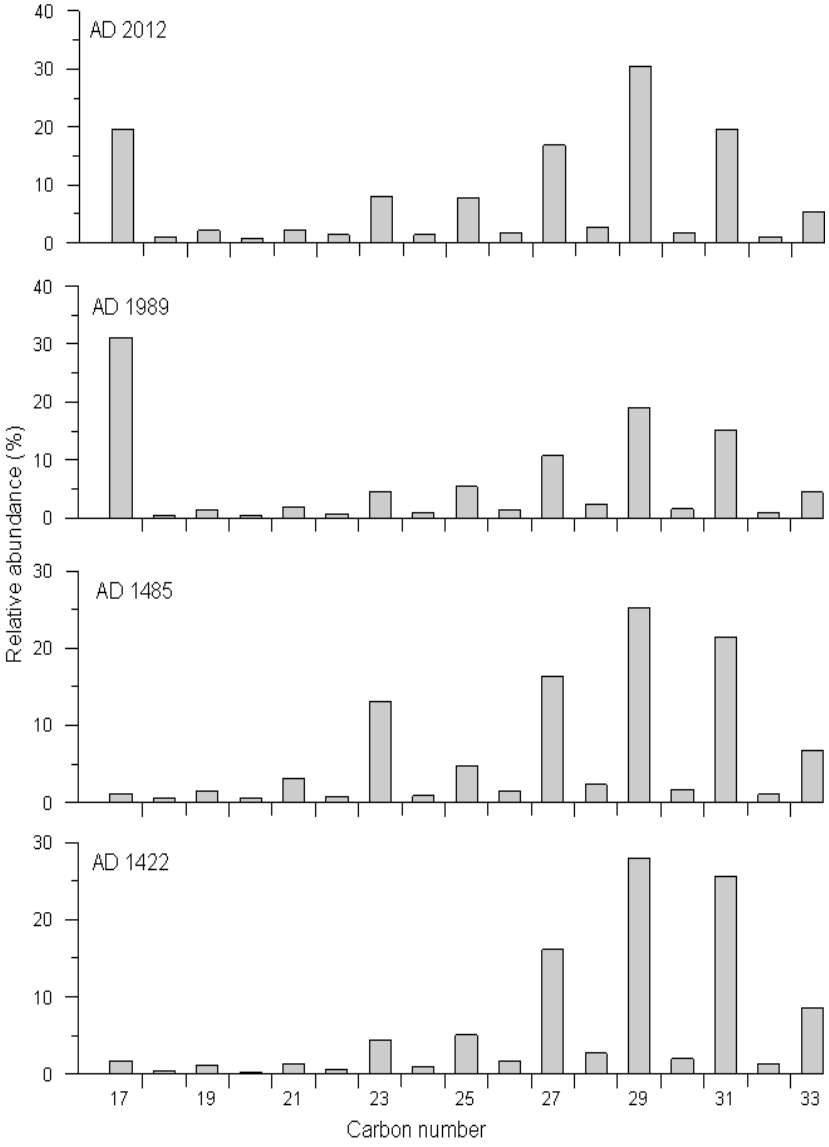

Figure 6-7 Distribution of *n*-alkane homologues formed in different time

6.4. Conclusion

Compared with TEX_{86}-estimated temperatures, the F(IIa)-based temperatures were more realistic throughout the last 110 years and the Spörer Minimum, which could be due to the fact that TEX_{86} reflects seasonal signals in the lake and could be easily preserved in the sediment core as well as biases from soil inputs and methanogenic inputs while F(IIa) reflects signals from the catchment soils without seasonality or the signals of seasonality is not strong enough to be revealed. However, the records since AD 1970s until present revealed that the temperature signals from the lake water column or from the catchment soils were in line with global warming, furtherly indicating that soil signals are not significant in a very short time scale (monthly) (Chapter 3) but a running average of 5 years is possible to reflect mean air temperature changes recorded by soil brGDGTs.

A combination of alkyl lipids data from Lake Montcortés and instrumental climatic data (precipitation and temperature) explains the environmental changes spanning last 110 years and the XV-XVII century (covering the Spörer Minimum). Our result shows that *n*-alkanes in the Lake Montcortés are more enriched in the XX century rather than the onset of LIA. ACL index of *n*-alkanes tends to reveal vegetation shift while CPI values of *n*-alkanes might be related to temperature variations based on a high-resolution (5-10 years) sediment core. P_{aq} index could not only reflect changes of submerged aquatic inputs and terrestrial/emergent aquatic inputs, but also indicate source variations within terrestrial inputs if the vegetation shift was sufficiently significant.

6.5. References

Benito, G., Thorndycraft, V. R., Rico, M., S??nchez-Moya, Y., & Sope??a, A. (2008). Palaeoflood and floodplain records from Spain: Evidence for long-term climate variability and environmental changes. *Geomorphology*, *101*(1-2), 68–77. doi:10.1016/j.geomorph.2008.05.020

Blaga, C. I., Reichart, G.-J., Heiri, O., & Sinninghe Damsté, J. S. (2009). Tetraether membrane lipid distributions in water-column particulate matter and sediments: a study of 47 European lakes along a north–south transect. *Journal of Paleolimnology*, *41*(3), 523–540. doi:10.1007/s10933-008-9242-2

Bray, E. , & Evans, E. (1961). Distribution of *n*-paraffins as a clue to recognition of source beds. *Geochimica et Cosmochimica Acta*, *22*(1), 2–15. doi:10.1016/0016-7037(61)90069-2

Büntgen, U., Esper, J., Verstege, A., Nievergelt, D., Frank, D. C., & Wilson, R. J. S. (2007). Climatic response of multiple tree-ring parameters from the Spanish Central Pyrenees. *Trace*, *5*, 60–72.

Clark, R. C., & Blumer, M. (1967). Distribution of *n*-paraffins in marine organisms and sediment. *Limnology and Oceanography*, *12*(1), 79–87. doi:10.4319/lo.1967.12.1.0079

Corella, J. P., Benito, G., Rodriguez-Lloveras, X., Brauer, a., & Valero-Garcés, B. L. (2014). Annually-

resolved lake record of extreme hydro-meteorological events since AD 1347 in NE Iberian Peninsula. *Quaternary Science Reviews*, *93*, 77–90. doi:10.1016/j.quascirev.2014.03.020

Corella, J. P., Brauer, A., Mangili, C., Rull, V., Vegas-Vilarrúbia, T., Morellón, M., & Valero-Garcés, B. L. (2012). The 1.5-ka varved record of Lake Montcortès (southern Pyrenees, NE Spain). *Quaternary Research*, *78*(2), 323–332. doi:10.1016/j.yqres.2012.06.002

Corella, J. P., Brauer, A., Valero-garcés, B. L., Muñoz, A., & Mangili, C. (2010). Paleoclimatic and sedimentological interpretation of the Lake Montcortès varved sedimentary record of the last 1500 years, *12*, 14698.

Dorado Liñán, I., Büntgen, U., González-Rouco, F., Zorita, E., Montávez, J. P., Gómez-Navarro, J. J., … Gutiérrez, E. (2012). Estimating 750 years of temperature variations and uncertainties in the Pyrenees by tree-ring reconstructions and climate simulations. *Climate of the Past*, *8*(3), 919–933. doi:10.5194/cp-8-919-2012

Eglinton, G., & Hamilton, R. J. (1950). Leaf Epicuticular, *156*.

Escala, M., Fietz, S., Rueda, G., & Rosell-Melé, A. (2009). Analytical considerations for the use of the paleothermometer tetraether index86 and the branched vs isoprenoid tetraether index regarding the choice of cleanup and instrumental conditions. *Analytical Chemistry*, *81*(7), 2701–2707. doi:10.1021/ac8027678

Escala, M., Rosell-Melé, A., & Masqué, P. (2007). Rapid screening of glycerol dialkyl glycerol tetraethers in continental Eurasia samples using HPLC/APCI-ion trap mass spectrometry. *Organic Geochemistry*, *38*(1), 161–164. doi:10.1016/j.orggeochem.2006.08.013

Ficken, K. J., Li, B., Swain, D. L., & Eglinton, G. (2000). An *n*-alkane proxy for the sedimentary input of submerged/floating freshwater aquatic macrophytes. *Organic Geochemistry*, *31*, 745–749.

Gottfried, M., Pauli, H., Futschik, A., Akhalkatsi, M., Barančok, P., Alonso, B., … Grabherr, G. (2012). Continent-wide response of mountain vegetation to climate change. *Nature Climate Change*, *2*(February), 5. doi:10.1038/nclimate1329

Hopmans, E. C., Weijers, J. W. ., Schefuß, E., Herfort, L., Sinninghe Damsté, J. S., & Schouten, S. (2004). A novel proxy for terrestrial organic matter in sediments based on branched and isoprenoid tetraether lipids. *Earth and Planetary Science Letters*, *224*(1-2), 107–116. doi:10.1016/j.epsl.2004.05.012

Huguet, C., Fietz, S., & Rosell-Melé, a. (2013). Global distribution patterns of hydroxy glycerol dialkyl glycerol tetraethers. *Organic Geochemistry*, *57*, 107–118. doi:10.1016/j.orggeochem.2013.01.010

Loomis, S. E., Russell, J. M., Eggermont, H., Verschuren, D., & Sinninghe Damsté, J. S. (2014). Effects of temperature, pH and nutrient concentration on branched GDGT distributions in East African lakes: Implications for paleoenvironmental reconstruction. *Organic Geochemistry*, *66*, 25–37. doi:10.1016/j.orggeochem.2013.10.012

Loomis, S. E., Russell, J. M., Ladd, B., Street-Perrott, F. A., & Sinninghe Damsté, J. S. (2012). Calibration and application of the branched GDGT temperature proxy on East African lake sediments. *Earth and Planetary Science Letters*, *357-358*, 277–288. doi:10.1016/j.epsl.2012.09.031

Luo, P., Peng, P. A., Lü, H. Y., Zheng, Z., & Wang, X. (2012). Latitudinal variations of CPI values of long-chain *n*-alkanes in surface soils: Evidence for CPI as a proxy of aridity. *Science China Earth Sciences*, *55*(7), 1134–1146. doi:10.1007/s11430-012-4401-8

Luterbacher, Xoplaki, Dietrich, Rickli, Jacobeit, Beck, … Wanner. (2002). Reconstruction of sea level pressure fields over the Eastern North Atlantic and Europe back to 1500. *Climate Dynamics*, *18*(7), 545–561. doi:10.1007/s00382-001-0196-6

Mango, F. D. (1997). The light hydrocarbons in petroleum: A critical review. *Organic Geochemistry*,

26(7-8), 417–440. doi:10.1016/S0146-6380(97)00031-4

Meyers, P. A., Maring, H. B., & Bourbonniere, R. A. (1980). Alkane and alkanoic acid variations with depth in modern sediments of Pyramid Lake. *Physics and Chemistry of the Earth*, *12*(C), 365–374. doi:10.1016/0079-1946(79)90119-8

Mügler, I., Sachse, D., Werner, M., Xu, B., Wu, G., Yao, T., & Gleixner, G. (2008). Effect of lake evaporation on δD values of lacustrine *n*-alkanes: A comparison of Nam Co (Tibetan Plateau) and Holzmaar (Germany). *Organic Geochemistry*, *39*(6), 711–729. doi:10.1016/j.orggeochem.2008.02.008

Naeher, S., Peterse, F., Smittenberg, R. H., Niemann, H., Zigah, P. K., & Schubert, C. J. (2014). Organic Geochemistry Sources of glycerol dialkyl glycerol tetraethers (GDGTs) in catchment soils , water column and sediments of Lake Rotsee (Switzerland) – Implications for the application of GDGT-based proxies for lakes. *Organic Geochemistry*, *66*, 164–173.

Niemann, H., Stadnitskaia, a., Wirth, S. B., Gilli, a., Anselmetti, F. S., Sinninghe Damsté, J. S., … Lehmann, M. F. (2012). Bacterial GDGTs in Holocene sediments and catchment soils of a high Alpine lake: application of the MBT/CBT-paleothermometer. *Climate of the Past*, *8*(3), 889–906. doi:10.5194/cp-8-889-2012

Otto, A., & Simpson, M. J. (2005). Degradation and Preservation of Vascular Plant-derived Biomarkers in Grassland and Forest Soils from Western Canada. *Biogeochemistry*, *74*(3), 377–409. doi:10.1007/s10533-004-5834-8

Pearson, E. J., Juggins, S., Talbot, H. M., Weckström, J., Rosén, P., Ryves, D. B., … Schmidt, R. (2011). A lacustrine GDGT-temperature calibration from the Scandinavian Arctic to Antarctic: Renewed potential for the application of GDGT-paleothermometry in lakes. *Geochimica et Cosmochimica Acta*, *75*(20), 6225–6238. doi:10.1016/j.gca.2011.07.042

Peterse, F., van der Meer, J., Schouten, S., Weijers, J. W. H., Fierer, N., Jackson, R. B., … Sinninghe Damsté, J. S. (2012). Revised calibration of the MBT–CBT paleotemperature proxy based on branched tetraether membrane lipids in surface soils. *Geochimica et Cosmochimica Acta*, *96*, 215–229. doi:10.1016/j.gca.2012.08.011

Powers, L., Werne, J. P., Vanderwoude, A. J., Sinninghe Damsté, J. S., Hopmans, E. C., & Schouten, S. (2010). Applicability and calibration of the TEX86 paleothermometer in lakes. *Organic Geochemistry*, *41*(4), 404–413. doi:10.1016/j.orggeochem.2009.11.009

Rielley, G., Collier, R. J., Jones, D. M., & Eglinton, G. (1991). The biogeochemistry of Ellesmere Lake, U.K. I, Source correlation of leaf wax inputs to the sedimentary lipid record. *Organic Geochemistry*, *17*(6), 901–912. Retrieved from http://cat.inist.fr/?aModele=afficheN&cpsidt=4957619

Rull, V., González-Sampériz, P., Corella, J. P., Morellón, M., & Giralt, S. (2010). Vegetation changes in the southern Pyrenean flank during the last millennium in relation to climate and human activities: the Montcortès lacustrine record. *Journal of Paleolimnology*, *46*(3), 387–404. doi:10.1007/s10933-010-9444-2

Rull, V., & Vegas-Vilarrúbia, T. (2015). Crops and weeds from the Estany de Montcortès catchment, central Pyrenees, during the last millennium: a comparison of palynological and historical records, 699–710. doi:10.1007/s00334-015-0525-z

Sachse, D., Radke, J., & Gleixner, G. (2004). Hydrogen isotope ratios of recent lacustrine sedimentary *n*-alkanes record modern climate variability. *Geochimica et Cosmochimica Acta*, *68*(23), 4877–4889. doi:10.1016/j.gca.2004.06.004

Schouten, S., Hopmans, E. C., Schefuß, E., & Sinninghe-Damste, J. S. (2002). Distributional variations in marine crenarchaeotal membrane lipids: A new tool for reconstruting ancient sea-surface temperatures? *Earth and Planetary Science Letters*, *204*, 265–274.

Scussolini, P., Vegas-Vilarrúbia, T., Rull, V., Corella, J. P., Valero-Garcés, B., & Gomà, J. (2011).

Middle and late Holocene climate change and human impact inferred from diatoms, algae and aquatic macrophyte pollen in sediments from Lake Montcortès (NE Iberian Peninsula). *Journal of Paleolimnology*, *46*(3), 369–385. doi:10.1007/s10933-011-9524-y

Sinninghe-Damsté, J. S., Hopmans, E. C., Pancost, R. D., Schouten, S., & Geenevasen, J. a. J. (2000). Newly discovered non-isoprenoid glycerol dialkyl glycerol tetraether lipids in sediments. *Chemical Communications*, (17), 1683–1684. doi:10.1039/b004517i

Spötl, C., Nicolussi, K., Patzelt, G., & Boch, R. (2010). Humid climate during deposition of sapropel 1 in the Mediterranean Sea: Assessing the influence on the Alps. *Global and Planetary Change*, *71*(3-4), 242–248. doi:10.1016/j.gloplacha.2009.10.003

Sun, Q., Chu, G., Liu, M., Xie, M., Li, S., Ling, Y., … Lü, H. (2011). Distributions and temperature dependence of branched glycerol dialkyl glycerol tetraethers in recent lacustrine sediments from China and Nepal. *Journal of Geophysical Research: Biogeosciences*, *116*(1), 1–12. doi:10.1029/2010JG001365

Tierney, J. E., Mayes, M. T., Meyer, N., Johnson, C., Swarzenski, P. W., Cohen, A. S., & Russell, J. M. (2010). Late-twentieth-century warming in Lake Tanganyika unprecedented since AD 500. *Nature Geoscience*, *3*(6), 422–425. doi:10.1038/ngeo865

Tierney, J. E., & Russell, J. M. (2009). Distributions of branched GDGTs in a tropical lake system: Implications for lacustrine application of the MBT/CBT paleoproxy. *Organic Geochemistry*, *40*(9), 1032–1036. doi:10.1016/j.orggeochem.2009.04.014

Weijers, J. W. H., Schouten, S., van den Donker, J. C., Hopmans, E. C., & Sinninghe Damsté, J. S. (2007). Environmental controls on bacterial tetraether membrane lipid distribution in soils. *Geochimica et Cosmochimica Acta*, *71*(3), 703–713. doi:10.1016/j.gca.2006.10.003

Zink, K. G., Vandergoes, M. J., Mangelsdorf, K., Dieffenbacher-Krall, A. C., & Schwark, L. (2010). Application of bacterial glycerol dialkyl glycerol tetraethers (GDGTs) to develop modern and past temperature estimates from New Zealand lakes. *Organic Geochemistry*, *41*(9), 1060–1066. doi:10.1016/j.orggeochem.2010.03.004

Chapter 7

Conclusions and future work

The aim of the project is to validate the use of biomarker proxies to obtain high resolution (i.e. multidecadal) records of temperature and precipitation in the Iberian Peninsula for the late Holocene. In order to achieve the main aim, the project has focused on the monitoring of modern sedimentation processes and of the putative sources of the targeted biomarkers in lake Montcortés, in NW Spain, and the study of laminated sedimentary sequences recovered from the lake.

We examined the *n*-alkanes and core GDGT distributions from different soils that were collected each month and one round of plant sample collection (for *n*-alkane analysis) in the same catchment. We found that different types of vegetation showed large variability on concentration, distribution and $\delta^{13}C$ values of long chain *n*-alkane homologues. However, concentration of *n*-alkanes just slightly varied in different soil sites (spatial heterogeneity) and in different sampling months (seasonal variability). The absence of seasonality in soil could be due long turnover time of *n*-alkanes. The composition of soil *n*-alkanes distinctively reflected lipid features from dominant plants overlying soils (such as grass or woodland plants), indicating degradation effects in plant-soil system are not significant. Abundance or flux of lipid biomarkers in suspended particulate matter (SPM) and settling particulate matter (STM) in the upper water column showed markedly seasonal variations, which were to some extent affected by transport processes (i.e. precipitation/runoff, wind), aquatic production (in summer and autumn) and annual lake circulation (in winter). Moreover, the abundance of SPM *n*-alkanes and *n*-alkanoic acids decreased at three depths from the upper to the bottom water column and their degrading rates were not similar in different seasons, e.g. the former degraded faster in spring while the latter in summer. Low CPI values *n*-alkanes (~1) from SPM in the water column indicate that anthropogenic inputs (such as petrogenic sources) make contribution of *n*-alkanes to the lake.

GDGT concentrations varied largely in different soils as well as within the same soils in different sampling months. MBT and CBT index showed large variability in different soil sites but without seasonality in the same soils. The soils could be separated into two groups: Group A, the MBT/CBT temperature estimates (based on global soil dataset calibration) were close to mean annual air temperatures (MAT); Group B, underestimated MAT (or just close to winter temperatures). The heterogeneity of these estimates between different soils might be affected by soil humidity (dry and alkaline soils tend to underestimate temperatures). The sediment in the lake has the estimated values closer to group B, it means that MBT/CBT estimates are not reliable for absolute temperature reconstruction in the lake. In addition, our

data suggested that CBT values of soils are correlated to pH values on a global scale, but on a regional or catchment scale, the MBT values are more correlated to pH values. isoGDGT-derived TEX_{86} values in the soils gave warmer signals and were unchangeable throughout the year. Forest soils in the catchment presented no TEX_{86} values due to low production of isoGDGTs. In the lake system, the TEX_{86}-reconstructed monthly temperatures at three depths of the water column and sediment trap were highly correlated to variations of CTD-measured temperatures in the thermocline water but the mean values were much closer to the surface temperatures. Nevertheless, the estimated mean annual lake temperatures from the surface water or thermocline water could be comparable with other sites on a global calibration plot. TEX_{86}-temperature biases might be due to warm signals from the catchment soils and dissolved oxygen could be a constraint factor influencing the accurate temperature reconstruction.

We tested the proxies derived from lipid biomarker to instrumental records on a 5-year scale. Temperature estimates from TEX_{86}, MBT/CBT, CBT and relative abundance of GDGT-IIa were performed. All the reconstructed temperature trends were to some extent correlated to mean annual instrumental air temperatures in the region (1949-1992). Biases of TEX_{86} estimates might be due to methanogenic inputs as well soil inputs or from seasonal signals, GDGT-0/GDGT-4 ratio could be an indicator for these two inputs in the lake. The temperature estimates using the fractional abundance of GDGT-IIa were the closest ones to the instrumental actual MAT. ACL values and compound specific $\delta^{13}C$ values of *n*-alkanes were very stable in last 100 years and independent from temperature and precipitation variability. CPI values might be correlated to temperature variations.

Finally, we used GDGT-based proxies to reconstruct past climate changes in the 15^{th} -17^{th} century on a decadal resolution. TEX_{86} index provide warmer signals in this period compared with modern time, particularly at the beginning of 15 century and at the end of 16 century, which we explain that higher TEX_{86} signals were from the catchment soils. On the other hand, temperatures derived from abundance of GDGT-IIa showed a cooling starting from 15^{th} century, indicating the beginning of the Little Ice Age. Thus, a combination of TEX_{86} and GDGT-IIa temperature could provide more reliable explanation for paleoclimatic reconstruction in lake Montcortés. The results all together reveal the high potential of *n*-alkanes and GDGTs in reconstructing past environmental changes the study area where these two families of biomarkers could be as good continental proxies. However, significant

heterogeneity of GDGT proxies suggested that a good knowledge of sampling site in the catchment soils is extremely necessary to accurately interpret the climatic variations.

There are also a number of perspectives of this work: More details on characteristics of biomarkers should be unveiled before the applications for the past reconstructions, e.g. what are overtimes of lipid biomarker in the soils? Why proxies derived from different sources providing original environmental information presented similar concentration/flux variations in the water column. In this thesis, we could apply GDGTs to reconstruct past temperature in quantity on a regional and decadal scale, but how about precipitation reconstruction? Information of *n*-alkanes is not so straightforward with instrumental records. It requires more understanding on source origins, transport, residence time of lipid biomarker as well as lake dynamics of circulation. Thus, the future work on soil lipids age and δD of long chain *n*-alkanes would be very important.

Figures and tables

Figure 1-1 (a) Observed changes in global average surface temperature. The three surface temperature datasets are originated from Hadley Centre/Climate Research Unit of the University of East Anglia, UK (black line), US National Oceanic and Atmospheric Administration (orange line) and Goddard Institute for Space studies, NASA (blue line). Top panel: annual mean values, bottom panel: decadal mean values including the estimate of uncertainty for HadCRUT4. (b) Changes in annual surface temperatures between 1901 and 2012 derived from data maintained by US National Oceanic and Atmospheric Administration. (Source: IPCC AR5, 2014) ----------4

Figure 1-2 (a) Winter (December-March) index of the NAO based on the difference of normalized sea level pressure (SLP) between Lisbon, Portugal and Stykkisholmur/Reykjavik, Iceland since 1864. The SLP values at each station were normalized by removing the long-term mean and by dividing by the long-term standard deviation. Both the long-term means and standard deviations are based on the period 1864-1983. Normalization is used to avoid the series being dominated by the greater variability of the northern station. (b) The principal component (PC) time series of the leading EOF of annual SLP anomalies over the Atlantic sector (20-80 °N, 90°W-40°E) serves as an alternative index (see Hurrell et al. (2003) and Hurrell et al. (1995)). (c) The annual PC timeseries is shown below in color, and the station based index is given by the thick black line. The correlation between the two is 0.91 over the period 1899-2014. The black dots on the EOF panel show the location of the stations used in the annual station-based index (Phillips, 2016) ----------7

Figure 1-3 Structures of crenarchaeol-based IPLs (Lengger et al., 2012) ----------11

Figure 1-4 Phylogenetic tree showing the topology of relationships between orders of Archaea based on 16S rRNA sequences. The major kingdoms of Archaea are the Korarchaeota, Crenarchaeota, Thaumarchaeota, and Euryarchaeota.Within the Euryarchaeota, the euryarchaeal group comprising Thermoplasmatales and their relatives (A), as well as all Thaumarchaeota and Crenarchaeota studied to date, are known for synthesizing GDGT(glycerol dialkyl glycerol tetraether) lipids containing cyclopentane rings. Only the Thaumarchaeota are known to make crenarchaeol. Abbreviation: DHVE, deep-sea hydrothermal vent Euryarchaeota (Pearson and Ingalls, 2013) ----------12

Figure 1-5 Structures of isoprenoid GDGTs and branched GDGTs ----------13

Figure 2-1 Location of Lake Montcortès in the Iberian Peninsula and Digital Terrain Model (5 m resolution) of the Pallars Sobira region and location of Lake Montcortès, Cabdella and La Pobla de Segur meteorological station (Corella et al., 2014). (b) Geologic map of Lake Montcorès catchment and (c) Locations of the sediment core (modified from Corella et al., 2012) ----------28

Figure 2-2 General location of soil sampling sites (Ms1-Ms6, yellow triangle) and plants (red triangle) as well as sediment trap (yellow dot) in Lake Montcortés, Catalan Eastern Pyrenees ----------32

Figure 2-3 Photos of pumping and filtering samples from water----------33

Figure 2-4 Schematic chart of analytical methods in the laboratory ----------35

Figure 2-5 Chromatogram of C_{23}-C_{35} *n*-alkanes in the reference sediment from Lake Montcortés based on retention time----------40

Figure 2-6 Chromatograms of the GDGT analysis in HPLC-APCI-MS system: isoprenoid, branched GDGTs and GR standard (Gemma, 2013)----------42

Figure 2-7 The injections of increasing concentrations of GR standard and peak area using Agilent HPLC-TOF-MS and Dionex HPLC –Thermo Finnigan TSQ-MS response to GDGT-0 (black dots) and to compound GR (red dots) (see details from Escala, 2009)----------43

Figure 2-8 Meteorological data from September 2013 to April 2015 were from a weather station at La Pobla de Segur (a) daily accumulated precipitation (dark grey bar), (b) mean monthly air temperatures (MMAT, solid diamond), and (c) wind velocity (hollow diamond). In here we show CTD values at the depths where water samples were taken once per month; blue, orange and green crosses stand for samples from the surface (0m), thermocline (5-12m) and the bottom (20-22m) for (b) water temperature and for (c) dissolved oxygen (DO). Bulk sediment mass fluxes in the sediment trap in Lake Montcortés are shown as grey bars in the upper most graph (a)----------45

Figure 3-1 Concentration of *n*-alkanes, average chain length (ACL) and Carbon preference index (CPI) from three soils in the Lake Montcortés catchment from September 2013 to November 2014--60

Figure 3-2 Distribution of *n*-alkanes in plants, soils and surface sediments----------64

Figure 3-3 The compound specific δ13C values of different plants----------65

Figure 3-4 Carbon isotopic compositions of *n*-alkanes in soils in lake Montcortés catchment from September 2013 to November 2014----------67

Figure 3-5 The relationship between (a) soil water content and concentration of brGDGTs from three sampling sites throughout the year (September 2013-November 2014), (b) soil water content and brGDGT concentration from 6 sampling sites (Ms1-Ms3 on average).----------69

Figure 3-6 Ternary diagrams with relative abundance of GDGT-I, GDGT-II and GDGT-III----------70

Figure 3-7 Concentrations of brGDGTs (a) and isoGDGTs (b) analyzed in the different soils from September 2013 to November 2014 in the Lake Montcortés catchment----------71

Figure 3-8 Variations of MBT, CBT and TEX_{86} proxies derived from GDGTs in soils during the sampling period (September 2013 to November 2014)----------72

Figure 3-9 Linear regression plots of (a) measured soil pH vs. CBT, (b) measured soil pH vs. MBT--75

Figure 4-1 Concentration of *n*-alkanes from suspended particulate matter (SPM) in the water column from October 2013 to November 2014. The top is specific carbon isotopic composition of *n*-alkanes from SPM of surface waters----------89

Figure 4-2 Concentration of *n*-alkanoic acids from suspended particulate matter (SPM) in the water column from October 2013 to November 2014----------91

Figure 4-3 Degrading rate of nC_{23} and nC_{29} concentration from the epilimnion to the hypolimnion----93

Figure 4-4 Sediment trap flux of *n*-alkanes (black bar) and *n*-alkanoic acids (grey bar) and *n*-alkyl lipid-related proxies. The top is compound specific $\delta^{13}C$ of *n*-alkane homologues (nC_{25}-nC_{31}) from the sediment trap from October 2013 to April 2015----------97

Figure 4-5 Chromatography of *n*-alkane distribution in the sediment trap, (a) November 2014, dominated by C_{23} alkane ; (b) December 2014, dominated by C_{29} alkane----------98

Figure 4-6 Suspended particulate matter (SPM) of water column containing *n*-alkanes and *n*-alkanoic acids correlated with the mean daily accumulated precipitation from the meteorological station-----101

Figure 4-7 The relationship between mean daily precipitation /wind velocity and sediment trap flux of *n*-alkanes (a, c)/*n*-alkanoic acids (b, d) in Lake Montcortés----------102

Figure 5-1 Concentrations of isoGDGTs (a) and brGDGTs (b) of SPM in the water column from September 2013 to November 2014 (c) isoGDGT flux (grey bar) and brGDGT flux (black bar) in the sediment trap from October 2013 to April 2015 in Lake Montcortés----------116

Figure 5-2 Fractional abundance of isoprenoid GDGTs in the water column (0 m, 5-12 m, 20-22 m), the sediment trap and surface sediment (0–2 cm)----------120

Figure 5-3 Fractional abundance of branched GDGTs in the water column (0 m, 5-12 m, 20-22 m), the sediment trap and surface sediment (0–2 cm)----------121

Figure 5-4 TEX_{86}-derived lake temperature from SPM at three depths of water column (a) and comparison of CTD-measured temperature at thermocline (5-12 m depth) and reconstructed temperatures from SPM in the water column and sediment trap----------123

Figure 5-5 Linear regression and correlation of TEX_{86} in water column and sediment trap in Lake Montcortés----------126

Figure 5-6 MBT/CBT estimated temperature from SPM at three depths of water column and sediment trap vs. the instrumental mean monthly air temperature and CTD-measured lake bottom water temperature----------128

Figure 6-1 GDGT concentration and proxies in XX^{th} century and $XV\text{-}XVII^{th}$ century----------143

Figure 6-2 (a-c) The correlation between instrumental mean/summer/winter air temperature anomaly (5 years running average) and TEX_{86} temperature anomaly; (d-f) The correlation between instrumental mean/summer/winter air temperature anomaly (5 years running average) and MBT/CBT temperature anomaly; The correlation between instrumental mean/summer/winter air temperature anomaly (5 years running average) and CBT temperature anomaly; The correlation between instrumental mean/summer/winter air temperature anomaly (5 years running average) and F(IIa) temperature anomaly (1949-1992).----------144

Figure 6-3 The relationship between TEX_{86} and GDGT-0/GDGT-4 ratios in lake sediment and soils (soil data from Chapter 3)----------146

Figure 6-4 GDGT-reconstructed temperatures and instrumental mean air temperatures spanning last 110 years and the XV-XVIIth century----------148

Figure 6-5 Concentration, ratios and carbon isotope of *n*-alkanes in XXth century and XV-XVIIth century----------150

Figure 6-6 Mean $\delta^{13}C$ values of *n*-alkanes in XXth century and XV-XVIIth century----------151

Figure 6-7 Distribution of *n*-alkane homologues in sediment core formed in different time----------153

Table 2-1 List of selected plants and types ----------31

Table 2-2 Names and usage of internal standards----------36

Table 3-1 Water content, TOC, pH and distribution of GDGTs in soils and surface sediment----------57

Table 3-2 Relative abundance of odd chain n-alkane homologues and ratios in soils and surface sediments----------58

Table 3-3 The *n*-alkane concentration, ratios and carbon isotopes of different vegetation specimens in the Lake Montcortés catchment----------61

Table 3-4 GDGT concentration and ratios in soils and surface sediment----------68

Table 4-1 *n-A*lkane concentrations and ratios in the water column from Sep. 2013 to Nov. 2014-----90

Table 4-2 Compound specific $\delta^{13}C$ values (‰) of long odd chain n-alkanes in SPM and sediment trap----------99

Table 5-1 Concentrations of isoGDGTs and brGDGTs, TEX_{86} (Schouten et al., 2002), MBT and CBT values, reconstructed MAT (Weijers et al., Peterse 2012) for SPM at three depths of water column from October 2013 to November 2014.----------118

Abbreviations

IPCC---Intergovernmental Panel on Climate Change

NAO---North Atlantic Oscillation

GDGTs--- Glycerol dialkyl glycerol tetraethers

BrGDGTs---Banched GDGTs, applied to chemical structures that are composed of a methylated carbon chain.

IsoGDGTs---Isoprenoid GDGTs, applied to chemical structures that are based on the isoprene unit (isoterpene or 2-methyl-1,3-butadiene).

SST---Surface see temperature

LST---Surface lake temperature

MAT---Mean annual air temperature

CBT---Cyclisation ratio of branched tetraethers

MBT--- Methylation index of branched tetraethers

SPM---Suspended particulate matter

CC---Column chromatography

GF/F---Glass fibre filters

DCM---Dichloromethane

MeOH---Methanol

2-pro---isopropanol

DE---Diethyl ether

AA---Acetic acid

BF_3---Boron trifluoride

GC---Gas chromatography

FID---Flame ionization detector

IRMS---isotope ratio mass spectrometer

PTFE---Polytetrafluorethylene

HPLC---High Performance Liquid Chromatography

APCI--- Atmospheric pressure chemical ionization

LOI---Loss on ignition

Appendix 1 Concentration of n-alkanes and ratios in soil samples (a)

	C_{23}	C_{24}	C_{25}	C_{26}	C_{27}	C_{28}	C_{29}	C_{30}	C_{31}	C_{32}	C_{33}
Ms1											
Sep-13	0.23	0.00	0.78	0.28	2.92	1.04	10.38	0.85	16.20	0.57	5.43
Oct-13	0.26	0.11	0.63	0.29	2.73	1.06	5.62	0.54	8.18	0.44	3.05
Nov-13	0.40	0.16	0.95	0.31	3.01	0.93	10.20	0.84	12.33	0.56	3.39
Dec-13	0.20	0.08	0.36	0.13	1.34	0.43	4.33	0.37	6.00	0.27	2.24
Jan-14	0.22	0.08	0.51	0.15	1.57	0.60	6.26	0.63	10.17	0.51	3.85
Feb-14	0.18	0.06	0.42	0.15	1.47	0.70	4.73	0.52	7.55	0.44	3.41
Mar-14	0.19	0.08	0.45	0.16	1.32	0.63	3.68	0.47	5.39	0.37	2.21
Apr-14	0.25	0.09	0.54	0.18	1.80	0.73	6.57	0.63	10.13	0.42	3.46
May-14	0.16	0.06	0.37	0.12	1.13	0.55	3.35	0.46	5.87	0.46	2.77
Jun-14	0.29	0.09	0.71	0.24	2.44	1.05	6.58	0.76	10.14	0.66	3.92
Jul-14	0.31	0.13	0.80	0.26	2.58	0.96	9.39	0.93	13.65	0.57	4.41
Aug-14	0.15	0.00	0.38	0.16	1.71	0.63	6.80	0.69	10.90	0.57	4.11
Sep-14	0.18	0.05	0.46	0.15	1.79	0.63	6.96	0.61	10.40	0.46	3.32
Oct-14	0.23	0.10	0.62	0.21	1.89	0.88	5.06	0.69	8.79	0.57	3.71
Nov-14	0.29	0.09	0.67	0.24	2.34	0.87	8.74	0.87	14.64	0.63	5.09
Ms1											
Sep-13	0.37	0.16	2.34	0.29	4.34	0.42	6.08	0.30	3.10	0.15	0.68
Oct-13	0.34	0.15	2.12	0.26	3.85	0.32	3.15	0.21	2.24	0.13	0.66
Nov-13	0.40	0.16	2.31	0.29	4.16	0.43	3.56	0.22	2.46	0.18	0.83
Dec-13	0.18	0.10	0.82	0.16	2.13	0.41	5.00	0.30	2.82	0.16	0.74
Jan-14	0.56	0.25	3.49	0.43	6.09	0.53	5.33	0.37	3.49	0.20	0.47
Feb-14	0.42	0.18	2.75	0.31	4.89	0.39	4.63	0.26	2.91	0.15	0.68
Mar-14	0.68	0.29	4.25	0.48	7.04	0.51	5.05	0.30	2.83	0.15	0.52
Apr-14	0.09	0.06	0.35	0.09	0.87	0.24	1.70	0.17	2.07	0.16	0.86
May-14	0.36	0.16	2.51	0.31	4.96	0.54	6.40	0.38	4.47	0.23	0.78
Jun-14	0.39	0.18	2.15	0.34	4.62	0.70	9.71	0.50	4.87	0.23	1.02
Jul-14	0.42	0.21	2.05	0.36	4.61	0.78	9.80	0.51	4.40	0.24	0.78
Aug-14	0.23	0.11	1.23	0.19	3.26	0.55	8.12	0.39	3.53	0.00	0.64
Sep-14	0.28	0.14	1.40	0.23	3.65	0.67	8.83	0.46	4.31	0.20	0.86
Oct-14	0.13	0.07	0.82	0.13	2.27	0.38	5.55	0.27	2.58	0.13	0.47
Nov-14	0.21	0.05	1.34	0.19	3.05	0.44	6.21	0.25	2.45	0.07	0.36
Ms3											
Sep-13	0.12	0.00	0.24	0.13	1.06	0.66	4.13	0.68	9.19	0.92	5.42
Oct-13	0.22	0.05	0.37	0.14	1.26	0.62	4.12	0.42	6.89	0.36	1.64
Nov-13	0.13	0.05	0.39	0.21	1.98	1.12	3.97	0.38	5.33	0.46	3.25
Dec-13											
Jan-14	0.08	0.46	0.31	0.16	2.57	1.34	6.17	0.70	10.88	0.60	2.84
Feb-14	0.38	0.11	0.67	0.35	3.18	1.83	6.47	0.55	8.71	0.77	6.38
Mar-14	0.09	0.00	0.27	0.18	1.60	0.90	3.39	0.35	4.63	0.46	3.22
Apr-14	0.17	0.00	0.44	0.26	2.35	1.42	4.44	0.41	6.30	0.37	2.07
May-14	0.17	0.07	0.27	0.16	1.23	0.59	4.33	0.40	5.56	0.46	2.68
Jun-14	0.21	0.08	0.55	0.37	3.12	1.63	8.26	0.65	9.78	0.74	4.64
Jul-14	0.21	0.07	0.47	0.28	2.43	1.40	7.20	0.77	12.46	0.88	5.48
Aug-14	0.16	0.00	0.39	0.12	1.41	0.64	4.44	0.43	6.62	0.53	4.40
Sep-14	0.30	0.07	0.60	0.16	1.70	0.85	3.74	0.42	5.96	0.58	4.95
Oct-14	0.10	0.00	0.32	0.19	1.73	0.96	3.69	0.36	5.50	0.44	3.01
Nov-14	0.24	0.00	0.37	0.05	0.99	0.45	2.71	0.34	4.42	0.49	3.92

Appendix 1 Concentration of n-alkanes and ratios in soil samples (b)

	Concentration of total n-alkanes	CPI_{24-34}	ACL_{25-33}	C_{23}/C_{29}	Paq
Ms1	µg/g $_{TOC}$				
Sep-13	454	12.76	30.1	0.02	0.04
Oct-13	274	7.91	29.8	0.05	0.06
Nov-13	400	10.37	29.8	0.04	0.06
Dec-13	213	11.11	30.0	0.05	0.05
Jan-14	295	10.84	30.2	0.04	0.04
Feb-14	243	9.01	30.2	0.04	0.05
Mar-14	210	7.26	29.9	0.05	0.07
Apr-14	300	10.79	30.1	0.04	0.05
May-14	210	7.78	30.2	0.05	0.05
Jun-14	338	8.09	30.0	0.04	0.06
Jul-14	379	10.53	30.0	0.03	0.05
Aug-14	279	11.31	30.3	0.02	0.03
Sep-14	326	11.40	30.1	0.03	0.04
Oct-14	267	7.91	30.1	0.05	0.06
Nov-14	369	11.19	30.2	0.03	0.04
Ms1					
Sep-13	271	12.31	28.3	0.06	0.23
Oct-13	258	11.13	28.1	0.11	0.31
Nov-13	265	10.34	28.1	0.11	0.31
Dec-13	214	10.36	28.9	0.04	0.11
Jan-14	403	10.89	27.9	0.10	0.31
Feb-14	268	12.20	28.1	0.09	0.30
Mar-14	279	11.31	27.6	0.13	0.38
Apr-14	122	8.26	29.6	0.05	0.11
May-14	318	11.68	28.5	0.06	0.21
Jun-14	328	11.36	28.7	0.04	0.15
Jul-14	331	10.10	28.6	0.04	0.15
Aug-14	248	13.75	28.8	0.03	0.11
Sep-14	294	11.08	28.8	0.03	0.11
Oct-14	197	12.12	28.8	0.02	0.10
Nov-14	240	13.66	28.5	0.03	0.15
Ms3					
Sep-13	453	8.41	30.7	0.03	0.03
Oct-13	345	9.02	29.9	0.05	0.05
Nov-13	306	6.72	30.0	0.03	0.05
Dec-13					
Jan-14	556	6.59	29.9	0.01	0.02
Feb-14	392	7.00	30.1	0.06	0.06
Mar-14	275	6.99	30.2	0.03	0.04
Apr-14	279	6.40	29.7	0.04	0.05
May-14	329	8.39	30.1	0.04	0.04
Jun-14	625	7.55	29.9	0.03	0.04
Jul-14	562	8.31	30.3	0.03	0.03
Aug-14	344	10.12	30.4	0.04	0.05
Sep-14	356	8.34	30.3	0.08	0.09
Oct-14	297	7.37	30.1	0.03	0.04
Nov-14	241	9.53	30.5	0.09	0.08

Appendix 2 Water content, TOC and pH in catchment soils

		Water content	TOC	Measured pH
		%	%	
Ms1	Sep-13	41	8.52	-
	Oct-13	28	8.35	-
	Nov-13	37	8.27	7.4
	Dec-13	36	7.37	7.7
	Jan-14	28	8.32	7.3
	Feb-14	38	8.06	-
	Mar-14	24	7.13	-
	Apr-14	47	8.28	-
	May-14	15	7.28	-
	Jun-14	36	7.96	6.6
	Jul-14	32	8.97	-
	Aug-14	37	9.36	-
	Sep-14	29	7.68	6.9
	Oct-14	36	8.51	-
	Nov-14	48	9.32	-
Ms2	Sep-13	32	6.73	-
	Oct-13	15	5.20	-
	Nov-13	18	5.67	7.4
	Dec-13	25	6.00	6.6
	Jan-14	16	5.26	7.0
	Feb-14	34	6.57	7.1
	Mar-14	34	7.91	-
	Apr-14	24	5.46	-
	May-14	27	6.64	6.7
	Jun-14	40	7.53	6.7
	Jul-14	26	7.29	6.6
	Aug-14	30	7.36	6.8
	Sep-14	34	7.15	-
	Oct-14	29	6.48	7.8
	Nov-14	32	6.08	7.7
Ms3	Sep-13	18	4.98	-
	Oct-13	3	4.67	8.0
	Nov-13	4	5.64	8.0
	Jan-14	3	4.70	-
	Feb-14	34	7.51	7.7
	Mar-14	10	5.49	-
	Apr-14	30	6.53	-
	May-14	5	4.83	7.6
	Jun-14	15	4.81	8.1
	Jul-14	8	5.63	-
	Aug-14	11	5.56	-
	Sep-14	14	5.42	-
	Oct-14	14	5.48	-
	Nov-14	22	5.80	7.8
Ms4	Jan-16	66	4.29	-
Ms5	Jan-16	28	7.34	-
Ms6	Jan-16	13	15.07	-

"-" indicates no measured data, "n.d." indicates data is not to be calculated

Appendix 3 GDGT concentration and indices in catchment soils

		isoGDGTs	brGDGTs	TEX_{86}	CBT	MBT	MBT´	MAT1	MAT2
		µg/g $_{TOC}$	µg/g $_{TOC}$						
Ms1	Sep-13	3.84	18.21	0.58	-0.02	0.28	0.29	10.0	8.3
	Oct-13	1.97	12.27	0.69	0.03	0.30	0.31	10.1	8.4
	Nov-13	4.10	41.97	0.60	-0.01	0.27	0.28	9.6	7.6
	Dec-13	5.36	12.08	0.60	-0.17	0.30	0.31	11.3	10.2
	Jan-14	2.74	17.14	0.67	0.10	0.28	0.29	9.2	7.1
	Feb-14	1.16	12.80	0.63	0.30	0.31	0.31	8.8	6.4
	Mar-14	1.60	13.23	0.69	0.38	0.28	0.28	7.4	4.3
	Apr-14	3.75	58.03	0.65	-0.05	0.28	0.29	10.0	8.3
	May-14	1.25	11.88	0.70	0.49	0.30	0.31	7.6	4.6
	Jun-14	2.51	5.03	0.78	0.48	0.30	0.31	7.6	4.6
	Jul-14	3.14	59.26	0.62	0.03	0.27	0.27	9.1	7.0
	Aug-14	3.62	21.33	0.65	0.00	0.30	0.31	10.5	9.1
	Sep-14	2.61	13.10	0.63	0.18	0.32	0.32	9.8	8.0
	Oct-14	4.12	27.49	0.70	0.44	0.34	0.35	9.0	6.9
	Nov-14	2.00	17.98	0.67	-0.53	0.28	0.29	12.8	13.0
Ms2	Sep-13	0.09	11.87	n.d.	0.41	0.31	0.31	5.4	8.1
	Oct-13	0.13	12.13	n.d.	0.57	0.35	0.35	6.0	8.5
	Nov-13	0.22	27.31	n.d.	0.49	0.29	0.29	3.8	7.1
	Dec-13	0.09	11.03	n.d.	0.54	0.39	0.39	8.3	9.9
	Jan-14	0.04	34.33	n.d.	0.47	0.31	0.31	5.1	7.9
	Feb-14	0.05	32.98	n.d.	0.44	0.31	0.32	5.4	8.1
	Mar-14	0.11	29.55	n.d.	0.42	0.29	0.30	4.7	7.7
	Apr-14	0.52	27.77	n.d.	0.48	0.33	0.34	6.1	8.5
	May-14	0.07	32.02	n.d.	0.42	0.32	0.32	5.7	8.3
	Jun-14	0.07	16.62	n.d.	0.53	0.33	0.33	5.4	8.1
	Jul-14	0.08	30.99	n.d.	0.55	0.27	0.27	2.0	6.0
	Aug-14	0.17	17.07	n.d.	0.41	0.34	0.35	7.2	9.2
	Sep-14	0.09	17.76	n.d.	0.50	0.36	0.37	7.3	9.3
	Oct-14	0.27	12.88	n.d.	0.29	0.30	0.30	6.1	8.5
	Nov-14	0.18	9.25	n.d.	0.18	0.21	0.22	2.9	6.6
Ms3	Sep-13	2.51	1.83	0.75	0.55	0.17	0.2	-2.9	2.8
	Oct-13	2.08	1.67	0.76	0.53	0.16	0.2	-2.9	3.4
	Nov-13	1.97	6.83	0.74	0.41	0.17	0.2	-1.3	4.3
	Jan-14	2.31	5.26	0.73	0.48	0.15	0.2	-3.2	2.7
	Feb-14	5.18	9.17	0.73	0.52	0.14	0.2	-3.9	2.6
	Mar-14	5.62	9.95	0.74	0.58	0.12	0.1	-5.7	1.4
	Apr-14	4.21	6.23	0.79	0.23	0.16	0.2	-0.1	5.1
	May-14	1.75	2.90	0.75	0.60	0.11	0.1	-6.4	1.0
	Jun-14	2.17	4.18	0.73	0.46	0.16	0.2	-2.3	3.7
	Jul-14	2.74	6.99	0.73	0.47	0.13	0.1	-4.0	2.7
	Aug-14	2.36	1.42	0.74	0.45	0.15	0.2	-2.9	3.5
	Sep-14	3.42	2.12	0.78	0.49	0.14	0.2	-3.5	3.0
	Oct-14	2.52	1.49	0.79	0.41	0.13	0.2	-3.2	3.2
	Nov-14	2.99	2.10	0.74	0.48	0.12	0.1	-4.4	2.7
Ms4	Jan-16	0.02	0.07	0.77	0.28	0.15	0.1	-1.4	3.8
Ms5	Jan-16	0.05	0.37	0.70	0.38	0.33	0.33	6.9	8.9
Ms6	Jan-16	0.05	1.68	0.81	0.35	0.20	0.20	0.9	5.2

"-" indicates no m"-" indicates no measured data, "n.d." indicates data is not to be calculated

Appendix 4 Concentration and ratios of n-alkanes in the sediment core of Montcortés

Age (A.D.)	Concentration of n-alkanes	ACL_{25-33}	CPI_{24-34}	P_{aq}	C_{17}/C_{29}
	µg/g dw				
2012	10.25	28.9	10.0	0.24	0.64
2010	11.34	28.9	9.1	0.22	0.55
2009	9.26	29.0	10.4	0.22	0.60
2004	13.16	29.2	9.3	0.20	0.60
1999	11.94	29.1	8.6	0.20	0.56
1994	11.33	29.0	8.6	0.24	0.99
1989	14.26	29.1	7.8	0.22	1.63
1984	12.58	29.0	7.7	0.23	1.68
1979	10.09	29.1	8.0	0.22	1.88
1974	10.66	29.0	8.3	0.22	2.00
1969	10.83	29.2	10.0	0.20	2.07
1964	13.71	29.0	10.0	0.27	1.26
1959	13.83	29.1	9.6	0.28	0.62
1954	14.51	29.0	9.7	0.25	0.72
1949	10.43	29.1	11.6	0.22	0.24
1939	10.80	29.1	7.0	0.21	0.18
1929	9.25	29.2	9.5	0.20	0.12
1919	10.50	29.2	9.8	0.21	0.17
1907	5.88	29.1	8.8	0.20	0.58
1902	7.13	29.2	9.4	0.19	0.05
1584	3.80	29.5	9.2	0.17	0.18
1572	3.38	29.7	9.3	0.12	0.09
1559	7.20	29.3	9.4	0.17	0.12
1547	9.37	29.3	9.6	0.15	0.07
1534	8.86	29.2	9.7	0.15	0.04
1522	8.46	29.2	10.0	0.15	0.03
1509	9.58	29.2	10.2	0.15	0.02
1497	8.58	29.2	10.2	0.23	0.03
1485	6.47	29.2	10.2	0.28	0.05
1472	4.49	29.3	9.1	0.25	0.06
1460	3.24	29.5	10.4	0.20	0.13
1447	2.68	29.5	8.8	0.18	0.08
1435	3.38	29.3	9.6	0.14	0.09
1422	3.86	29.4	9.8	0.15	0.06
1410	3.46	29.6	9.5	0.13	0.10

Appendix 5 Concentration and ratios of GDGTs in the sediment core of Montcortés

Age (A.D.)	isoGDGT	brGDGT	TEX_{86}	GDGT-0	CBT	MBT	MBT'
	µg/g dw	µg/g dw		/GDGT-4			
2012	0.64	5.64	0.49	29.89	0.46	0.20	0.20
2010	0.78	7.30	0.49	33.31	0.51	0.21	0.21
2009	0.62	5.55	0.50	24.45	0.47	0.22	0.23
2004	0.82	7.51	0.50	16.39	0.47	0.22	0.23
1999	1.15	8.03	0.48	30.21	0.50	0.23	0.23
1994	1.12	9.29	0.45	38.53	0.50	0.24	0.24
1989	1.01	9.50	0.42	51.57	0.56	0.23	0.23
1984	1.43	8.08	0.41	56.45	0.56	0.23	0.24
1979	0.39	2.60	0.42	37.94	0.57	0.22	0.22
1974	0.99	7.10	0.44	37.89	0.63	0.19	0.20
1969	0.67	4.81	0.52	15.53	0.59	0.19	0.20
1964	1.12	7.40	0.53	30.10	0.61	0.19	0.20
1959	1.01	6.56	0.50	28.70	0.61	0.20	0.20
1954	1.05	5.91	0.46	36.03	0.60	0.20	0.20
1949	0.56	3.89	0.49	15.75	0.49	0.20	0.20
1939	0.73	4.45	0.52	25.66	0.51	0.20	0.20
1929	0.68	3.20	0.49	25.40	0.47	0.21	0.21
1919	0.70	3.91	0.52	20.61	0.53	0.20	0.20
1907	0.73	4.07	0.50	19.98	0.48	0.20	0.20
1902	0.47	3.22	0.54	17.11	0.41	0.20	0.21
1584	0.47	6.21	0.57	5.84	0.61	0.23	0.23
1572	0.45	4.37	0.58	3.96	0.56	0.23	0.23
1559	0.83	10.41	0.53	24.70	0.62	0.24	0.24
1547	0.97	12.44	0.55	25.54	0.62	0.23	0.24
1534	0.77	9.96	0.58	32.83	0.62	0.22	0.22
1522	1.43	17.40	0.55	47.75	0.64	0.23	0.23
1509	0.83	11.57	0.59	19.24	0.63	0.23	0.23
1497	0.75	10.72	0.54	22.87	0.60	0.24	0.24
1485	0.65	6.29	0.57	22.66	0.58	0.23	0.23
1472	0.51	3.90	0.56	17.99	0.57	0.23	0.24
1460	0.41	2.91	0.57	9.52	0.52	0.23	0.23
1447	0.38	2.87	0.57	15.04	0.51	0.23	0.23
1435	0.40	3.29	0.51	15.81	0.53	0.23	0.24
1422	0.45	4.05	0.57	11.83	0.52	0.23	0.23
1410	0.42	3.11	0.59	9.14	0.58	0.22	0.22

Appendix 6 GDGT-estimated temperatures in the sediment core of Montcortés

Age (A.D.)	LST	MAT1	MAT2	MAT-(Zink, 2010)	F(IIa)-T
	°C	°C	°C	°C	°C
2012	13.2	-0.6	4.3	10.2	10.6
2010	13.3	-0.5	4.3	9.9	9.8
2009	13.4	0.6	5.1	10.1	9.6
2004	13.6	0.7	5.1	10.1	9.6
1999	12.2	0.6	5.0	10.0	9.4
1994	10.6	1.3	5.5	10.0	9.9
1989	9.4	0.1	4.7	9.6	9.2
1984	8.7	0.3	4.8	9.6	8.9
1979	9.1	-0.6	4.3	9.5	8.8
1974	10.3	-2.4	3.2	9.1	8.5
1969	14.7	-1.9	3.5	9.4	9.3
1964	15.2	-2.1	3.4	9.2	9.2
1959	13.6	-1.7	3.6	9.2	9.5
1954	11.6	-1.8	3.5	9.3	9.3
1949	12.9	-0.8	4.1	10.0	9.7
1939	14.6	-1.0	4.1	9.9	9.9
1929	13.1	0.0	4.6	10.1	10.1
1919	14.6	-1.0	4.0	9.7	9.8
1907	13.5	-0.7	4.2	10.1	9.5
1902	15.7	0.3	4.8	10.5	9.7
1584	17.5	-10.0	189.9	9.2	7.8
1572	18.3	-11.5	133.2	9.6	9.0
1559	15.1	-9.2	320.1	9.1	9.1
1547	16.5	-9.5	382.8	9.2	8.9
1534	17.8	-10.1	305.9	9.1	9.5
1522	16.6	-9.3	536.4	9.0	9.1
1509	18.6	-9.6	355.9	9.1	9.6
1497	16.0	-9.6	329.8	9.3	9.7
1485	17.6	-10.7	192.5	9.4	9.4
1472	16.8	-10.9	118.5	9.5	9.7
1460	17.7	-12.8	88.1	9.8	10.1
1447	17.5	-13.0	86.7	9.9	9.8
1435	14.2	-12.2	99.9	9.8	9.7
1422	17.2	-12.5	123.3	9.8	9.9
1410	18.6	-11.4	93.9	9.4	9.1